NASA Contractor Report 179613

Propfan Test Assessment
Propfan Propulsion System
Static Test Report

Contract NAS3-24339

September 1987

(NASA-CR-179613) PROPFAN TEST ASSESSMENT PROPFAN PROPULSION SYSTEM STATIC TEST REPORT
Contractor Report, Feb. - Jun. 1986
(Lockheed-Georgia Co.) 238 p Avail: NTIS
HC A11/MF A01
CSCL 21E G3/07

N87-29536

Unclas
0099053

NASA

NASA Contractor Report 179613

Propfan Test Assessment Propfan Propulsion System Static Test Report

D. M. O'Rourke
Lockheed-Georgia Company
Marietta, Georgia

Prepared for
Lewis Research Center
under Contract NAS3-24339

National Aeronautics
and Space Administration

Lewis Research Center
Cleveland, Ohio 44135

Lockheed

FOREWORD

This report presents the results of the PTA Static Test Program performed at the Rohr Brown Field facility in Chula Vista, California. Evaluation of the Hamilton Standard SR-7L propfan and the Allison 501-M78B drive system was accomplished under NASA-Lewis contract NAS3-24339.

This report was prepared by the Lockheed-Georgia Company with support from Allison, Hamilton Standard, and Rohr, and is also identified by Lockheed Report Number LG86ER0173 for Lockheed internal control purposes. Substantial inputs were provided by Harold Bartel, Wynn Daughters, Clark Price, and Cliff Withers of Lockheed, Mark Price and Denny Warner of Allison, and Chuck de George, Doug Leishman, and Jay Turnberg of Hamilton Standard.

The Static Test Program itself involved a great number of people from all the companies involved. Cliff Withers was the PTA Test Manager responsible for the overall conduct of the test. Clark Price and Eddie Fletcher of Lockheed oversaw the installation, functional checkout, and initial runs of the propfan propulsion system. Mark Price and Larry Nightingale of Allison provided guidance on drive system operation, and Jay Turnberg, Chuck de George, and Gary Godek of Hamilton Standard ensured proper operation of the propfan. Tony Bradlaugh-Dredge and Steve Bryan provided support from the Rohr main plant in Chula Vista.

Special thanks should be extended to Bill Buchanan and the Brown Field facility crew. Bill, Don Roth, and Les Travis managed the resources and manpower smoothly, and were extremely helpful in obtaining and reducing data. The Brown Field technicians and operators provided competent and timely assistance when required.

Lockheed

TABLE OF CONTENTS

Lockheed

TABLE OF CONTENTS (cont.)

Lockheed

LIST OF FIGURES

LIST OF FIGURES (cont.)

Lockheed

LIST OF FIGURES (cont.)

Lockheed

LIST OF FIGURES (cont.)

LIST OF FIGURES (cont.)

LIST OF TABLES

Lockheed

1.0 SUMMARY

The Propfan Test Assessment (PTA) propulsion system successfully completed over 50 hours of extensive static ground tests, including a 36 hour endurance test. All major systems performed as expected, verifying that the large-scale 2.74m (9 foot) diameter propfan, engine, gearbox, controls, subsystems and flight instrumentation will be satisfactory with minor modifications for the upcoming PTA flight tests on the GII aircraft in early 1987.

A test envelope was established for static ground operation to maintain propfan blade stresses within limits for propfan rotational speeds up to 105% (1783 rpm) and power levels up to 3880 kW (5200 SHP).

Maximum propfan blade angle slew rate observed during the power transient was 7 deg/sec, compared to a design slew rate of 9 deg/sec. Power turbine speed overshoots were observed to be within approximately 3% for each propfan speed transient. These transient tests verified stable, predictable response of the engine power and propfan speed controls.

The drive system provided the necessary power up to a maximum propfan disc loading of 503.6 kW/D^2 (62.7 SHP/D^2) during the static test with a Measured Gas Temperature (MGT) margin of 55° C (100° F) below the Maximum Continuous rating. Engine oil consumption was virtually non-existent for the entire test. Installed engine TSFC was better than expected, probably due to the excellent inlet performance coupled with the supercharging effect of the propfan.

The drive system exhibited a 1 to 2% power deterioration during the 36 hours of endurance testing. This performance degradation was probably due to compressor efficiency loss caused by the ingestion of dirt and hydraulic fluid that leaked from the propfan control rear lip seal. Following the test, the compressor was cleaned with a commercial engine wash and water in an effort to restore the power loss.

Propfan near and far field noise was measured over a range of tip speeds and power loadings. The measured noise exhibited characteristics typical of an open rotor operating under static conditions where random turbulent flow enters the disc area and the blades are likely to be stalled. The near and far field noise spectra contained three dominant components, propfan blade tones, propfan random noise, and compressor/propfan interaction noise. Propfan blade tones in the far field were identified up to the fifth order. However, the contribution beyond the first order was minimal. Propfan random noise was observed at low frequencies (500 to 1500 Hz), and was a significant contributor to the near and far field spectra. This random noise governed the overall sound pressure level at most operating conditions. Compressor/propfan interaction tones (tones at frequencies equal to the sums of or differences between the propfan and compressor blade passage frequencies) were strongest at azimuthal angles ranging from 15^{o} to 60^{o} in the forward quadrant. At low tip speeds, these tones were masked by the propfan random noise. No significant turbine noise or combustion noise was evident.

Propfan propulsion system refurbishment prior to flight test includes:

1. Rework the gearbox mounted electromechanical actuator to increase the torque capability by approximately 70% for propfan speed control input.

2. Replace the propfan control rear lip seal to minimize hydraulic fluid leaks.

3. Replace the engine power lever potentiometer to improve engine power lever response.

4. Replace the gearbox lateral accelerometer (V_5) bracket.

5. Replace The aft compressor vertical (V_3) accelerometer with the aft compressor lateral (V_7) signal for the cockpit display.

6. Refurbish the reduction gearbox and replace the main drive gear roller bearing.

Propfan propulsion system limitations during ground, taxi, and flight tests of the GII testbed aircraft based on static test operation include:

1. Limit or avoid reverse thrust operation to prevent possible overspeed, handling problems at some taxi speed conditions, lubrication fluid and fuel heating problems, and gearbox roller bearing skidding problems.

2. Set propfan minimum speed limit at 50% N_p to ensure sufficient lubrication oil pressure for power section and gearbox.

3. Set power section minimum torque limit at 474.5 N-m (350 ft-lbs) to prevent skidding of main drive gear roller bearing.

2.0 INTRODUCTION

The Lockheed-Georgia Company is the prime contractor for the Propfan Test Assessment (PTA) program to flight test the government furnished Hamilton Standard 2.74m (9-ft) diameter SR-7L propfan from the Large-Scale Advanced Propfan (LAP) program. PTA flight test objectives are to evaluate the structural integrity and acoustic characteristics of the LAP installed on the left wing of a Gulfstream Aerospace GII testbed aircraft. The PTA propulsion system consists of the SR-7L propfan, an Allison drive system consisting of a modified Model 570 industrial gas turbine engine and a modified Allison T56 reduction gearbox, and a Rohr Industries forward nacelle and acoustically treated tailpipe.

The SR-7L propfan was previously tested at Wright-Patterson Air Force Base under static conditions, and in the Modane, France wind tunnel up to 0.83 Mach. Allison previously tested the modified Model 570 engine (a derivative of the XT-701 Heavy Lift Helicopter engine), the modified T56 reduction gearbox, and the modified XT-701 engine control system. This Allison drive system is capable of delivering approximately 2237 kW (3000 shaft horsepower) continuously at 0.8 Mach at 10,668m (35,000 feet) pressure altitude, and 4474 kW (6000 horsepower) intermittently under sea level static conditions, and has in-flight starting capability.

A PTA Propfan Propulsion System Detail Design Review (DDR) was held on November 21,1985, and a Static Test Readiness Review was held on April 3, 1986, both at the NASA-Lewis Research Center. The Propfan Propulsion System was assembled, instrumented, and installed on the Rohr-Brown Field engine test stand near Chula Vista, CA, and static tests were conducted from May 19 to June 27, 1986. Tests included a functional system checkout, propfan dynamic balancing and stress survey, a media demonstration on June 3, a simulated flight 36 hour endurance test, reverse thrust operation, and concurrent tests of the PTA systems and acoustic characteristics.

This report presents the results of the Propulsion System Static Tests accomplished at the Rohr Industries, Inc. static test facility at Chula Vista, California.

3.0 OBJECTIVES

The goals of the propfan propulsion system static test were to experimentally qualify and obtain baseline data for the propulsion system, including its related subsystems, under static conditions prior to the start of the Propfan Test Assessment (PTA) flight test program. In order to fulfill these goals, the specific objectives of the PTA static test program were to:

- Functionally checkout the propfan propulsion system
- Substantiate the structural integrity of the propfan
- Verify safe and stable operation of the propfan propulsion system
- Functionally checkout operational and research instrumentation
- Define propfan and drive system static noise characteristics
- Obtain drive system baseline vibration data
- Verify drive system sea level performance
- Evaluate modified propfan blade seal
- Verify system endurance capability at static conditions by completing simulated flight cycles.

4.0 TEST HARDWARE DESCRIPTION

4.1 PROPFAN PROPULSION SYSTEM

The propulsion system for the Propfan Test Assessment static tests was an integrated system consisting of the Hamilton Standard SR-7L propfan, the Allison Model 501-M78B drive system, the Rohr Quick Engine Change (QEC) nacelle, and related subsystems. The aft nacelle that will be used on the GII testbed aircraft during flight testing was not installed for the static tests. Figure 4.1 shows the arrangement of the propfan propulsion system components.

4.2 PROPFAN

The Large-Scale Advanced Propfan assembly, shown in Figure 4.2, is a 2.74 meter (9 foot) diameter, 8-bladed tractor type propeller rated for 4476 kW (6000 SHP) at 1698 rpm. It is designed to be mounted on a standard 60A splined propeller shaft. The LAP has a hydraulically actuated blade pitch change system and a hydromechanical pitch control that allows the propfan to operate in a speed governing mode. The design of the actuator and control is based on proven technology used in Hamilton Standard's military and commercial propellers.

4.2.1 Propfan Assembly

The structural configuration of the SR-7L blade consists of a central aluminum spar, a fiberglass shell which overhangs the leading and trailing edges of the spar and a nickel sheath that covers the leading edge of the outer two-thirds of the blade. The remaining internal cavities are filled with low density rigid foam. A cut-away view of the blade is shown in Figure 4.3.

The blade design makes use of a NACA series 16 airfoil outboard and a series 65 circular arc airfoil inboard. Each blade has an activity factor

of 227 with 45° of blade sweep at the tip. The blades were designed with pre-deflection so that they would assume the desired aerodynamic shape at the cruise operating condition.

The blade tip trailing edge swings through a radius of 35.2 cm (13.84 inches) from the pitch axis. The maximum aft position occurs when the blade pitch angle is 98.3° at 3/4 radius. The normal maximum blade pitch angle is 90°.

The propfan blades are retained in the hub by a single row of ball bearings. The balls ride in two hardened steel races. One race is integral to the rim of the hub arm bore. The other race is machined into two ring halves that bear on the blade shank. Blade pitch change forces are transmitted from the actuator to the blade through a trunnion attached to the blade shank.

The spinner and bulkhead are essentially a reinforced fiberglass shell, supported by the hub and actuator. The spinner has an aerodynamic shape to facilitate proper inflow to the propfan blades. The bulkhead provides a mounting surface for much of the instrumentation hardware in the rotating field.

4.2.2 Propfan Controls

The pitch change system is comprised of two components, a pitch change actuator and a propeller control. The pitch change actuator is located within the propeller hub, and the propeller control is mounted on the propeller drive shaft. The pitch change actuator consists of a translating piston with an integral yoke to engage the blade rollers, a 4-way metering valve assembly, a pitch lock screw, a ground adjustable low pitch stop and a servo piston and ball screw to drive the pitchlock screw and beta valve.

To change pitch, a hydraulic signal from the control causes the half area servo to move and turn the ball screw. To increase pitch, the rotary

output of the ballscrew turns the pitchlock screw which advances the screw a small amount relative to the actuator piston. This rearward motion of the screw reduces the pitchlock gap and moves the 4-way valve relative to the piston, which directs supply oil to the increase pitch chamber of the actuator. The actuator moves in the opposite direction to the motion of the valve and causes the blade to change pitch. The beta valve is returned to null and the pitchlock gap is re-established. The pitchlock gap in steady-state is maintained at about the equivalent of 1^{o} blade angle and is always ready to limit the decrease pitch if oil pressure is lost. If this decrease of 1^{o} blade pitch occurs in flight, the prop speed will remain within approximately 2.5% of the set value.

4.2.2.1 Pitch Change Actuator

The pitch change actuator is designed to present state of the art technology and low development risk technique that has been used on a number of existing propeller systems. The design uses mostly steel for the load carrying member, and all surfaces subject to sliding seal wear are chrome plated to increase durability. The actuator is designed to conservative stress and deflection levels to minimize development effort while maintaining a reasonable but not minimum weight.

The pitch change mechanism is designed such that any malfunction will either cause the system to pitchlock or to feather. An additional safety feature on the SR-7L is a ground adjustable low pitch stop. This will limit the minimum blade angle under all in-flight circumstances. During the PTA Static Test this adjustable stop was generally set at the 20^{o} blade pitch position, although it was set at 35^{o} for one series of tests. The adjustable stop was set at approximately -5^{o} for reverse testing.

4.2.2.2 Pitch Change Control

The control for the SR-7L is a modified 54H60 unit. The 54H60 is a hydromechanical control in use on the Lockheed C-130 and P-3 airplanes. Since the first production unit was placed in service in 1956, there have been

over 11,000 built and they have logged over 73 million hours. The 54H60 is very similar to the 54460 controller, presently in service on the C-2 and E-2 airplanes. It provides the constant speed governing function and the capability to either manually or electrically feather the propeller. Because of physical restraints on the installation, no beta, i.e., direct blade angle, control is provided. An engine supplied overspeed electrical signal is available in the event of a malfunction of the on speed governor. The control utilizes this signal through the feather solenoid to cause the blade angle to increase until the propeller speed is at the overspeed setting and modulates there.

The primary functions of the blade pitch control are to generate the hydraulic pressure for the actuator and establish the increase or decrease pitch hydraulic pressure signal transmitted to the pitchlock and servo assembly. Hydraulic pressure is produced by two pumps contained in the stationary control and driven by the propeller shaft. A pump, driven by an auxiliary electric motor, provides hydraulic pressure for the blade angle changes when the propfan is not rotating. The increase/decrease pitch hydraulic signal is produced by a flyweight governor and a governor valve, which senses changes in rotational speed and sets the hydraulic pressure signal accordingly to re-establish the set point speed. This results in a blade pitch angle rate of change that is proportional to the difference between the actual RPM and the set point RPM.

The control has a single mechanical input positioned by an electromechanical actuator mounted on the Allison gearbox. This input signal will set the governing speed, feather the propeller, and reset the governor for reverse. The reverse blade angle is set by the pitch change mechanism. The output of the control is metered pressure to a half area servo piston in the pitch change mechanism. The control also includes an electrical feather override which will feather the propeller upon command, or in the event of overspeed regardless of the position by the mechanical pitch controller input.

Increasing metered pressure will cause the propeller to decrease pitch. Decreasing pressure will cause the propeller to increase pitch. Feather is accomplished by dumping metered pressure to drain.

4.3 DRIVE SYSTEM

The Allison Model 501-M78B drive system, shown in Figure 4.4, has the capability of delivering up to 4474 kW (6000 SHP) to the propfan. The major components of the drive system are the power section, reduction gearbox, and engine controls. The power section is a slightly modified version of the Model 570 industrial engine. A modified T56 reduction gearbox reduces engine power turbine speed through two gear stages to propfan speed. The drive system is controlled by a slightly modified XT701 control system.

4.3.1 Power Section

The power section is a slightly modified version of a Model 570 industrial engine, which was derived from the Model XT701 turboshaft engine developed in the Army Heavy Lift Helicopter program. Primary differences between the XT701 and the 570 are the elimination of the XT701 compressor bleed air system and change from a titanium to steel compressor case. Certain other minor mechanical and electronic features also were modified for increased durability and reduced cost for industrial applications.

The Model 501-M78B power section incorporates two rotor systems: a gas generator rotor, and power turbine rotor. The gas generator includes a thirteen-stage compressor, a diffuser/combustor, and a two-stage gas generator turbine. The power turbine system is made up of a two-stage power turbine and shafting to couple the turbine to the torquemeter.

The power section is described by the major engine assembly sections shown in Figure 4.5. These include:

- Air inlet housing assembly
- Compressor assembly
- Diffuser/combustor assembly
- Turbine assembly
- Accessory gearbox.

4.3.1.1 Air Inlet Housing Assembly

The air inlet housing has an outer ring and an inner hub connected by six radial struts. It supports the front of the compressor and provides mounting for an accessory gearbox. The front flange of the inlet housing mounts the adapter ring and torquemeter housing that transmits mount loads from the reduction gearbox to the power section. The Model 501-M78B inlet housing is identical to the Model 570 part except for a minor modification to mount the adapter ring and torquemeter.

The 501-M78B contains an integral torquemeter assembly which provides a means of measuring the power output from the engine. The torquemeter assembly is located in the hub of the air inlet housing assembly.

The torquemeter assembly operates on a simple principle. When torque is transferred through a shaft, the shaft twists. The greater the torque, the greater the twist. As long as the limits of the metal are not exceeded, the shaft will return to its original shape when the torque is removed. By measuring the magnitude of twist of the calibrated shaft, the amount of torque being transmitted through the shaft can be calculated.

4.3.1.2 Compressor Assembly

Compressor assemblies for Model 501-M78B and 570 power sections are identical. The thirteen-stage assembly is an axial-flow design incorporating variable inlet guide vanes and five stages of variable stator vanes. A variable geometry compressor system is used to position vanes at their optimum angle at any operating condition. In addition to preventing

stall during engine starts variable vanes allow the compressor to operate at higher efficiency under partial load conditions.

The compressor consists of a rotor assembly, case, and vane assembly. The compressor rotor assembly is a titanium drum which retains the blades for stages 2 through 13.

The compressor case assembly is the structural member between air inlet housing and diffuser. This assembly consists of two compressor case halves which retain five stages of variable vanes and eight stages of fixed vanes.

4.3.1.3 Diffuser/Combustor Assembly

Model 501-M78B diffuser/combustor assembly is identical to Model 570 which incorporates a triple-pass diffuser and annular combustor.

The diffuser consists of an outer and inner case wall, connected by eight hollow radial struts. An inner case wall provides structural support for the center bearing sump assembly, and serves as the combustion inner casing. The outer diffuser case wall serves as the combustion outer casing. It provides mounting for sixteen fuel nozzles, four spark ignitors, and four borescope inspection ports.

To obtain high endurance life, sixteen airblast fuel nozzles provide atomized, evenly distributed fuel flow to the combustion liner. Once combustion occurs, the four spark ignitors automatically cease operation.

4.3.1.4 Turbine Assembly

The power section contains a two-stage gas generator turbine and a two-stage power turbine. The rematched turbine aerodynamics resulting from modified first-stage vanes allows sea level, maximum continuous operation at a gas generator corrected speed of 98.3 percent and Power Turbine Inlet Temperature (TIT) of 808°C (1486°F).

The turbine case is designed to contain any single turbine blade failure. To further minimize damage in the event of failure, a sequential failure order is incorporated in the design. If turbine blades fail, the turbine rotor can no longer accelerate, thus minimizing the probability of turbine wheel failure.

4.3.1.5 Accessory Gearbox

An accessory drive gearbox assembly, mounted on the bottom of the air inlet housing, is a fixed-ratio gearbox driven by the gas generator rotor system. It drives all the engine accessories, including oil pump, centrifugal breather, and fuel pump. Also, the air starter unit drives the engine through this gearbox.

4.3.2 Reduction Gearbox

The T56 reduction gearbox incorporates limited changes to ensure compatibility of the engine power turbine with propfan speed and rotation direction requirements.

The 501-M78B reduction gear assembly, shown in Figure 4.6, has four magnesium alloy castings which provide structural support for two stages of reduction gearing and accessory drive gear train. These structural members are:

- Front case
- Bearing diaphragm
- Rear case
- Rear case liner diaphragm.

The rear case provides the front attachment for the extension shaft housing. Within this housing is the torque transmission shaft, which provides the input to the input pinion. Two struts connected between the rear case and the power section air inlet housing, along with the torquemeter housing, provide rigidity required to maintain alignment between

power section and reduction gear assembly. On each side of the rear case are large engine mounting pads. Engine mounts, connected to these pads, support the engine within its nacelle. The rear case inner diaphragm and rear case provide structural support for the accessory drive gear train.

Two stages of gearing provide change in direction of rotation and overall speed reduction of 6.797:1. When power turbine speed is 11,500 rpm, (100 percent) rotating "down" inboard, propeller shaft speed is 1692 rpm, rotating "up" inboard.

Reduction gear assembly lubrication is independent of the power section system although both utilize a common oil supply tank. The reduction gear assembly system provides for lubrication of the gears and bearings of the first and second stage reduction gearing, and supplies oil required for propeller brake operation. Gears and bearings of the accessory drive gear train are lubricated by oil mist. Oil is scavenged by a nose scavenge pump and a main scavenge pump located in the front case.

The propfan brake is located in the accessory train. This brake is designed to prevent windmilling when the propfan is feathered in flight. It is a friction-type brake, consisting of a stationary inner cone and a rotating outer member. During normal engine operation, reduction gear oil pressure holds the brake released. As reduction gear oil pressure drops off, effective hydraulic forces decrease and spring forces move the outer member into contact with the inner cone. The propfan brake resists rotation with 247 N-m (182 ft-lbs) of torque when propeller is not rotating, and withstands 1532 N-m (1130 ft-lbs) reverse torque.

4.3.3 Controls

Control of the 501-M78B engine is provided by what is basically an XT701 control system, originally designed for turboshaft multi-engine helicopter applications. With minor modifications, this control is suitable for the propfan application. The engine control has two major components: a hydromechanical fuel metering system and a supervisory control. Unlike

T56 powerplants, there are no direct coordinating devices provided between engine and propeller control; each is controlled separately.

A hydromechanical fuel control, similar to those used with military TF39 and TF34 and commercial CF6 engines, is used for the PTA propfan engine.

4.4 QEC NACELLE

The QEC nacelle provides an aerodynamic shaped envelope for the drive system and its related subsystems, such as the starter supply, fuel supply, lubrication and oil cooling, and electrical subsystems.

The QEC nacelle consists of the nacelle cowling that encloses the engine drive system and includes the engine air inlet duct and the oil cooler air inlet and exhaust ducts, the engine mounting system, and mounting structure to the aft nacelle that will be connected to the QEC for flight testing on the GII testbed aircraft.

4.4.1 Nacelle Cowling

The nacelle cowling consists of graphite/epoxy skins, frames and longerons. The side panels of the nacelle are removable for access to the drive system and engine components.

The upper cowling panel accomodates the inlet ducting for the engine air intake and oil cooler, and the exhaust ducting for the oil cooler. A graphite/epoxy S-shaped duct assembly is located between the engine air inlet and the engine compressor case. Anti-icing for the engine air intake lip is not provided. Graphite/epoxy ducts are located between the oil cooler and oil cooler air inlet and exhaust.

V-frames and upper and lower cowlings terminate at the upper and lower frames which attach to the Lockheed forward firewall bulkhead of the aft nacelle.

4.4.2 Drive System Mounting

The mounting system for the Allison 501-M78B engine is similar to the Allison T56 installation in the Lockheed P-3. It consists of a suspension system and supporting truss, longerons and frames.

The suspension system consists of seven mountings and provides restraint in pitch, yaw and torque. The main mounts are located on each side of the gearbox and are designed to react to loads in all three directions. The gearbox top and bottom front mounts resist fore and aft loads. The gearbox bottom mount also resists vertical loads in the event of main mount failure. The aft upper and side mounts are located on the rear casing of the engine and resist vertical and lateral loads, respectively.

4.4.3 QEC Mounting Structure

The mounting structure consists of two machined forward frame members located adjacent to the gearbox, V-frames, aft diagonals and upper and lower longerons. The forward frames are manufactured from aluminum plate and graphite/epoxy. The upper portion of the frames are graphite/epoxy designed to accommodate the engine air inlet contour for the Allison 501-M78B engine, and the lower portion is machined from aluminum plate with constant bevel angles. The V-frames are fabricated from the P-3 demountable powerplant nacelle V-frames with new lower aft end fittings.

4.5 ACOUSTICALLY TREATED TAILPIPE

The acoustically treated tailpipe was designed to be installed into and mate with the attachment fittings in the aft nacelle. Since the aft nacelle was not used during static test, the tailpipe was attached directly to the test stand at the test facility. As a goal, the tailpipe was designed and fabricated to provide for 15 dB exhaust system noise suppression throughout the engine combustor frequency spectrum.

4.6 SYSTEMS

4.6.1 Propulsion System Controls and Instruments

The propulsion system functions for the static test were controlled and monitored by a control console (Figure 4.7) and instrument panel (Figure 4.8). These panels were those that will be used in the GII testbed flight station.

The control console contains the switches and levers which control engine starting and normal shutdown, emergency shutdown, engine power, prop speed, and prop feather and unfeather. The results of the actions taken on the control console are displayed as performance or engine health parameters on the instrument panel.

Power, which is a function of power turbine (prop) speed and torque, is controlled by both the prop speed control lever and the power control lever, and monitored on the N_p and torque indicators.

4.6.2 Fuel System

The QEC fuel system used during static testing was identical to the fuel system to be used on the GII testbed aircraft.

The PTA QEC fuel system consists of a fuel/oil heat exchanger, a fuel/oil heat exchanger/strainer assembly, a low pressure switch, a pressure relief valve, a temperature sensor and indicator, the PTA engine fuel system, and associated plumbing. The engine fuel system consists of a fuel pump assembly, fuel control, fuel flowmeter, manifold drain valve, fuel manifold, and fuel nozzles.

Fuel enters the QEC through a quick connect/disconnect fitting at the QEC firewall. A flexible fire resistant fuel line runs to the prop pitch control oil cooler assembly. A C-130 fuel heater/strainer assembly with

the thermostatic oil bypass and fuel strainer removed is used to cool the prop control oil.

Fuel exiting the prop oil cooler flows through flexible line to another C-130 fuel heater, this one with only the thermostatic oil bypass removed, which is used to partially cool engine oil as well as strain solid particles from the fuel. A fuel low pressure switch and a pressure relief valve are connected to the fuel strainer outlet. The pressure switch warns the flight crew of low supply pressure during engine operation, and the relief valve protects the fuel system components from overpressure due to thermal expansion of the trapped fuel while the engine is not operating.

A flexible line directs fuel from the engine oil cooler to the engine inlet. A boss for a temperature sensor is inserted in this line. An MS28034-3 resistance bulb senses the fuel temperature entering the engine which is indicated on the instrument panel.

Upon entering the engine, fuel passes through the 501-M78B fuel pump assembly and the fuel control. The fuel control ports fuel pressure to the CVG actuator to control the variable compressor vanes. Metered fuel from the fuel control flows through the flowmeter and the manifold drain valve to the fuel manifold and fuel nozzles.

4.6.3 Engine Lubrication System

The QEC lubrication system used during static testing was identical to the oil system to be used on the GII testbed aircraft.

The PTA oil system consists of the engine oil system, scavenge oil filters, an air/oil heat exchanger, a fuel/oil heat exchanger, pressure and temperature sensors, and interconnecting plumbing. The drive system oil system consists of gearbox and power section oil filters, pressure and scavenge pumps, and an oil reservoir. The working fluid is MIL-L-23699C synthetic base oil.

Lubricating oil is stored and deaerated in a nacelle mounted oil tank with a capacity of 43.5 l (11.5 gallons). An MS28034-1 temperature sensor, mounted in the oil tank sump, supplies a signal to an indicator on the instrument panel. Oil flows through a motor operated shutoff valve controlled by either a switch on the control panel in conjunction with the engine electronic control, or the emergency engine shutdown T-handle. Two supply lines run from the oil sump, one to the power section, the other to the gearbox.

Power section oil is delivered through a flexible fire resistant line to the power section pressure pump in the accessory gearbox. Pressurized oil passes through a filter before being distributed to jets throughout the power section. A pressure sense line is located just downstream of the filter. This line is connected to a pressure transducer, which sends a signal to a pressure gage on the instrument panel, and a pressure switch, connected to a light also on the instrument panel which indicates low oil pressure.

After circulating through the power section, oil collects in four separate sumps to be scavenged. Oil flows through four scavenge pumps, connected in parallel, past a magnetic chip detector, and through a nacelle mounted scavenge oil filter. This oil filter has a popout indicator to warn of impending oil bypass. Power section oil then flows through a modified C-130 fuel heater assembly (described in Section 4.6.2) before combining with the gearbox scavenge oil.

Oil is supplied to and distributed in the reduction gearbox in a manner similar to the power section oil system. Gearbox oil is scavenged by two pumps, flows past a magnetic chip detector, and through a scavenge oil filter to the point where it is combined with the partially cooled power section scavenge oil.

Drive system scavenge oil flows through an air/oil cooler assembly and back into the oil tank until it is recirculated.

4.6.4 Prop Control Oil Cooling System

The working fluid in the prop pitch control circuit is MIL-H-5606 hydraulic fluid. The prop oil cooling system consists of a fuel-oil heat exchanger, a temperature sensor and indicator, and associated plumbing.

Prop control oil (hydraulic fluid) flows from the propfan assembly through flexible line to the modified C-130 fuel heater described in Section 4.6.2. The fluid travels through a flexible line past a temperature sensor. An MS28034-3 resistance bulb senses the fluid temperature returning to the propfan assembly for display on the instrument panel. A flexible line returns fluid to the propfan.

4.6.5 Starting System

The PTA starting system consists of an air turbine starter, a starter control valve, and associated ducting. The starter is bolted to the power section accessory gearbox, and a pawl and ratchet type clutch engages the starter shaft during starting.

Power was supplied to the starter in the form of high pressure air from a ground start cart through the control valve. This valve regulates pressure to the starter to 193 kPa (28 psig) maximum with a pressure rise rate of approximately 27.6 kPa (4 psi) per second. These limitations were necessary to prevent damage to the accessory gearbox.

The QEC starter supply ducting is 7.62 cm (3-inch) diameter stainless steel connected by standard V-band couplings.

4.7 SYSTEM LIMITS

4.7.1 Engine Limits

During the static test, the engine was operated within the limits specified in the Allison 501-M78B Model Specification. These limits are summarized in the following table:

501-M78B Engine Maximum Limits

	Maximum Continuous	Transient
Speed, rpm (%)		
Gas generator	14300 (100)	14700 (102.8)
Power turbine	12075 (105)	12535 (109)
Gearbox	1777 (105)	1844 (109)
Temperature, °C (°F)		
Compressor inlet	39 (103)	39 (103)
Power turbine inlet (starting)	677 (1250)	677 (1250)
Power turbine inlet (operating)	808 (1486)	846 (1555)
Torque, N-m (ft-lb)	4972 (3667)	4972 (3667)
Vibration, cm/sec (in/sec)		
15-40 Hertz	2.54 (1.0)	3.81 (1.5)
150-250 Hertz	1.91 (0.75)	3.05 (1.2)
Power, kW (SHP)	3729 (5000)	4474 (6000)
Oil inlet temperature, °C (°F)		
Above flight idle	85 (185)	100 (212)
Flight idle or below (30 minute limit)	100 (212)	

In addition to the above limits, an effort was made to avoid operation below 475 N-m (350 ft-lb) torque, which is the approximate torque load required to prevent the reduction gearbox main drive gear roller bearing from skidding. Low power turbine speed running (below approximately 50% N_p) was also avoided, since that condition could have resulted in lower than recommended gearbox oil pressures.

4.7.2 Propfan Limits

Due to stall buffet conditions discovered in LAP Static Rotor Testing at Wright-Patterson AFB, during the endurance tests the propulsion system was limited to the following speeds and powers:

Percent RPM	Power	Torque
75.0	1491 kW (2000 hp)	1238 N-m (913 ft-lb)
87.5	2312 kW (3100 hp)	2194 N-m (1618 ft-lb)
100.0	3505 kW (4700 hp)	2910 N-m (2146 ft-lb)
105.0	3952 kW (5300 hp)	3128 N-m (2307 ft-lb)

Based on the results of the propfan stress survey, these limits were revised for the endurance tests as discussed in Sections 8.4 and 8.6. After analyzing the results of the endurance tests, lower torque limits were specified for future static testing as noted in Section 9.2.1.2.

4.7.3 QEC/Engine Surface Temperature Limits

During static testing, thermocouples were applied to the engine surfaces and QEC nacelle structure to monitor surface and ambient temperatures. These temperatures were monitored to insure that limits were not exceeded. The maximum allowable air temperature surrounding the engine forward of the vertical firewall was 121°C (250°F) while the engine was running, and 135°C (275°F) while the engine was not operating. Aft of the vertical firewall, the limit was 371°C (700°F) whether the engine was operating or not. The limit temperatures for the QEC/engine surfaces for which limits were defined are shown below:

Limiting Component Surface Temperatures, °C (°F)

Component	Minimum	Maximum
Hydromechanical fuel control	-55 (-67)	120 (248)
Fuel pump	-54 (-67)	121 (250)
Electronic engine control	-55 (-67)	125 (257)
Ignition exciters	-54 (-67)	121 (250)
Prop speed control actuator	-54 (-67)	121 (250)

5.0 TEST FACILITY DESCRIPTION

5.1 TEST SITE

The Brown Field Test Facility consisted of a 30,350 m^2 (7 1/2 acre) fenced area situated within a 42,500 m^2 (10.5 acre) plot located on the north side of Brown Field Airport, 16 km (10 miles) from the Rohr main plant in Chula Vista. The prevailing wind conditions (speed and direction), mild temperatures and near sea level elevation 160 m (524 feet) of the site provided a high percentage of run windows with minimal data corrections. The test site was located in an area that was virtually flat with no obstructions for at least 1.6 km (1 mile) in any direction, thus making the site ideally suited for acquiring engine noise data.

Three engine test stands with bidirectional thrust measurement systems used for the testing of turbojet, turbofan and turboprop engines over a wide range of forward and reverse thrust capabilities were available at the test site. These stands, coupled with a computerized data acquisition and reduction system, provided a static test facility for use in the development of FAA certification testing of aircraft powerplant components and engine thrust calibrations. The thrust range capability of the three test stands and the accuracy of the instrumentation permit engine performance and thrust reverser testing of all current aircraft turbojet, turbofan and turboprop engines and nacelle systems.

Test stand operation was controlled and monitored from a soundproof control building equipped with an engine control station. The control room was environmentally conditioned to provide temperature and humidity stability for instrumentation systems, thus ensuring satisfactory data accuracies and instrument reliability. Air-conditioned trailers provided office space for engineering personnel and customer representatives. A layout of the test site is shown in Figure 5.1. As noted, the propfan propulsion system was mounted on the B-60 test stand and faced west.

5.2 TEST STAND

The PTA propulsion system was mounted on the B-60 test stand which provided an overhead structure mounting arrangement. This arrangement is shown in Figure 5.2. The single component thrust system was designed and manufactured by Aero Systems Engineering to measure the operating performance of aircraft turbine engines rated up to and including 267 kN (60,000 pounds) thrust. The thrust bed was designed to provide systems accuracies of $\pm$0.1 percent of the rated capacity of the installed thrust load measurement string over the temperature range of $21^{o}C \pm 17C^{o}$ ($70^{o}F \pm 30^{o}F$).

A specially prepared sound field instrumented with microphone arrays was provided as part of the test stand capability. The design of the sound field is such that direct correlation of engine noise data taken at other FAA certified facilities can be made. A detailed description of the sound field is provided in Section 5.6.

5.2.1 Adaptions and Interfaces

The propfan/engine/nacelle assembly was mounted on the B-60 test stand using the same structural mount points as defined for later use in the aircraft. A supporting series of structural beams was used to support the assembly and transfer all loads into the stand thrust measuring system.

A series of baffles was installed on the stand to protect the thrust bed, instrumentation lines, etc., from the direct blast of the propfan airflow.

Interface connections were made at the canted bulkhead in a manner similar to the aircraft installation. The air start line, engine fuel supply and all electrical connections were located on this bulkhead. The electrical connections were used for engine operational instrumentation, as well as for research instrumentation.

From the bulkhead, the fuel and start lines were routed to the facility air start cart and fuel supply system. The instrumentation lines were routed to various locations, i.e., both to the main control room where the engine display and data recording system was located and to the instrumentation van where the Hamilton Standard and dynamic strain gage recording devices were located.

5.3 FUEL SYSTEM

The fuel farm consisted of five underground tanks ranging in capacity from 15,100 to 37,900 liters (4,000 to 10,000 gallons). Total fuel capacity at the Brown Field Test Facility was 132,500 liters (35,000 gallons). Each tank had its own fill, vent, suction, and return lines. Tank selection was made by opening the suction and return valves to the tank. A 300 l/min (80 gpm) at 550 kPa (80 psig) pump driven by a 5.6 kW (7.5 hp) electric motor, was used to supply fuel to the B-60 test stand. The system was designed so that fuel could be pumped from and returned to any one of the five storage tanks.

The fuel system incorporated a pressurized 1135 liter (300 gallon) emergency fuel tank. In the event of an electrical failure during test operations, fuel from the emergency tank could have entered the B-60 fuel line. This would have allowed sufficient fuel flow to the operating engine to permit a normal engine shutdown.

5.3.1 Flow Measurement

The flow measuring section was horizontally mounted and vibration isolated. This section was located on the intermediate level of the stand about 18 meters (60 feet) from the engine fuel control. Fuel temperatures were also measured at this location.

5.3.2 Fuel System Operation

The amount of fuel used during an engine run was measured and recorded as part of the run log data.

5.4 ENGINE START SYSTEM

Air supply required to start the test engine was ducted from a facility start cart capable of supplying approximately 54.4 kg/min (100 lb/min) of air at 255 kPa (37 psig).

5.5 ENGINE PERFORMANCE DATA ACQUISITION/REDUCTION SYSTEM

The Brown Field data system consisted of a minicomputer with an analog subsystem and display terminals.

The minicomputer capabilities were:

- 29 digital input channels
- 192 analog channels
- Data resolution--16384 counts full scale
- Amplifier per channel
- Accuracy--0.04 percent full scale
- Secondary storage on dual tape and dual disc units

During the tests, the computer operator's terminal was normally configured as the data system control console. Any on-line changes and/or direct commands to the program were input via this console.

The engine operator's terminal displayed up to 16 channels of observed or corrected data. Wind speed and direction as well as critical engine parameters were continually monitored. An audible alarm limit check function was also available for monitoring critical parameters.

Data output was displayed on a 300 line-per-minute line printer from which multiple hard copies were available. The data were also recorded on a magnetic tape. The recorded data were reformatted into several specifically required formats.

A supplementary data acquisition and reduction system was used to acquire the dynamic and static strain gage data and related temperature data associated with the acoustic tailpipe research instrumentation. The system included the following major items and support equipment:

- FM tape recorder, 28 track
- Strain gage signal conditioning and signal amplifier modules (20 channels)
- IRIG "B" time code generator/reader
- Digital signal processor with display
- X-Y plotter
- CRT oscillograph
- Miscellaneous associated monitoring and calibrating equipment

The supplementary system was housed with the Hamilton Standard propfan instrumentation equipment in the instrumentation van located near the engine test stand.

Quick look data reduction was accomplished on site. A more capable data reduction capability was available for post test run data analysis.

5.5.1 Data Acquisition

During stabilized engine tests, data were normally acquired after the engine has stabilized on a specified set point. Data were acquired over at least a 30-second time span. During this 30 seconds, a complete scan of all data parameters was made each second. The computer utilized these individual scans to perform the specified calculations. The computer updated the calculations with new data each second until a total of 30 seconds of data were obtained. The final data output is the average of 30 second data runs.

After the final scan and calculations were completed, hard copy data were printed on a line printer. Each of the 30 individual data scans was also recorded on magnetic tape.

An eight channel strip chart recorder was provided in the instrumentation van for monitoring, in real time, selected propfan and engine parameters by Hamilton Standard engineering personnel.

Selected data channels were monitored during the engine runs and "quick-look" plots of selected parameters were made upon completion of the runs to verify data quality and to diagnose any problems.

5.5.2 Data Reduction

There were two forms of data reduction for engine testing: on-line and off-line.

The on-line data reduction method of Paragraph 5.5.1 was performed by the data reduction program defined. The hardcopy output was the result of these calculations. This provided a quick look at the engine parameters to evaluate the overall quality of the engine performance data. The instrumentation parameters were also evaluated from a quality standpoint.

Off-line data reduction was accomplished by play-back of the raw data from the magnetic tape through a playback program. This provided the following features:

- Allowed manual input of pre- and post-test thrust calibration data
- Allowed the use of a conversion generated program to access the data to calculate curve fit coefficients and check within-run and run-to-run data quality by statistical data analysis
- Allowed the generation of computer generated plots of engine gas generation curves
- Allowed the conversion of the data to several other desired formats
- Allowed individual one-second time slice data to be printed out for diagnostic or engineering investigation purposes.

A dual channel digital signal analyzer was available for on-line monitoring and data reduction. A dual channel signal analyzer, as well as the digital signal analyzer, was used for more intensive off-line dynamic data reduction.

5.6 ACOUSTIC DATA ACQUISITION

The Brown Field acoustical data acquisition system was a 69-channel dynamic data system with a magnetic tape recorder. It was capable of recording data on FM tape and accomplishing real time data analysis.

The system was capable of acquiring acoustic data from three groups of microphones, each group being recorded separately on a 28 track tape recorder. The recording system consisted of 69 acoustic amplifiers, each having fixed gain settings of -20 dB to +40 dB in 5 dB steps. These amplifiers fed 25 FM record amplifiers.

During recording all input signals were monitored simultaneously on 25 oscilloscopes; the recorded signals could also be checked individually.

During the acoustic tests, an analyzer provided on-line 1/3 octave band analysis for approximately 5 microphone locations. These data were printed out, as well as plotted, for instant review of selected noise data. However, this on-line data did not have microphone corrections for environmental conditions, pre-and post-test piston phone calibrations, line loss, or cable response calibrations.

5.6.1 B-60 Acoustic Field

All acoustic data were gathered in a smooth concrete sound measurement field and on or to the right of the propfan propulsion system centerline, as shown in Figure 5.3. The forward quadrant of the field was defined by a 90 degree arc of 53.3 m (175 feet) radius about the microphone reference point. This reference point was a defined location on the ground below the engine centerline approximately 2.74 m (9 feet) aft of the propfan disc.

The aft quadrant of the field was a rectangle defined by a line 53.3 m (175 feet) to the right of the engine centerline and a line 86.9 m (285

feet) aft of the reference point. The field also extended 4.57 m (15 feet) along the non-measurement (left) side of the engine centerline. The acoustic field satisfied the following criteria:

- The surface was light-colored to minimize thermal gradients.
- The field was concrete poured 14 cm (5-1/2 inches) thick.
- The field was sloped for drainage an average of 1 cm in 48 (1/4 inch per foot).
- Elevation changes were less than 1 cm in 240 (1 inch in 20 feet) distance. This change is with respect to the plane defined for drainage. In addition, there were no abrupt changes in elevation.

Some of the acoustic data were obtained with an acoustic barrier erected alongside the propulsion system. The barrier, shown in Figure 5.4, was constructed of two offset layers of wood planking. The barrier was 12.2 m (40 feet) in length and 9.1 m (30 feet) in height. In the forward position, the forward end of the barrier was 9.4 m (31 feet) forward of the propeller plane. In the aft position, the forward end of the barrier was 5.8 m (19 feet) aft of the propeller plane.

5.6.2 Microphone Arrays

Provisions were made for locating microphone arrays to measure both near field and far field noise.

Microphones could be positioned at 19 locations in the far field and 7 locations in the near field. Figure 5.5 defines the locations according to azimuth angle and distance from the microphone reference point. The near field microphones were mounted on poles 4.9 m (16 feet) above ground to measure noise in the horizontal plane of the propfan centerline. Four of the far field microphones (#16 at 60°, #17 at 90°, #18 at 120°, and #19 at 90°) were also pole mounted at the propfan centerline height. The other far field microphones, numbers 1 through 15 on the 45.7 m (150 foot) semicircle, were ground flush.

The ground flush mount consisted of a wire tripod support that suspended the microphone in an inverted position with the diaphragm parallel to and approximately 1.27 cm (1/2 inch) above the concrete surface.

The pole mount consisted of a plastic staff supporting the microphone in an upright vertical position at the extreme end of the staff, with the microphone diaphragm parallel to the ground.

All seven near field, and 18 of the far field microphones (#19 was removed) were in place during acoustic testing without the acoustic barrier. During testing with the acoustic barrier in position, the near field microphones and poles were removed. Noise measurements were then limited to the 19 far field microphones. When the barrier was placed in the forward position, the microphones at 70^{o} through 110^{o} sensed discharge noise while propfan noise was partially blocked, as shown in Figure 5.6. The barrier-aft position, shown in Figure 5.7, permitted the microphones at 100^{o} through 130^{o} to sense propfan noise while discharge noise was partially blocked. This was to provide insight on whether discharge noise contributed to the total noise in the lateral quadrant.

5.7 SHOP

The shop was a 186 m^2 (2,000 ft^2) two-story building housing a small array of power tools, such as bandsaws, grinders, drill presses and press brake. These were used to perform minor equipment repairs and also to fabricate special equipment to support test set-ups. A large storage loft and instrumentation repair area were also in this building.

The full machine shop and fabrication portions of the test laboratory were available for support for any major fabrication and/or repair beyond the capability of the on-site equipment.

6.0 TEST INSTRUMENTATION

6.1 PROPFAN

The Propfan FM electronic instrumentation system provided the capacity to transmit 33 channels of information from transducers on the rotating portion of the propfan to data collection and monitoring equipment in the stationary field. Electric power for the instrumentation system and signals from the transducers were transmitted across the rotating/stationary interface by a brush block and slip rings. The configuration of the propfan allowed for only eight slip rings. The need to transmit 33 channels of information therefore necessitated the use of multiplexing. The DC signals from 32 of the transducers in the rotating field were divided into two groups of sixteen and converted to frequency modulated signals by voltage controlled oscillators. Each group was then multiplexed by a mixer, allowing 32 channels to be transmitted through two slip rings. The groups of sixteen channels were then detranslated in the stationary field to four groups of four multiplexed channels (IRIG Standard/A through 4A) for recording. Simultaneously, discriminators demodulated each channel for real time monitoring of data. One discriminator was tuned to the center frequency of each channel. A schematic of the electronic data acquisition system is presented in Figure 6.1.

The FM electronic instrumentation system provided inherent noise immunity for data transmission. The frequency response of the system was 0 to 1000 Hz. Overall accuracy of the system was $\pm$3% RSS. Time correlation between channels is $\pm$13.8 microseconds.

Transducers installed on the propfan included strain gages to measure vibratory strain in the blade structure, pressure transducers to measure the actuator high and low pitch pressures, a potentiometer to measure the blade pitch angle, and a 1P sensor for measuring the propfan rotational speed. A flow switch was also located in the stationary propfan pitch control to warn if a hydraulic pump failure occurred.

The instrumentation system allowed for up to ten strain gages to be installed on each blade, though a maximum of 30 gages were active at any one time. Sixteen active gages could be selected from blades one through four and an additional sixteen could be selected from blades five through eight. Selection of the desired combination of strain gages was accomplished using eight programmable connectors mounted on the propfan hub. Programming of the connectors required jumper wires to connect the sockets of patch boards in the connectors. A total of sixty gages were applied to the propfan blades for the static engine tests. The gage locations are shown in Figures 6.2 through 6.5 and the active gages are indicated. The inactive gages were positioned to be used as back-ups in the event of primary gage failure. The strain gage pairs on the blade shanks and vee shear pairs on the blade aerodynamic surfaces were wired to act as one gage.

Data from the propfan instrumentation was recorded on a 14 track IRIG tape recorder. Real time monitoring of data was accomplished using two, four channel oscilloscopes and a spectrum analyzer. The oscilloscope provided a time domain display of eight channels simultaneously. The spectrum analyzer provided a frequency domain display of one channel at a time.

The performance of the instrumentation system was satisfactory throughout the test. Low strain gage signal noise levels were achieved as well as a high degree of reliability. The brush block employed a new leaf spring and brush design, which exhibited good wear and ring tracking characteristics. One set of brushes was used for the entire fifty hours of testing. The new design also minimizes brush bounce which had previously been a major source of strain gage signal noise. The blade angle measurement seemed to exhibit a significant amount of hysteresis throughout the test. It is estimated that the hysteresis resulted in a $\pm 2^{o}$ uncertainty in the blade angle measurement.

6.2 DRIVE SYSTEM

The data parameters measured on the drive system during static testing can be divided into two groups: operational and research instrumentation. Operational instrumentation parameters, shown in Figure 6.6, were those which related directly to drive system health or were required by the engine operator to set a specific test point. These data were displayed on the PTA instrument panel which was located in the engine control room, and which will be located in the flight station of the GII testbed aircraft. Other data parameters, shown in Figures 6.7 through 6.10, were monitored and recorded for information and diagnostic purposes only. These parameters, classified as research instrumentation parameters, were not used to set test points.

6.2.1 Operational Instrumentation

Operational instrumentation on the drive system included the following parameters:

Parameter	Range	Accuracy
Gearbox Lateral Vibration (V_5)	3.81 cm/sec (1.5 in/sec)	± 0.38 cm/sec (± 0.15 in/sec)
Engine Vertical Vibration (V_3)	3.81 cm/sec (1.5 in/sec)	± 0.38 cm/sec (± 0.15 in/sec)
Low Rotor Speed	0-13,225 rpm	± 65 rpm
High Rotor Speed	0-15,000 rpm	± 65 rpm
Torque	-136 to 5423 N-m (-100 to 4000 ft-lb)	± 68 N-m (± 50 ft-lb)
Measured Gas Temperature	-18 to 850°C (0 to 1555°F)	± 15°C ± 27°F
Oil Tank Outlet Temperature	-50 to 150°C (-58 to 300°F)	± 2°C ± 4°F
Propfan Oil Temperature	-50 to 150°C (-58 to 300°F)	± 2°C ± 4°F
Gear Box Oil Pressure	0 to 1380 kPa (0 to 200 psia)	± 2%
Power Section Oil Pressure	0 to 1035 kPa (0 to 150 psia)	± 2%
Fuel Flow Rate	0 to 2090 kg/hr (0 to 4600 lb/hr)	± 23 kg/hr (± 50 lb/hr)
Fuel Inlet Temperature	0 to 100°C (32 to 212°F)	± 0.5°C ± 0.9°F
Low Fuel Inlet Pressure	0/1	N/A

6.2.2 Research Instrumentation

Research instrumentation on the drive system included the following parameters:

Parameter	Range	Accuracy
Gearbox Vertical Vibration (V_1)	3.81 cm/sec (1.5 in/sec)	± 0.38 cm/sec (± 0.15 in/sec)
Engine Vertical Vibration (V_2)	3.81 cm/sec (1.5 in/sec)	± 0.38 cm/sec (± 0.15 in/sec)
Engine Vertical Vibration (V_4)	3.81 cm/sec (1.5 in/sec)	± 0.38 cm/sec (± 0.15 in/sec)
Engine Lateral Vibration (V_6)	3.81 cm/sec (1.5 in/sec)	± 0.38 cm/sec (± 0.15 in/sec)
Engine Lateral Vibration (V_7)	3.81 cm/sec (1.5 in/sec)	± 0.38 cm/sec (± 0.15 in/sec)
Engine Lateral Vibration (V_8)	3.81 cm/sec (1.5 in/sec)	± 0.38 cm/sec (± 0.15 in/sec)
Power Lever Position	0 to 120 deg	± deg
Propfan Speed Lever Position	-40 to +40 deg	± 0.3 deg
Ignition On/Off	0/1	N/A
Compressor Discharge Gas Temp.	-18 to 371°C (0 to 700°F)	± 4°C (± 7°F)
Compressor Inlet Air Temperature	-54 to 54°C (-65 to 130°F)	± 0.6°C (± 1.0°F)
Compressor Inlet Pressure	0 to 172 kPa (0 to 25 psia)	± 2%
Gearbox Oil Temperature	0 to 177°C (32 to 351°F)	± 2°C ± 4°F
Power Section Oil Temperature	0 to 177°C (32 to 351°F)	± 2°C ± 4°F
Compressor Discharge Pressure	0 to 1380 kPa (0 to 200 psig)	± 0.5%
Fuel Manifold Pressure	0 to 3450 kPa (0 to 500 psia)	± 2%
Oil Cooler Differential Pressure	± 14 kPa (± 2 psid)	± 2%

6.3 NACELLE

Thermocouples were installed inside the QEC nacelle to determine the environment surrounding the engine. The temperatures measured do not necessarily reflect the temperatures that will be encountered during

flight testing since the aft nacelle was not installed for static testing, but the data were helpful in ensuring that no hot spots existed in the isolated QEC nacelle. The locations of the QEC mounted thermocouples are shown in Figures 6.11 and 6.12.

The data parameters with range and accuracy which were measured in the nacelle are listed below.

Parameter	Range	Accuracy
Top Lord Mount Temperature	0 to 260°C	± 2.2°C
Left Lord Mount Temperature	0 to 260°C	± 2.2°C
Aft Lord Mount Temperature	0 to 260°C	± 2.2°C
Bottom Lord Mount Temperature	0 to 260°C	± 2.2°C
Side Lord Mount Temperature	0 to 260°C	± 2.2°C
Electronic Control Surface Temp.	0 to 177°C	± 2.2°C
Electronic Control Ambient Temp.	0 to 177°C	± 2.2°C
Turbine Case - Fwd Flange Temp.	0 to 538°C	± 4.0°C
Turbine Case - Aft Flange Temp.	0 to 538°C	± 4.0°C
Fuel Control Surface Temperature	0 to 177°C	± 2.2°C
Fuel Control Ambient Temperature	0 to 177°C	± 2.2°C
Ignition Exciter Surface Temp.	0 to 177°C	± 2.2°C
Burner Case Surface Temperature	0 to 538°C	± 4.0°C
Tailpipe Bellmouth Surface Temp.	0 to 600°C	± 4.0°C
Electro Mech Actuator Amb. Temp.	0 to 177°C	± 2.2°C
Starter Valve Ambient Temperature	0 to 177°C	± 2.2°C
Oil Line #1 Temperature	0 to 177°C	± 2.2°C
Oil Line #2 Temperature	0 to 177°C	± 2.2°C
Oil Line #3 Temperature	0 to 177°C	± 2.2°C
Cowl Skin Surface Temperature	0 to 260°C	± 2.2°C
Cowl Frame Upper Surface Temp.	0 to 260°C	± 2.2°C
Cowl Frame Lower Surface Temp.	0 to 260°C	± 2.2°C
Bulkhead Upper Surface Temp.	0 to 260°C	± 2.2°C
Oil Cooler Inlet Ambient Temp.	0 to 177°C	± 2.2°C
Oil Cooler Outlet Ambient Temp.	0 to 177°C	± 2.2°C
Zone 2 Ambient Temperature	0 to 177°C	± 2.2°C
Oil Cooler Duct Temperature	0 to 177°C	± 2.2°C

6.4 ACOUSTIC TAILPIPE

Ten high temperature, weldable strain gages were installed to measure longitudinal static strains and circumferential dynamic strains on the acoustic tailpipe inner and outer skins, and four weld-on thermocouples were attached to the tailpipe skin to measure tailpipe environment, as

shown in Figure 6.13. Strain gage SGT1 through SGT6 were longitudinal gages. Gages SGT7 through SGT10 were oriented circumferentially on the tailpipe. The four strain gages designated as SGT1, SGT2, SGT3 and SGT4 were used to measure both static and dynamic strains. The remaining six gages, SGT5 through SGT10, were used for dynamic strain measurement only.

One chromel-alumel (type K) thermocouple was tack-welded to each static strain gage mounting flange and provided temperature data to make corrections to the static strain data. These thermocouples are identified as TTG1, TTG2, TTG3 and TTG4 in Figure 6.13.

6.5 ACOUSTIC INSTRUMENTATION

The principle elements of the acoustic test instrumentation were the microphones, the amplifiers and the tape recorder. The 26 microphones, located at the angles and positions as illustrated in Figure 5.4, were 1.27 cm (1/2 inch) condenser microphones with companion preamplifiers. The microphone signals were routed into 26 acoustic amplifiers having selectable fixed-gain settings covering a 60 dB range. The conditioned signals were then routed to a 28-track FM tape recorder.

6.5.1 Microphone Calibrations

In the week prior to test, a series of four or five microphone pistonphone calibrations were performed. The pistonphone applied a sound pressure level of 124 dB at a frequency of 250 Hz and all microphones were normalized to a 250 mV output for this sound pressure level. A pistonphone calibration was also performed immediately before and after every engine run in which acoustic data were taken.

Prior to each test series, the following annotations and calibration signals were recorded on the magnetic tape at 76 cm/sec (30 ips), using FM at a center frequency of 54 kHz:

(1) Voice annotation identifying the program, tape number, date, test stand, engine number, engine type, engine configuration and recorder speed.

(2) With all the microphones disconnected, a sine wave of 250 Hz, and 250 mVRMS (equivalent to 124 dB, S..L.) was recorded for 60 seconds with all the acoustic amplifiers set at 0 dB.

(3) With all the microphones disconnected and all acoustic amplifiers set at -20 dB, a peak noise signal of approximately 1 VRMS for 60 seconds was recorded.

(4) With all the microphones connected and all the amplifier gains set to +30 dB, ambient acoustic noise for a duration of approximately 60 seconds was recorded.

In recording acoustic test data when the engine was on a given test point a further test signal of 25 mVRMS at 250 Hz was recorded on tape for 15 seconds just prior to the taking of data. The purpose of this signal which was fed to the acoustic amplifiers was to establish the attenuator setting during data reduction. It should be noted that the acoustic amplifier attenuator settings were also printed out with each set of engine performance data.

The propfan speed/phase signal (1P) described in Section 6.1 was also recorded on the acoustic data tape.

6.6 AMBIENT AND FACILITY INSTRUMENTATION

The Brown Field Test Facility had the capability of measuring ambient conditions, such as ambient pressure and temperature, relative humidity, and wind speed and direction, as well as some engine performance parameters such as gross thrust, fuel flow, and fuel inlet temperature and specific gravity.

The measurement of gross thrust was accomplished by a dual bridge strain gage type load cell located on the thrust bed of the engine.

Fuel flow was measured by two turbine flowmeters plumbed in series. These were horizontally mounted and vibration insulated near the engine centerline, and were located on the intermediate level of test stand about 18 m (60 feet) from the engine fuel control.

Platinum resistance temperature detectors were inserted in the fuel flow stream approximately 0.3 m (1 foot) upstream and downstream of the flow meters. These probes were located on the engine support structure.

Fuel samples were collected and shipped to the Rohr Material Laboratory located at Chula Vista. Specific gravity was determined by standard hydrometry.

Wind speed (WSPD) was measured by a cup anemometer mounted on a pole approximately 4.9 m (16 feet) above ground 49 m (160 feet) away from the engine centerline and at an angle of approximately 45 degrees from the engine under test. This anemometer generated 50 pulses per revolution. Wind direction (WDIR) was measured by a 360 degree linear potentiometer type instrument located on the same pole as WSPD anemometer.

Relative humidity data were collected by a probe located on the same pole as WSPD and WDIR. The sensing element of the probe was a thin film capacitor reacting to humidity with extremely short time constant. The corresponding change in capacitance was electronically conditioned to produce a high level (0-5 VDC) signal directly proportional to 0-100% relative humidity. A platinum resistance temperature detector was mounted along with relative humidity probe to measure ambient temperature.

Ambient pressure was measured using a digital barometer unit located inside the control room and plumbed to ambient atmosphere approximately 30.5 m (100 feet) from the test engine.

The ranges and accuracies for the ambient and test facility measurements are listed below:

Parameter	Range	Accuracy
Gross Thrust	-107 N to 267 kN (-24 to 60K lb)	± 0.25% fs
Fuel Flow	0 to 246 liters/min (0 to 65 gpm)	± 0.35% rdg
Fuel Inlet Temperature	-18 to 38°C (0 to 100°F)	± 0.6°C (± 1.0°F)
Fuel Specific Gravity	0.73 to 0.87	±0.15%
Wind Speed	0 to 32 km/hr (0 to 20 mph)	± 0.8 km/hr (± 0.5 mph)
Wind Direction	0 to 360 deg	± 5.0 deg
Relative Humidity	0 to 100%	± 5.0%
Ambient Temperature	-18 to 38°C (0 to 100°F)	± 0.3°C (± 0.5°F)
Ambient Pressure	0 to 105 kPa (0 to 15.3 psia)	± 0.07% FS

6 Load Calibrations

The measuring load cell used to measure gross thrust was mechanically loaded in series with a standard load cell. The results were compared and necessary adjustments were made to correct any zero or scaling offsets. The reference load cell was calibrated by an authorized calibration agency using standards that are traceable to the National Bureau of Standards.

The calibration of the fuel flowmeters was performed by an outside vendor using a flow calibration stand. The data was supplied in the form of flow versus output frequency. The calibration of the signal conditioning and data acquisition system was performed by inputting a frequency based upon the flowmeter calibration.

The fuel temperature probe was suspended in a temperature bath along with a standard probe for calibration. Various temperatures were established and the output of the test probe was compared to the output of the standard probe. The electrical output of the measuring system was converted to engineering units.

The calibration of the wind speed translator and data acquisition system of the cup anemometer was performed by inputting a frequency proportional to the rotational speed of the anemometer.

The precision wind vane was rotated upon a calibration fixture. The directional alignment of this fixture is checked once per year. Wind direction was converted to analog voltage calibrated into degrees of angle.

The sensing element of the relative humidity probe was a thin polymer film capacitor reacting to humidity with an extremely short time constant. The probe was suspended in the vapor cloud of saturated salt solutions of LiCl (12.4% RH), NaCl (75.5% RH), and K_2SO_4 (97.2% RH). Adjustments were then made to read the values shown in parentheses.

7.0 TEST PROCEDURES

7.1 TEST SCHEDULE

During static testing at Rohr, the propfan propulsion system was operated for over 50 hours in 45 test runs. The first 27 runs were primarily devoted to balancing, checkout, or demonstration. The next 17 runs were primarily endurance and acoustics runs, and a reverse thrust test was completed on the last run. Table 7.1 shows the purpose of each run and the accumulated run times.

The general order in which the tests were conducted is described below:

(1) Functional Checkout	Runs 1 - 3
a) Dry Motor	
b) Wet Motor	
c) Idle Run Checks	
o Normal/Emergency Shutdowns	
(2) Propfan Dynamic Balance	Runs 4 - 9
(3) Low Power Governing Check	Runs 10 - 12
(4) Propfan Stress Survey	Runs 13 - 14
(5) Transient Tests	Run 15
(6) Media Demonstration	Runs 16 - 18
(7) Endurance Testing	Runs 24 - 40
a) Pre-endurance Calibration	
b) Endurance Tests	
c) Post-endurance Calibration	
(8) Reverse Thrust Test	Run 41
(9) Propfan Auxiliary Pump Motor Test	

The choice of test points for the static test was constrained by operating limitations of the propfan, the gas turbine engine, and the reduction gearbox discussed in Section 4.7. The operating envelope for the Endurance Test phase is illustrated in Figure 7.1. The lower limit of the operating envelope is determined by a minimum 475 N-m (350 ft-lb_f) engine torque to prevent skidding of the reduction gearbox main drive bearing. A minimum power turbine/propfan RPM of 53% of design speed was required to provide sufficient oil flow to the reduction gear surfaces for continuous operation. A maximum power turbine/propfan speed of 105% was determined

TABLE 7.1. ENGINE RUN LOG

DATE	RUN NO.	PURPOSE OF TEST	START CONDITION	SHUTDOWN CONDITION	RUN TIME (MINUTES)	TOTAL RUN TIME MIN/HR-MIN
5-19-86	1	IDLE LEAK CHECK	ON LP STOP	FEATHER	02	02
5-20-86	2	FUNCTIONAL CHECK-SHUTDOWN	LP STOP	MANUAL	03	05
	2(a)	FUNCTIONAL CHECK-SHUTDOWN	LP STOP	FIRE HANDLE	02	07
	2(b)	FUNCTIONAL CHECK-SHUTDOWN	LP STOP	OVERSPEED	10	17
5-22-86	3	BALANCE AND STRESS SURVEY	FEATHER	CB TO EEC	21	38
	4	BALANCE AND STRESS SURVEY	FEATHER	RUN/STOP	13	51
	5	BALANCE AND STRESS SURVEY	FEATHER	RUN/STOP	10	61 (1:01)
5-23-86	6	BALANCE AND STRESS SURVEY	FEATHER	RUN/STOP	10	71
	7	BALANCE AND STRESS SURVEY	FEATHER	RUN/STOP	10	81
	8	BALANCE AND STRESS SURVEY	FEATHER	RUN/STOP	09	90
	9	BALANCE AND STRESS SURVEY	FEATHER	RUN/STOP	15	105
	10	LOW POWER CHECK	FEATHER	RUN/STOP	16	121 (2:01)
5-27-86	11	PROP GOVERN ADJUST	FEATHER	RUN/STOP	09	130
	12	LOW POWER CHECK	FEATHER	RUN/STOP	23	153
	13	PROP STRESS SURVEY	FEATHER	RUN/STOP	26	179 (2:59)
5-28-86	14	PROPFAN STRESS SURVEY	73°	RUN/STOP	22	201
5-29-86	15	MEDIA RUN CONDITIONS ACCELERATION/DECEL STRESS SURVEY	FEATHER	RUN/STOP	115	316 (5:16)
6-3-86	16	MEDIA RUN CHECKS	FEATHER	RUN/STOP	07	323
	16A	MEDIA RUN CHECKS	FEATHER	RUN/STOP	05	328 (5:28)
6-4-86	17	MEDIA RUNS	FEATHER	RUN/STOP	08	336
	17A	MEDIA RUNS	FEATHER	RUN/STOP	12	348
	18	MEDIA RUNS	FEATHER	RUN/STOP	14	362 (6:02)
6-6-86	19	PROPFAN BALANCE CHECK	FEATHER	RUN/STOP	07	369
6-9-86	20	PROPFAN BALANCE CHECK	FEATHER	RUN/STOP	19	388 (6:28)
6-10-86	21	PRE-ENDURANCE CALIB	FEATHER	RUN/STOP	40	428
	22	PROPFAN BALANCE CHECK	FEATHER	RUN/STOP	34	462
6-11-86	23	VIBRATION CHECK (V_3)	FEATHER	RUN/STOP	38	500 (8:20)
6-12-86	24	PRE-END NO. 1 ENDURANCE	FEATHER	LP STOP	274	774 (12:54)
6-16-86	25	ENDURANCE NO. 2	FEATHER	RUN/STOP	186	960
	26	ENDURANCE NO. 3	FEATHER	RUN/STOP	184	1144 (19:04)
6-17-86	27	ENDURANCE NO. 4	FEATHER	RUN/STOP	188	1332
	28	ENDURANCE NO. 5	FEATHER	RUN/STOP	182	1514 (25:13)
6-18-86	29	ENDURANCE NO. 6	FEATHER	RUN/STOP	185	1699
	30	ENDURANCE NO. 7	FEATHER	RUN/STOP	183	1882 (31:21)
6-19-86	31	ENDURANCE NO. 8	FEATHER	RUN/STOP	192	2074
	32	ENDURANCE NO. 9	FEATHER	RUN/STOP	183	2257 (37:36)
6-20-86	33	ENDURANCE NO. 10	FEATHER	RUN/STOP	184	2441
	34	ENDURANCE NO. 11	FEATHER	RUN/STOP	183	2624 (43:43)
6-23-86	35	ENDURANCE NO. 12 (BARRIER AT 9.5 FT)	FEATHER	RUN/STOP	13	2637
	36	c/o J. PARKER	FEATHER	RUN/STOP	30	2666 (44:26)
6-24-86	37	ENDURANCE NO. 12 (BARRIER AT 16 FT)	FEATHER	RUN/STOP	184	2851 (47:31)
6-26-86	38	PROPFAN BALANCE AFTER BLADE CHANGE	FEATHER	RUN/STOP	38	2889
	39	POST ENDURANCE CALIB	FEATHER	RUN/STOP	63	2952
6-27-86	40	ACOUSTICS: BARRIER SHIELD EXHAUST	FEATHER	RUN/STOP	65	3017 (50:17)
	41	REVERSE: STRESS SURVEY	-5°(LPSTOP)	-5°	15	3032 (50:32)

by the propfan governi g range. The power turbine/propfan 100% speed is defined as 11,500 powe turbine RPM, or 1692 propfan RPM. The upper boundary of the operat ng envelope was based on blade vibratory stress restrictions determine during the Propfan Stress Survey.

7.1.1 Functional Chec out

The engine dry motor functional check was conducted by following the normal engine start rocedure except that the test stand fuel valve remained closed and th fuel pump remained off. The wet motor was performed with the fuel upply on, but the circuit breaker to the engine ignitors was pulled. he engine was then started and run at idle to check the engine/propfan com atibility. Five different shutdown checks were performed:

- o Normal Shut own (Run/Stop Switch)
- o Manual Fuel Shutdown
- o Simulated E gine Overspeed Shutdown
- o Loss of Ele trical Power Shutdown
- o Fire Handle Shutdown.

7.1.2 Propfan Balanci g

Dynamic balancing of t e propfan and specialized rotating instrumentation were required to attai acceptable vibration levels over the entire operating speed range. Ba ancing was conducted using data collected from the gearbox horizontal (V_L and vertical (V_1) accelerometers. Data from accelerometers located c the gas turbine were also recorded during the balancing procedure. he unfiltered signals from the gearbox accelerometers were analyzed by a trim balancer, which determined the 1P amplitude and phase of the vibr tory response. Vibration data were collected at 55%, 75%, 81%, 88%, an 94% speed for the base propfan, and with a trial weight of 74 grams add d to the forward balance ring at a radius of 20.87 cm (8.125 in). The ch ge in 1P amplitude and phase angle caused by the trial weight were note for each rotational speed. The mass and orientation of the weight req ired to balance the propfan was determined using a single plane balancing calculation.

7.1.3 Low Power Governing Check

The low power governing test consisted of selecting set point speeds of 75%, 87.5%, 100%, and 105% on the propfan speed control lever, then slowly increasing power until the propfan began to govern. Governing was indicated by the blade pitch angle lifting off the low pitch stop and RPM remaining constant with increasing power. The low pitch stop was set at 20° for these runs. If governing did not commence at the set point speed, the control speed trim adjustment on the propfan was employed to fix the governing speed at the correct value. Speed trim adjustment continued until the desired governing range of 75% to 105% of the design speed was achieved.

7.1.4 Stress Survey

The stress survey was conducted with the blade angle set by the low pitch stop and also with the propfan operating in a governing mode. Low pitch stop settings of 20° and 35° were employed during the stress survey. Below the minimum governing speed, the propfan operated on the low pitch stop setting. The 35° setting permitted high power test points to be run at rotational speeds below the minimum governing RPM. Testing on the low pitch stop was accomplished by setting the propfan speed control lever to 105% so that rotational speed was controlled by the application of engine power. During the governing portion of the stress survey, rotational speed was controlled with the propfan speed control lever and power was controlled with the engine power lever. The blade angle was greater than the low pitch stop position during governing.

7.1.5 Transient Tests

The purpose of the transient test was to evaluate the dynamic response of the propfan propulsion system to time dependent variations in engine power and speed set point. The blade vibratory response to these transients was also monitored. The transients were initiated by manually actuating

either the engine power lever or the propfan speed control lever. The severity of the transients was altered by varying the rate at which the power or speed levers were moved. Conducting the transient test in this manner resulted in the system response being affected by the dynamics of the turbine engine fuel control and the propfan control input lever actuator. These devices had features which limited the maximum rate at which engine power or propfan speed set point could be changed no matter how quickly the control levers were moved. A slow transient and a fast transient were run in both directions along each operating curve. Engine power lever position, propfan speed lever position, propfan RPM, engine torque, and propfan blade pitch angle were recorded and plotted as functions of time for each transient. Acoustic tailpipe static and dynamic strains and temperatures also were recorded during the power lever transient to full power and for a prescribed time at power. Dynamic strain data also were recorded during the fast speed lever transient.

7.1.6 Media Demonstration

Two propulsion system runs were made to demonstrate propfan performance for media personnel. For each run, propfan speed was set at 75%, 87.5%, and 94% of design speed and the system was run with the propfan resting on the low pitch stop. A higher power run up to 105% speed and 3655 kW (4900 SHP) was then made for NASA and management representatives.

7.1.7 Endurance Test

The endurance portion of the static test consisted of twelve repetitions of a simulated three hour flight cycle plus pre- and post-endurance calibrations. Acoustic data were recorded for three configurations during these tests.

7.1.7.1 Pre-endurance Calibration

The pre-endurance calibration consisted of two parts: a seven point calibration and a three point calibration. The seven point calibration

involved setting the propfan rotational speed at 100% and varying engine power between 1640 and 3280 kW (2200 and 4400 SHP). Data were taken at seven steady state conditions between the low and high power settings. The three point calibration was performed by setting the propulsion system at three set points and taking data when steady state conditions were reached. The system was set at 76% N_p speed and 1340 kW (1800 SHP), 87.5% N_p speed and 2160 kW (2900 SHP), and 105% N_p and 3580 kW (4800 SHP) for the three point calibration.

7.1.7.2 Endurance Testing

Twelve repetitions of a three-hour simulated flight cycle were performed to determine if any excessive wear might occur in either the propfan assembly or the drive system, especially the reduction gearbox. Of primary concern in the propfan assembly were the propfan actuator and the blade retention hardware.

Each endurance cycle consisted of setting the propfan propulsion system on twelve different set points and recording engine and propfan performance data at each steady state point. Data were recorded more than once for some set points so that seventeen sets of data were obtained for each cycle. Propfan rotational speed ranged from 77% to 105% and engine power from 1940 to 3430 kW (2600 to 4600 SHP) over the course of a cycle.

All acoustic data were recorded during endurance runs 27 (endurance cycle number 4), 37 (endurance cycle number 12), and 40 (after the post-endurance calibration). In order to assess the potential masking of propfan noise by drive system noise, some of the acoustic data were obtained with an acoustic barrier erected alongside the propulsion system as described in Section 5.6.1. In run 27, there was no acoustic barrier. In run 37, the barrier was in the forward position; in run 40 it was in the aft position.

7.1.7.3 Post-endurance Calibration

After completion of the twelve endurance cycles, the seven point and three point calibrations described in Section 7.1.7.1 were repeated to determine any engine performance degradation which may have occurred during endurance tests.

7.1.8 Reverse Thrust Test

Testing was conducted to verify safe and stable operation of the propfan propulsion system while producing reverse thrust. The reverse thrust test was accomplished with the blade angle set at -5^{o} by the adjustable low pitch stop. The propfan speed control lever was set at 105% and the test conducted with the propfan on the low pitch stop so that propfan speed would be controlled by the engine power lever. Data were recorded at six power settings corresponding to 75%, 81%, 87%, 94%, 100%, and 103% propfan speeds. Power was then reduced and a slow power transient which changed propfan speed from 75% to 103% was performed.

7.1.9 Propfan Auxiliary Pump Motor Test

The propfan auxiliary pump motor is a 3.7 kW (5 hp) three-phase electric motor designed to supply power to the propfan auxiliary pump which provides hydraulic pressure for blade angle changes when the propfan is not rotating. This motor is rated for 400 Hz supply power. However, the frequency of the power that will be supplied on the GII testbed aircraft is a function of GII main engine speed, and may vary between 350 Hz and 500 Hz.

A test was conducted with the propfan propulsion system shut down to determine the performance of the propfan auxiliary pump motor at supply frequencies other than 400 Hz. A variable frequency three-phase power source was used to provide between 300 Hz and 500 Hz to the auxiliary pump motor, and supply current and voltage were recorded while the motor was started and run. Strip chart data were recorded for supply frequencies of 300, 350, 400, 450, and 500 Hz.

8.0 TEST RESULTS

All tests specified in the Reference 1 test plan were accomplished except for the stress survey tests with the propfan in feather and the feather checks. These tests were deleted to avoid exceeding drive system operating limits, and because of the limited useful data they would have provided. Some engine power test conditions were modified slightly as a result of propfan stress survey results.

8.1 FUNCTIONAL CHECKOUT

Dry and wet motor tests were successfully conducted before the PTA engine was started. These tests verified the integrity of the oil and fuel system plumbing. The engine was then started and run at idle and the following shutdown functional checks were accomplished:

- o Normal Shutdown (Run/Stop Switch)
- o Manual Fuel Shutdown
- o Simulated Engine Overspeed Shutdown
- o Loss of Electrical Power Shutdown
- o Fire Handle Shutdown.

All systems operated as intended, verifying the low power compatibility of the propulsion system configuration.

During the functional checkout, it was discovered that the relationship between power lever angle and engine output power was not linear. To achieve the high idle condition (approximately 300 kW or 400 SHP), nearly half the displacement of the power lever was required.

Three buckles formed on the inner skin of the acoustic tailpipe during the first engine run and remained, unchanged, for the rest of the static test program. The buckles were located on the lower inner skin surface along the propulsion system vertical centerline.

8.2 PROPFAN BALANCING

Balancing of the propfan was accomplished by the addition of 147 grams to the forward balance ring at a 20.87 cm (8.125 in) blade radius. Once balancing was accomplished, vibration levels were independent of blade angle for a constant RPM. No additional balancing of the propfan was required throughout the duration of static tests. Replacement of components on the rotating portion of the propfan and changing the low pitch stop setting did not adversely affect the balance.

8.3 LOW POWER GOVERNING CHECK

During the low power governing check, the preload of the servo governor speeder spring was altered using the speed trim adjustment to achieve the desired governing range of 75% to 105% of the propfan design speed. Three engine runs were required to adjust the servo governor to obtain this range. These tests verified that the desired governing range could be attained with the available travel on the propfan speed control input lever.

8.4 STRESS SURVEY

The propfan blade vibratory strain levels were monitored continuously during the stress survey to avoid exceeding vibratory stress limits, which were based on the fatigue endurance limit of the blades. At each steady state test point, vibratory strain data were recorded for thirty seconds. Power absorbed and thrust produced by the propfan were also logged for each steady state operating point. Figure 8.1 shows a plot of the stress survey test points. The data gathered during these tests were used to define operating limits for subsequent endurance tests. The analysis of the data obtained during the stress survey is presented in Section 9.2.1.

8.5 TRANSIENT TESTS

Figures 8.2 and 8.3 show the conditions at which propfan speed and power transient tests were run. Plots of the propfan and engine control dynamic response to speed and power lever transients are presented in Figures 8.4 through 8.11. Figures 8.4 and 8.5 show the response to ramp changes in the speed set point between 87.5% and 100% propfan speed. The time intervals to traverse this speed set point range were four seconds and two seconds, respectively. Figures 8.6 and 8.7 show the responses to essentially step changes in power lever position between 1268 kW (1700 SHP) and 2089 kW (2800 SHP) at 87.5% propfan speed. Figures 8.8 and 8.9 show the responses to more severe transients, step changes in power lever position between 1350 kW (1810 SHP) and 2700 kW (3620 SHP) at 95% speed. Propfan blade peak vibratory strain response to a fast speed transient from 87.5% to 100% and back to 87.5% propfan speed at a constant 2240 kW (3000 SHP) power setting is shown in Figure 8.10. Peak vibratory strain response to a fast power transient at 95% speed is shown in Figure 8.11.

Acoustic tailpipe strains and temperatures were recorded and the data were examined after the static test. More meaningful data were observed during runs with longer dwell times at high power. These data are presented in Section 8.6.

8.6 ENDURANCE TESTS

The endurance tests were run basically within the operating envelope defined in Figure 8.12. This envelope was defined initially based on the engine and propfan limitations discussed in Section 4.7, and revised based on the results of the propfan stress survey. Specific set points chosen for the endurance run were designed to explore the entire envelope while avoiding any problem areas. For example, a critical speed was found at 94% design speed during the balancing procedure, while another condition that induced higher than normal test stand vibrations was running with power section output power near 2240 kW (3000 SHP). Prolonged operation near these resonance areas, once they were identified, was avoided during static testing.

The simulated flight cycle performed for each endurance run is shown in Figure 8.13. Typical power section torque, corrected power turbine shaft power, gas generator turbine speed, and corrected fuel flow are shown plotted versus corrected measured gas temperature in Figures 8.14 through 8.17.

Similar propulsion system set points were run in the pre- and the post-endurance calibrations to determine any engine performance degradation that may have occurred during endurance testing.

Acoustic tailpipe strains and temperatures from the post-endurance calibration (Run 39) were examined. The maximum observed stresses for the inner and outer tailpipe skins were 83,400 kPa (12,100 psi) and 74,500 kPa (10,800 psi), respectively. The inner skin maximum temperature was 471°C (880°F). The maximum temperature observed on the outer skin was 368°C (694°F). The greatest temperature differential observed between the inner and outer skins was 226°C (407°F).

8.6.1 Acoustics Tests

The specific operating conditions existing during the endurance tests during which acoustic data were recorded are tabulated in Tables 8.1, 8.2, and 8.3.

Lockheed

TABLE 8.1. OPERATING CONDITIONS FOR RUN 27

PARAMETER	UNITS	QUANTITY											
RECORD	NO.	5	6	7	8	9	10	11	12	13	14	15	16
PROP ROT SPEED	% RPS RPM	97.5 27.5 1650	97.5 27.48 1649	97.5 27.48 1649	97.5 27.53 1652	87.3 24.62 1477	87.4 24.63 1478	76.7 21.63 1298	104.9 29.58 1775	104.9 29.58 1775	104.9 29.58 1775	104.8 29.55 1773	103.5 29.2 1752
PROP TIP SPEED	M/SEC FT/SEC	237 778	237 777	237 777	237 778	212 696	212 696	186 612	255 836	255 836	255 836	255 836	252 826
PROP THRUST	N LBS	28024 6300	30693 6900	32250 7250	32250 7250	25800 5800	23353 5250	18683 4200	36031 8100	36920 8300	35586 8000	32694 7350	29581 6650
PROP TORQUE	NM FT. LBS.	10025 7394	12384 9134	16332 12046	17379 12818	13402 9885	9481 6993	11027 8133	19765 14578	18647 13753	15677 11563	12402 9147	10250 7560
PROP POWER	KW HP	1732 2323	2139 2868	2820 3782	3007 4032	2073 2780	1468 1968	1499 2010	3674 4927	3466 4648	2914 3908	2303 3088	1881 2522
PROP 1ST ORDER BPF	Hz	220	220	220	220	197	197	173	237	237	237	237	233.7
COMPRESSOR ROT SPEED	RPM	12787	13055	13400	13500	13003	12549	12634	13846	13741	13469	13205	12934
COMPRESSOR 1ST ORDER BPF	Hz	4049	4134	4243	4275	4118	3978	4001	4385	4351	4265	4182	4096
BLADE ANGLE β	DEG	21.1	22.6	26.7	28.5	28.3	25.0	30.3	28.0	28.1	27.4	24.7	23.5
PWR COEFF. C_p		.438	.541	.714	.757	.730	.516	.778	.746	.703	.591	.469	.397
THRUST COEFF C_T		.534	.586	.615	.613	.614	.554	.575	.503	.608	.586	.540	.500

TABLE 8.2. OPERATING CONDITIONS FOR RUN 37 (BARRIER FORWARD)

PARAMETER	UNITS	QUANTITY											
RECORD	NO.	4	5	6	7	8	9	10	11	12	13	14	15
PROP ROT SPEED	% RPS RPM	97.5 27.5 1649.7	98. 27.62 1657.2	97.9 27.61 1656.8	97.9 27.61 1656.9	87.6 24.69 1481.4	87.6 24.7 1482	76.2 21.5 1288.6	104.9 29.58 1774.6	104.8 29.55 1772.8	104.7 29.53 1772	104.6 29.5 1770.5	104.1 29.35 1760.9
PROP TIP SPEED	M/SEC FT/SEC	237 777.4	238 781	238 780.8	238 780.0	213 698.1	213 698.4	185 607.2	255 836.2	255 835.4	255 835	254 834.3	253 829.8
PROP THRUST	N LBS	25800 5800	30025 6750	32427 7300	32250 7250	25800 5800	23353 5250	18683 4200	37143 8350	36920 8300	35586 8000	31138 7000	29358 6600
PROP TORQUE	NM FT LBS	9508 7013	11800 8703	16560 12214	17173 12666	13463 9930	9359 6903	10936 8066	19775 14585	18533 13669	15942 11758	11333 8359	10319 7611
PROP POWER	KW HP	1643 2203	2048 2746	2873 3853	2980 3996	2089 2801	1453 1948	1476 1979	3675 4928	3441 4614	2958 3967	2101 2818	1903 2552
PROP 1ST ORDER BPF	Hz	220.0	221.0	220.9	220.9	197.5	197.6	171.8	236.6	236.4	236.3	236.1	234.8
COMPRESSOR ROT SPEED	RPM	12753	13001	13456	13518	12982	12525	12593	13780	13656	13425	12969	12847
COMPRESSOR 1ST ORDER BPF	Hz	4038	4117	4261	4281	4111	3966	3988	4364	4324	4251	4107	4068
BLADE ANGLE β	DEG	23.9	25.7	31.1	31.2	30.6	27.4	34.2	29.9	29.9	29.9	27.4	26.9
PWR COEFF C_P		.415	.511	.717	.744	.729	.507	.783	.746	.701	.603	.430	.396
THRUST COEFF C_T		.492	.567	.614	.610	.610	.552	.584	.612	.610	.588	.515	.491

TABLE 8.3. OPERATING CONDITIONS FOR RUN 40 (BARRIER AFT)

PARAMETER	UNITS	QUANTITY											
RECORD	NO.	4	5	6	7	8	10	11	12	13	14	15	16
PROP ROT SPEED	% RPS RPM	98.3 27.72 1663	97.9 27.6 1656	97.8 27.57 1654.4	97.7 27.56 1653.8	87.6 24.7 1481.8	87.5 24.69 1481.1	76 21.44 1286.2	104.9 29.58 1774.9	104.9 29.58 1775	104.8 29.55 1773.2	104.7 29.53 1771.7	103.7 29.24 1754.6
PROP TIP SPEED	M/SEC FT/SEC	239 783.6	238 780.4	238 779.6	238 779.3	213 698.3	213 697.9	185 606.1	255 836.4	255 836.5	255 835.6	254 834.9	252 826.8
PROP THRUST	N LBS	24910 5600	30025 6750	32250 7250	30693 6900	25800 5800	23353 5250	18683 4200	37143 8350	36920 8300	35586 8000	31138 7000	29581 6650
PROP TORQUE	NM FT LBS	9813 7238	12006 8855	16640 12273	17257 12728	13835 10204	9640 7110	11050 8150	19666 14505	18497 13643	15368 11335	11116 8199	10174 7504
PROP POWER	KW HP	1709 2292	2082 2792	2883 3866	2989 4008	2147 2879	1495 2005	1488 1996	3655 4902	3438 4611	2854 3827	2063 2766	1869 2507
PROP 1ST ORDER BPF	Hz	221.7	220.8	220.1	220.5	197.6	197.5	171.5	236.6	236.7	236.4	236.2	233.9
COMPRESSOR ROT SPEED	RPM	12795	13012	13473	13541	13060	12577	12614	13791	13675	13397	12973	12855
COMPRESSOR 1ST ORDER BPF	Hz	4052	4120	4266	4288	4136	3983	3994	4367	4330	4242	4108	4071
BLADE ANGLE β	DEG	20.5	23.4	27.1	28.5	28.3	23.9	30.9	27.3	27.3	26.9	23.0	22.7
PWR COEFF - C_P		.422	.520	.723	.750	.749	.522	.794	.742	.698	.581	.421	.393
THRUST COEFF - C_T		.467	.568	.611	.582	.610	.552	.586	.612	.608	.587	.515	.499

The atmospheric conditions during the three acoustic runs were within prescribed limits. Conditions at the beginning, at the midpoint, and at the end of Run 27 were as follows:

	Beginning	Midpoint	End
Max Wind (m/sec)	1.61	3.4	3.84
(MPH)	3.6	7.6	8.6
Avg Wind (m/sec)	1.43	2.77	2.68
(MPH)	3.2	6.2	6.0
Amb Pressure (kPa)	99.77	99.77	99.77
(PSIA)	14.47	14.47	14.47
Amb Temp (^{o}C)	15.8	19.9	22.1
(^{o}F)	60.4	67.8	71.8
Rel Humidity (%)	93.9	79.7	73.0

Atmospheric conditions prevalent during Runs 37 and 40 were very similar.

8.7 REVERSE THRUST TEST

The propfan propulsion system performed satisfactorily during the reverse thrust test. The propfan adjustable low pitch stop was set to the -5^{o} position and the engine was started and the test performed with the propfan on the low pitch stop. Blade stresses were low and the propfan reached approximately 103% design speed. The set points for which data were recorded are shown on the -5^{o} low pitch stop line in Figure 8.1.

9.0 DISCUSSION OF TEST RESULTS

9.1 PROPFAN PROPULSION SYSTEM

9.1.1 Thrust

No accurate measurement of propfan installed thrust was attempted during static testing due to a number of non-quantified parameters, including the absence of an aerodynamic aft nacelle, an uncalibrated exhaust nozzle, and test stand and afterbody drag. Propfan thrust is shown in Figure 9.1. Measured thrust is the actual observed thrust corrected to standard day conditions. Estimated installed thrust is the predicted PTA propulsion system thrust for the GII testbed aircraft installation calculated using the Allison 501-M78B engine cycle deck, Hamilton Standard SR-7L propfan SP06A83 performance predictions, and PTA QEC and aft nacelle drag estimates. As expected, thrust values measured on the static test stand are 10% to 20% below what was estimated for the flight installation. This difference is probably due to two factors: propfan blade inefficiency during static operation at high blade angles, and static test stand drag.

LAP Static Rotor Tests at Wright Patterson showed that static thrust generated by the isolated propfan corresponds very well with predicted static thrust for blade angles below approximately 26°. However, as blade angle is increased above 26°, propfan static performance diverges from predictions. The 26° blade angle is reached at approximately 1120 kW (1500 SHP) at 75%, 1715 kW (2300 SHP) at 87.5%, 2160 kW (2900 SHP) at 100%, and 2985 kW (4000 SHP) at 105% design speeds. Propfan blade inefficiency may account for about half of the difference between measured and estimated installed thrusts at the highest powers run for each tip speed.

9.1.2 Specific Fuel Consumption

Since accurate thrust measurements could not be made, as discussed in Section 9.1.1, accurate calculation of thrust specific fuel consumption

(TSFC) was not attempted. The measured TSFC curve in Figure 9.2 reflects the uncalibrated test stand installation conditions at 100% propfan design speed, and is higher than curves of predicted installed TSFC.

The predicted TSFC curve in Figure 9.2 is the estimated TSFC obtained by using the Allison 501-M78B engine cycle deck, Hamilton Standard performance estimates for the LAP, and Lockheed estimates of installed losses on the PTA GII testbed aircraft, and is purely a computational result.

Estimated installed TSFC shown in Figure 9.2 is a combination of test stand measured fuel flow, shaft power derived from measured torque and measured propfan speed, and computed thrust, again using the Allison 501-M78B/Hamilton Standard LAP integrated thrust estimates. It should be noted that the LAP Static Rotor Test conducted at Wright Patterson Air Force Base showed that Hamilton Standard thrust estimates correlated well with measured data in the lower power regions. Therefore, the estimated installed TSFC curve probably shows the best estimate of TSFC for the PTA testbed aircraft installation.

Analysis of these data help substantiate the static performance predictions of the integrated propfan propulsion system.

Installed engine performance is presented as Brake Specific Fuel Consumption (BSFC) in Figure 9.3. BSFC is an indicator of drive system efficiency, relating available input power in the form of kg/hr (lb/hr) of fuel flow to shaft output power in kW (SHP). The measured installed BSFC during static testing was approximately 4% to 5% less than the uninstalled BSFC measured during dynamometer testing of the power section at Allison. This performance improvement is probably due to excellent inlet duct performance coupled with the supercharging effects of the LAP.

This combination of inlet duct performance and propfan supercharging is shown in Figure 9.4. Pressure ratios up to about 1.07 were observed at the compressor face. This is considerably higher than estimates that were used in installed performance calculations. Just what this improvement

means in overall efficiency of this tractor propulsive system arrangement is not totally apparent and is certainly a candidate for further study to quantify the effects of supercharging on improvements in net thrust and specific fuel consumption.

9.1.3 Vibration Data

As noted in Section 6.2, propulsion system vibration was monitored by accelerometers in eight locations. Although only two locations were used by the engine operator for health indication, all eight were displayed and recorded on the data acquisition system.

A critical speed was found near 94% propfan design speed during the balancing procedure. Prior to balancing, the vibratory response was magnified 8.25 times at the critical speed as shown in Figure 9.5. The mode shape defined by data acquired from accelerometers V_1, V_2, and V_4 was determined to be vertical bending as illustrated in Figure 9.6. The mode shape indicates that the major source of flexibility is in the structure connecting the engine to the gearbox. Once balancing was accomplished, the propfan propulsion system could be operated at the critical speed without exceeding vibration limits. This critical speed will most likely exist in the flight structure, but it should pose no problem when the propfan is balanced.

Although the recorded values (30 second averages) of the various vibration sensors remained within limits after the propfan was balanced, the overall signal from a given unfiltered accelerometer would occasionally exceed the established limits. When these signals were reviewed either in real time on a spectrum analyzer, or after the test from a spectrum analysis plot, the amplitudes of the vibrations within the band widths of concern did not exceed limits. Vibration limits were defined for two band widths: 15 to 40 Hz (900 to 2400 RPM), which encloses the normal range of the propfan rotational speed, and 150 to 250 Hz (9000 to 15000 RPM), which is approximately the range of the gas generator and power turbine normal rotational speeds.

Spectrum analysis plots of each of the eight accelerometer signals are shown in Figures 9.7 through 9.14 for static test run number 20, a propfan balance checkout run. The location of each accelerometer is shown in Figure 6.8. The data shown are ten second averages with the propfan running at 100% of design speed (1692 RPM) on the low pitch stop (low power).

Based on the data recorded during static testing, accelerometer position V_5 (reduction gearbox lateral) appears to be an acceptable choice as a location for monitoring propulsion system health. The V_3 (compressor rear frame vertical) position was also used during the static test for monitoring by the engine operator. Based on spectrum analyses of signals from all eight accelerometer locations on the drive system, it appears that the V_7 (compressor front frame lateral) location may provide a more appropriate indication. Throughout the static test, V_7 appeared to be somewhat more sensitive to compressor unbalance and considerably more sensitive to propfan unbalance than V_3.

9.1.4 Subsystems Performance

Propulsion subsystems characteristics were measured and recorded concurrent with propfan and drive system performance during static testing.

9.1.4.1 Oil Cooler Performance

Data for both the propfan and engine/gearbox oil cooling circuits were recorded during static testing to analyze their suitability for flight tests. The relatively long periods of static operation provided sufficient time for thermal stabilization and substantiate the capability of the cooling systems to maintain the lubrication oil temperatures below established limits.

9.1.4.1.1 Propfan Oil Cooling

The propfan fluid cooling system maintained the hydraulic fluid temperature at or below 87°C (188°F) throughout the endurance test cycles. Fluid

cooling is dependent upon not only the heat rejection rate from the propfan, but also the fuel flow rate. Therefore, the more critical periods with respect to propfan fluid cooling occurred at high propfan speed and relatively low engine power. Prolonged operation under these conditions resulted in relatively high prop fluid temperatures as well as high engine fuel pump inlet temperatures. As shown in Figure 9.15, the maximum prop fluid temperatures occurred during endurance testing at the 105% propfan design speed, 1865 kW (2500 SHP) test condition. These maximum temperatures occurred at test stand supplied fuel temperatures of approximately 27°C (80°F), which were considerably higher than the estimates of 10 to 16°C (50 to 60°F) for the stored fuel.

Both propfan fluid temperature and fuel engine inlet temperature increased rapidly during the reverse thrust test. Propfan hydraulic fluid reached 114°C (237°F) within approximately 15 minutes after starting the engine. Fuel inlet temperature exceeded 100°C (212°F) at shutdown.

9.1.4.1.2 Engine Oil Cooling

The power section and gearbox oil cooling system provided sufficient cooling throughout the static test to maintain the oil temperature within the engine specification limits. Figure 9.16 shows drive system oil temperature as a function of engine output power and propfan speed. Extrapolating these data show that the drive system oil cooling system can maintain the engine oil temperature at or below 100°C (212°F) at maximum power static conditions for hot day (39°C or 103°F) operation. A 100°C oil temperature is considered the maximum transient (five minute) limit by Allison.

Significant improvement in the cooling air circuit through the air/oil heat exchanger is anticipated for the testbed aircraft installation. Since the static test stand strut fairing was located directly behind the air exit door, it is believed that air flow through the heat exchanger was impeded. The cooling capacity of the GII testbed aircraft installation, based upon test results of this system under static conditions, should be satisfactory under all flight conditions.

Reverse thrust operation was the most severe condition for lubrication oil cooling. During the reverse thrust test, engine/gearbox oil temperature reached a maximum of 85°C (183°F) within 15 minutes of engine startup. The primary reason that oil temperatures did not increase beyond this value is that the low power input to the propfan resulted in low drive system heat rejection to the lubricating oil.

9.1.4.2 QEC Surface and Air Temperatures

Measured QEC surface and internal nacelle air temperatures during the static tests indicated satisfactory temperature levels, but since the aft nacelle was not part of the test configuration, the results of this test do not necessarily represent those that will result on the complete GII testbed aircraft configuration.

Maximum surface and air temperatures consistently occurred after engine shutdown following an endurance operating cycle. The maximum recorded air temperature inside the QEC, which occurred near the fuel control, was 66°C (150°F). Corrected to hot day conditions (39°C or 103°F), this is equivalent to 84°C (183°F), well below the limit of 120°C (248°F).

Typical maximum recorded surface temperatures are shown below:

Component	Recorded Temperature	Corrected to Hot Day 39°C
Fuel control	71°C (159°F)	89°C (192°F)
Electronic engine control	41°C (106°F)	59°C (139°F)
Ignition exciters	74°C (165°F)	92°C (198°F)
Prop speed control actuator	36°C (96°F)	54°C (129°F)

QEC cowl frame, cowl skin, bulkhead and engine mount surface temperatures were monitored throughout the conduct of the static tests to verify that limit temperatures were not exceeded and that sufficient cooling air was available for static operation.

Table 9.1 presents a tabulation of the maximum temperatures recorded during the static tests and verifies that the limit temperatures were never approached. Correction of the temperature data to hot day conditions also indicates that limits would not have been exceeded during hot day operation.

The measurement codes identifying the thermocouple locations tabulated in Table 9.1 are shown below:

TSFL	Surface Temperature - Lower Cowl Frame
TSCS	Surface Temperature - Cowl Skin
TSFU	Surface Temperature - Upper Cowl Frame
TSBU	Surface Temperature - Upper Bulkhead
TLMS	Engine Mount Temperature - Side
TLMT	Engine Mount Temperature - Top
TLML	Engine Mount Temperature - Left
TLMA	Engine Mount Temperature - Aft
TLMB	Engine Mount Temperature - Lower

9.1.4.3 Acoustic Tailpipe Stress and Temperature Survey

The strains and temperatures measured in all areas of the acoustic tailpipe were lower than those assumed by a theoretical analysis performed prior to the static test program. That analysis showed an expected fatigue life of 15,000 thermal cycles, while an estimated 300 engine runs will be accumulated during static and flight testing. The analysis estimated an outer skin maximum stress of 113,800 kPa (16,500 psi) compared to the 74,500 kPa (10,800 psi) that was observed. For the inner skin, it was estimated that the stress would equal 487,500 kPa (70,700 psi), much greater than the 83,400 kPa (12,100 psi) measured.

Although tailpipe temperatures were lower than predicted, e.g. 471°C (880°F) versus 649°C (1200°F) for the inner skin, the maximum differential temperature between the inner and outer skins was greater than predicted. The analysis used a value of 167°C (300°F) while the measured value was 226°C (407°F). This implies that yielding could occur earlier than expected, but the tailpipe should possess the same fatigue life that was predicted.

TABLE 9.1. QEC MAXIMUM OBSERVED TEMPERATURES

ENDURANCE CYCLE DATA POINT NO.	KW	SHP	TAMB (°C)	TSFL (°C)	TSCS (°C)	TSFU (°C)	TSBU (°C)	TLMS (°C)	TLMT (°C)	TLML (°C)	TLMA (°C)	TLMB (°C)	TMGT (°C)
1	1492	2000	23	27	24	24	30	24	23	51	23	25	572
2	2238	3000	23	30	28	27	33	28	24	66	24	70	608
3	2984	4000	23	30	29	29	33	31	26	69	23	62	683
4,5	3282	4400	24	32	29	29	34	31	26	67	16	64	694
6,7,8	2144	2874	24	32	28	29	33	29	26	61	24	61	754
9	1492	2000	23	32	29	30	34	27	28	63	24	64	734
10,11,12	1492	2000	23	32	30	29	34	31	29	68	24	62	596
13	3770	5054	23	32	32	31	34	31	29	64	31	67	683
14	3506	4700	23	33	30	29	36	28	27	68	23	75	696
15	2984	4000	23	34	32	32	37	32	31	75	27	81	695
16	2238	3000	23	29	32	32	38	32	31	73	27	81	613
17	1492	2000	23	34	29	28	38	31	27	71	18	71	588
7.1.3*	2313	3100	23	28	27	26	31	26	26	65	22	71	619
9.2.3*	3432	4600	24	36	36	34	39	34	33	70	31	36	759
LIMIT TEMP (°C)				71	71	121	121	121	121	121	121	121	808

Since the analysis showed adequate static and fatigue life for the planned duration of the flight test program, the results obtained during the static tests substantiate the analytical prediction and confirm the durability of the acoustic tailpipe.

9.1.4.4 Engine Start Characteristics

The engine air turbine starter performed satisfactorily, with recorded start times in the 15 to 25 second range. These start times compare favorably with the estimated time of 20 seconds for a 21°C (70°F) day. No hot starts (transient MGT exceeding limit) or 'hung' starts (failure to accelerate to idle) were encountered during the static test phase. The engine progressed through its pre-fire acceleration, ignition, and post-light acceleration events to idle as predicted.

9.1.4.5 Propfan Speed Control Electromechanical Actuator

During the system checkout phase of the static tests, it was discovered that the gearbox-mounted electromechanical prop control actuator would not rotate the prop control input lever to the feather position. Bench test confirmed that the available torque of 7.91 N-m (70 in-lb) was marginal for the mechanical feather input torque requirement. Therefore, the actuator specification stall torque has been increased to 13.6 N-m (120 in-lb), with a control voltage of 26 VDC. Except for this, the actuator system functioned satisfactorily throughout the prop speed control range.

9.1.4.6 Propfan Auxiliary Pump Motor Operation

At the conclusion of the static test phase of this program, a test was conducted to determine whether the propfan auxiliary pump motor would operate on a variable frequency power equivalent to that available on the PTA testbed aircraft. The auxiliary pump motor was designed to operate on 115/200 VAC, 400 Hz, 3-phase power. The modified GII testbed aircraft provides 115/200 VAC, 3-phase power with the frequency varying from 300 to

500 Hz as a function of engine speed. Consequently, this test was conducted at electrical power frequency conditions of 300, 350, 400, 450 and 500 Hz. The results of the test are tabulated below:

FREQUENCY Hz	300	350	400	400	450	450	500
LOCKED ROTOR AMPS	101.1	99.3	95	92.8	91.1	93.5	92.1
RUNNING AMPS	27.5	29.8	23.6	22.6	23.21	23.2	24.6
LOCKED ROTOR VOLTAGE	189.2	189.6	190.7	191.2	191.6	191.0	193.7
RUNNING VOLTAGE	206.5	206.1	207.4	207.7	207.5	207.4	207.2

The prop auxiliary pump motor will produce the required power to feather and unfeather the propfan blades at all of the frequencies evaluated. The motor is less efficient at off-frequency conditions, but with the short duty cycle requirement of the motor, operation at the variable aircraft power frequencies should be satisfactory.

9.1.5 Propulsion System Controls

The non-linear relationship of the engine power lever displacement to engine power discovered during the functional checkout was determined to be too sensitive for setting precise test conditions at the higher power levels. A non-linear potentiometer was specified for use in the PTA Flight Test program to linearize the relationship between power lever angle and engine power at high powers.

The engine torquemeter display was somewhat confusing. A slight discrepancy was observed between the two pointer displays on the indicator. The hundreds scale pointer appeared relatively close to the DC output recorded by the data acquisition system, while the tens scale pointer was approximately 41 N-m (30 ft-lbs) lower. However, the calibration accuracy of the torquemeter was substantiated by good agreement that was observed between the power section power calculated using the DC output and Allison test data.

9.2 PROPFAN

9.2.1 Steady State Performance

The results of the stress survey and endurance tests indicated that, in general, the vibratory stress levels were lower for the same blade angle and RPM, than the levels observed during earlier LAP Static Rotor Tests. A maximum of 3960 kW (5314 SHP) was absorbed at 100% speed during the PTA stress survey. This compares with 3520 kW (4719 SHP) absorbed at 100% speed during the LAP Static Rotor Test for the same blade stress level.

The lower stress levels are attributed to a general headwind that was present during the stress survey and endurance tests, and the streamlined nature of the QEC nacelle. The headwinds resulted in the blades operating at a lower angle of attack for a given blade pitch angle and rotational speed. The streamlined nacelle provided well behaved flow downstream of the rotor disc and presented less downstream blockage than did the LAP Static Rotor Test Rig at Wright Patterson.

It was observed that the blade vibratory stress levels were dependent on the wind conditions. Differences in stress level could be noted from day to day where the only change in operating condition was a 2.2 m/s (5 mph) variation in wind speed or a 45^{o} variation in wind direction.

9.2.1.1 Stress Survey

From the stress survey test points 32 key conditions were selected for data analysis in terms of vibratory mean and infrequently repeating peak (IRP) strain. The mean vibratory strain is the average peak amplitude of a sample of strain gage data while the IRP vibratory strain is a statistical value representing the mean strain plus two standard deviations of the data sample. The IRP vibratory strain is used to define the boundaries of the blade continuous operating envelope. Figure 9.17 shows the test conditions selected for analysis.

The SR-7L exhibited high blade tip vibratory response that limited torque at constant speed conditions as shown in Figure 9.18. For constant speed operation the blade strain was relatively low until a critical torque condition was attained and the blade strain increased rapidly with increases in torque as occurred during LAP Static Tests. The only difference between the PTA test results and the LAP test results was that higher torque could be absorbed at a given strain level as seen in Figure 9.18.

The relationship between strain and torque becomes apparent when blade angle is introduced as the key variable. Figure 9.19 shows that torque increased with increasing blade angle and that the rate of torque increase with blade angle changed in the 25^{o} to 30^{o} range. Also included in Figure 9.19 is a comparison of measured torque and blade angle for the LAP and PTA tests. In all cases higher torque was measured during PTA tests than during LAP tests for a given blade angle. The higher blade angles required during LAP tests account for the increased blade strain noted in Figure 9.18.

Using blade angle as the key parameter affecting blade strain, the data in Figure 9.18 is replotted versus blade angle in Figure 9.20. The strain increased rapidly when the blade angle was increased above 25^{o} for all torques and rotational speeds plotted. This relationship with blade angle was also found during LAP tests. One factor that Figure 9.20 does not show is that a relationship existed between blade strain and rotational speed. For low rotational speeds, below 59% N_p (1000 RPM), the blade vibratory tip strain was low.

At the 34.2^{o} low pitch stop blade angle the blade strain increased from a low level at low rotational speed to high levels at 83% N_p (1407 RPM) that prevented further increases in rotational speed. Increasing rotational speed at a constant blade angle had two effects that altered blade response. One was an increase in aerodynamic loads due to increased dynamic pressure and the second was a decrease in the local section reduced frequency. Both of these factors adversely affected blade response.

Figure 9.21 shows the relationship between rotational speed and blade strain at a high blade angle and the distribution of strain along the blade radius. Although the blade angle measurement system indicated the low pitch stop blade angle to be 34.2°, the system had approximately a ±2° error. The low pitch stop was set at 35° blade angle.

As stated previously the blade vibratory response was dominated by activity on the tip bending gage as shown in Figure 9.21. The reason for the high tip bending response is evident from the examination of the frequency content of the strain gage signals. Spectral analysis of gage 13 at 1407 RPM and 34.2° blade angle shows that the primary blade response was at 95 Hz which corresponds to the second flatwise blade vibratory mode. The blade response was characterized during LAP Static Rotor Test as buffeting response, dominated by the second flatwise mode. However, substantial response existed at frequencies other than 95 Hz as shown in Figure 9.22.

To establish the blade natural frequencies and response frequencies, spectral analyses were performed on 18 test conditions. The blade natural frequencies compared very well with the measured frequencies from the LAP Static Rotor Tests. The pre-test predictions were in good agreement for the flatwise modes. The edgewise mode was higher than predicted because the blade retention was found to be stiffer than predicted. The torsion mode was lower than predicted and no reason is apparent for the lower than predicted result. The measured blade natural frequencies are shown in Figure 9.23.

Blade to blade strain variations are summarized in Figures 9.24, 9.25 and 9.26 for the inboard mid-blade and tip bending strain gages. Blade differences were on the order of 12.6% for the highly strained tip bending gage and 7% for the mid-blade bending gage. The blade to blade differences on the inboard bending gage were 20%, which is high because the strain amplitudes were low. Independent of strain level or gage location the blade-to-blade variation was on the order of 75 microstrain.

9.2.1.2 Endurance Tests

Detailed analysis of the strain data taken during the endurance cycles revealed that the strain limits were occasionally exceeded during the cycle. As a result a lower torque limit for future static testing was specified. This torque limited is defined by the dashed line in Figure 9.27.

The endurance test conditions for which detailed strain analyses were conducted are shown in Figure 9.28. Figures 9.29, 9.30, and 9.31 summarize the tip bending gage strain measurements for 77%, 87.5% and 105% rotational speed. The results show that the strain was generally below 400 microstrain and that the acoustic barrier did not significantly influence blade stressing. The blade strain variation with torque follows the same trends that occurred during the stress survey test.

9.2.2 Transient Response

Selected plots of the propfan control dynamic response to power and speed lever transients were presented in Figures 8.4 through 8.11. The results of the transient response tests showed that no adverse stressing of the propfan blades occurred during either fast or slow power or speed lever transients.

9.2.2.1 Prop Speed Lever Transients

For the two second speed lever traverse time (Figure 8.4), the speed set point was being changed at a rate close to the maximum capability of the control input lever actuator. The maximum speed overshoot observed was 3% and the settling time was on the order of three to four seconds. Although an overshoot in speed was noted in Figure 8.5 there seemed to be no corresponding overshoot in blade angle. The absence of overshoot and oscillation of the blade pitch angle during a transient was indicative of a very stable system. A lag time ranging from 1 to 2 seconds was apparent between initiation of the control lever traverse and an observed change in

RPM. The lag time appears to be roughly proportional to the control lever traverse time. Factors which may have contributed to this lag time are the dynamics of the control input lever actuator and dead band in the propfan control. Whirl rig testing of this propfan, conducted in Hamilton Standard's engineering laboratory, determined that the control dead band was larger than had been predicted by analysis.

Figure 8.10 showed the blade peak vibratory strain response to a fast speed transient at a constant power setting. High unsteady strain levels were indicated at low rotational speed and high blade angle transitioning to low, steady amplitude strain at high speed and low blade angle. A small spike in vibratory strain, which damped quickly, was noted during the transient from low to high blade angle (high to low speed).

9.2.2.2 Power Lever Transients

Figures 8.6 and 8.7 showed the responses to essentially step changes in power lever position between 1268 kW and 2089 kW (1700 and 2800 SHP) at 87.5% speed. Figures 8.8 and 8.9 showed the responses to more severe transients, step changes in power lever position between 1350 kW and 2700 kW (1810 and 3620 SHP) at 94% speed. The time rate of change of engine torque and RPM for these cases indicated that although the power lever set point was changed in a few tenths of a second, the actual change in turbine power output required two or three seconds to occur. This was probably the result of the rate limiting characteristics of the turbine fuel control. The maximum underspeed or overspeed observed for these transients was 12%, or 203 RPM. As was noted during the speed lever transients, the speed settling time for the power transients was very short and no blade angle overshoot occurred, confirming the stability of the system. The observed blade angle rate of change in the increasing angle direction was larger than in the decreasing direction. This characteristic was predicted by a computer simulation of the control system conducted during design. The magnitude of the overspeed and underspeed, which occurred during the power transients, was somewhat larger than predicted by the computer simulation. However, the response of the control

system was still well within acceptable limits if abrupt power changes were avoided.

Three factors can be identified which contributed to the larger than expected overspeed and underspeed during power transients. These factors are a larger than predicted control dead band, a lower than predicted governor gain, and a lower than predicted increase in propfan power absorbed with blade angle. As dead band increases a larger speed error is required to initiate a blade angle change that re-establishes the set speed. The larger dead band was the result of more friction and hydraulic leakage in the control system than was assumed in the analysis. The lower governor gain is indicated by a slower blade angle rate of change than was predicted by computer simulation for comparable transients. The maximum observed blade pitch rate was 7^{o} per second (reference Figure 8.6) as compared to a design slew rate of 9^{o} per second. The lower governor gain also may have resulted from higher than expected internal hydraulic leakage. The flattening of the curves of torque versus blade angle, seen in Figure 9.19 illustrates an aerodynamic cause of higher than expected overspeed and underspeed. The flattening of the torque curves was not predicted by aerodynamic analysis nor considered in the dynamic simulation of the control system. As a result a larger blade angle change than predicted was required to absorb a given change in engine power. The flattening of the torque curves occurred between 25^{o} and 30^{o} blade angle, the blade angle range over which much of the transient testing was conducted.

Figure 8.11 showed the blade peak vibratory strain response to a fast power transient at 95% N_p (1600 RPM). Low strain at low power and blade angle was observed smoothly transitioning to high strain at high power and blade angle. No perturbations in strain were noted despite a 9% overspeed and a 12% underspeed which occurred during the transient.

9.2.3 Aerodynamic Performance

Propfan aerodynamic performance data gathered during the stress survey and the endurance test are presented in Figures 9.32 and 9.33. The data were corrected for ambient temperature and pressure, non-dimensionalized and compared with analytical predictions and the results of the LAP Static Rotor Test. The large amount of scatter in the power coefficient versus blade angle data was the result of significant hysteresis and dead band in the blade angle instrumentation. However, the same data trends that were observed in the LAP test data were discernible in the PTA test data. The power coefficient began to fall short of predictions at blade angles above 30°. The plot of thrust coefficient versus power coefficient shows that the thrust measured during the PTA test seemed to be slightly lower than thrust measured during the LAP test in the lower blade angle range. However, the same maximum thrust coefficient was obtained for both tests. The reason for the lower thrust angle may be related to the 4.5 m/s (8 mph) headwind that was present throughout most of the test. The effect of a headwind was to reduce the angle of attack seen by the blades for a given blade pitch angle.

9.2.4 Mechanical Performance

Throughout the course of testing, significant oil leakage was observed from the rear lip seal area of the propfan control. Upon completion of testing the control was disassembled and the source of the leakage was found to be a void in the bond joint between the seal and its retainer. The leak was not due to a defect in the seal itself. The problem will be remedied prior to flight testing by bonding a new seal into the retainer and performing a static leak check of the control.

There were several instances during testing when the propfan failed to come out of the feather or reverse positions. Upon completion of testing, the actuator pitchlock and servo assembly was disassembled to investigate this problem. Several minute metal chips were found in the area of the ballscrew. These chips may have become lodged in the ballscrew on the

occasions when the actuator failed to move the blade angle out of feather or reverse. The pitchlock and servo assembly will be cleaned and the ballscrew replaced.

The modified blade seal design appeared to reduce oil leakage significantly. The new seal was also easier to install which facilitated blade installation. The test results verified that the speed set cam yields the desired speed governing range.

Teardown and inspection of the propfan and control following test revealed no unusual wear.

During the test program the blade strain continuous operating limits were exceeded for short periods of time. Post test fatigue evaluation showed that the blade spar, the primary load carrying structure, accumulated a summation of $n/N = 0.004$ at the blade tip due to buffeting response. The revised static torque limit in Figure 9.27 will prevent any further tip fatigue due to buffeting.

9.3 DRIVE SYSTEM

Allison supplied an abbreviated performance program to calculate engine performance data. This simplified program was developed based on the engine and test stand instrumentation available during the static test. In an attempt to compare the test results with the results obtained during power section and gearbox testing at Allison, this performance program corrected the data to sea level unity ram conditions. In the correction process, however, several assumptions were required. For example, since the engine exhaust static pressure was not instrumented, the ram pressure ratio across the engine was estimated. Important performance parameters such as calculated Burner Outlet Temperature (BOT) were not available since engine airflow could not be measured. Also, the effect on engine performance of inlet pressure and temperature distortion due to the inlet duct could not properly be accounted for with the single compressor inlet pressure/temperature probe.

9.3.1 Steady State Performance

The 501-M78B drive system provided necessary power for all portions of the static test while operating within engine specification limits. A maximum disc loading factor of 503.3 kW/m^2 (62.7 SHP/D^2) was provided with a comfortable Measured Gas Temperature (MGT) margin of 56°C (100°F) below the maximum continuous rating. Oil consumption was virtually nonexistent with a final oil loss (which included not only oil consumption and leaks, but also losses due to magnetic plug inspections) of approximately 0.38 liter (0.1 gallon) per operating hour. Stable operation was demonstrated at every required point during the test.

9.3.1.1 Sea Level, Unity Ram Performance

Figures 9.34 through 9.36 reflect performance comparisons from propulsion system testing at Rohr and power section testing at Allison. The static test data were taken from the pre-endurance performance calibration. The Allison data consisted of the final ambient performance calibration conducted on engine serial number 0085. Both sets of data were corrected to unity ram, allowing a comparison to validate instrumentation, correction factor accuracy, and engine health. Figure 9.34 shows that corrected gas generator speeds versus power section power were nearly identical for the two runs. This helped to verify the accuracy of engine instrumentation such as the torquemeter, rotor speeds, and the compressor inlet temperature and pressure probes. Figure 9.35 shows that corrected MGT data from the static test were slightly higher than the MGT measured on the Allison power section test stand. Installed static test MGT was within 1.5% of the power section uninstalled test data. Corrected fuel flow rates, shown in Figure 9.36, agree within 2.5% between the two test stands.

9.3.1.2 Ram Effect on Drive System Performance

Figures 9.37 through 9.39 compare the installed power section performance, which included the ram effect of the propfan, to unity ram results ob-

tained at Allison. · The data presented in these figures reflect the improvement in drive system performance due to the ram assist from the propfan. At the maximum corrected MGT run in the pre-endurance calibration at Rohr, 7% more power was produced by the power section than was produced under unity ram conditions on the isolated power section test at Allison. Extrapolation to the maximum continuous MGT rating shows that the power section could be expected to produce a 10% power margin above specification requirements.

9.3.2 Transient Response

During propfan speed transients at constant power settings, the propfan speed governor held power turbine overshoots to within approximately 3% as discussed in Section 9.2.2.1. Gas generator speed was unaffected since the power lever was not changed.

Gas generator speed was seen to be linear with power lever position during the power lever transient tests, and the propfan speed control held over- and underspeeds to a minimum. The transient response of the propfan propulsion system verified stable, predictable performance during speed lever or power lever transients.

9.3.3 Engine Power Degradation

Results from the pre- and post-endurance performance calibrations corrected to sea level static, unity ram conditions were presented in Figures 9.40 through 9.42. Comparison of the two calibration runs indicated that engine performance had degraded slightly during the 36-hour endurance test. Considerable dirt and propfan hydraulic fluid buildup was evident on the inlet duct and engine inlet guide vanes.

The post-endurance calibration showed an increase of approximately 2.5% in fuel flow (Figure 9.42) and a resultant MGT increase of $8^{o}C$ ($15^{o}F$) at the maximum power condition. The performance results were indicative of a loss in compressor efficiency. After completion of all scheduled testing,

the engine flow path was chemically cleaned for removal of propfan oil and dust deposits.

9.3.4 Drive System Teardown

After completion of the static test, the propfan propulsion system was disassembled for component refurbishment and shipment to be used in the PTA Flight Test Program. A borescope inspection of the engine power section was performed and no damage was found. The reduction gearbox was removed and shipped to Allison for inspection and refurbishment. Upon teardown at Allison, some distress of the main drive gear roller bearing was discovered. The bearing used during static testing was a specially designed round bearing as opposed to the eccentric bearings in production for installation in the C-130 and P-3 aircraft. No damage to any other component of the gearbox was apparent.

9.4 ACOUSTICS

Far field and near field acoustic data were obtained while operating the SR-7L propfan/engine drive system over a range of tip speeds and horsepowers. The data were also obtained with vertical wall barriers alongside the propfan and alongside the turbine discharge, in an attempt to separate the combustion noise from propfan noise.

9.4.1 Acoustic Data Processing

The acoustic data were machine processed to convert the electrical analog records into engineering units of noise level measurement - sound pressure in psi, and sound pressure level in decibels. The noise level data were displayed in three forms: sound pressure time history, narrow band constant bandwidth sound pressure level spectra, and 1/3-octave sound pressure level spectra.

9.4.2 Far Field Noise Characteristics

The far field noise characteristics of the SR-7L propfan were determined from the 15 ground-flush microphones at 45.7 m (150 feet). Both time-domain and frequency-domain data were evaluated. The sound pressure wave characteristics were examined, the various components of the noise spectrum were identified, the directivity of the significant components was determined, the influences of various propfan operational parameters were evaluated, and the possible masking of propfan noise by drive system noise was investigated.

9.4.2.1 Far Field Sound Pressure Signature Characteristics

Time domain analyses show that the sound pressure waves contained both periodic and random pressures. A typical example, shown in Figure 9.43, is the 90° azimuth location and a moderate power condition. The single 200-millisecond arbitrary sample spans 5.42 revolutions of the propfan. The lower curve was obtained by triggering the time sampling process with the propeller index pulse and averaging 50 samples. The randomly phased pressures averaged to near zero while the phase-correlated pressures averaged to a finite value. In this "laundered" pressure signature, individual blade characteristics could be identified. Weaker as well as stronger pressure waves (denoted by the "W" and "S" symbols) can be seen to repeat at intervals of 8 cycles, or one propfan revolution. This repetition of strong and weak pressure waves, supported by the blade to blade strain variations noted in Section 9.2.1.1, suggests that blade loading may have been dissimilar.

The time averaging process was repeated for a reduced time span to provide better visibility of a single wave. A single 8 millisecond sample is shown in the upper part of Figure 9.44, while the average of 50 wave samples is shown in the lower part.

9.4.2.2 Far Field Noise Spectrum Content

Figure 9.45 illustrates the features of the far field sound pressure level spectrum at 30° azimuth for a moderate power of 1732 kW (2323 SHP) and 100% tip speed. In all spectrum analyses of this type, the amplitudes were based on 30 averages obtained with free run triggering, no overlap, Hanning windowing, 19 Hertz effective bandwidth, and 800 line display resolution.

The first few orders of propfan blade noise were distinct at multiples of 220 Hertz. Other tones were evident near 4000 Hertz. One of these tones (though often not the strongest) always occurred at the compressor first-order blade frequency, while the rest occurred at sums of or differences between the compressor and the propeller blade frequencies. Broad-band random noise was evident throughout the audible range. It was strongest in the comparatively low frequency range of 500 to 1500 Hertz.

The level of the first-order propfan blade tone shown in Figure 9.45 was 98 dB; the second-order tone was 92; the third was 88. The third, fourth, and fifth order tones were contaminated by the random noise, and higher orders were totally masked.

The tone frequencies were determined more accurately by high-resolution spectrum analysis, wherein the analysis frequency range and bandwidth were reduced by a factor of 10, the display resolution was increased to 8000 lines, and 50 averages were obtained. In so doing, the cursor indication was accurate to within $\pm$0.62 Hertz. Figure 9.46 shows the results of such an analysis for the same microphone and power conditions as Figure 9.45.

The peaks adjacent to the compressor fundamental peak in Figure 9.46 are seen to be at exact multiples of 220 Hz (the propfan fundamental) above or below the 4052.5 Hz compressor tone. These tones in the vicinity of 4000 Hertz are not the 18th, 19th, 20th, etc., order of propfan noise alone, but appear to be the result of an interaction between the compressor and propfan wake. The noise frequency was seen to track compressor rotation

speed when power was changed; directivity of the tone noise was seen to agree with inlet rather than propfan noise directivity; and level of these tones remained constant at conditions where propfan tone levels changed.

The broad-band random noise shown in Figure 9.45 maximized near 800 Hertz, at a level of about 84 dB. This level is deceptively low because of the comparatively narrow (19 Hertz) analysis bandwidth used. In fact, the random noise governed the overall sound pressure level, OASPL, which, at 107 dB, was 9 dB above the highest tone level. The importance of this low frequency random noise was also visible in 1/3-octave analyses.

The low frequency random noise was attributed to stall on the propfan blades and/or possible inflow turbulence since the random noise behavior was consistent with the blade stress behavior. As flow separation increased, the random noise typically increased throughout the audible spectrum, but the increase in the low frequency portion of the noise spectrum was always more pronounced. For that reason, the random noise discussion and illustrations hereafter will refer to the "crest" of the low-frequency portion of the random noise spectrum.

The three spectrum components discussed above (propfan tone noise, compressor-related noise, and low frequency random noise) took on varying significance, depending on direction and power. In the following discussion they are examined at 60°, 90°, and 120° at two power conditions.

9.4.2.2.1 Directivity Effects on Spectrum Content

The variation in spectral characteristics with azimuthal location is shown in Figures 9.45, 9.47, 9.48, and 9.49 for a power of 1732 kW (2323 SHP) and a tip speed of 237 m/sec (778 ft/sec).

Figure 9.47 shows the noise spectrum at 60° for the same power and tip speed as the 30° spectrum of Figure 9.45. At 60°, the propfan tone noise was lower, the compressor/propfan interaction tone noise was higher, and the random noise crest was at a higher frequency than at 30°.

At 90° azimuth, shown in Figure 9.48, the propfan first-order tone level increased from the level at 60°, the compressor/propfan interaction noise decreased, and the random noise level was slightly lower.

At 120° azimuth, Figure 9.49, the propfan first-order tone noise decreased from the level at 90°, while the higher-order propfan tones increased slightly. The compressor-related noise also showed preference to higher orders, and the level of the random noise crest increased.

9.4.2.2.2 Power Effects on Spectrum Content

The variation in spectral characteristics with power is shown in Figures 9.47 through 9.58. Data at a power of 1732 kW (2323 SHP) are compared with data at 3007 kW (4032 SHP). The tip speed for both power levels was 237 m/sec (778 ft/sec).

At 60° azimuth, increasing the power from the 1732 kW (2323 SHP) case, shown in Figure 9.47, to 3007 kW (4032 SHP), Figure 9.50, increased the propfan first-order tone 7 dB while the random noise crest increased 13 dB. Most of the random noise increase occurred in the 500 to 1500 Hz range.

A 1/3-octave analysis of the noise at 60° azimuth, 1732 kW (2323 SHP), is shown in Figure 9.51. This analysis illustrated the greater significance of the random noise relative to the propfan tones. The random noise maximized in the 1600 Hertz band, where it was 4 dB above the propfan fundamental. The highest noise level occurred in the band containing the compressor/propfan interaction tones and random noise combined.

The 1/3-octave spectrum for the same 60° azimuth and 3007 kW (4032 SHP) maximized in the band containing the crest of the random noise, as seen in Figure 9.52.

At 90° azimuth, increasing propfan power increased the propfan tone noise by 3 dB and increased the random noise by 15 dB, as shown in Figures 9.48, and 9.53 through 9.55. The compressor related noise was totally masked by the random noise at the higher power setting.

At 120°, increasing the propfan shaft power increased propfan tone noise about 4 dB and increased the random noise crest about 15 dB as shown in Figures 9.49, and 9.56 through 9.58.

9.4.2.3 Far Field Noise Directivity

The strength of each of the principle noise components in the spectra was seen to vary significantly with direction, and the directionality varied with power. These effects are illustrated in the polar plots of Figures 9.59 through 9.67. All of the polar plots show ground level noise levels at 45.7 m (150 feet) from the reference point.

The propfan first-order blade noise directivity is shown in Figures 9.59 through 9.62 for the four tip speeds tested. For each tip speed case, data are shown for the maximum and minimum test powers, except for the lowest tip speed, where only the maximum power was tested.

The propfan low-frequency random noise directivity is shown in Figures 9.63 and 9.64 for the highest and lowest tip speeds, respectively. The radial scale quantity is the 19 Hertz band SPL at the crest of the smoothed random noise spectrum. The general shape of the polar plots was similar for all tip speeds. These figures show that, at a given tip speed, the random noise in all directions increased with increasing power, while at a given power, the random noise in all directions decreased with increasing tip speed.

The compressor/propfan interaction tone directivity is shown in Figures 9.65 through 9.67. The levels shown are those of the strongest compressor-related tone. These figures show that the tones were usually strongest at about 15°, and also strong at 40° to 60° azimuth. The

spectrum tended to be richer in tone content in the 15° area. Figures 9.65 and 9.66 show data only for the high tip speeds, because at low tip speeds the increased random noise masked the compressor related noise. Figure 9.67 shows a comparison of compressor/propfan interaction tone noise for three tip speeds. In this comparison the power conditions were similar though not identical. The compressor-related noise level and directivity characteristics were similar at all three tip speeds.

The manner in which the subjective annoyance of the total noise spectrum varied with direction is shown in Figures 9.68 and 9.69. In Figure 9.68 the "A" weighted overall level, dBA, is shown for four tip speeds, each for the minimum power tested. In Figure 9.69, dBA level is shown for five power conditions, each for the maximum tip speed tested. The levels were surprisingly uniform from straight ahead to 145° azimuth, despite the distinct directivity of individual noise components.

9.4.2.4 Far Field Noise Relation to Operational Parameters

The propfan first-order blade noise, the low-frequency random noise, and the compressor/propfan interaction noise were each plotted against appropriate control parameters.

The first-order blade noise at 100° azimuth is shown as a function of shaft power in Figure 9.70. The noise levels were tip speed dependent as well as power dependent. Similar plots were made for power coefficient C_P, measured thrust, and thrust coefficient C_T. The better describer of first-order blade noise was thrust. The relationship is shown in Figure 9.71. It suggests "lift" noise as the source, since thrust relates to the forward component of blade lift.

The low-frequency random noise at 130° azimuth is shown as a function of shaft power in Figure 9.72. At the higher tip speeds where there were sufficient data to show the trend, noise level was seen to increase roughly linearly with shaft power. At a given power, the random noise level decreased as tip speed increased. The relationship of random noise

to blade lift (measured thrust) is presented in Figure 9.73. At a given tip speed, random noise increased nonlinearly with thrust, while at a given thrust, random noise decreased as tip speed increased. Blade vibratory stress behaved in a similar fashion. All of these trends indicate that random noise was strongly related to blade stall. This random noise should be substantially lower in flight, where flow through the propeller disc will be clean and blade stall should be absent.

The random noise data of Figure 9.73 were correlated with thrust coefficient C_T. The result is shown in Figure 9.74, where the data are seen to converge toward a single nonlinear curve. An even better describer of the random noise level was found to be power coefficient, C_p. As shown in Figure 9.75, when plotted against C_p, the noise data for all tip speeds converge toward a single slightly nonlinear curve.

The compressor/propfan multiple-tone interaction noise at 50° azimuth is shown as a function of shaft power in Figure 9.76. In this figure the ordinate is the sound pressure level of the strongest interaction tone, regardless of the tone frequency. The strongest interaction tone frequency was always in the range of 4000 to 5500 Hertz. The tone level data followed a linear power relationship with rather flat slope, indicating only a mild sensitivity to power. The tone-level sensitivity to thrust was very similar. At the higher shaft power conditions, the compressor/propfan interaction noise was masked by the random noise. Frequency-wise, the compressor related tones were well removed from the propfan tones and did not contaminate the propfan tone measurement.

9.4.2.5 Masking of Propfan Far Field Noise by the Drive System

The drive system noise consisted primarily of combustion noise and compressor related noise. Since the exhaust velocities were relatively low, jet noise was minimal. Because compressor and turbine tone noise frequencies were far removed from propfan frequencies, they did not contaminate propfan noise measurements. The combustion noise was in the same frequency range as the propfan second, third, and fourth order tones, and

could have been contaminating. Combustion noise was also in the same frequency range as the propfan low frequency random noise, and because noise from both sources maximized at high power conditions, it was difficult to distinguish combustion noise from propfan random noise.

The approach used for separating combustion noise from propfan random noise was source shielding, using an acoustic barrier. The configuration and placement of the barrier in the forward and aft positions is described in Section 5.6.1.

Before applying the barrier noise data to the random noise case, the barrier performance was examined at the propfan first-order blade passage frequency and at compressor related frequencies, where no other sources should have influenced the data. Figure 9.77 illustrates the barrier effectiveness on propfan first-order noise for a tip speed of 255 m/sec (836 ft/sec), corresponding to a frequency of 236 Hertz. While the barrier provided line-of-sight shielding for the 30^{o} through 110^{o} far field microphones, the barrier provided noise reductions ranging from zero to as much as 20dB, depending on direction. The poor performance at 60^{o} and forward probably indicated either a combined flanking and reflection path, or a barrier resonance with attendant low transmission loss. The barrier was consistently effective in the 70^{o} to 110^{o} cone of interest where the propfan was shielded but the discharge noise was unimpeded.

In Figure 9.78 where the propfan first-order tone frequency was 220 Hz, the characteristics were similar but the barrier was less effective in the cone of interest.

The compressor tone noise, seen in Figures 9.79 and 9.80, was reduced by the barrier, although more reduction was achieved at 40^{o} to 60^{o} than in the cone of interest. Despite this, the barrier was effective on compressor noise frequencies in the cone of interest.

Random noise level in the 500 to 1500 Hertz range, where combustion noise was most likely to contribute, is shown in Figure 9.81 for the high power

high tip speed case. The levels shown are 19 Hertz bandwidth levels at the crest of the spectra. Figure 9.82 shows similar data for the high power/low tip speed case. Noise levels between the two conditions were essentially unchanged in the directions where the barrier did not shield the propfan. Within the cone of interest, the area where the propfan was shielded but the discharge was not shielded, noise levels were reduced significantly. This suggests that the low frequency random noise originated at the propfan. This conclusion is supported by the data shown in Figure 9.83, which shows the random noise level with the barrier in the aft position for a high power/high tip speed case. The random noise level in the cone of interest, where the engine discharge was shielded and the propfan was not shielded, was not reduced from the no-barrier configuration.

9.4.3 Near Field Noise Analyses and Characteristics

Near field noise was recorded at seven sideline microphone locations as discussed in Section 5.6.2. The sideline at 2.99 m (9.8 feet) from the propfan centerline is representative of the testbed fuselage exterior sidewall locations nearest the circumference of the propfan disc. Static test microphone locations, relative to the fuselage and the installed propfan, are shown in Figure 9.84.

Contamination from ground reflections should have been minimal at 30° through 90°, since the reflected path was two or more times the direct path. The data collected at these locations should approximate free field data, and PTA testbed aircraft fuselage surface levels could be about 6 dB higher than the static test acoustic data. At the 110°, 130°, and 145° locations, some ground reflection contamination could be present which could introduce deviations from free field levels. The deviations could range from about -6 dB to about +3 dB, depending on phase relation between direct and reflected waves. Testbed aircraft fuselage surface levels at these three locations could range from 3 to 12 dB higher than the data collected during static testing. No attempt has been made to correct the data for fuselage surface pressure doubling, ground effects, or atmospheric effects. All data shown are as measured.

C-2

9.4.3.1 Near Field Noise Spectrum Content

Narrow-band (19 Hertz bandwidth) sound pressure spectra were produced for each microphone and each power condition in the same manner as for the far field analyses. An example is shown in Figure 9.85. This moderate power example for the microphone at 30^{o}, which represents testbed FS 217, showed the same characteristic propfan tones, random noise, and compressor tones seen in the far field.

The sound pressure spectrum for the same power condition at 50^{o} (FS 322) is shown in Figure 9.86, and at 90^{o} (FS 421) in Figure 9.87. As with the far field data, the propfan tones and the propfan random noise were most prominent in the lateral quadrant, while the compressor tones in the lateral quadrant were barely discernible (the 50^{o} near field microphone was at roughly 90^{o} to the propfan).

The propfan blade passage tone levels at each microphone were read from the spectra for each of the various power conditions to reveal power effects, and variations in noise level fore and aft.

9.4.3.2 Near Field Noise Distribution Fore and Aft

Propfan first-order blade passage sound pressure levels at the seven equivalent fuselage stations are shown in Figure 9.88 for the highest tip speed, 252 to 255 m/sec (826 to 836 ft/sec). These data show the tone level maximized at equivalent FS 322, which was slightly aft of 90^{o} from the propfan. While the spacing of the microphones was too great to pinpoint the location of the maximum level, the microphone at equivalent FS 322 was within the directivity lobe of high levels observed in the far field, and should be within a few dB of the maximum.

The first-order blade noise distribution for 237 m/sec (778 ft/sec) tip speed is shown in Figure 9.89. At both 237 and 255 m/sec (778 and 836 ft/sec) tip speeds, the noise level was seen to peak at an intermediate

horsepower rather than the highest power. This behavior resembled that observed for the far field data. It was probably because the directivity was changing with power, and the single microphone at equivalent FS 322 was missing the maximum.

First-order blade noise distributions at the lower tip speed conditions are shown in Figures 9.90 and 9.91.

First-order blade noise distributions as a function of tip speed, for roughly equal shaft power conditions, are shown in Figure 9.92. In the region of the maxima the noise level increased systematically with tip speed. Aft of the maxima the noise levels were less dependent on tip speed.

For fuselage sonic fatigue design purposes, the near field noise was the highest at the high tip speeds, where worst case levels reached 141 dB. This was still well below the levels expected during high speed cruise. Since the testbed fuselage shell was reinforced to tolerate the cruise case, it should not be unduly affected by ground running.

Cabin noise levels that result from exterior surface noise being transmitted to the interior will be substantially higher in flight, because of the higher exterior noise during that condition. Crew ear protection provisions that are suitable for the flight case should therefore be adequate for ground running.

9.4.3.3 Near Field Sound Pressure Signature Characteristics

Instantaneous and time-averaged sound pressure signatures were obtained for selected conditions to reveal the nature of the pressure loading on the structure and to determine the non-uniformity, if any, of the pressure waves from the propfan blades.

Examples of a typical instantaneous and an average of 50 pressure wave samples of 200 milliseconds duration (about 5.5 propfan revolutions, or 44

blade passes) are shown in Figure 9.93 for equivalent fuselage station 322. The averaged wave shows the same characteristics as the far field data, i.e., certain blade signatures were consistently weaker (indicated by "W"), and others consistently stronger (indicated by "S"). Typically, the strongest and the weakest pressure signatures deviated from the average by about 10%.

A typical instantaneous and an average of 50 pressure wave samples of 8 milliseconds duration is shown in Figure 9.94 for the same equivalent fuselage station 322. The instantaneous wave illustrates the complex nature of the instantaneous pressure loading on the structure. Because random pressures coexisted with the discrete phase-correlated pressures, the instantaneous pressure loading varied a great deal between samples. In the time-averaged pressure wave, the randomly phased pressures averaged to near zero, leaving only the discrete phase-correlated pressure. The first-order wavelength was seen to dominate at the location and condition shown. The pressure distribution was slightly saw-toothed, but essentially sinusoidal.

10.0 CONCLUSIONS

All of the major objectives for the static test program were achieved. The propfan propulsion system operation was very satisfactory and should be suitable for upcoming flight tests with minor modifications.

The propulsion system and its related subsystems operated as they were intended to operate. Control inputs to the propfan and drive system provided stable, predictable responses. Instrumentation outputs were accurate. Fluid cooling was adequate, with fluid temperatures remaining within specification limits during normal running conditions. Compartment temperatures indicated that the nacelle cooling provisions permit a suitable environment for propulsion system operation. Operation in reverse thrust was hampered by inadequate fluid cooling and insufficient propfan power absorption to prevent reduction gearbox main drive bearing skidding.

Propfan blade stresses were lower than those encountered at similar operating conditions during the LAP Static Rotor Test. No adverse stressing was encountered during transient testing. Blade strain limits were occasionally exceeded during the endurance testing, and a revised torque limit has been defined for static operation as a result.

The propfan control dynamic response was very stable but slightly slower than predicted. Overspeed or underspeed conditions could occur if power changes were introduced too rapidly. The single plane balance procedure provided satisfactory results. Vibration levels were independent of blade angle. Replacement of components on the rotating portion of the propfan and changing the low pitch stop setting did not adversely affect the balance.

Drive system instrumentation provided accurate, readable displays to the engine operator. Research instrumentation outputs were also consistent and accurate. The performance of the Hamilton Standard instrumentation was satisfactory with the strain gage signals very reliable and free of noise.

Engine speed stability and propfan 1P signal quality were satisfactory for time domain averaging of acoustic pressures, and for high resolution frequency domain analyses. The far and near field noise spectra contained three components whose significance depended on power, tip speed, and direction. The components were propfan blade tones, propfan random noise, and compressor/propfan interaction noise. No significant turbine noise or combustion noise was evident. The combined noise of all sources, on an "A" weighted basis, was uniformly directional over the range of 0^{o} to 145^{o}. The static near field noise levels were well below the worst case cruise noise levels used for fuselage sonic fatigue analyses, and the fuselage structure should not be unduly affected by ground running. Crew ear protection provisions planned for flight operation should be adequate for ground operation.

All drive system vibration data were within the limits specified in the engine model specification. After the propfan was balanced, no vibration problems were experienced.

The drive system provided necessary power for all portions of the static test program while operating within the engine specification limits. The pre-endurance calibration data agreed with Allison predictions of drive system performance. The engine inlet duct performed better than predicted, with a large beneficial effect on drive system performance. Measured Gas Temperature exhibited a $56^{o}C$ ($100^{o}F$) margin below the maximum continuous limit. The 1 to 2% power degradation observed between the pre- and post-endurance calibrations was probably due to compressor contamination by hydraulic fluid and dirt. A post-test compressor wash was performed and should minimize power loss.

The modified propfan blade seal significantly reduced hydraulic fluid leakage. Although the propfan assembly leaked a significant amount of fluid, the majority of the leakage occurred past the prop control rear lip seal.

11.0 RECOMMENDATIONS

Recommended modifications to the propfan propulsion system prior to flight testing include:

1. Increase the prop speed control electro-mechanical actuator torque from 7.9 N-m (70 in-lb) to 13.6 N-m (120 in-lb) to allow the actuator to place the propfan control actuator lever into the feather position.

2. Replace the power lever potentiometer with a non-linear potentiometer to improve the linearity between the engine power lever and actual engine output power.

3. Replace the gearbox lateral accelerometer (V_5) bracket with a shorter, stiffer bracket.

4. Replace the reduction gearbox main drive gear roller bearing with a C-130/P-3 style eccentric bearing.

Recommended changes that do not require hardware or design modifications for flight testing include:

1. Correct propfan rear lip seal oil leakage by bonding a new seal to the retainer.

2. For cockpit vibration display, replace the aft compressor vertical (V_3) accelerometer signal with the aft compressor lateral (V_7) signal.

3. For normal operation, limit the minimum propfan/power turbine speed to 50% N_p.

4. For normal operation, limit the minimum torquemeter torque to 474.5 N-m (350 ft-lb).

5. Limit or avoid reverse thrust ground operation to stay above the minimum recommended torque limit and to avoid potential ground handling problems during taxi conditions.

6. Restrict ground static operation to be within the torque-speed envelope established by Hamilton Standard to reduce propfan blade stresses.

7. Utilize the Hamilton Standard method for calculating prop shaft moments from blade stress data.

Lockheed

APPENDIX A

LIST OF ABBREVIATIONS

BOT	Burner Outlet Temperature
BSFC	Brake Specific Fuel Consumption
CP	Power Coefficient
CT	Thrust Coefficient
CRT	Cathode Ray Tube
CVG	Compressor Variable Geometry
D	Propfan Diameter
FM	Frequency Modulation
IRIG	Inter-Range Information Group
IRP	Infrequently Repeating Peak
LAP	Large-Scale Advanced Propfan
MGT	Measured Gas Temperature
Ng	Gas Generator Speed
Np	Power Turbine/Propfan Speed
OASPL	Overall Sound Pressure Level
P	Propfan Revolution
PTA	Propfan Test Assessment
QEC	Quick Engine Change
SHP	Shaft Horsepower
SPL	Sound Pressure Level
TIT	Turbine Inlet Temperature
TSFC	Thrust Specific Fuel Consumption
VAC	Volts Alternating Current
VRMS	Root Mean Squared Volts

APPENDIX B

FIGURES

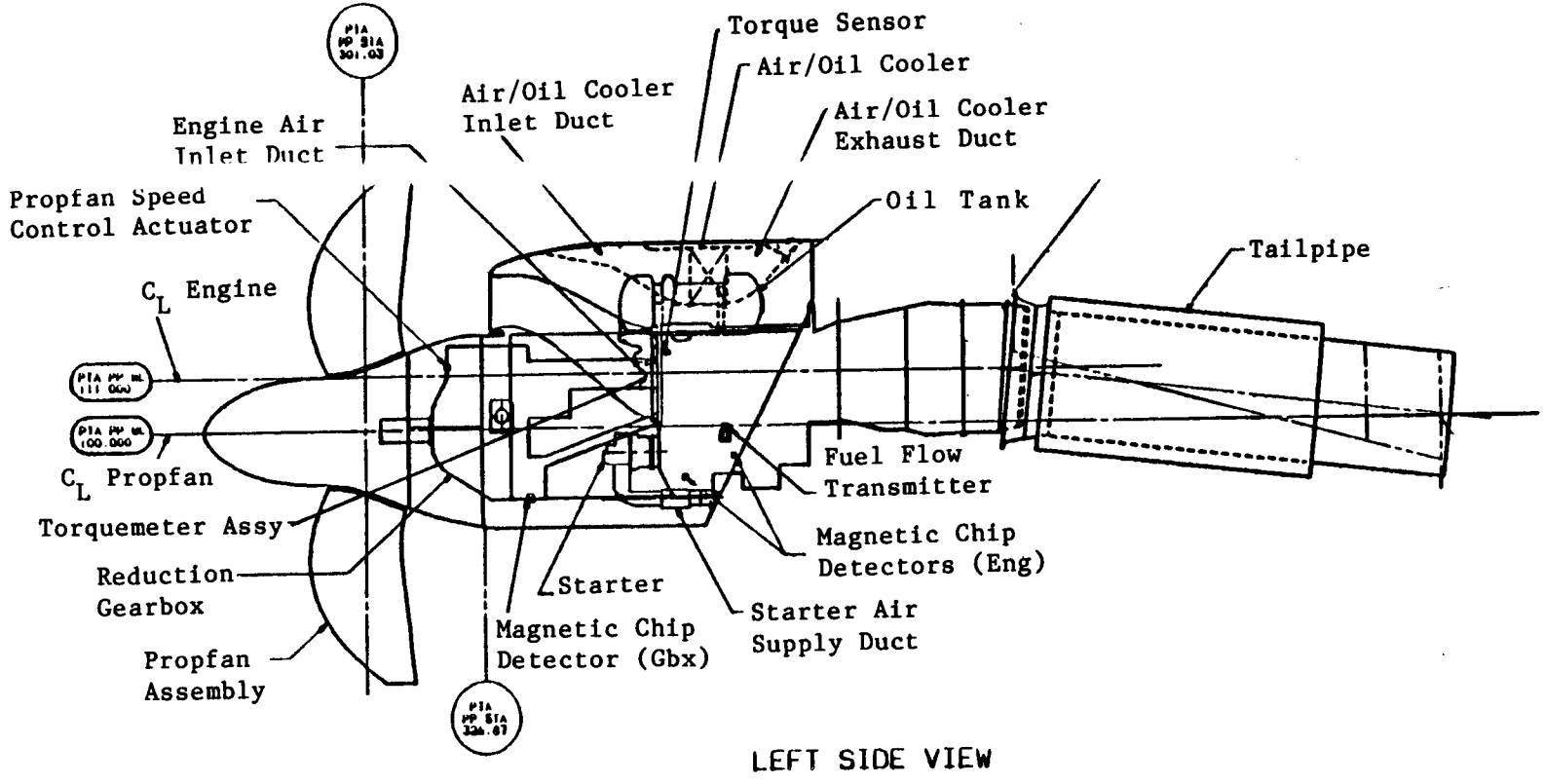

Figure 4.1. Propfan Propulsion System

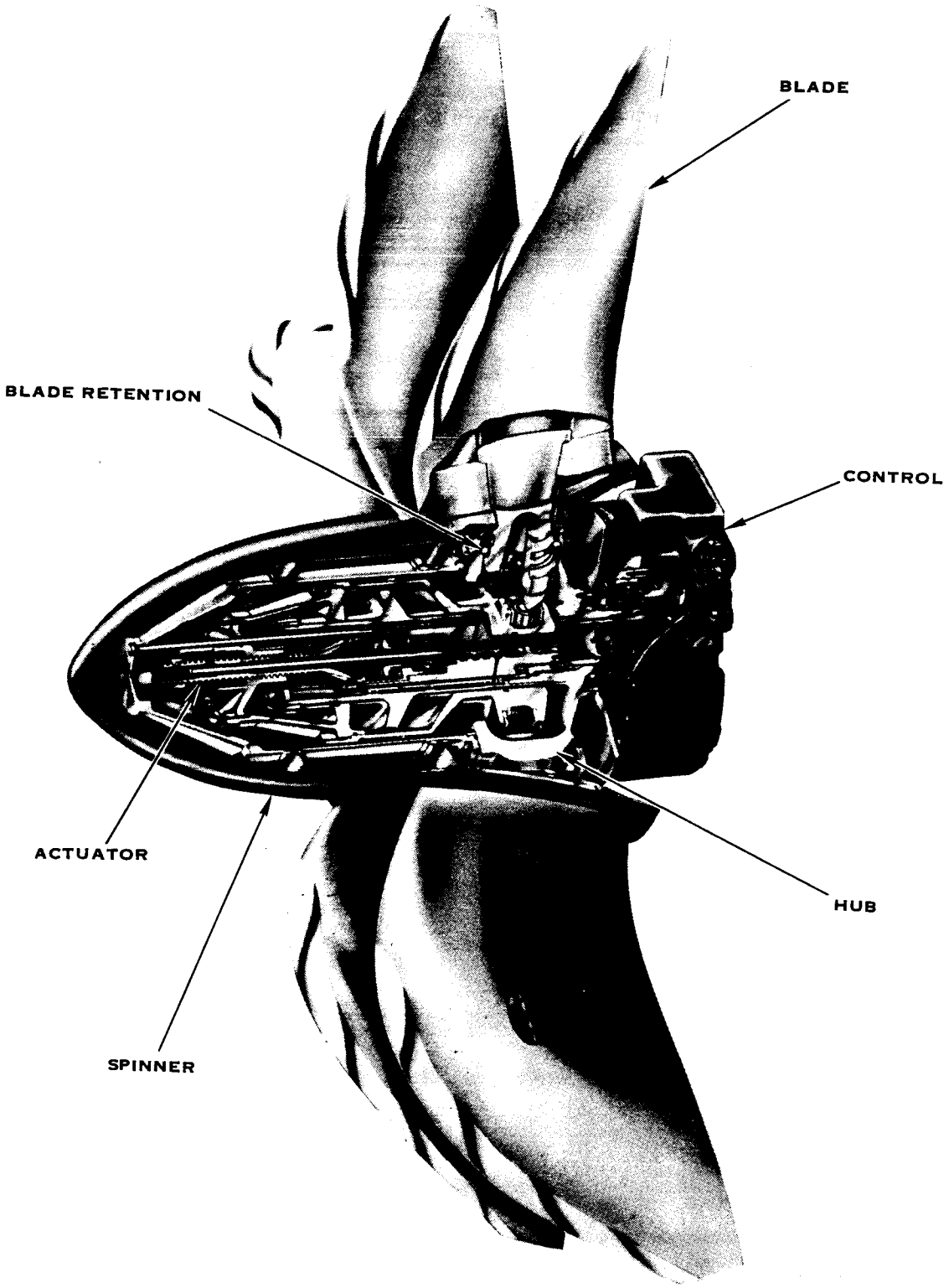

Figure 4.2. Large-Scale Advanced Propfan

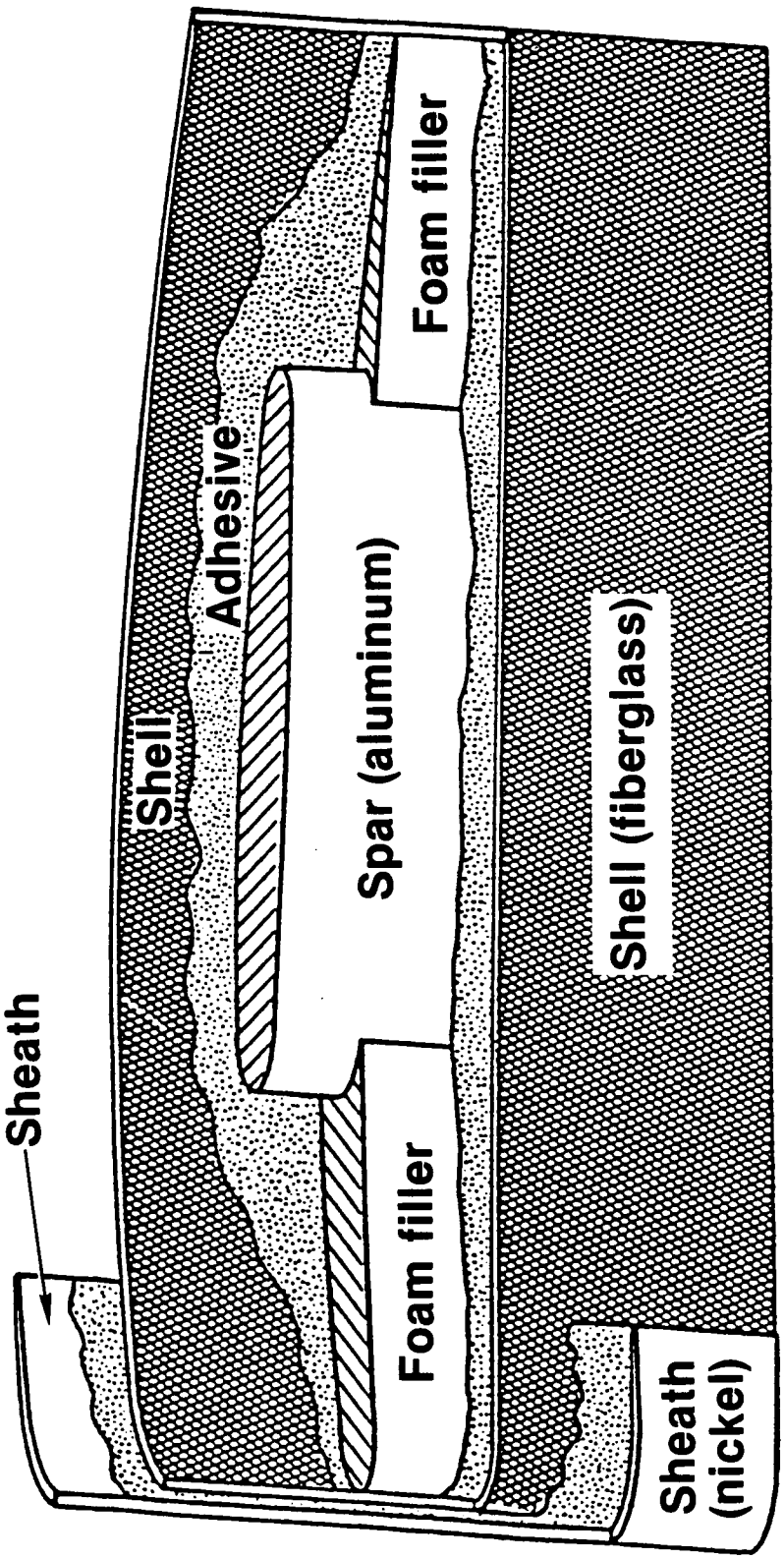

Figure 4.3. SR-7L Blade Cutaway View

Figure 4.4. Allison 501-M78B Drive System

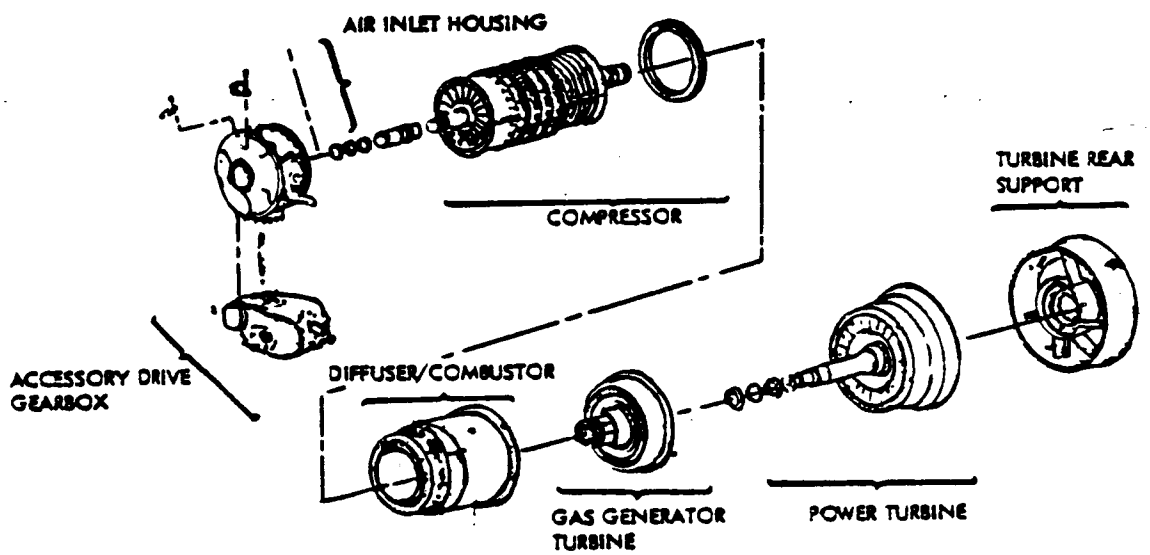

Figure 4.5. Major Power Section Components

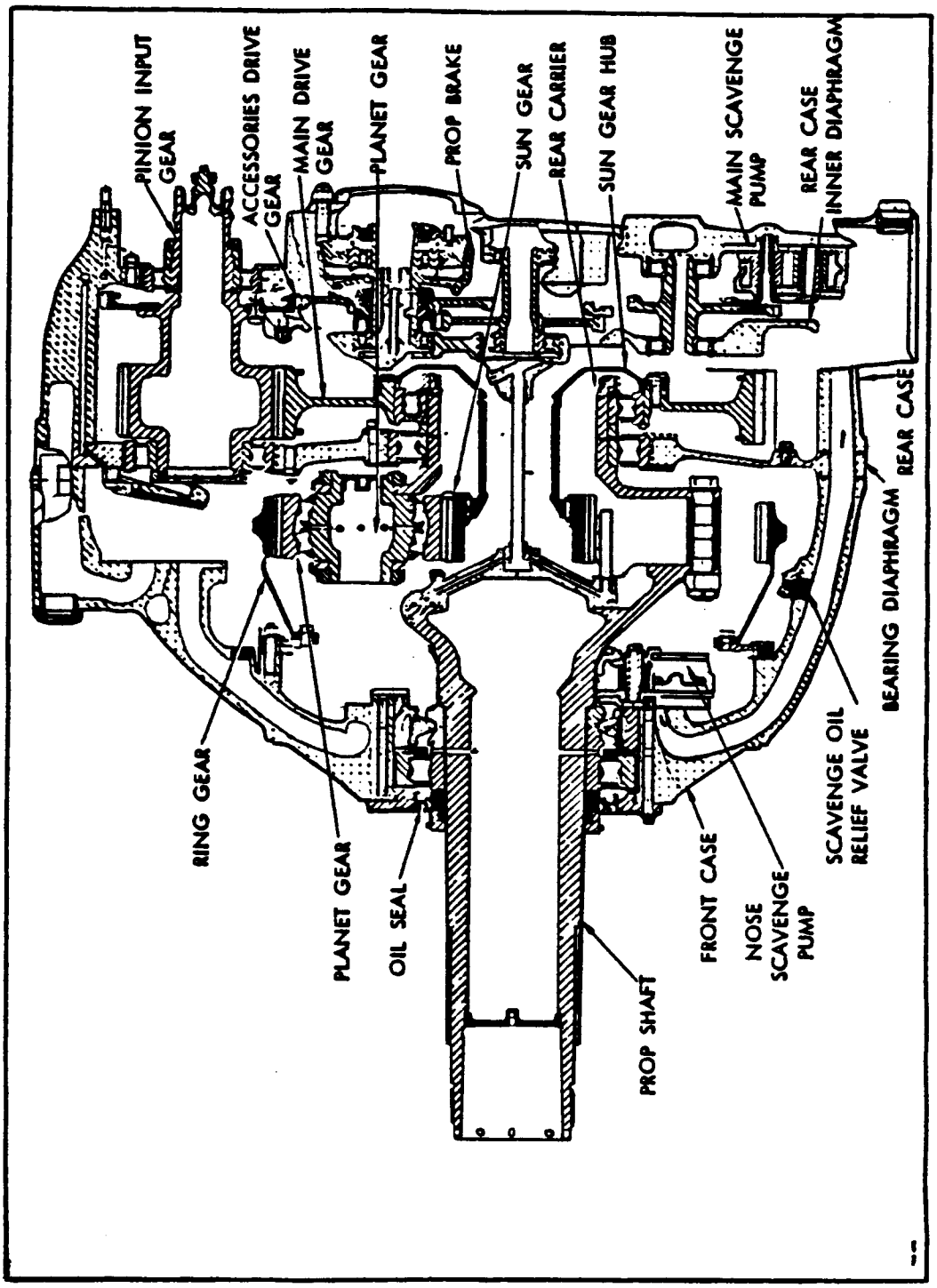

Figure 4.6. Reduction Gearbox Assembly

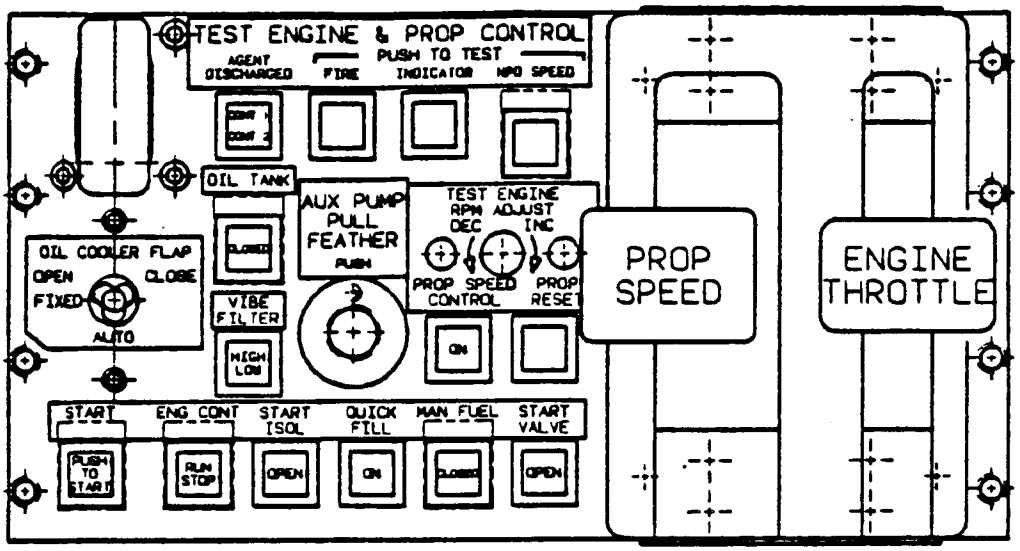

Figure 4.7. PTA Control Panel

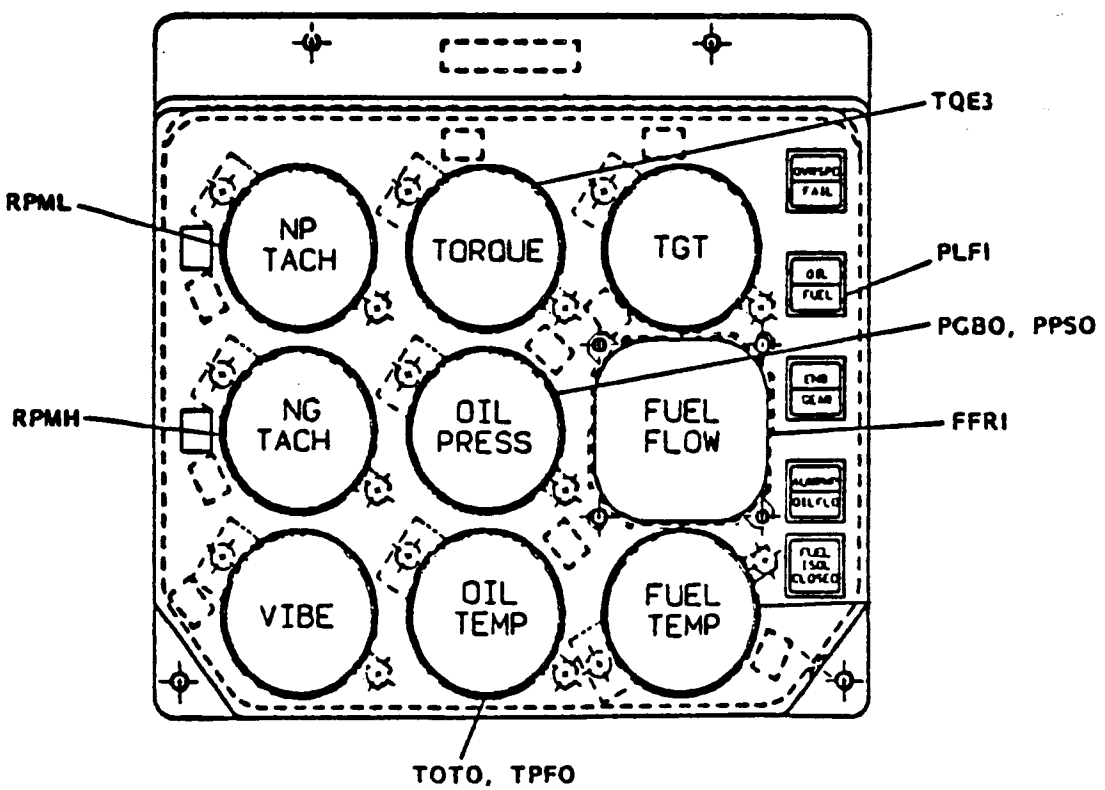

Figure 4.8. PTA Instrument Panel

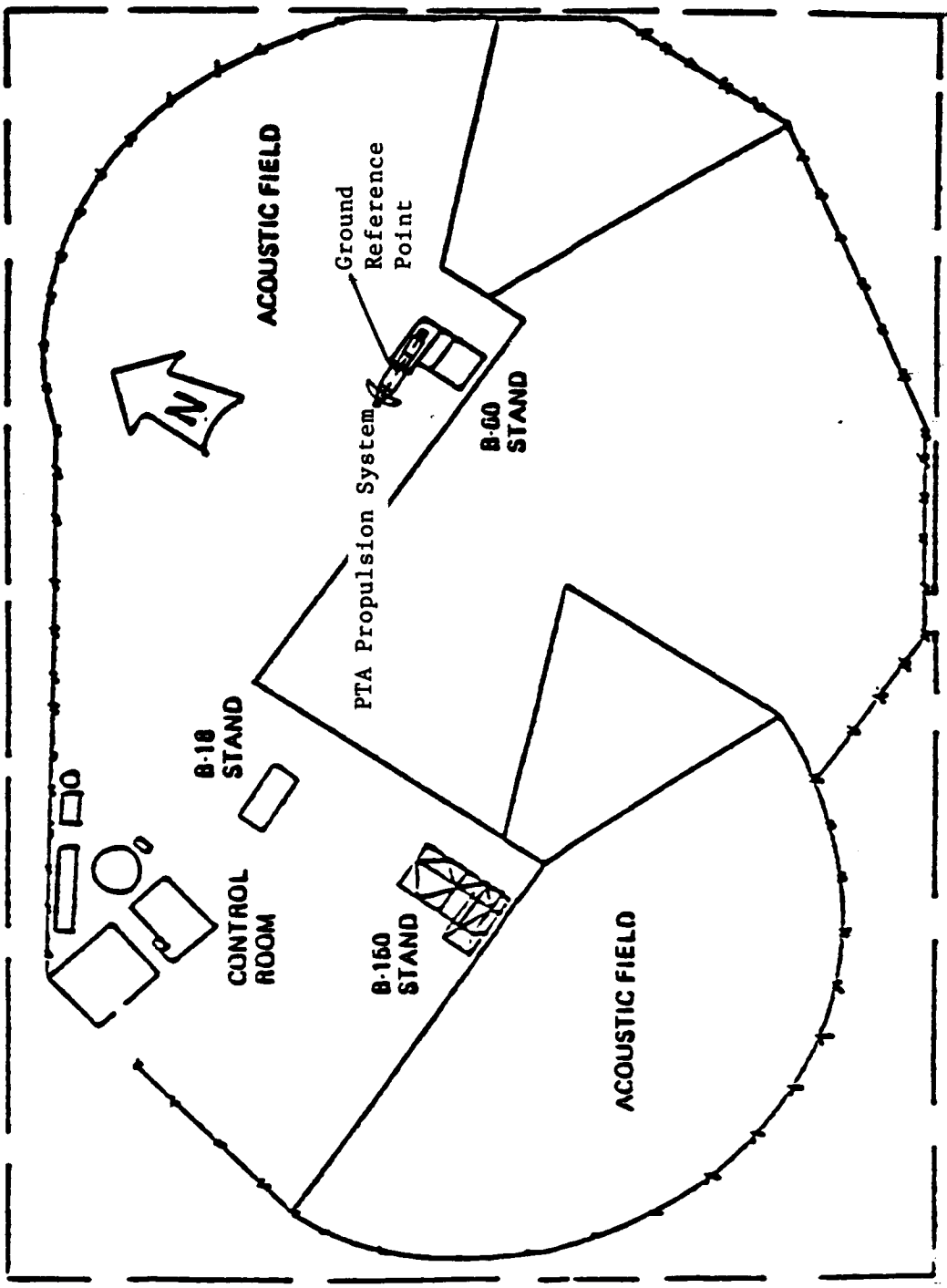

Figure 5.1. Rohr Brown Field Test Facility

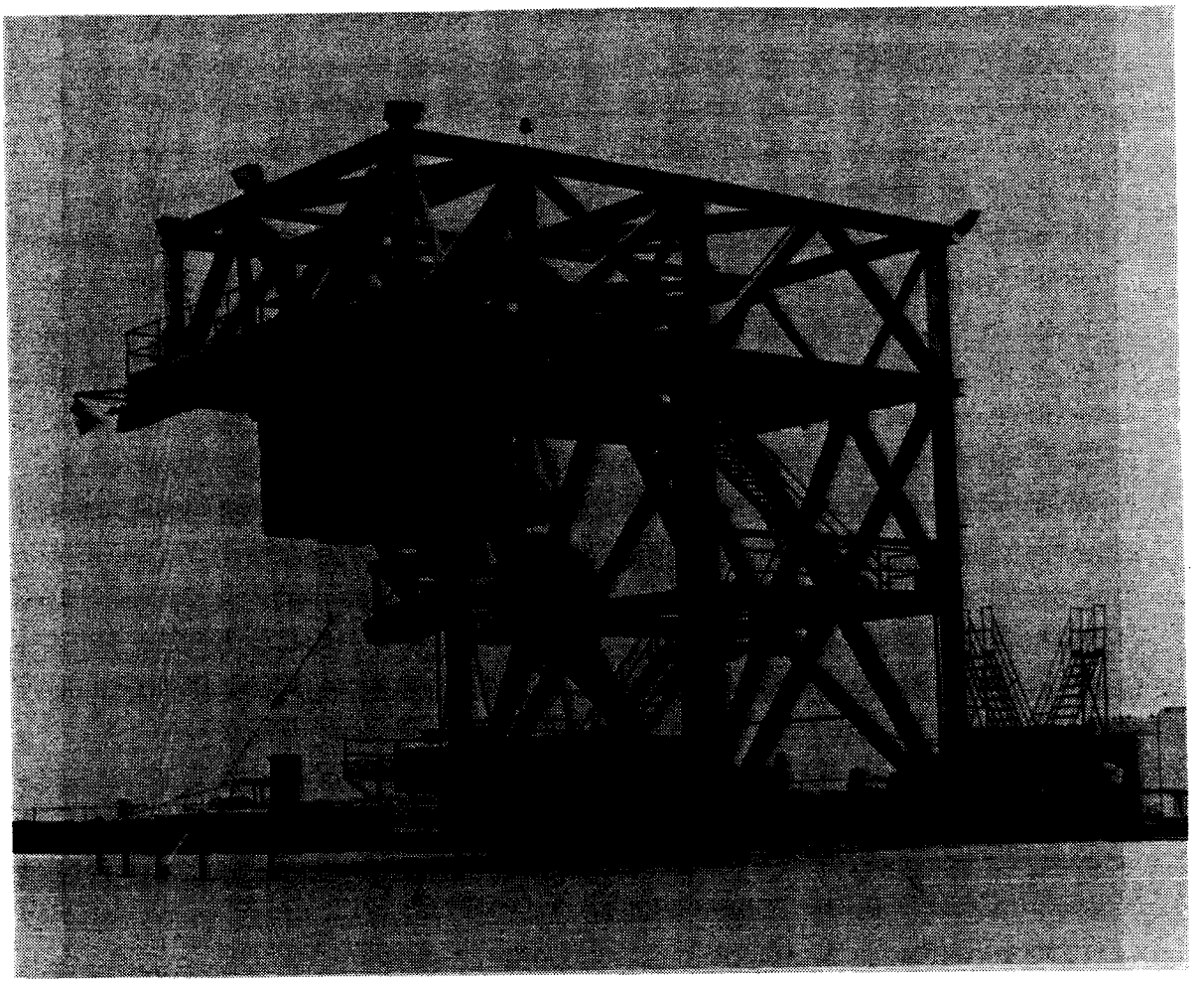

Figure 5.2. PTA Static Test Mounting Arrangement

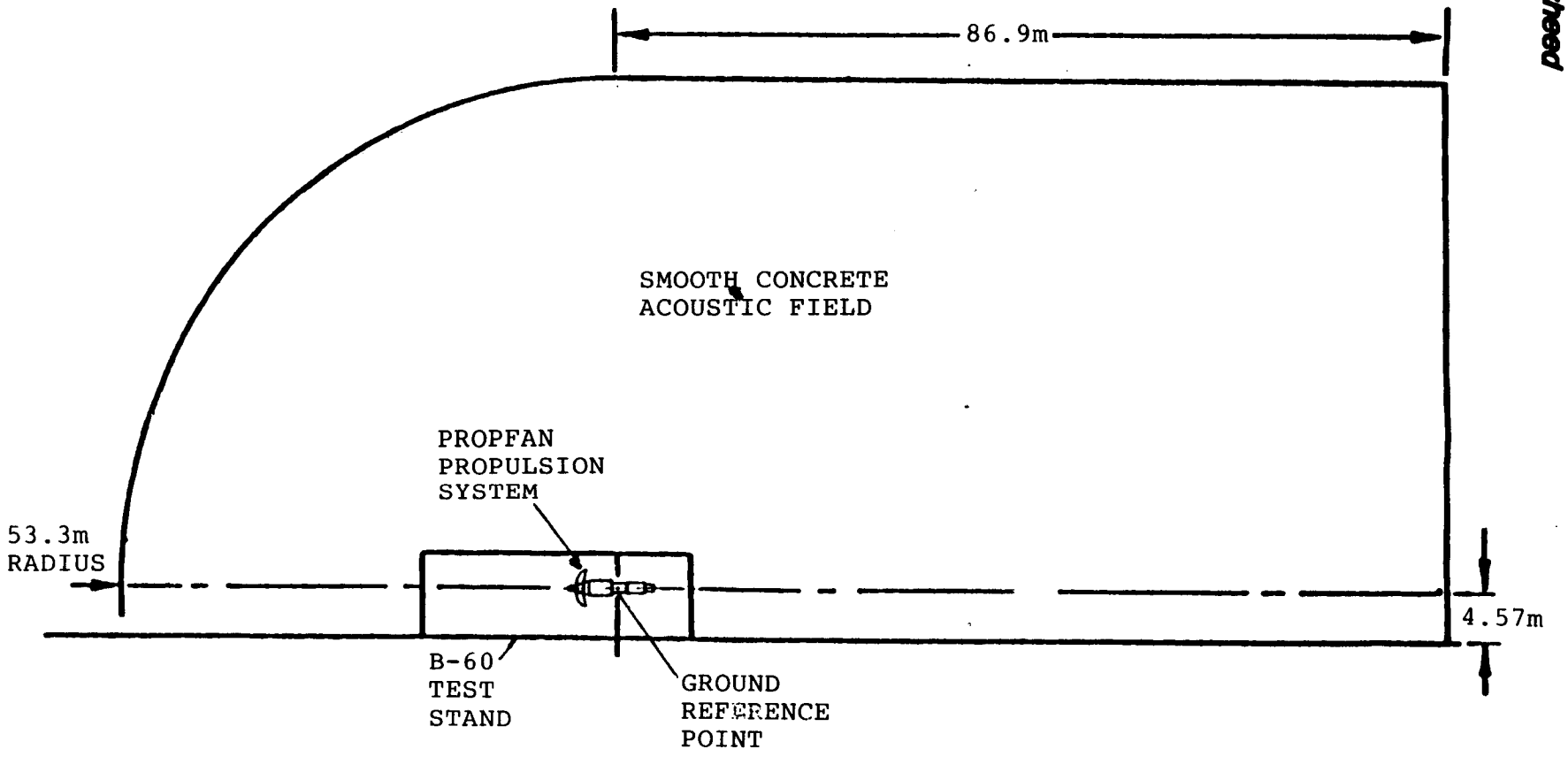

Figure 5.3 B-60 Test Stand Acoustic Field

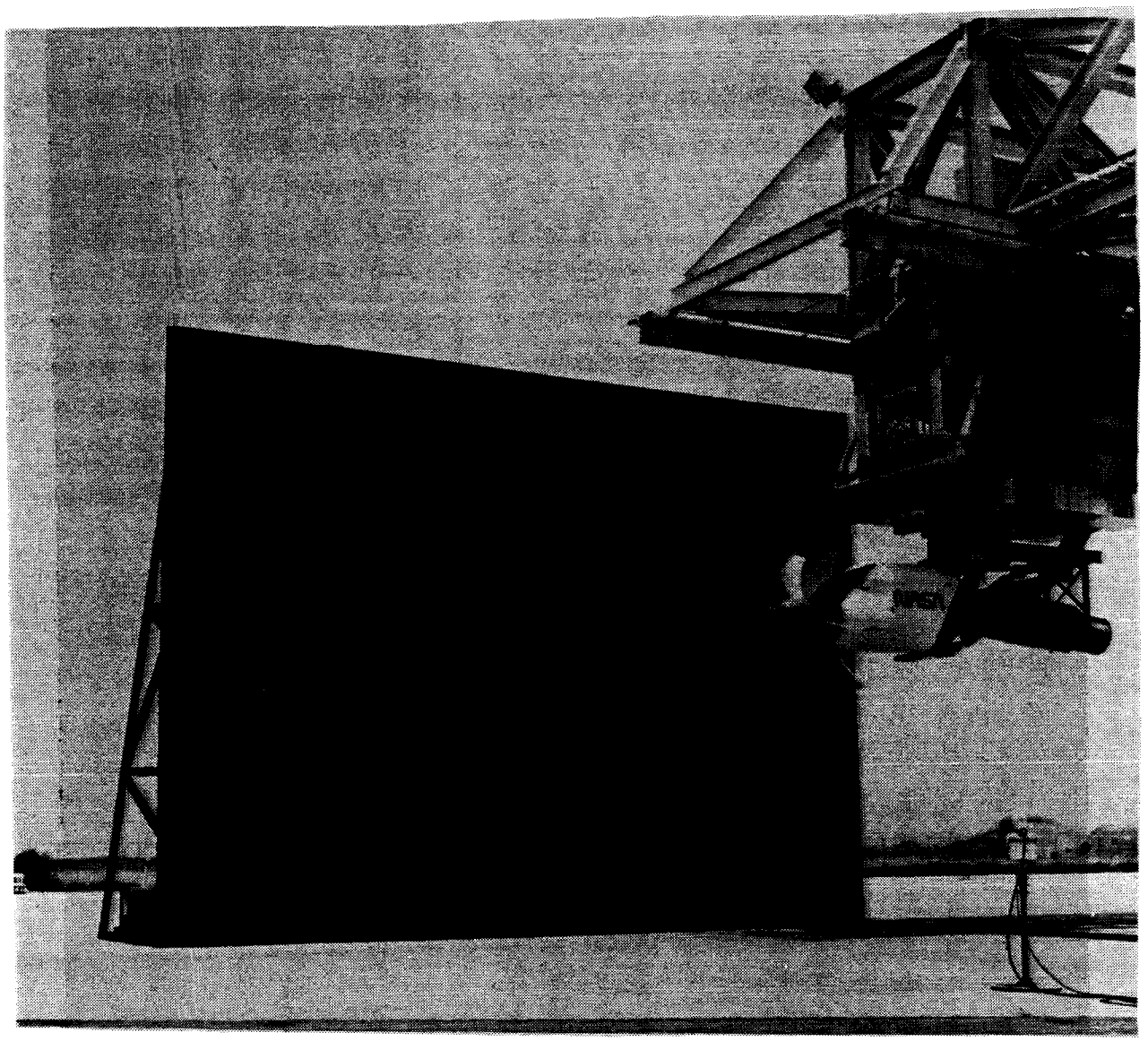

Figure 5.4. PTA Static Test Mounting Arrangement - Acoustic Barrier in Forward Position

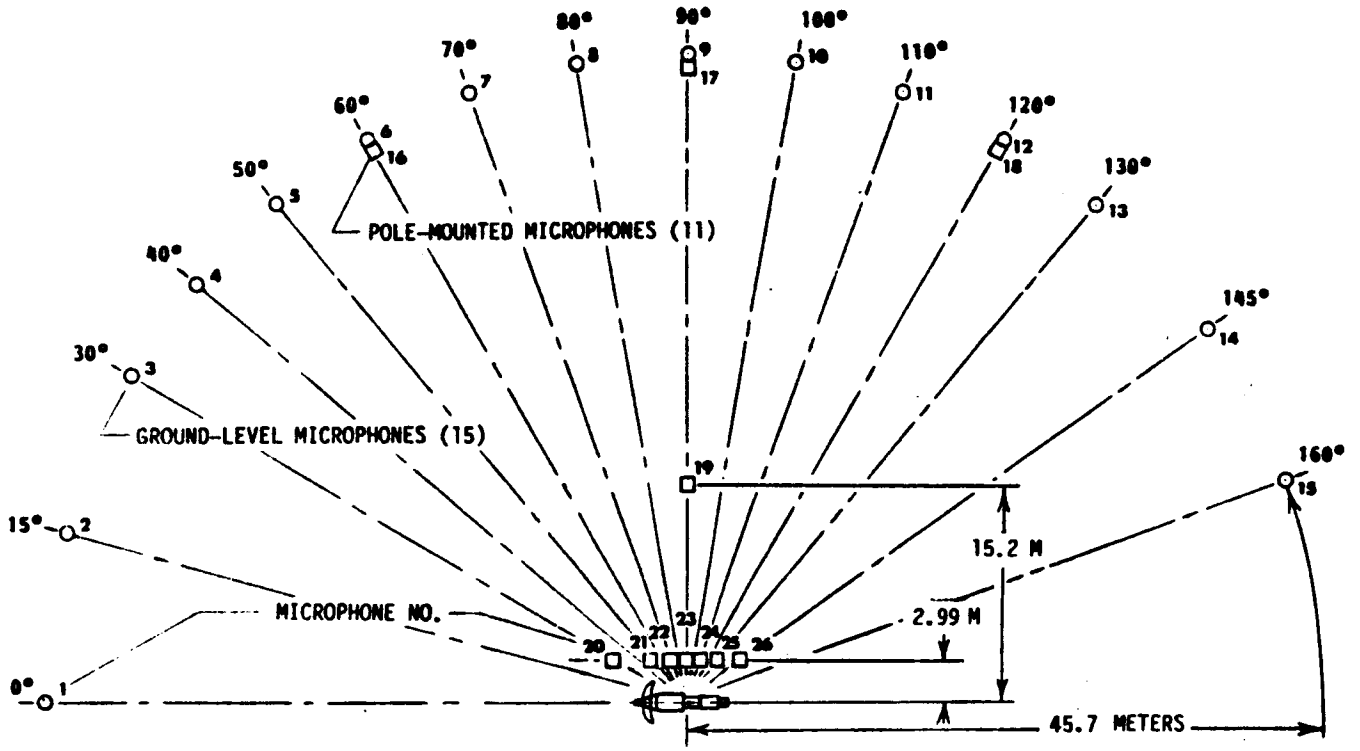

Figure 5.5. Sound Field Microphone Positions

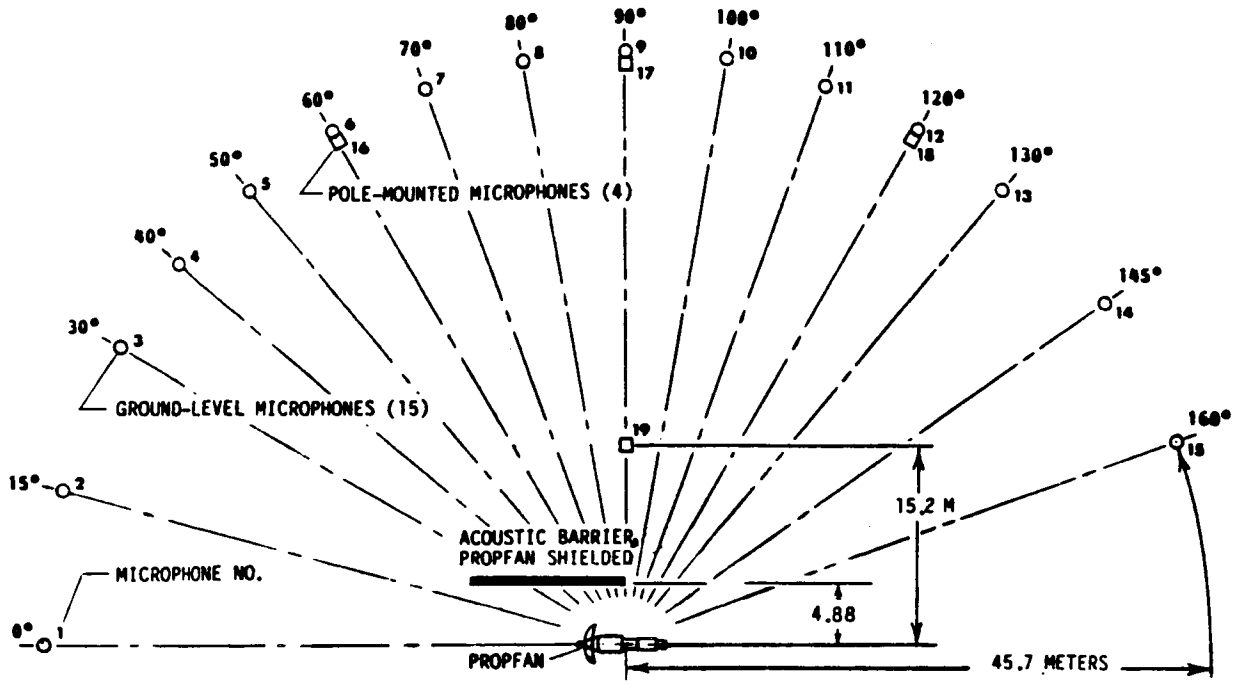

Figure 5.6 Sound Field Arrangement - Acoustic Barrier in Forward Position

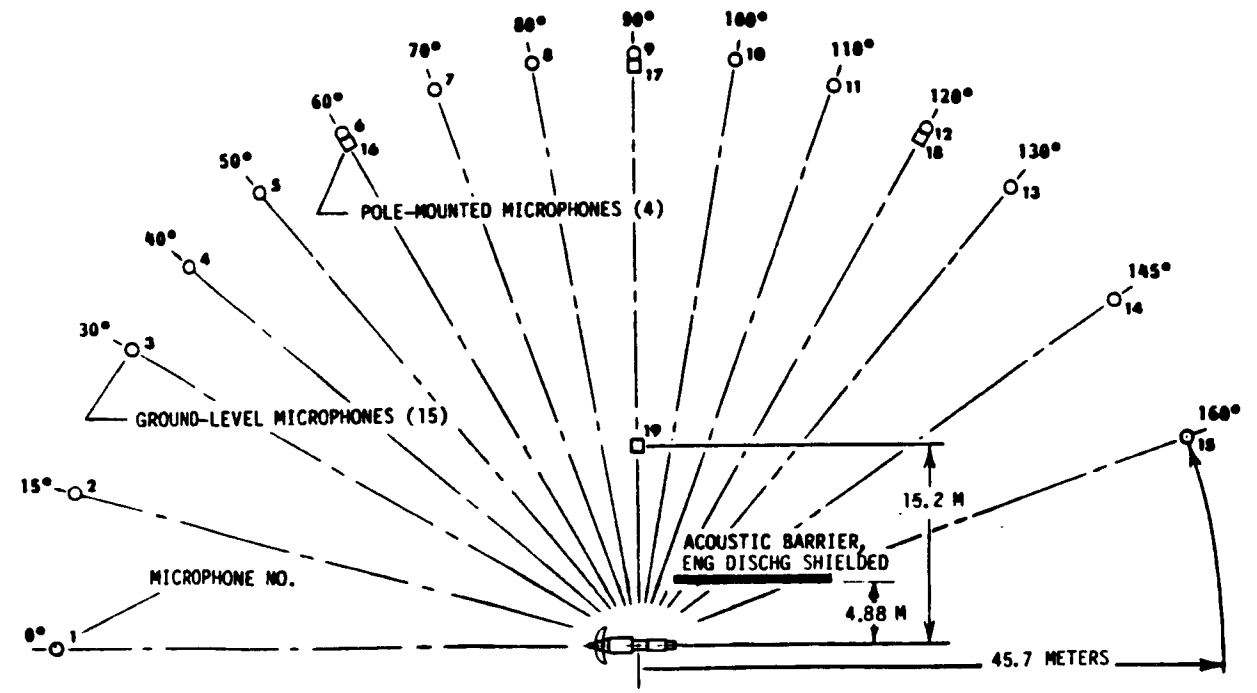

Figure 5.7 Sound Field Arrangement - Acoustic Barrier in Aft Position

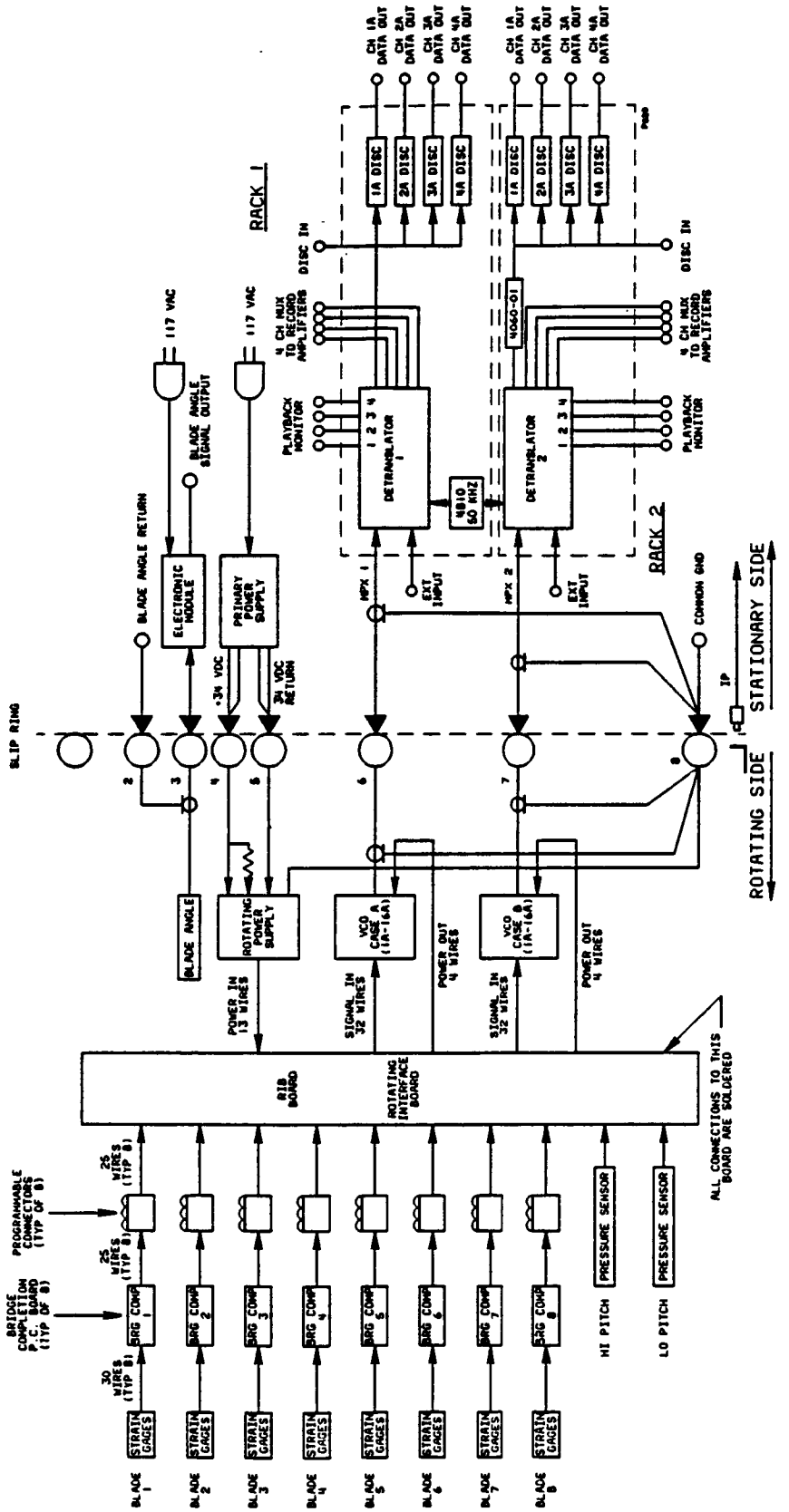

Figure 6.1. Propfan Instrumentation Schematic

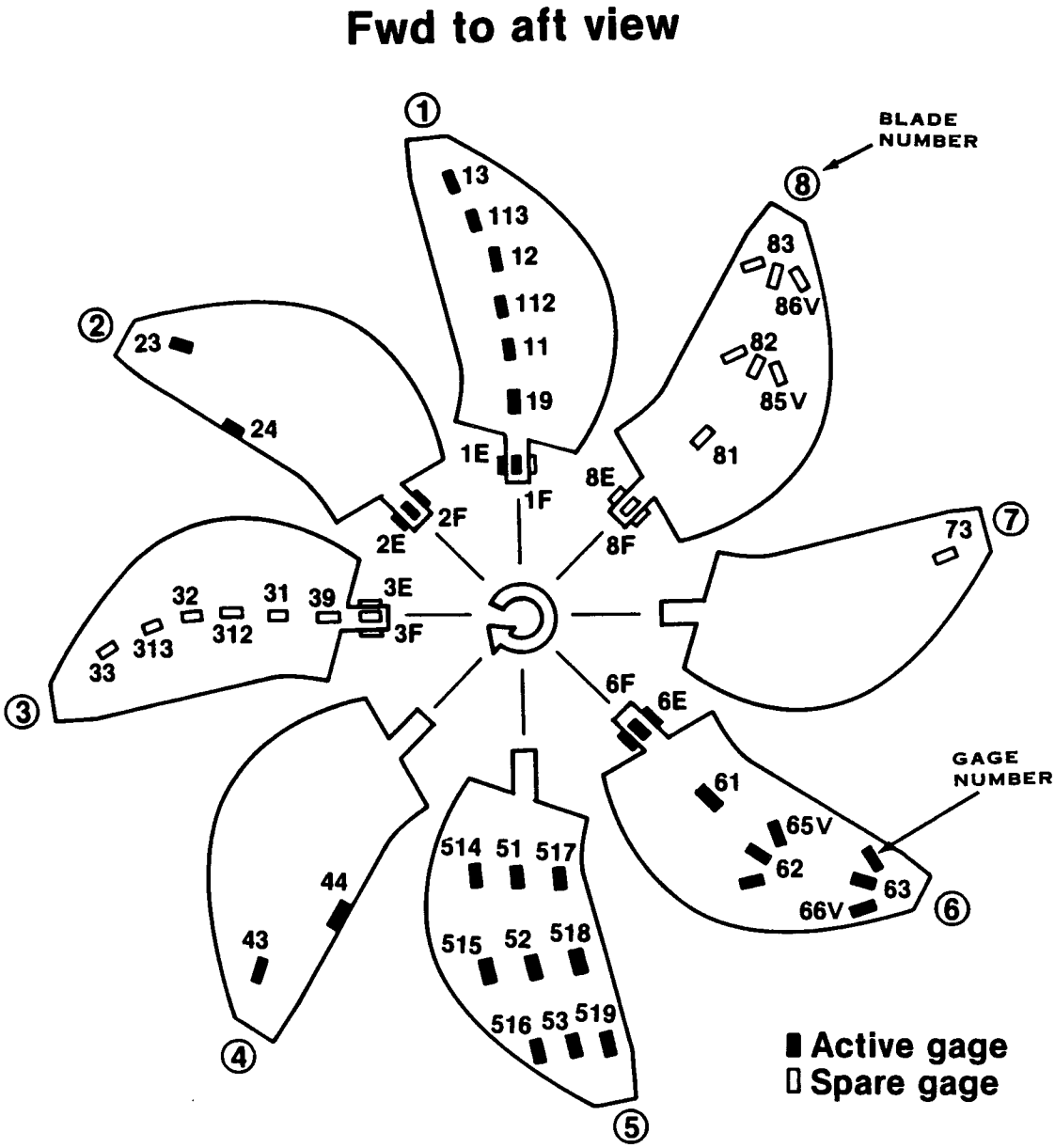

Figure 6.2. SR-7L Propfan Strain Gage Locations

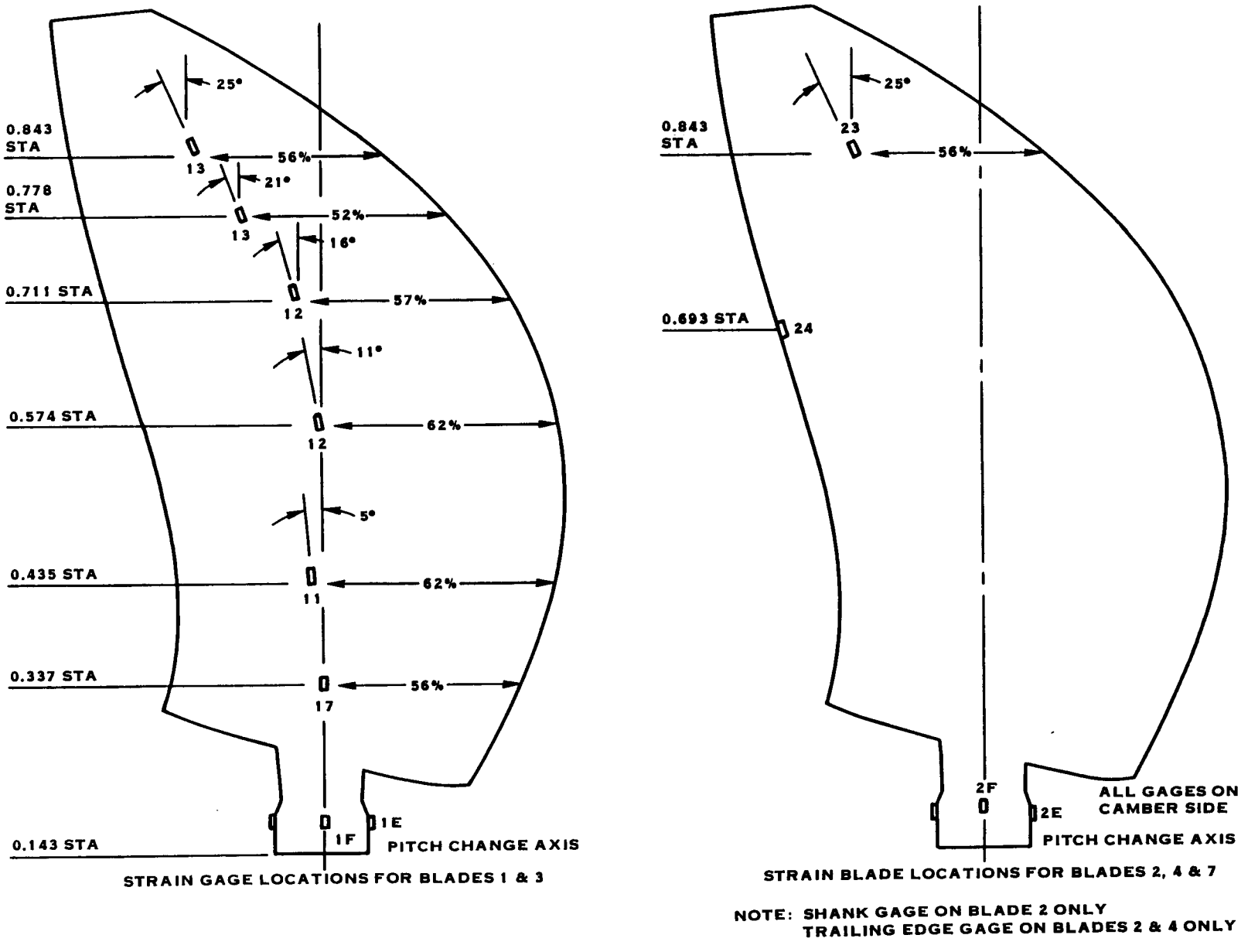

Figure 6.3. SR-7L Blade Strain Gage Locations

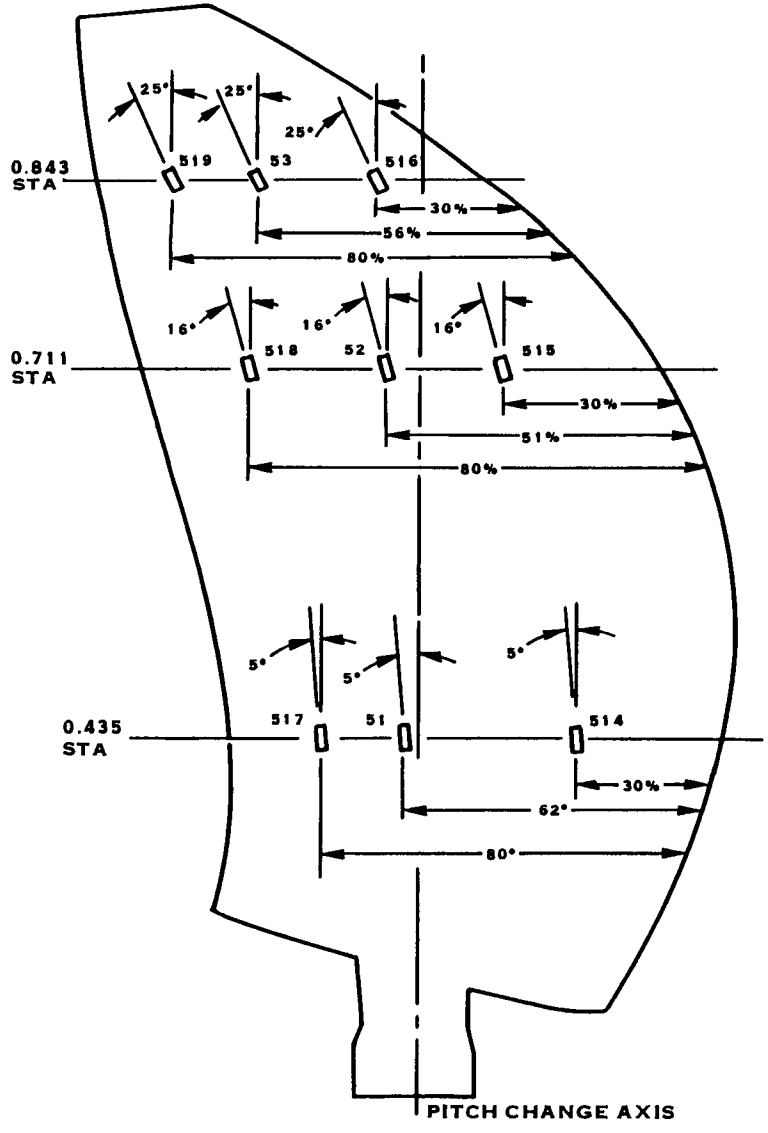

STRAIN GAGE LOCATIONS FOR BLADE 5

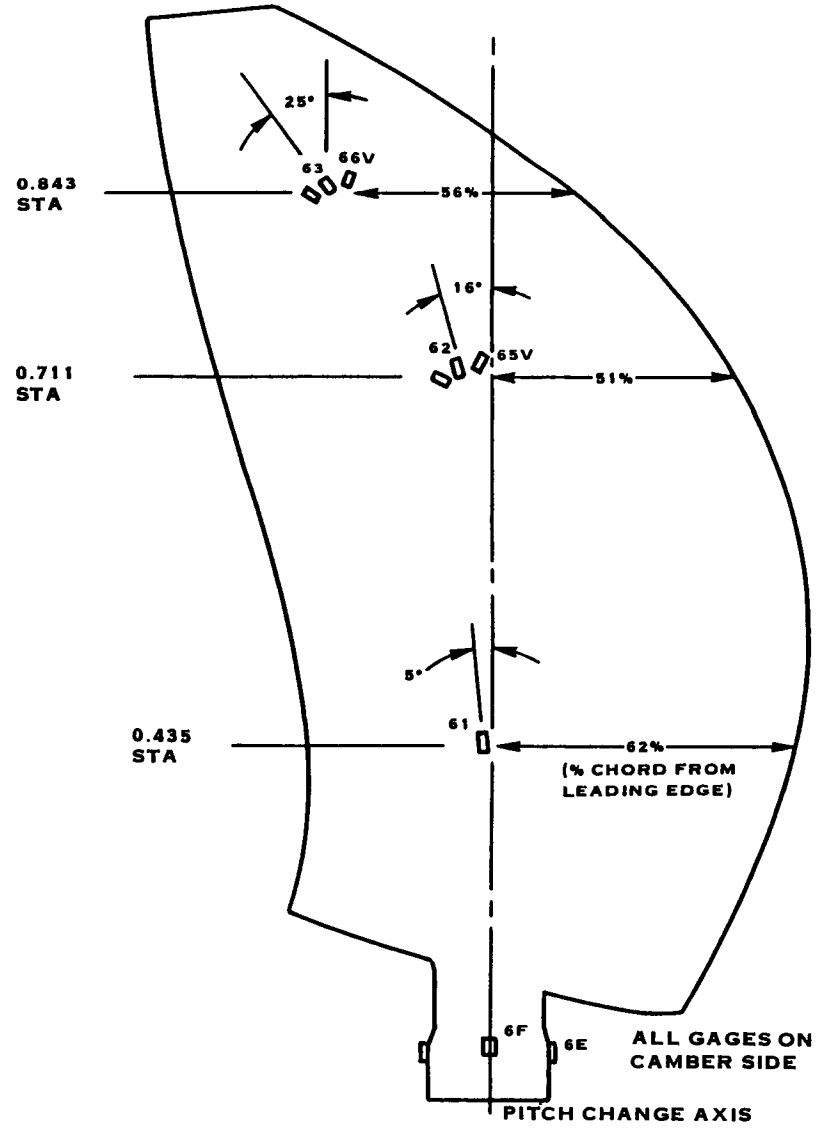

STRAIN GAGE LOCATIONS FOR BLADES 6 & 8

Figure 6.4. SR-7L Blade Strain Gage Locations

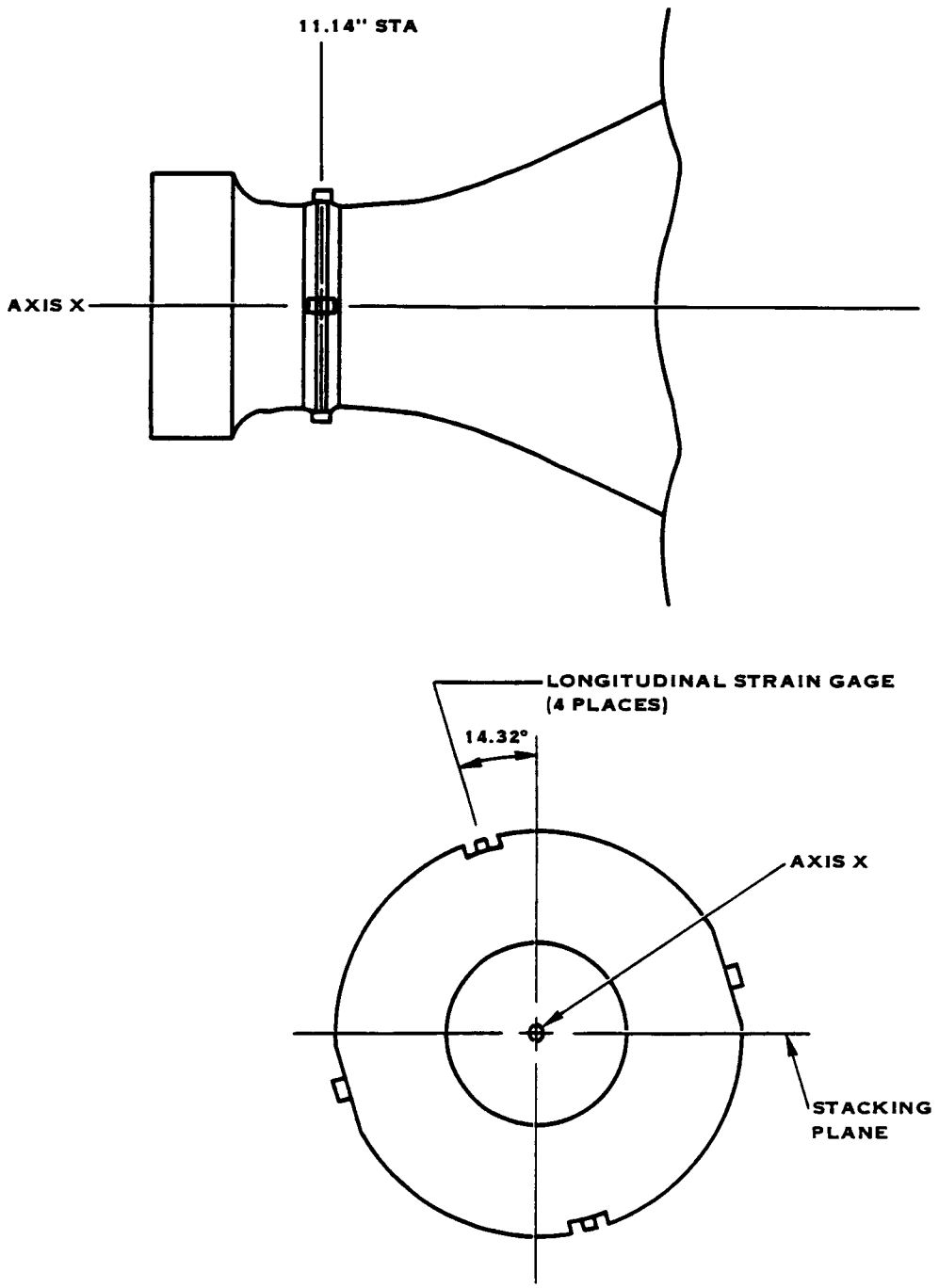

Figure 6.5. SR-7L Shank Strain Gage Locations

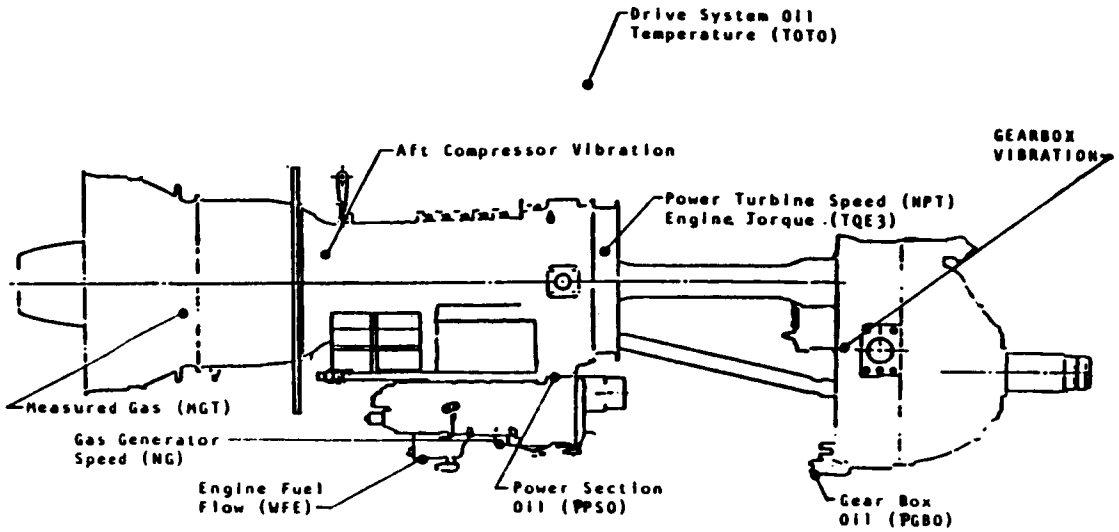

Figure 6.6. Drive System Operational Instrumentation

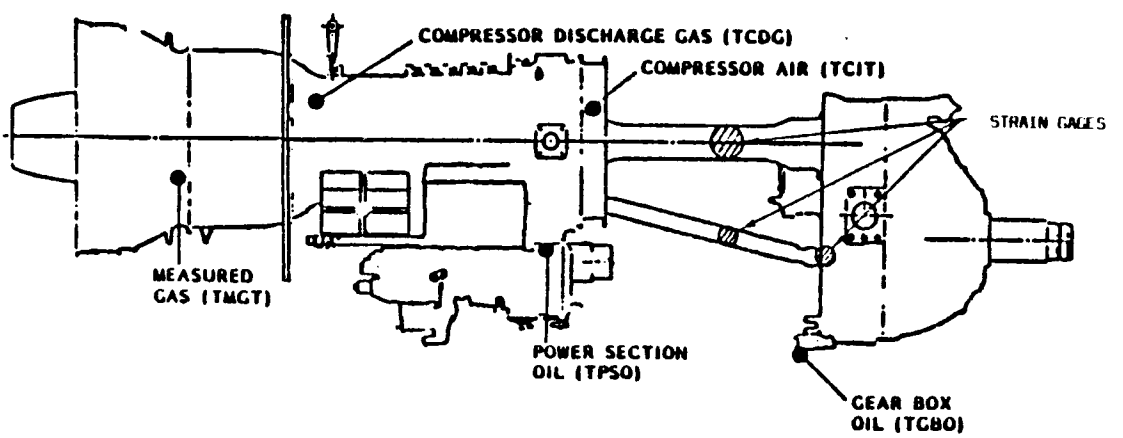

Figure 6.7. Drive System Strain Gage and Temperature Locations

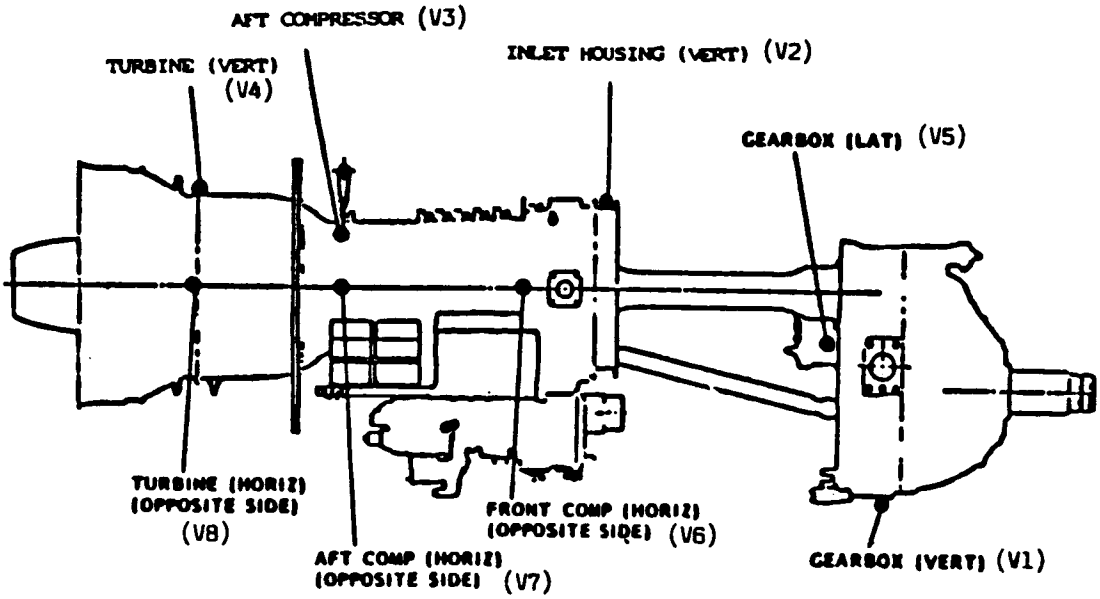

Figure 6.8. Drive System Vibration Locations

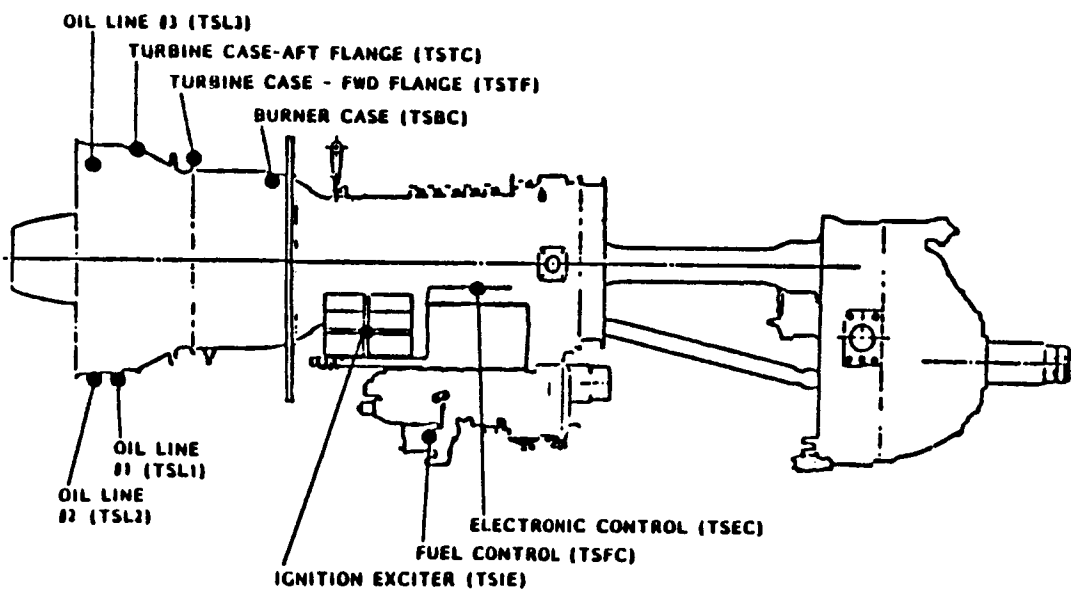

Figure 6.9. Drive System Temperature Locations

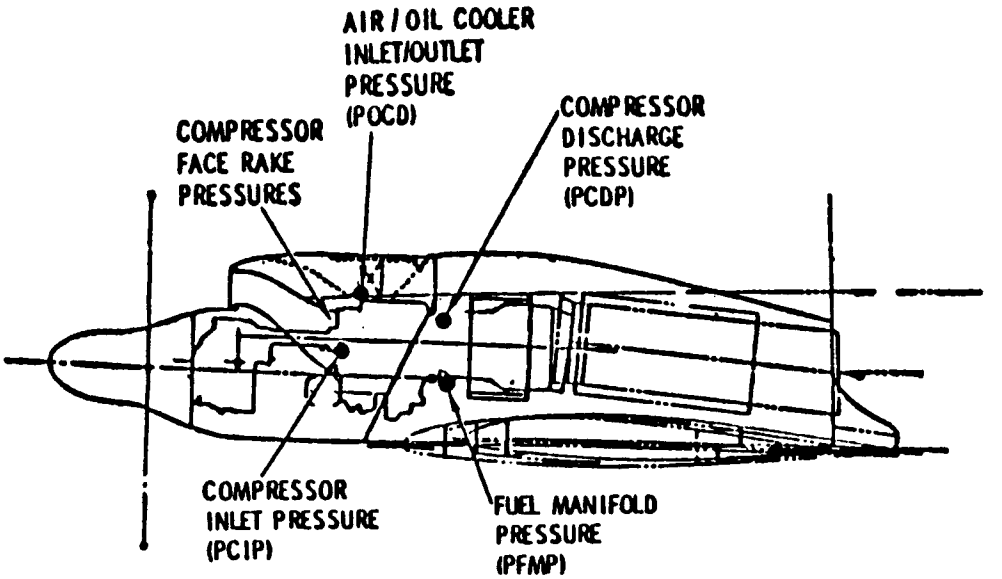

Figure 6.10. Drive System Pressure Transducer Locations

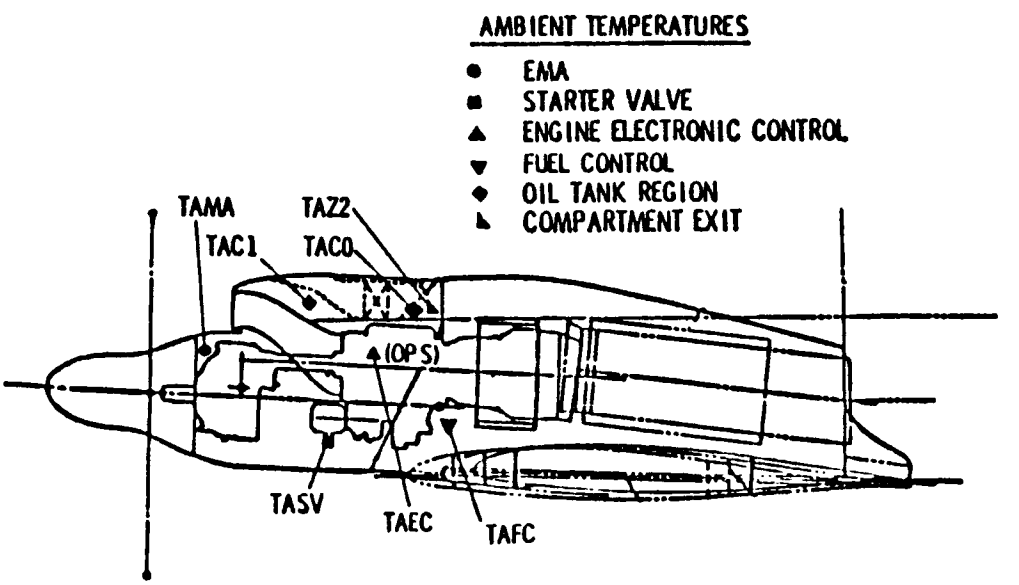

Figure 6.11. QEC Ambient Temperatures

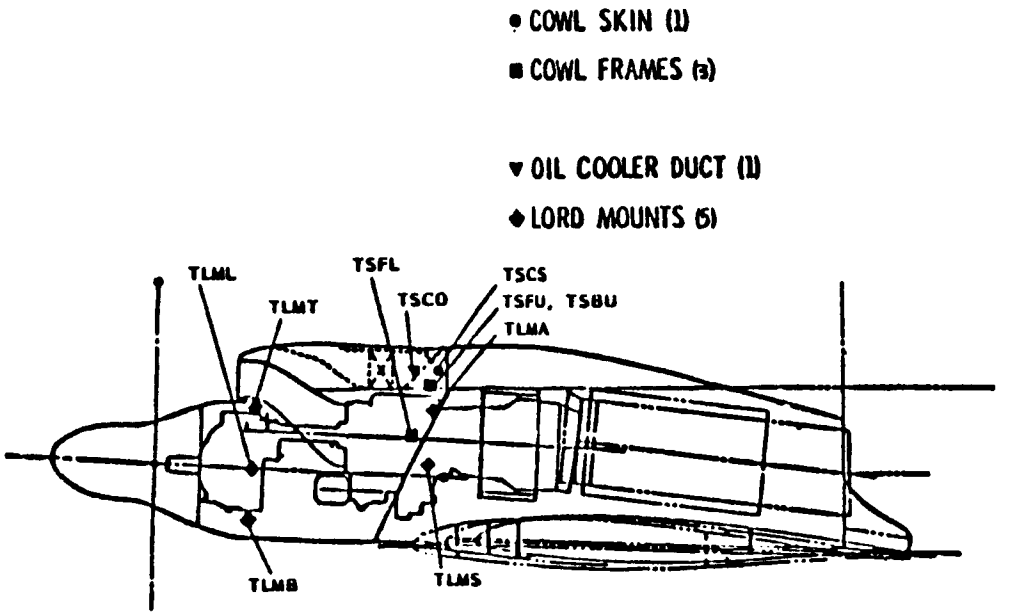

Figure 6.12. QEC Structural Temperatures

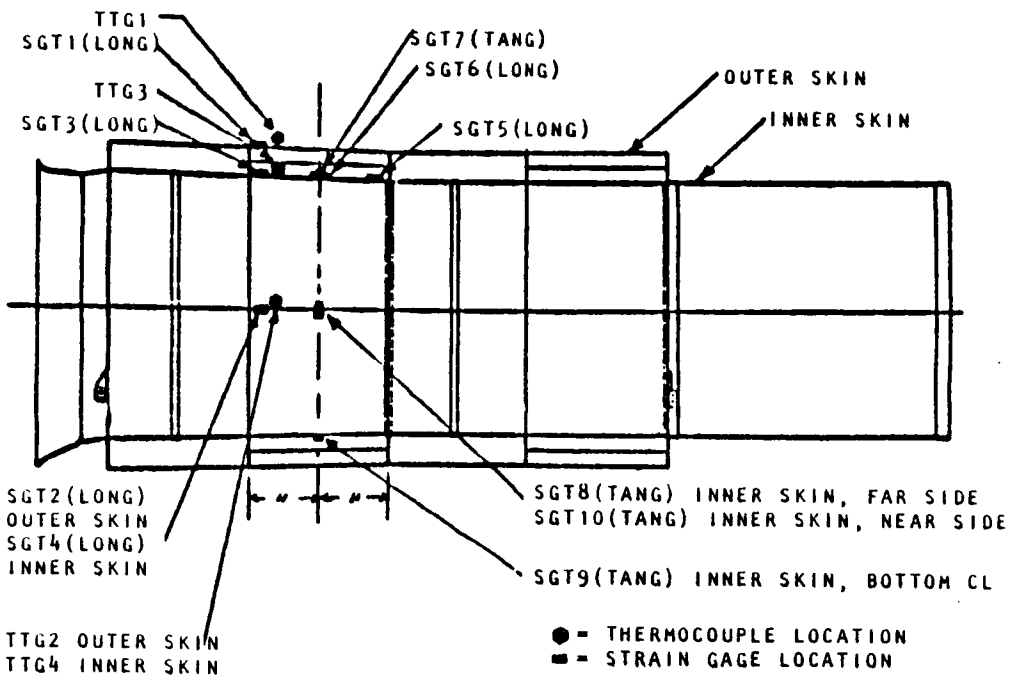

Figure 6.13. Acoustic Tailpipe Instrumentation

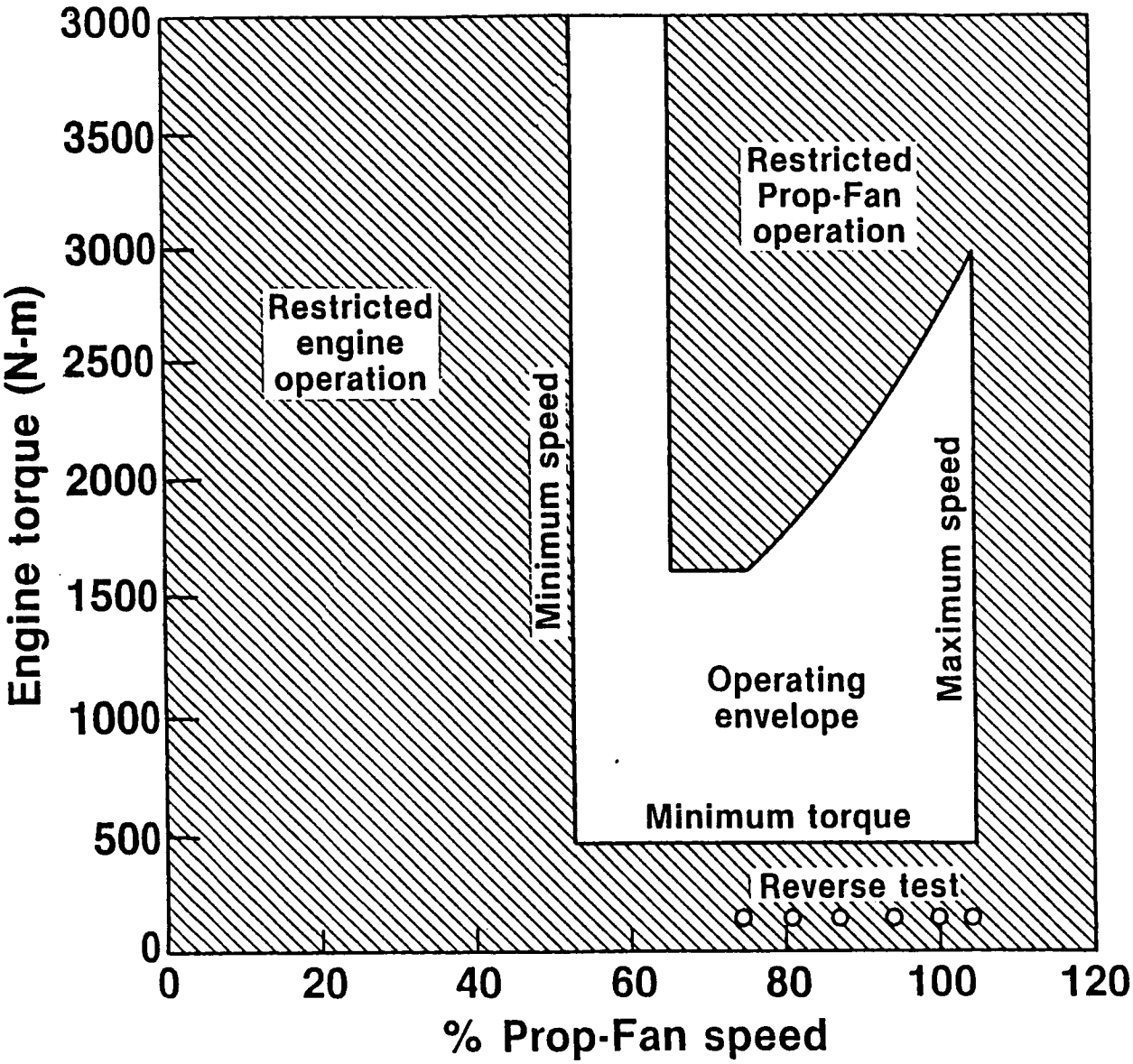

Figure 7.1. Static Test Operating Limitations

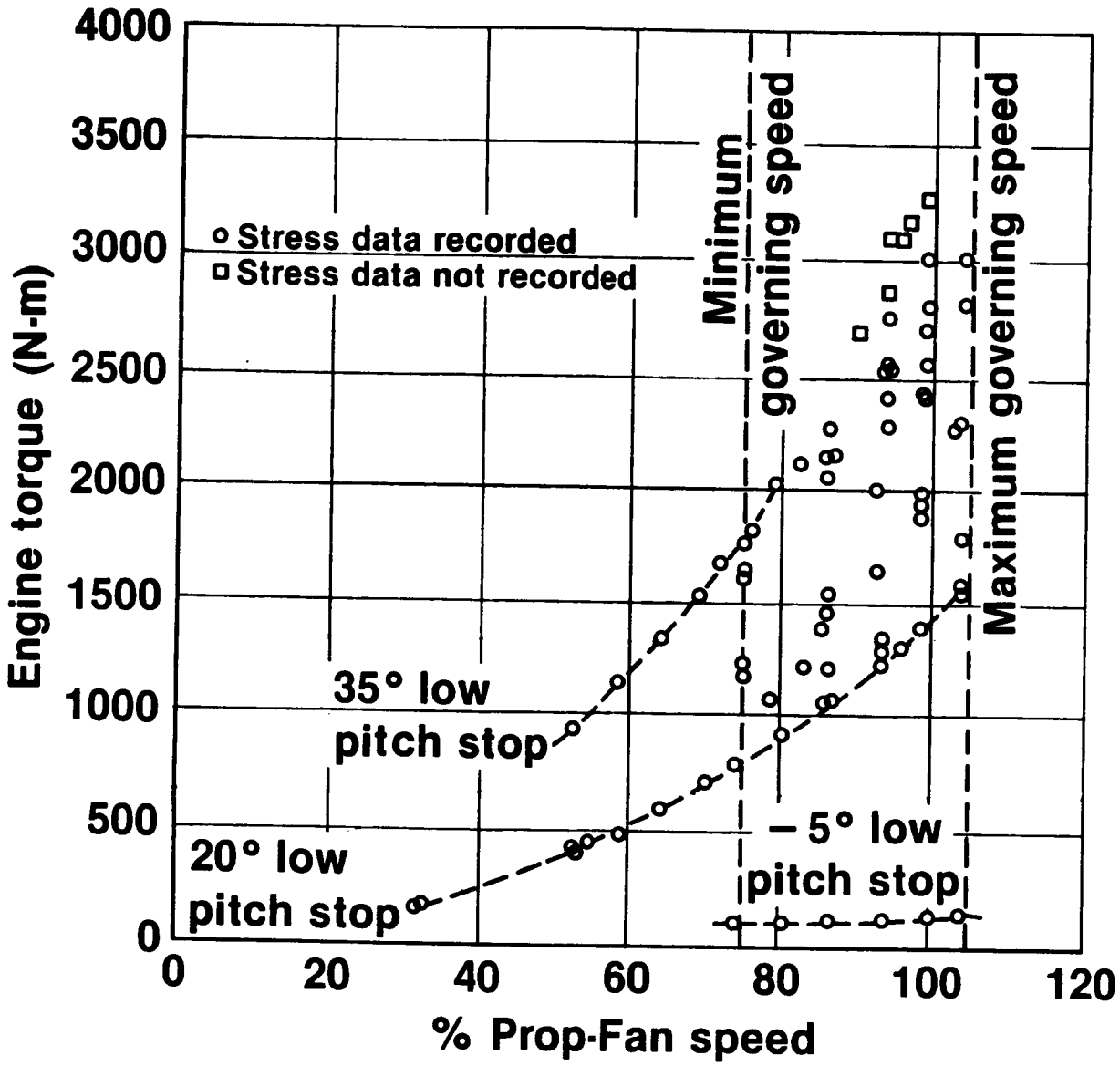

Figure 8.1. Stress Survey Test Points

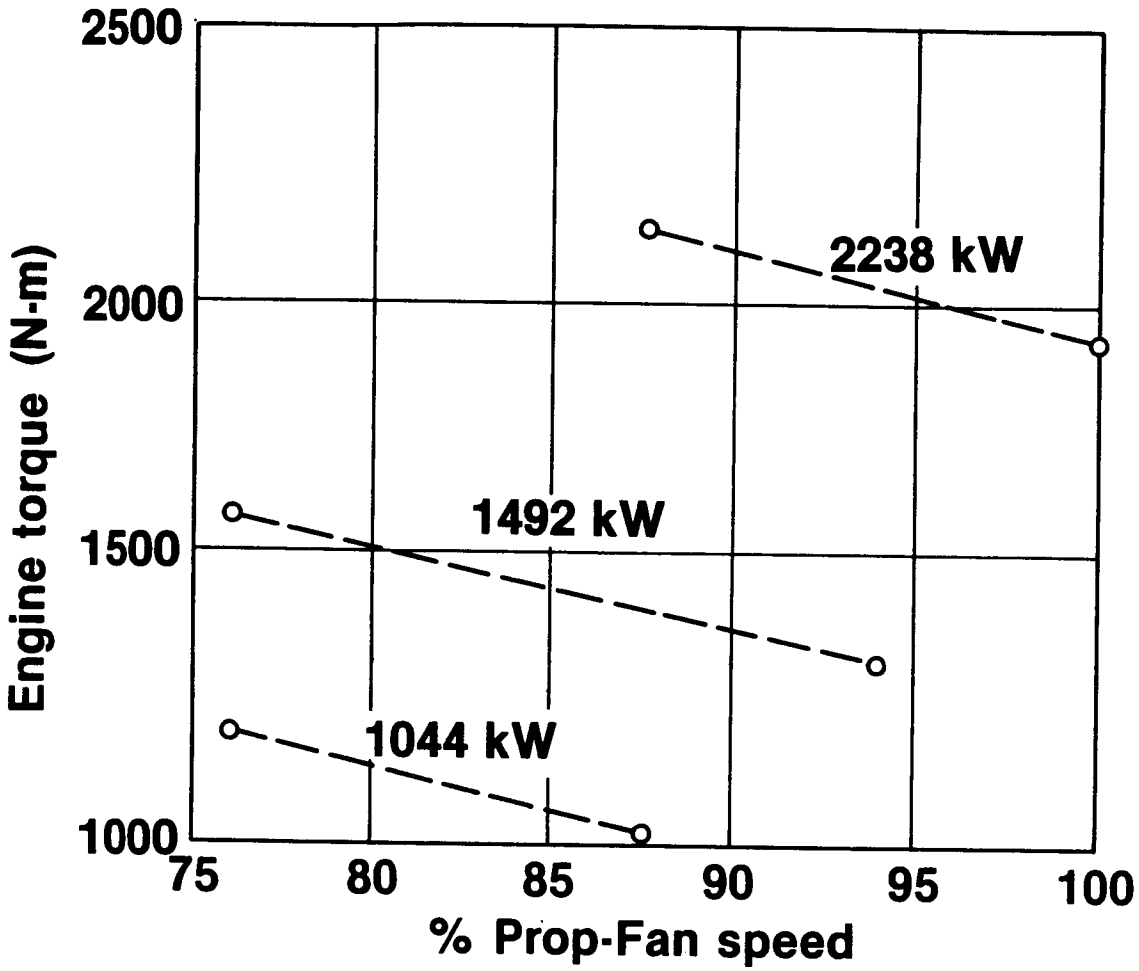

Figure 8.2. Speed Transient Conditions

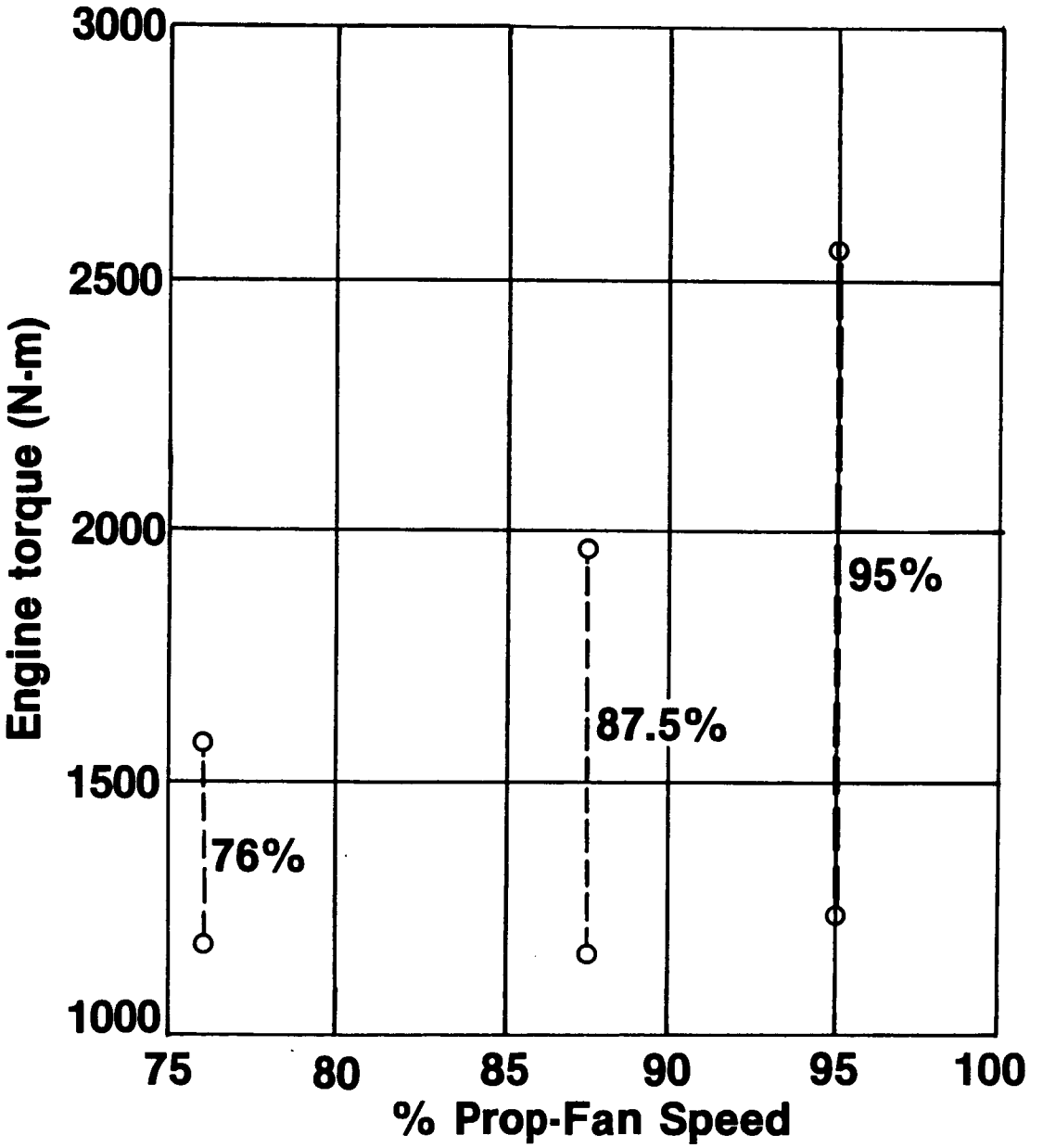

Figure 8.3. Power Transient Conditions

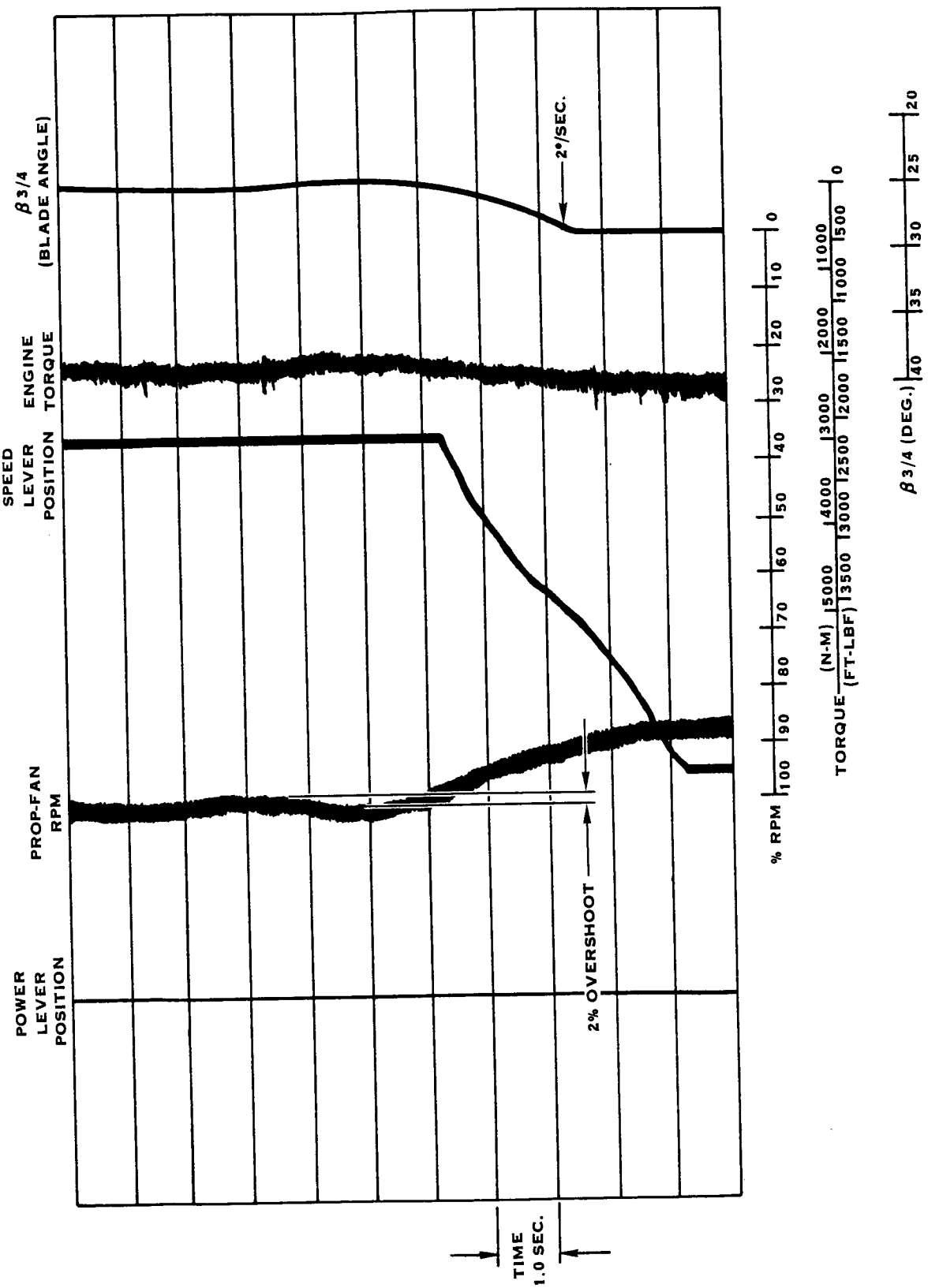

Figure 8.4. 4 Second Speed Lever Traverse - 87.5% to 100% Speed, 2238 kW

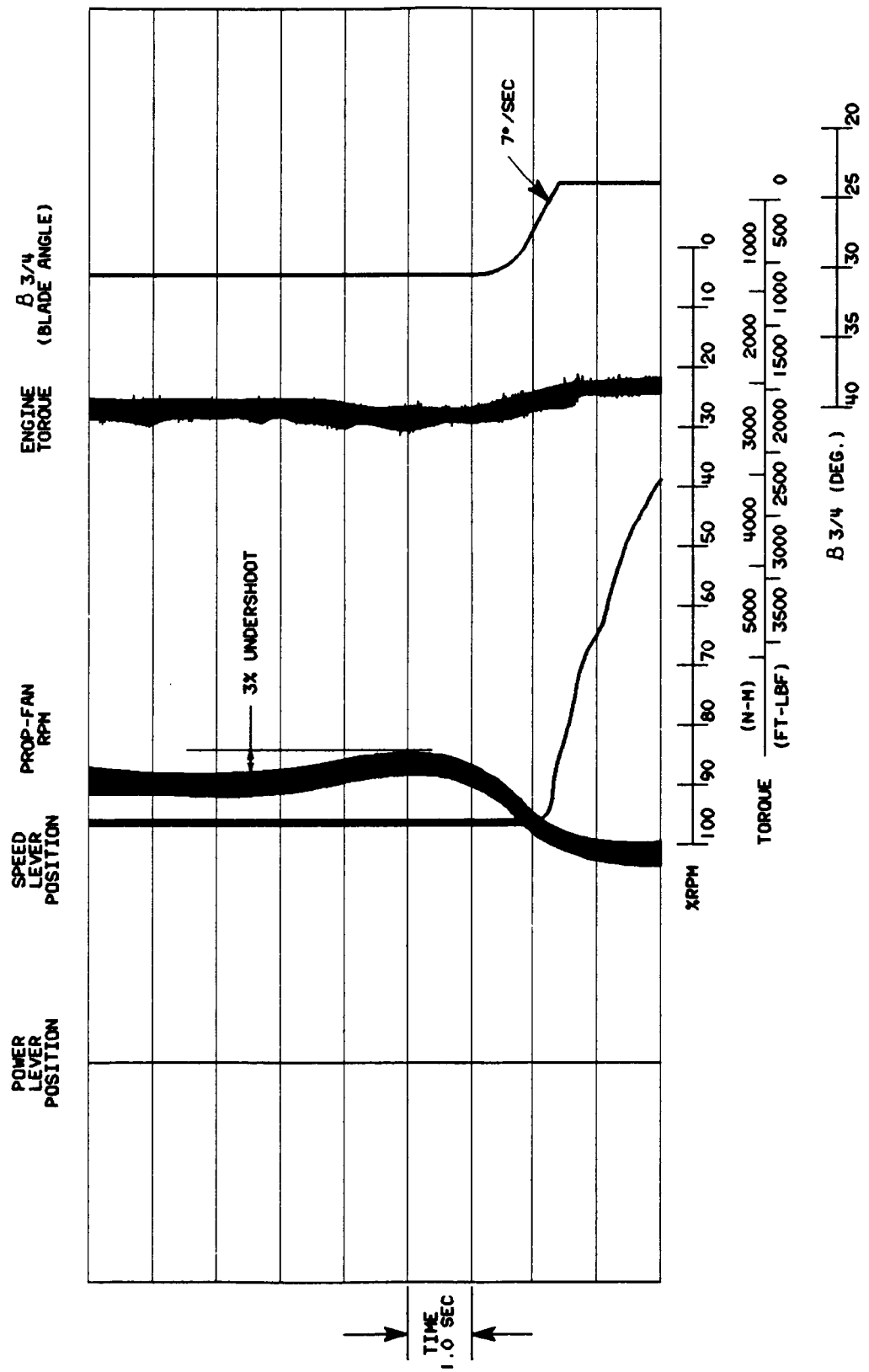

Figure 8.5. 2 Second Speed Lever Traverse - 100% to 87.5% Speed, 2238 KW

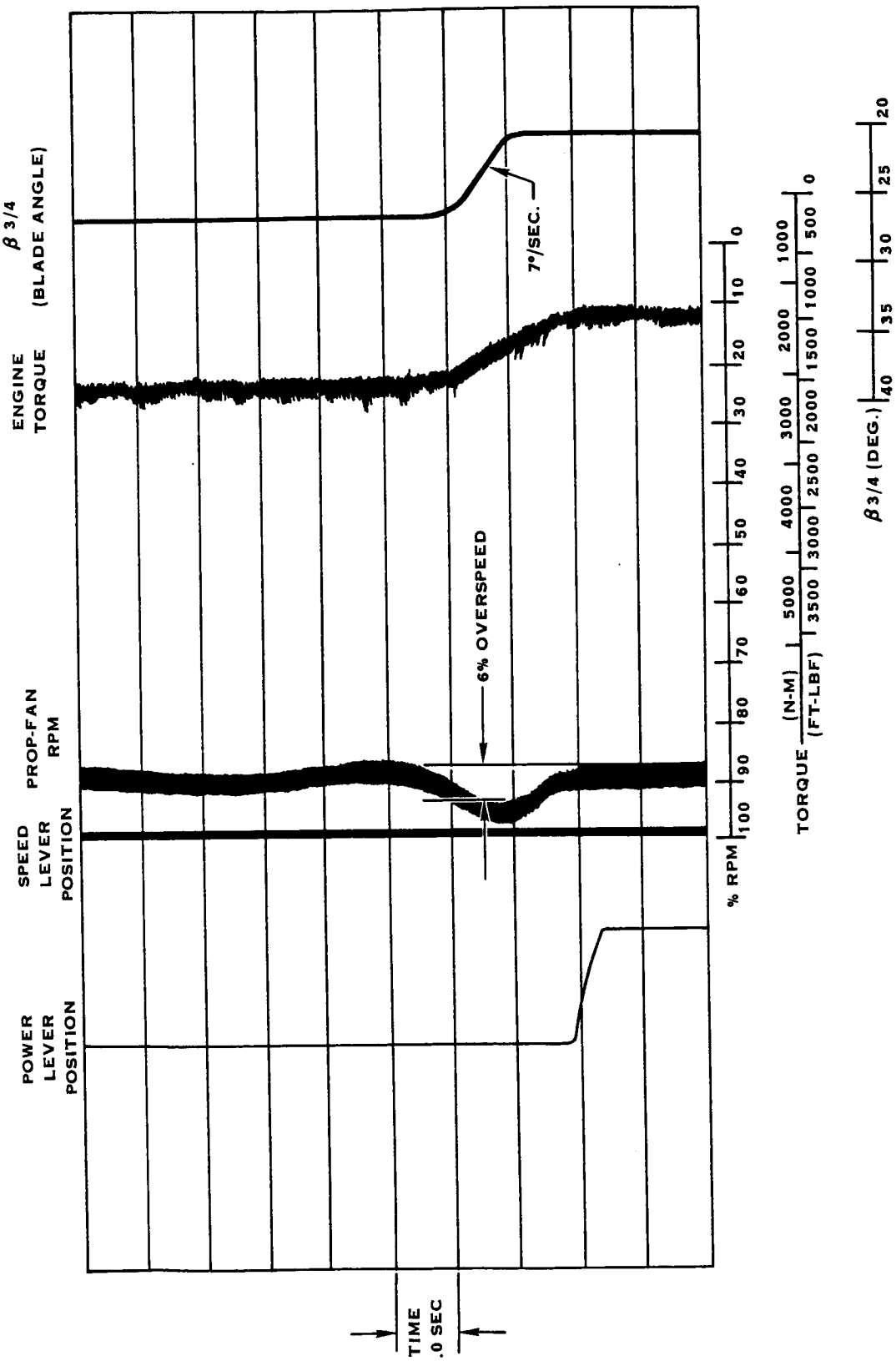

Figure 8.6. Step Change in Power Lever Position - 1268 kW to 2089 kW, 87.5% Speed

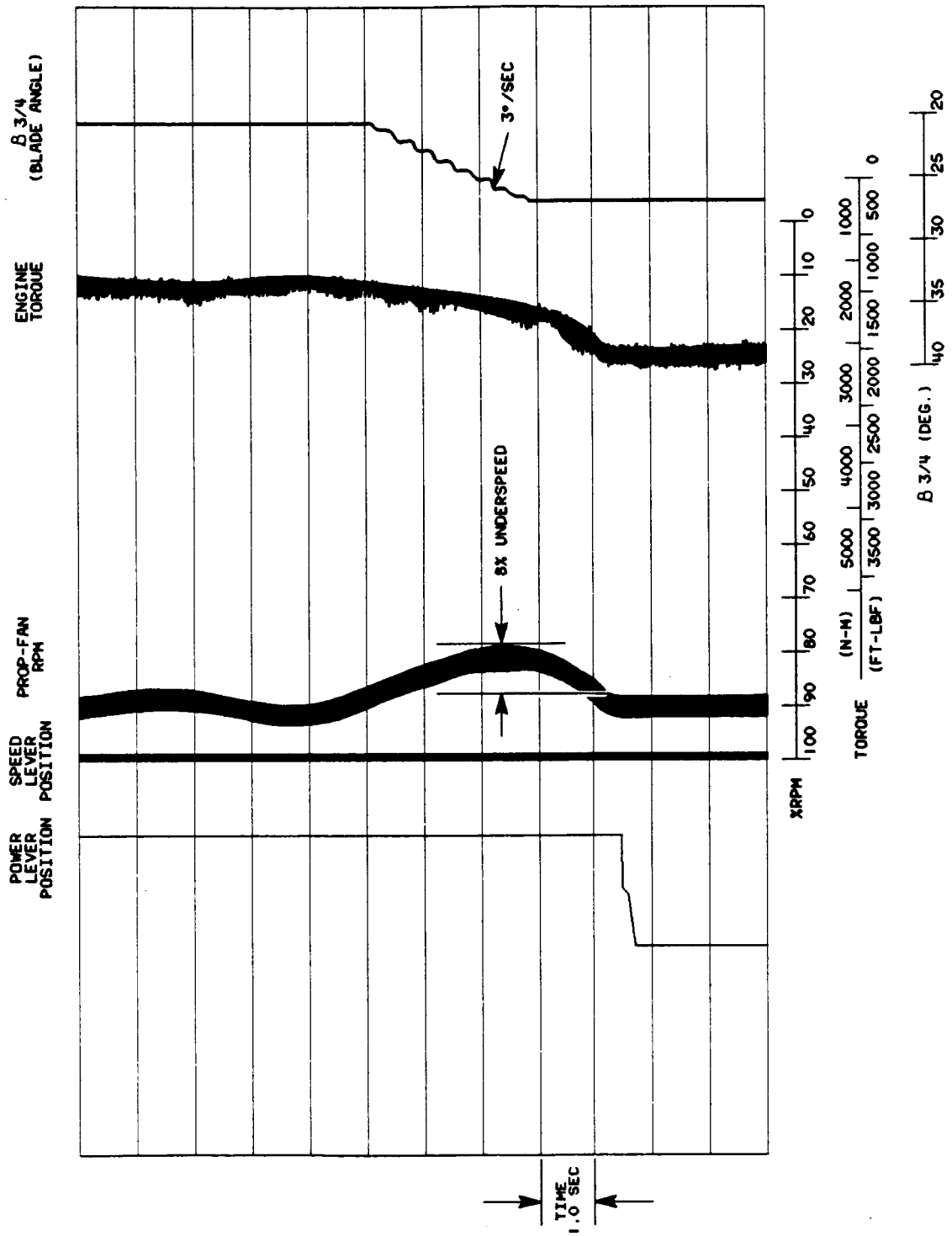

Figure 8.7. Step Change in Power Lever Position - 2089 kW to 1268 kW, 87.5% Speed

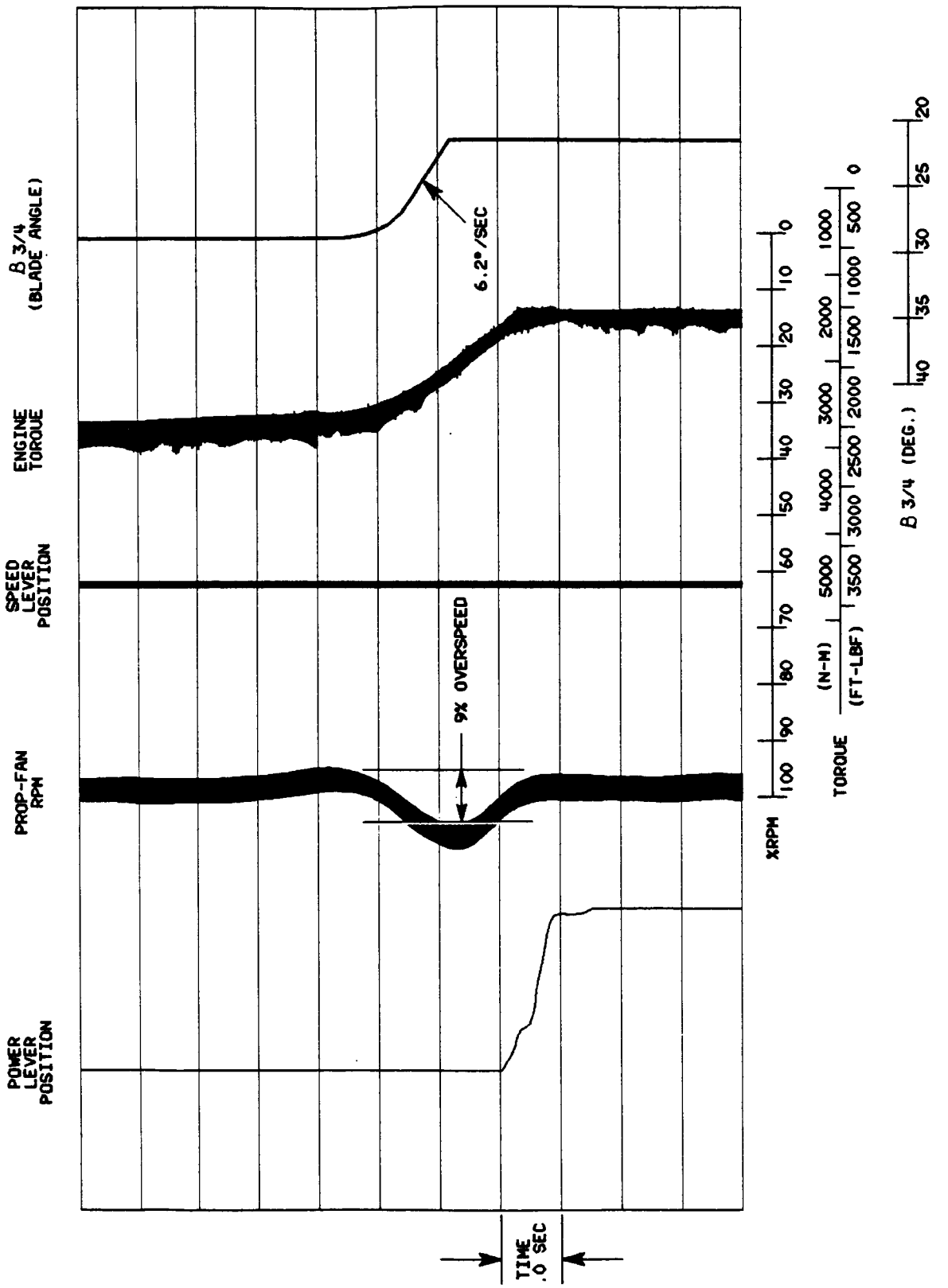

Figure 8.8. 1 Second Power Lever Transient - 1350 kW to 2700 kW, 95% Speed

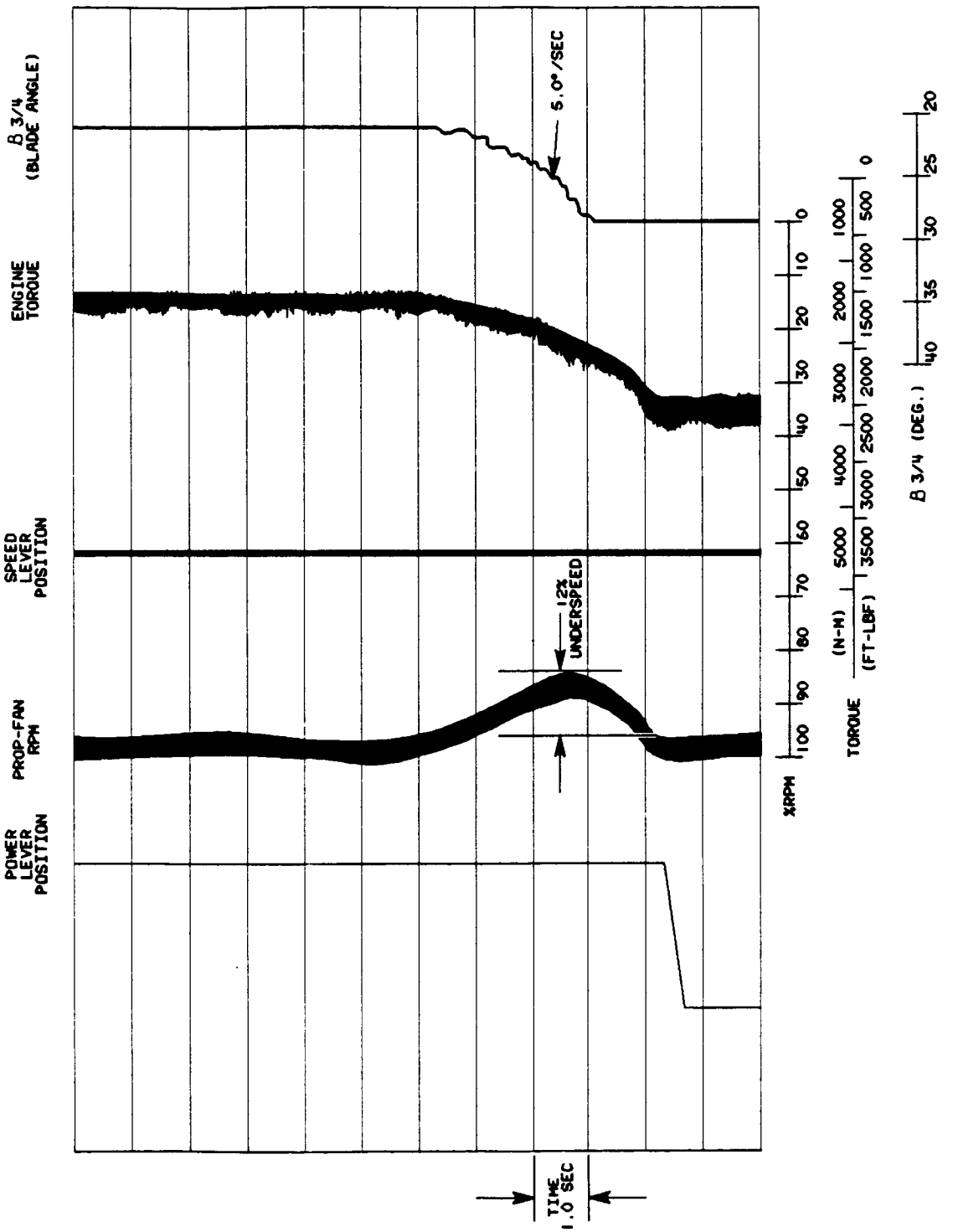

Figure 8.9. Step Change in Power Lever Position - 2700 kW to 1350 kW, 95% Speed

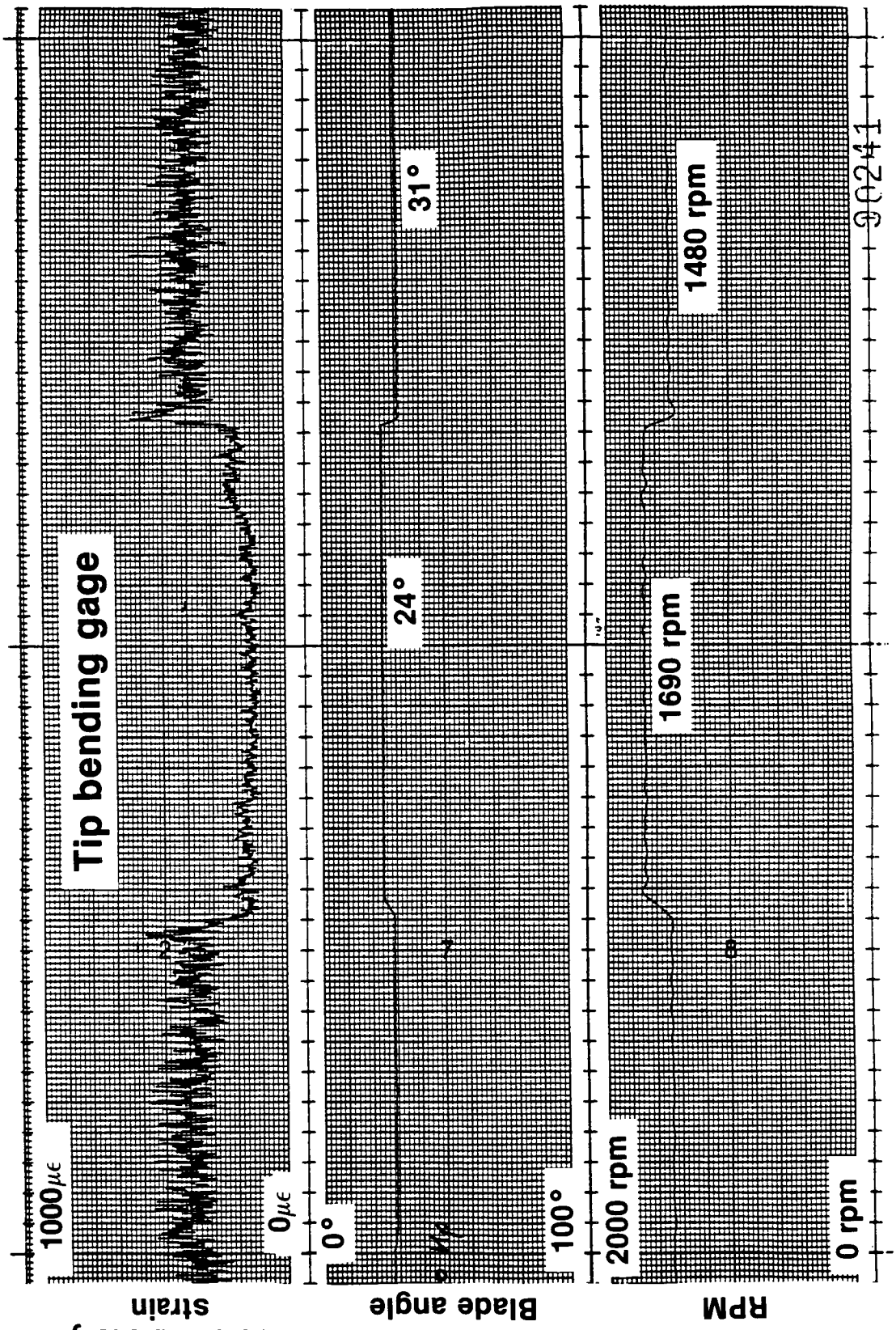

Figure 8.10. Fast Speed Lever Transient - 2240 kW

ORIGINAL PAGE IS
OF POOR QUALITY

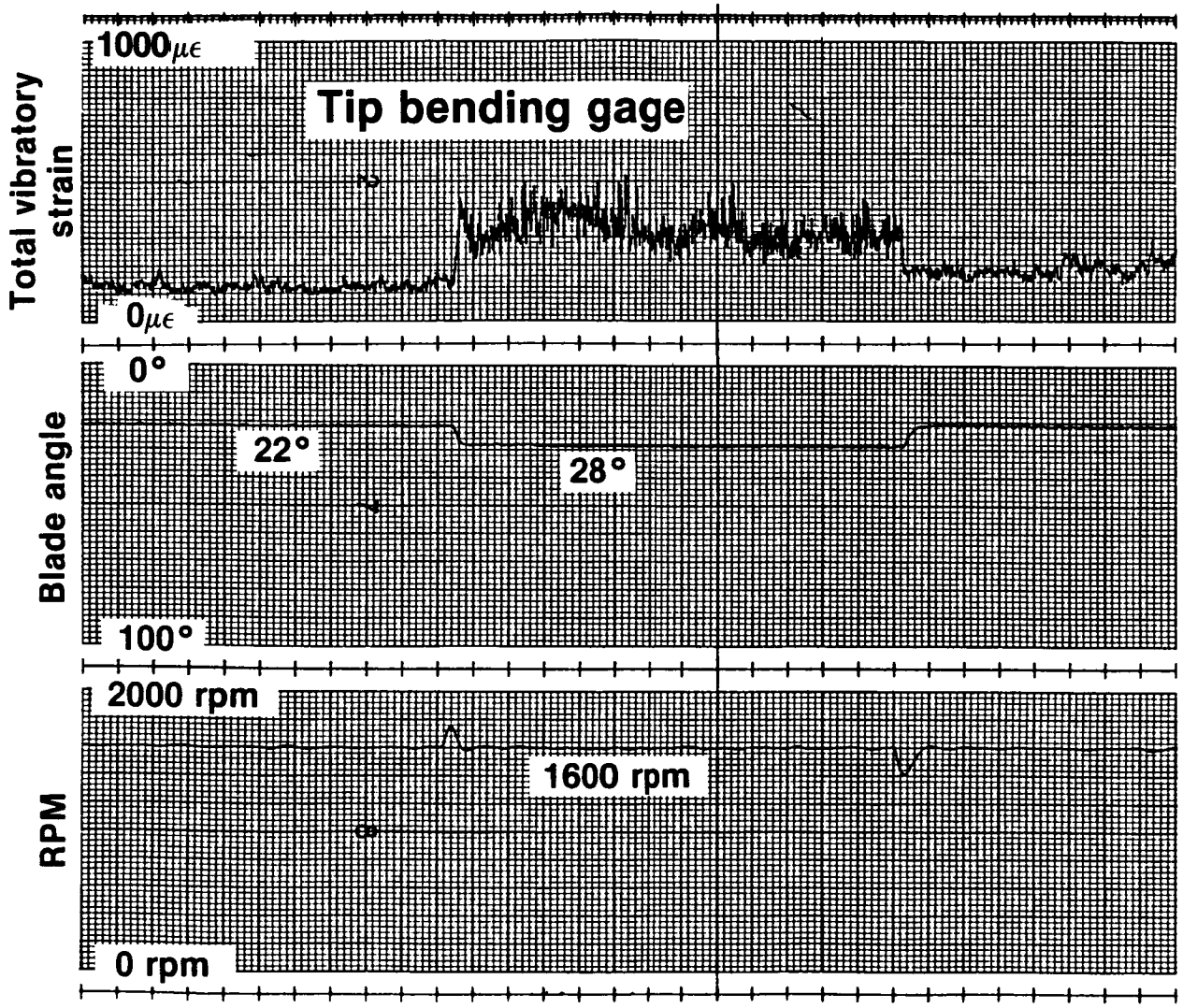

Figure 8.11. Fast Power Lever Transient - 95% Speed

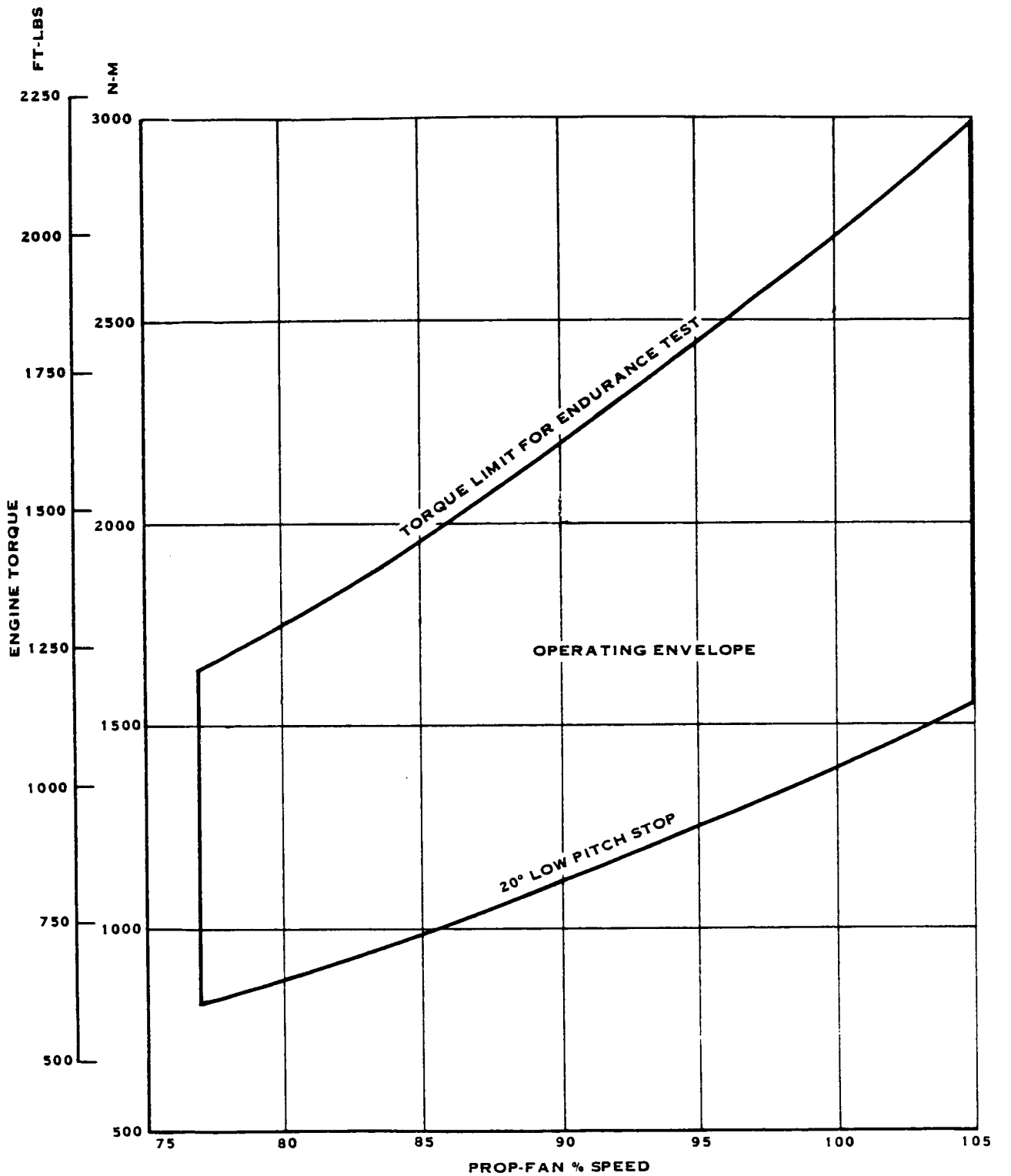

Figure 8.12. Operating Envelope for Endurance Test

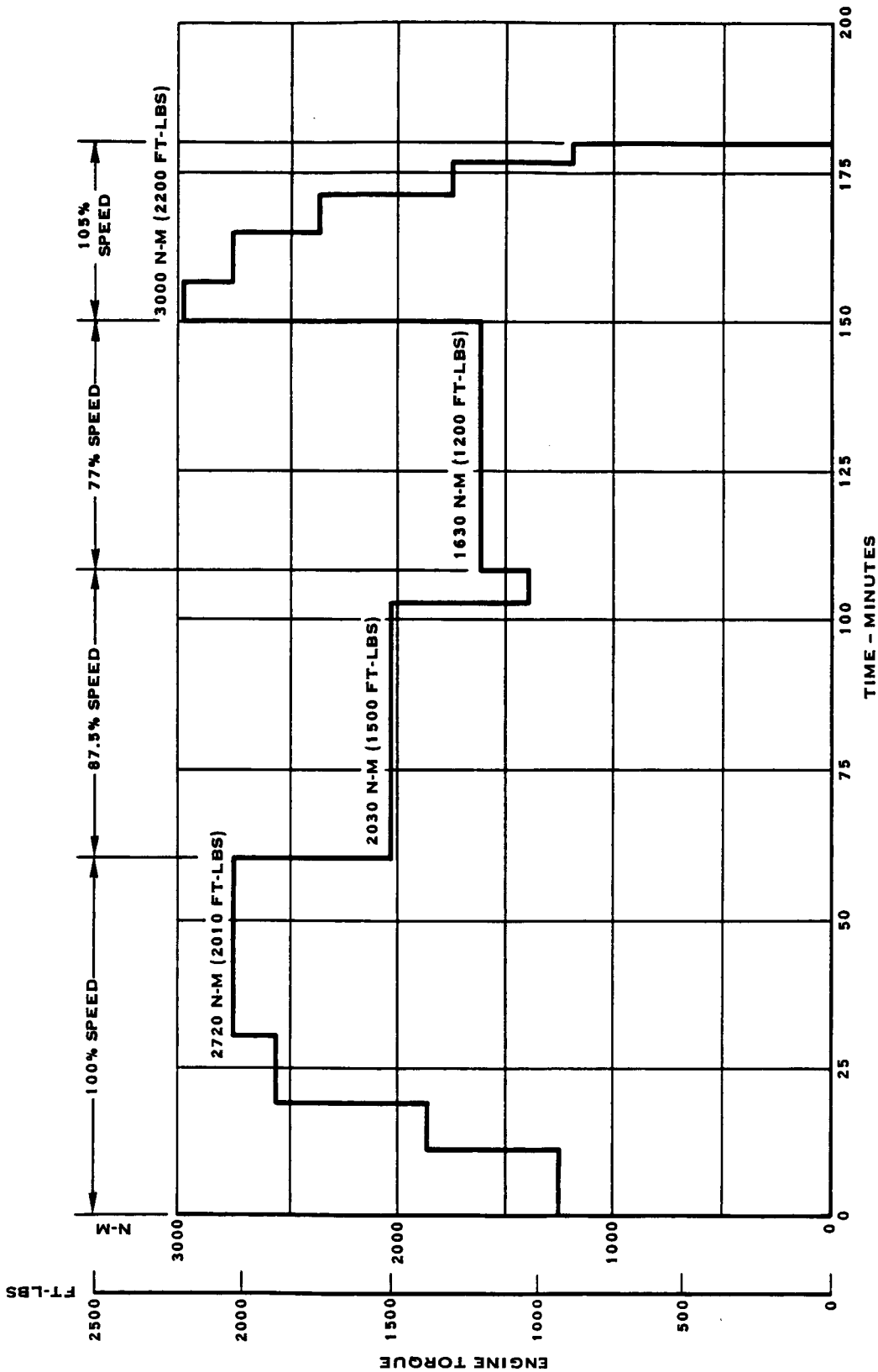

Figure 8.13. Simulated Flight Cycle

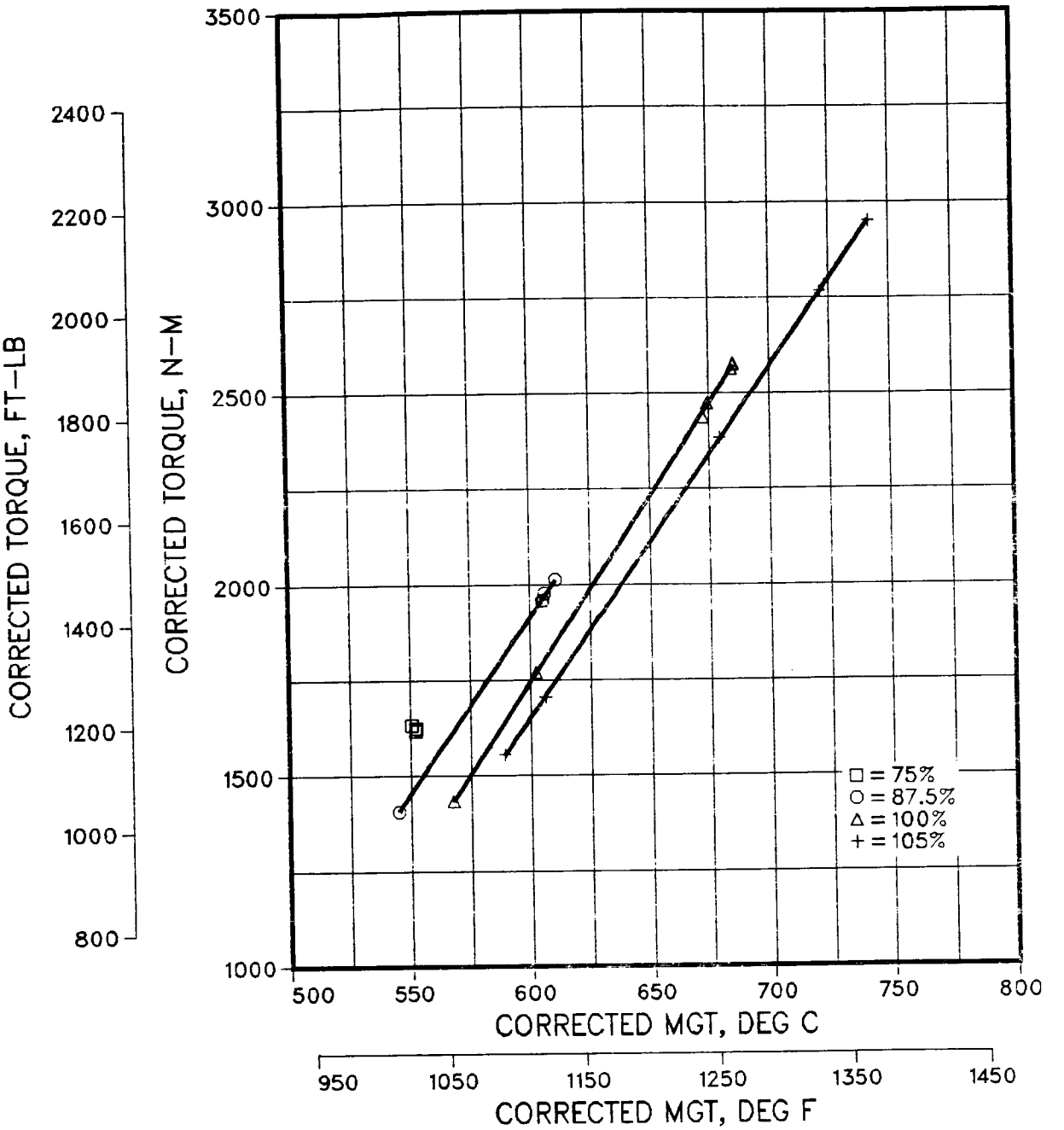

Figure 8.14. Unity Ram Torque - Endurance Cycle No. 12

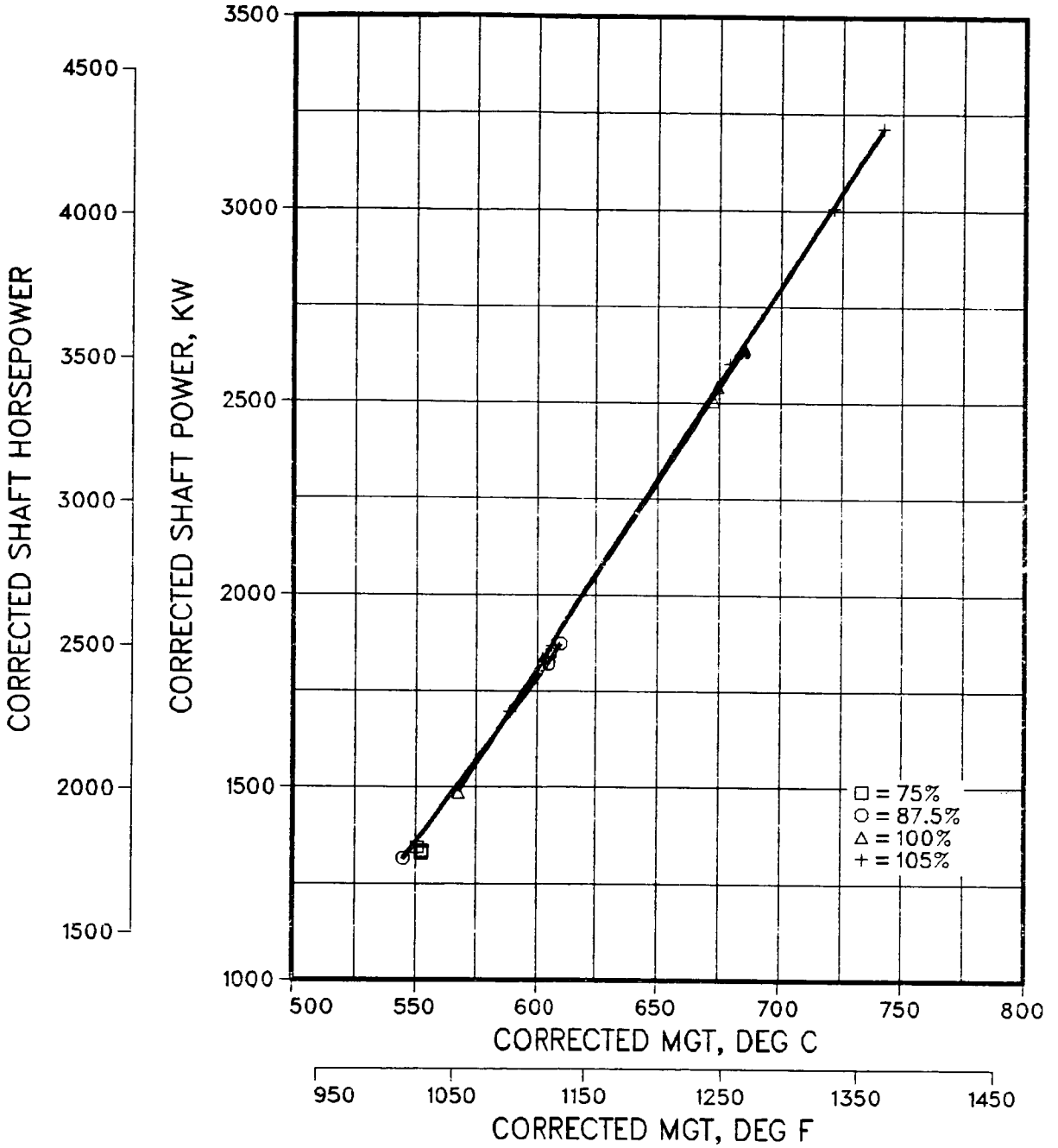

Figure 8.15. Unity Ram Power - Endurance Cycle No. 12

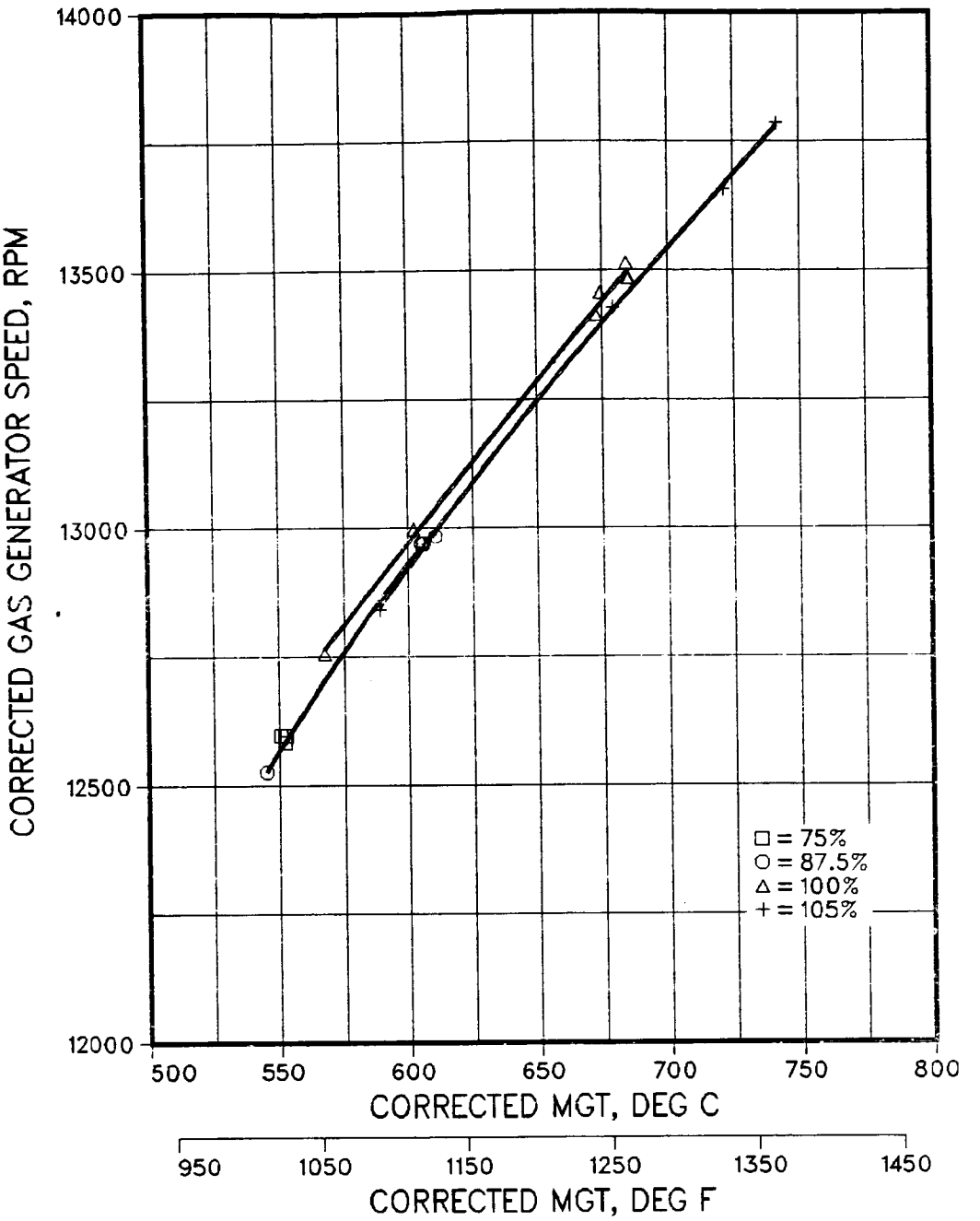

Figure 8.16. Unity Ram Gas Generator Speed - Endurance Cycle No. 12

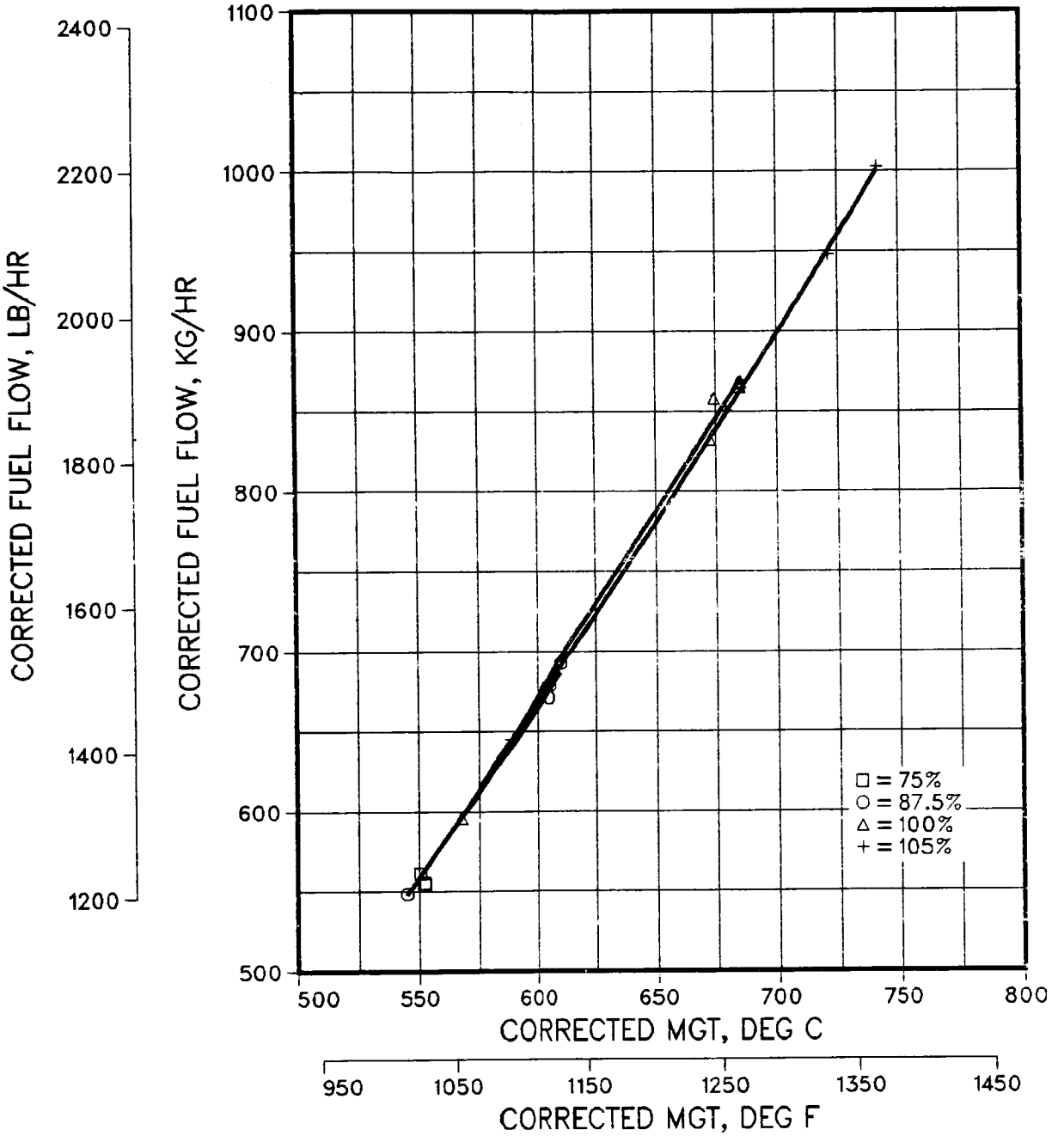

Figure 8.17. Unity Ram Fuel Flow - Endurance Cycle No. 12

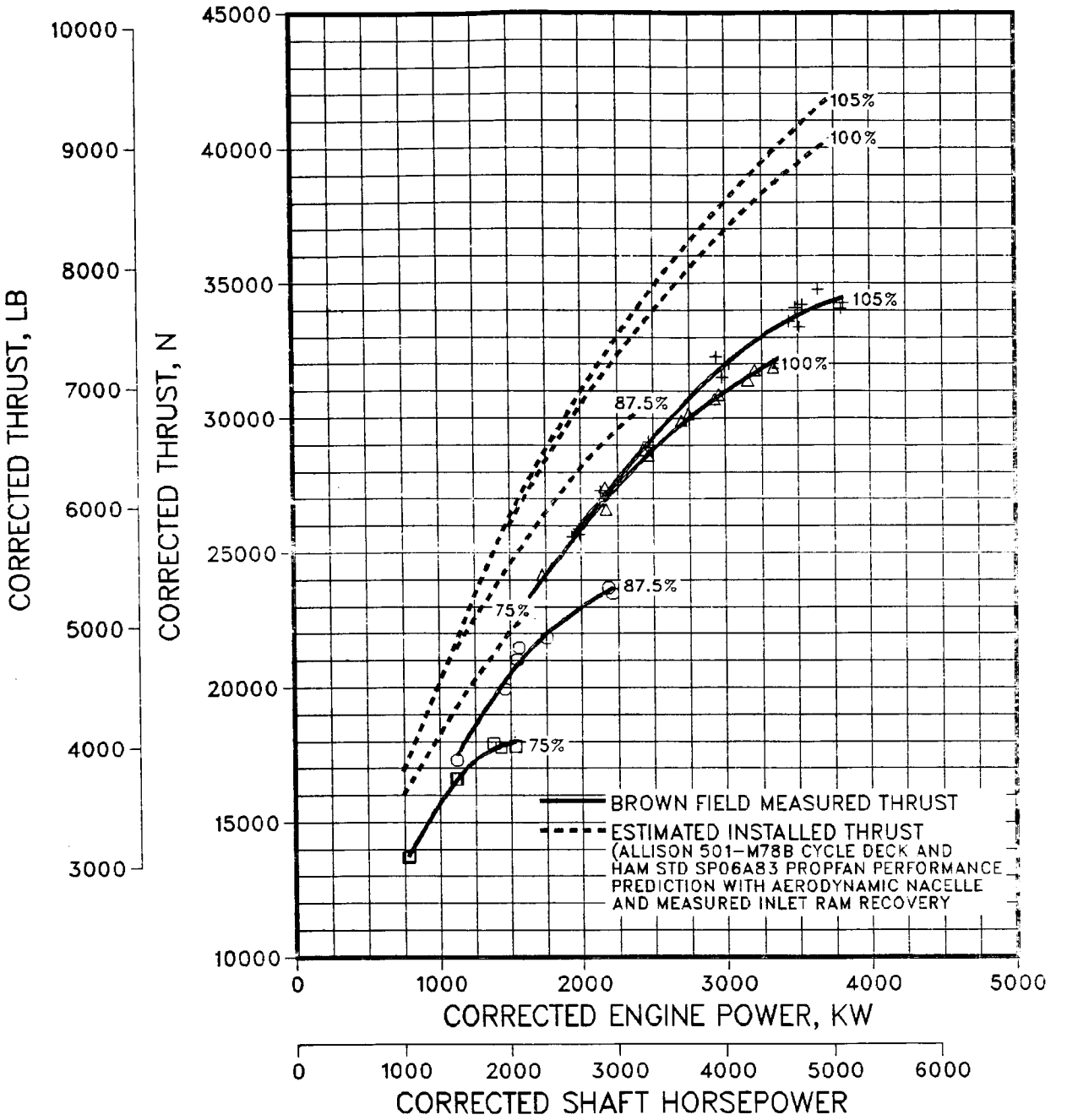

Figure 9.1. PTA Static Thrust

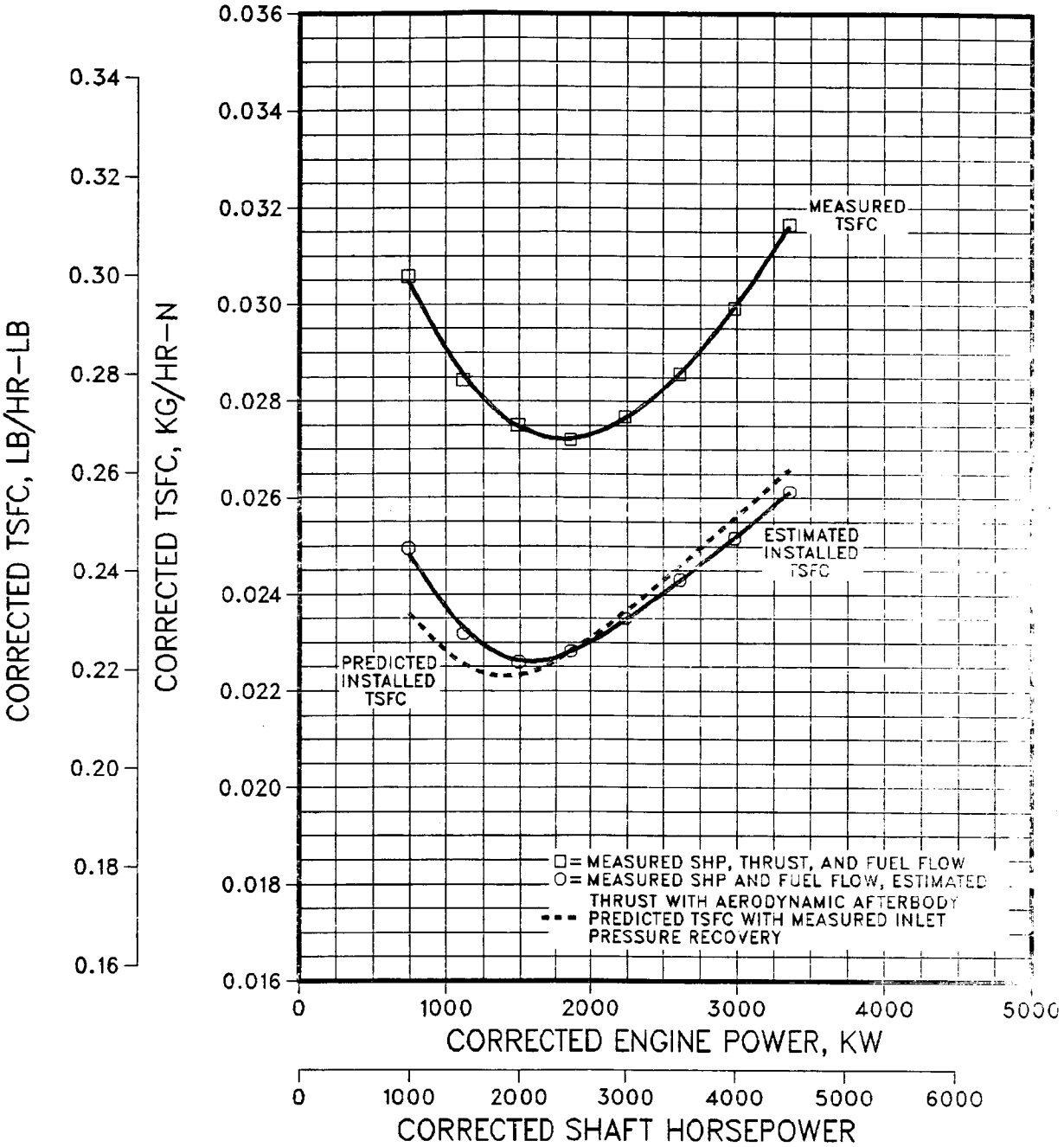

Figure 9.2. PTA Static TSFC - 100% Speed

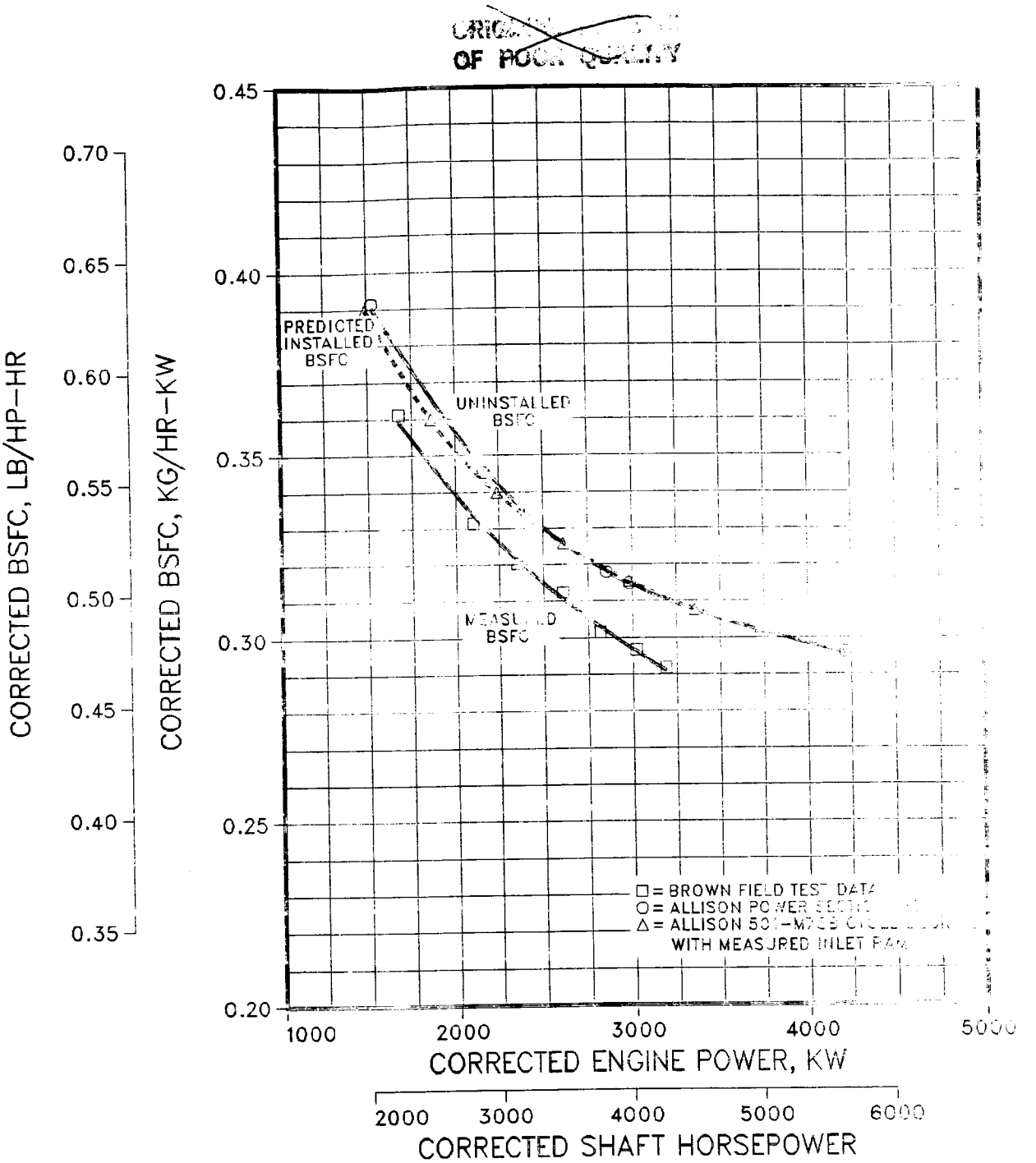

Figure 9.3. PTA Static BSFC - 100% Speed

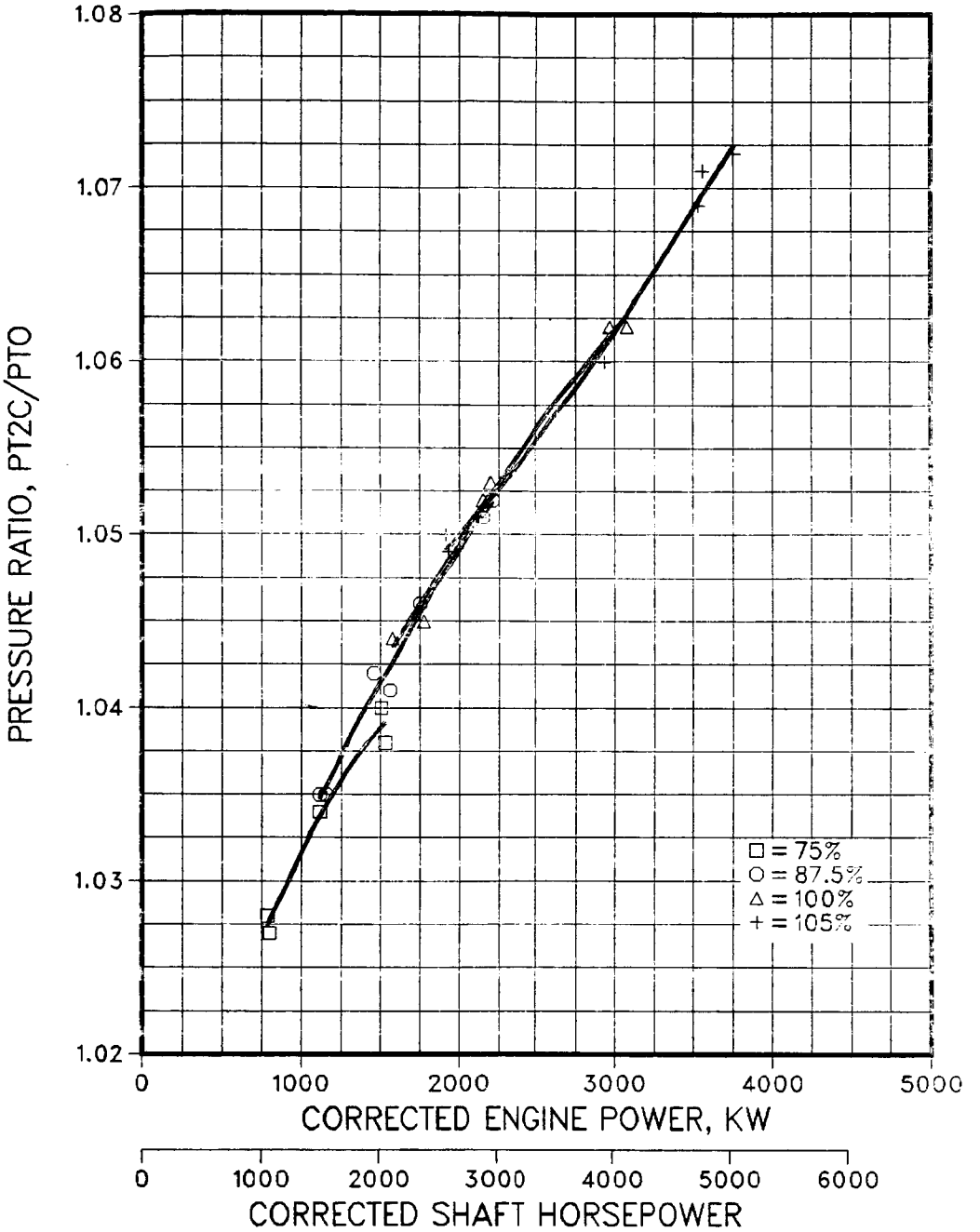

Figure 9.4. PTA Static Compressor Inlet Pressure Ratio

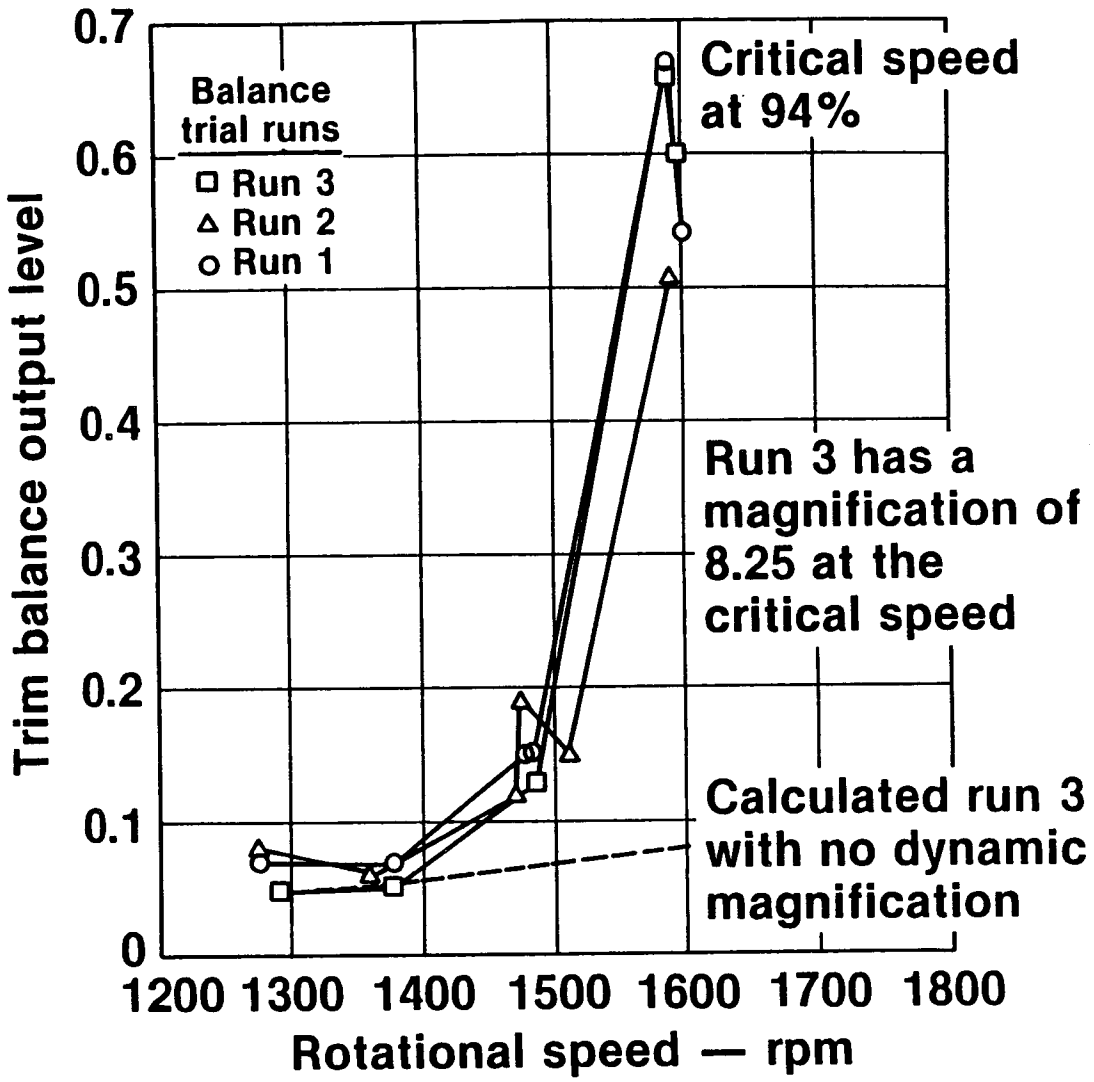

Figure 9.5. SR-7L Relative Vertical Acceleration on the Static Test Stand

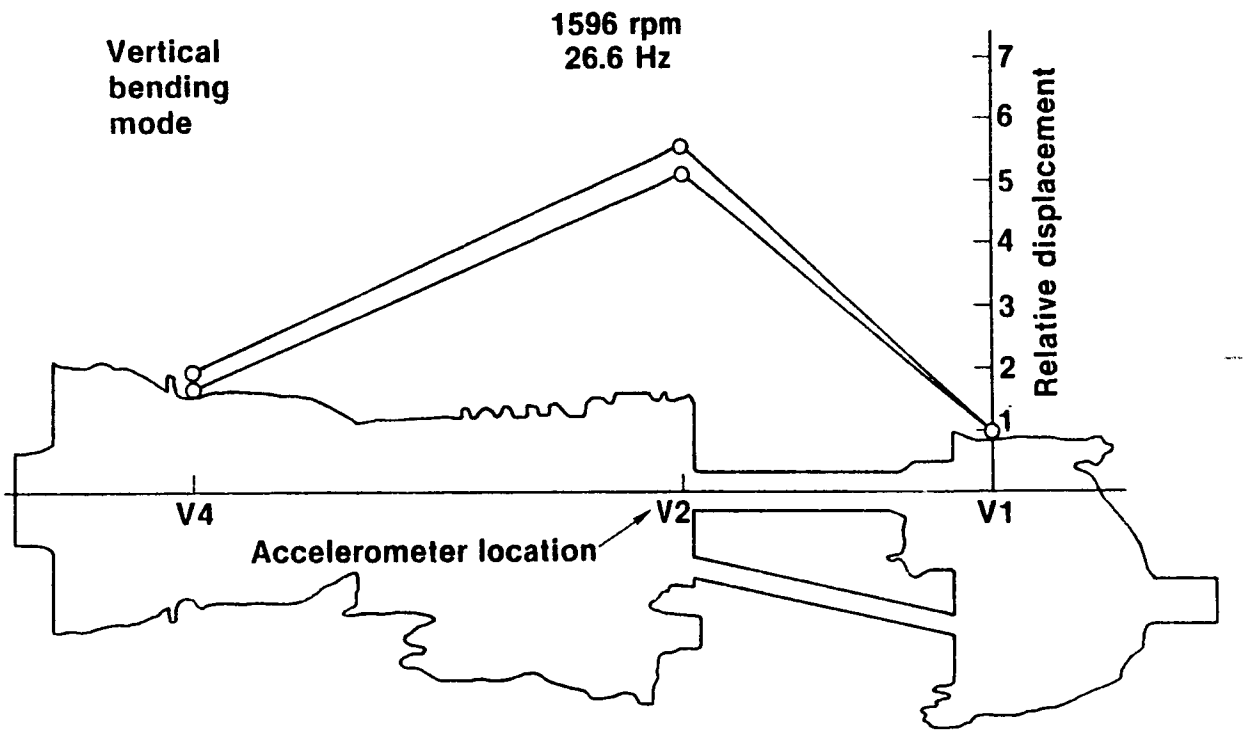

Figure 9.6. Propulsion System Vibration Mode Shape - 94% Speed

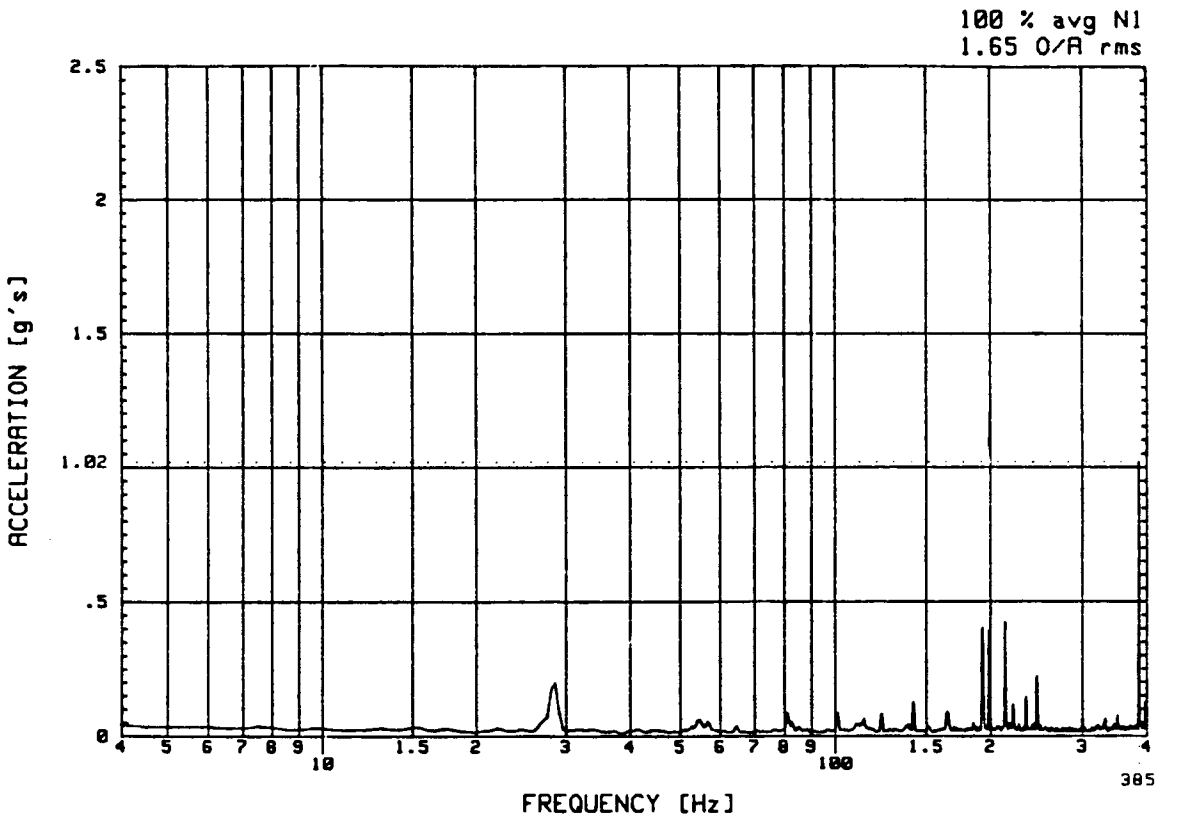

Figure 9.7. V1 Spectrum Analysis Plot - Run 20

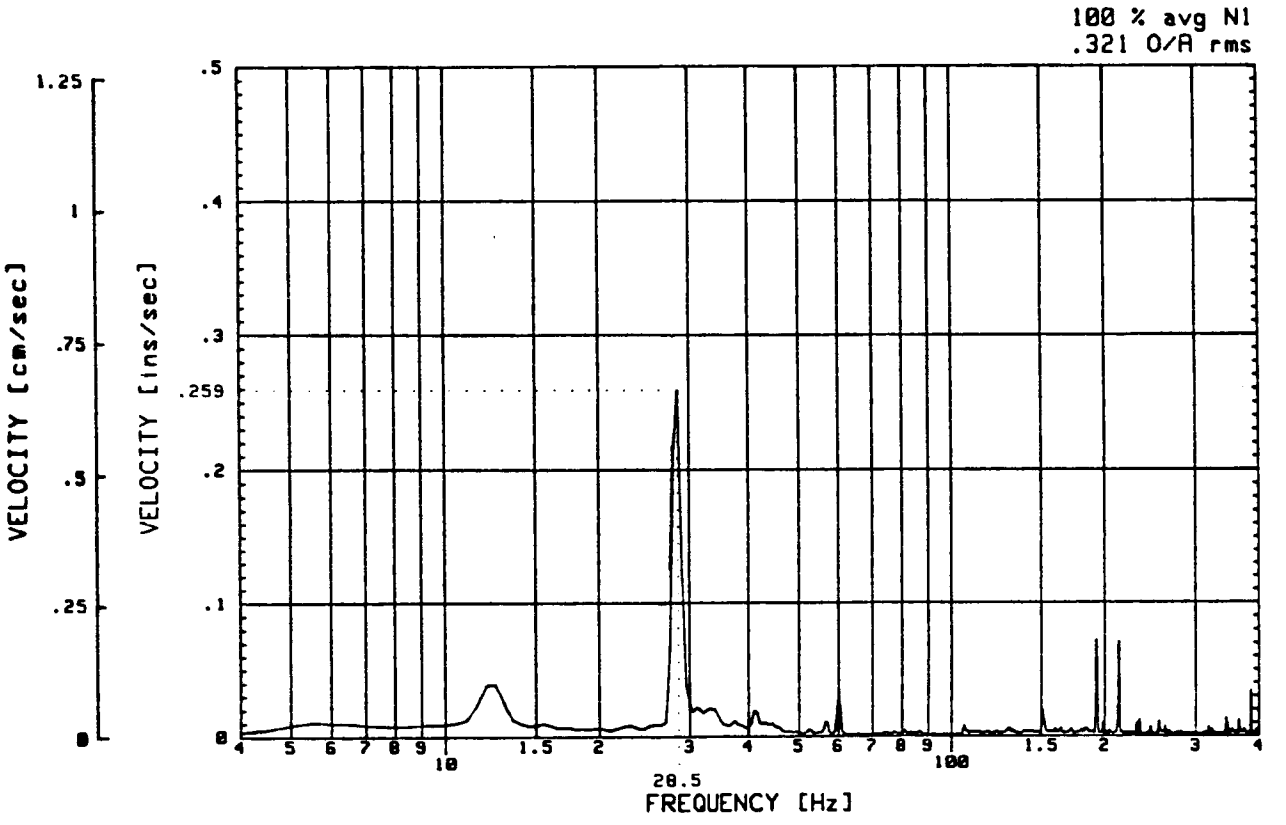

Figure 9.8. V2 Spectrum Analysis Plot - Run 20

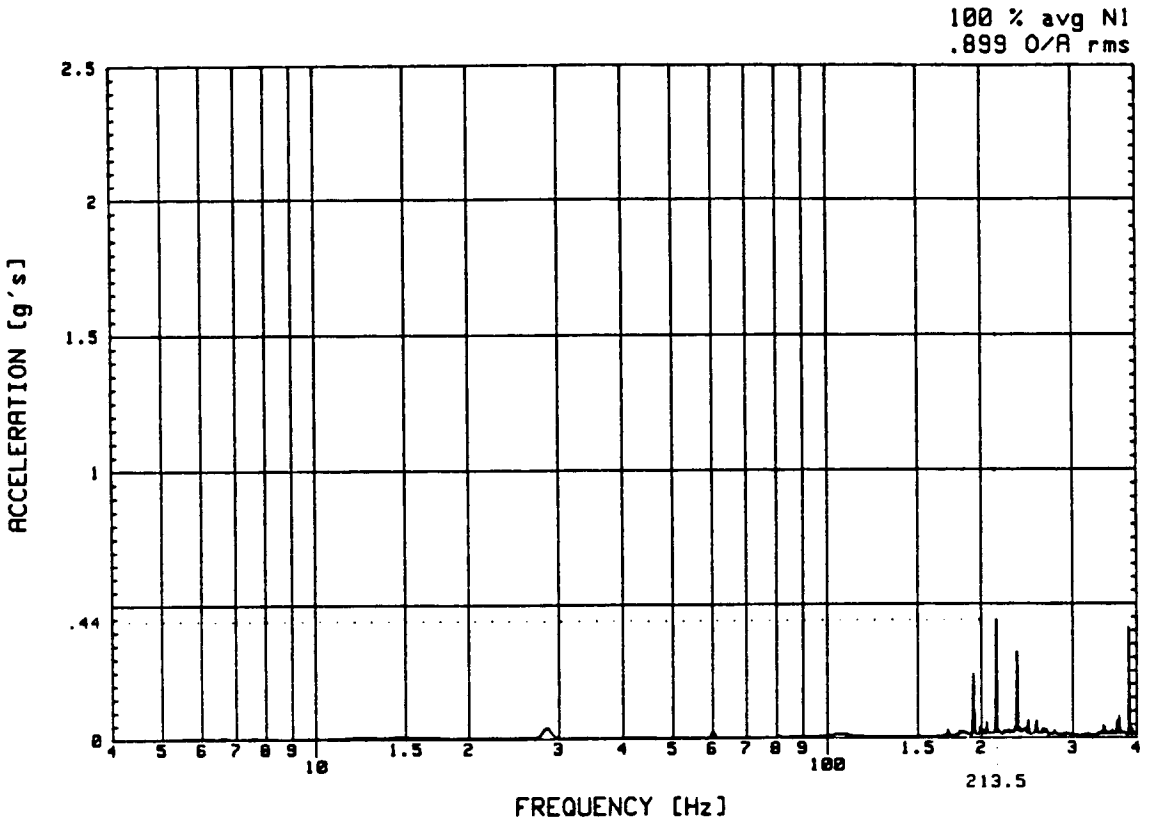

Figure 9.9. V3 Spectrum Analysis Plot - Run 20

ORIGINAL PAGE IS
OF POOR QUALITY

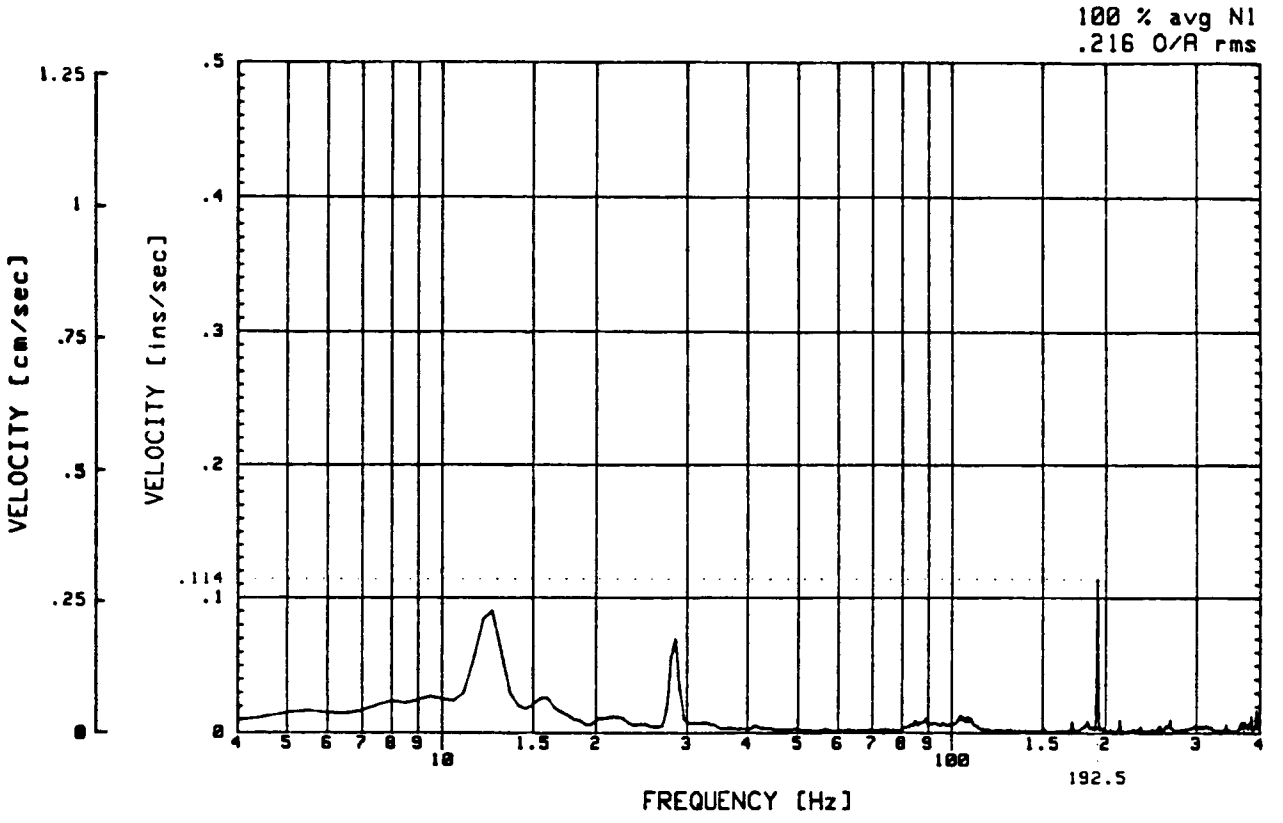

Figure 9.10. V4 Spectrum Analysis Plot - Run 20

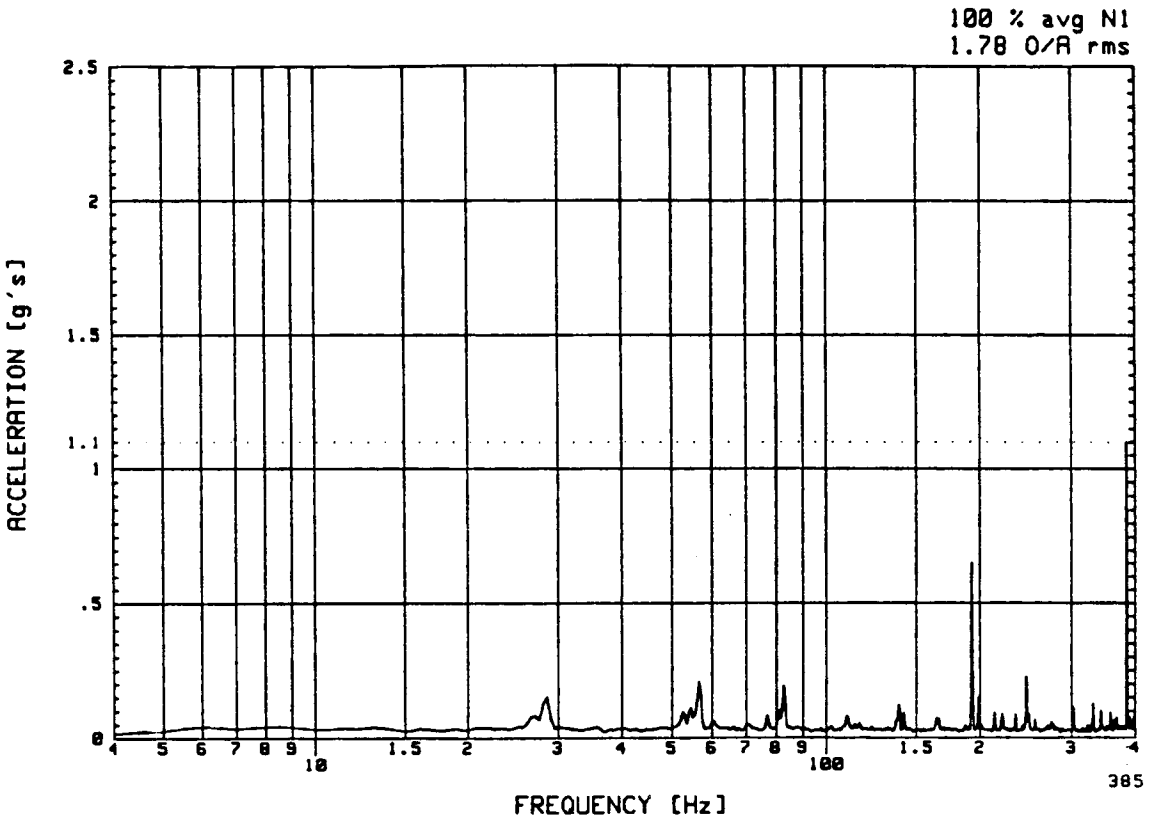

Figure 9.11. V5 Spectrum Analysis Plot - Run 20

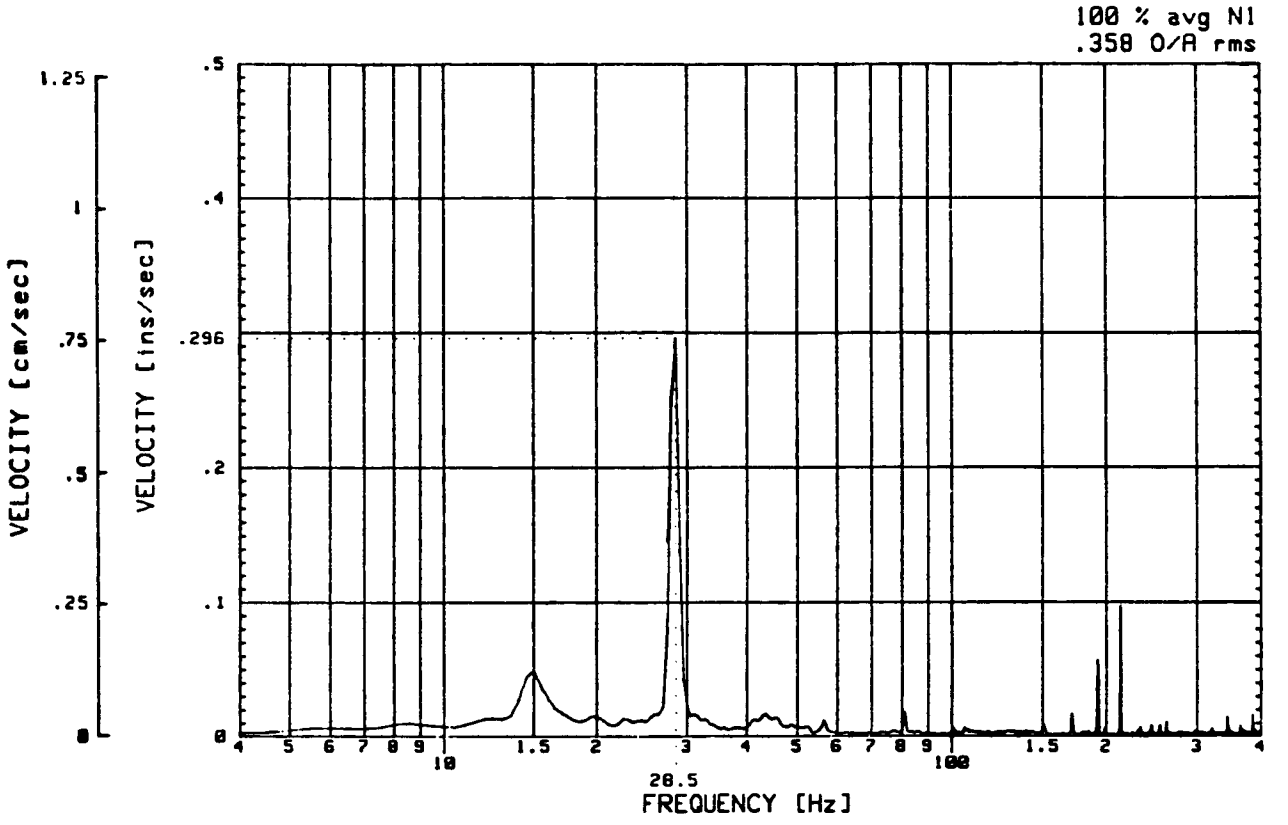

Figure 9.12. V6 Spectrum Analysis Plot - Run 20

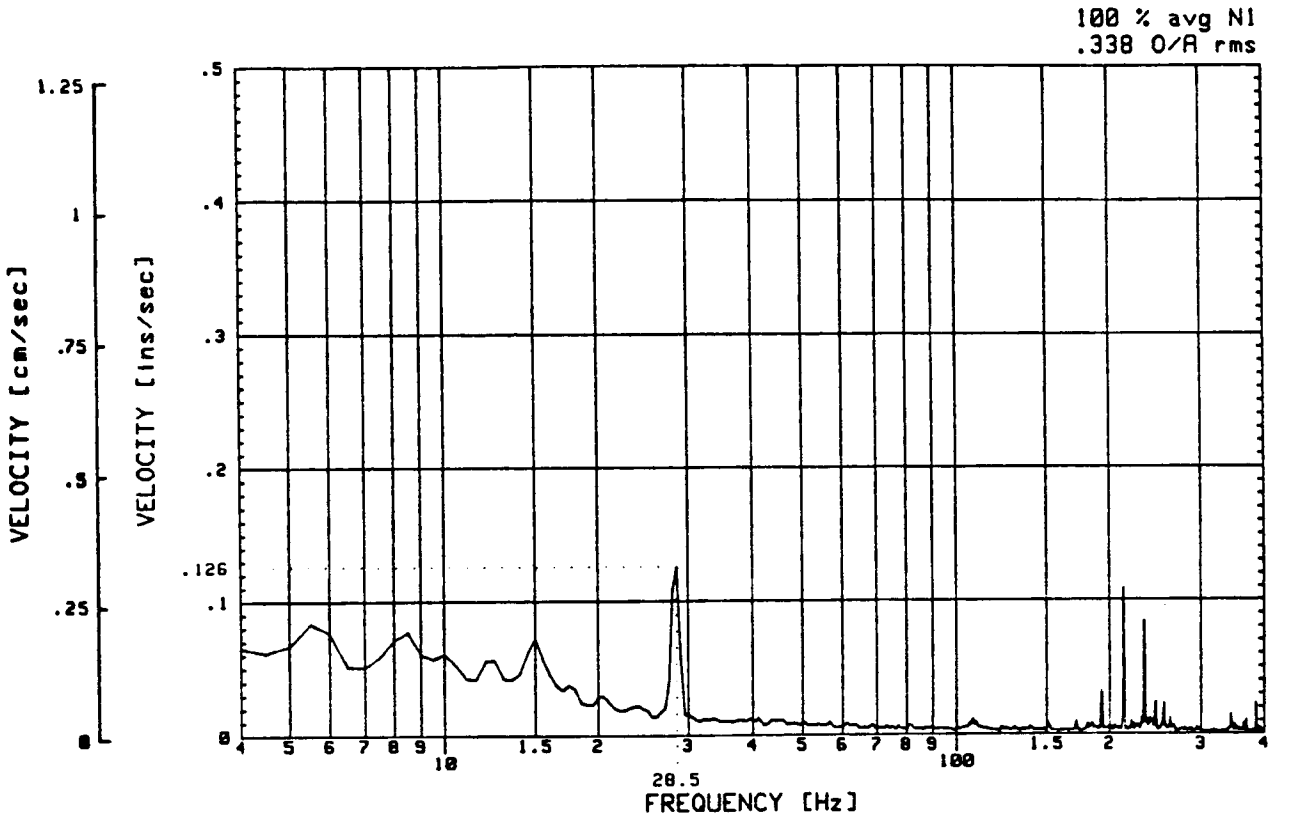

Figure 9.13. V7 Spectrum Analysis Plot - Run 20

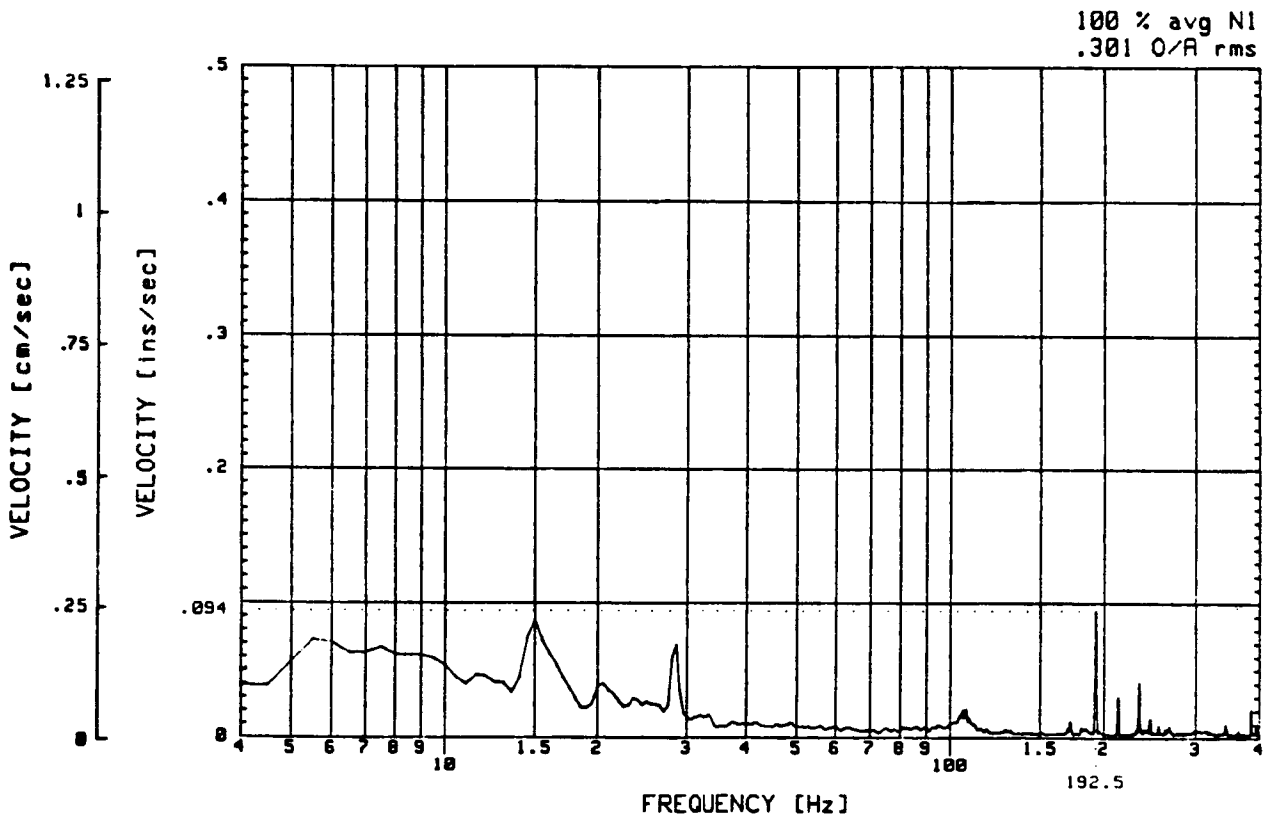

Figure 9.14. V8 Spectrum Analysis Plot - Run 20

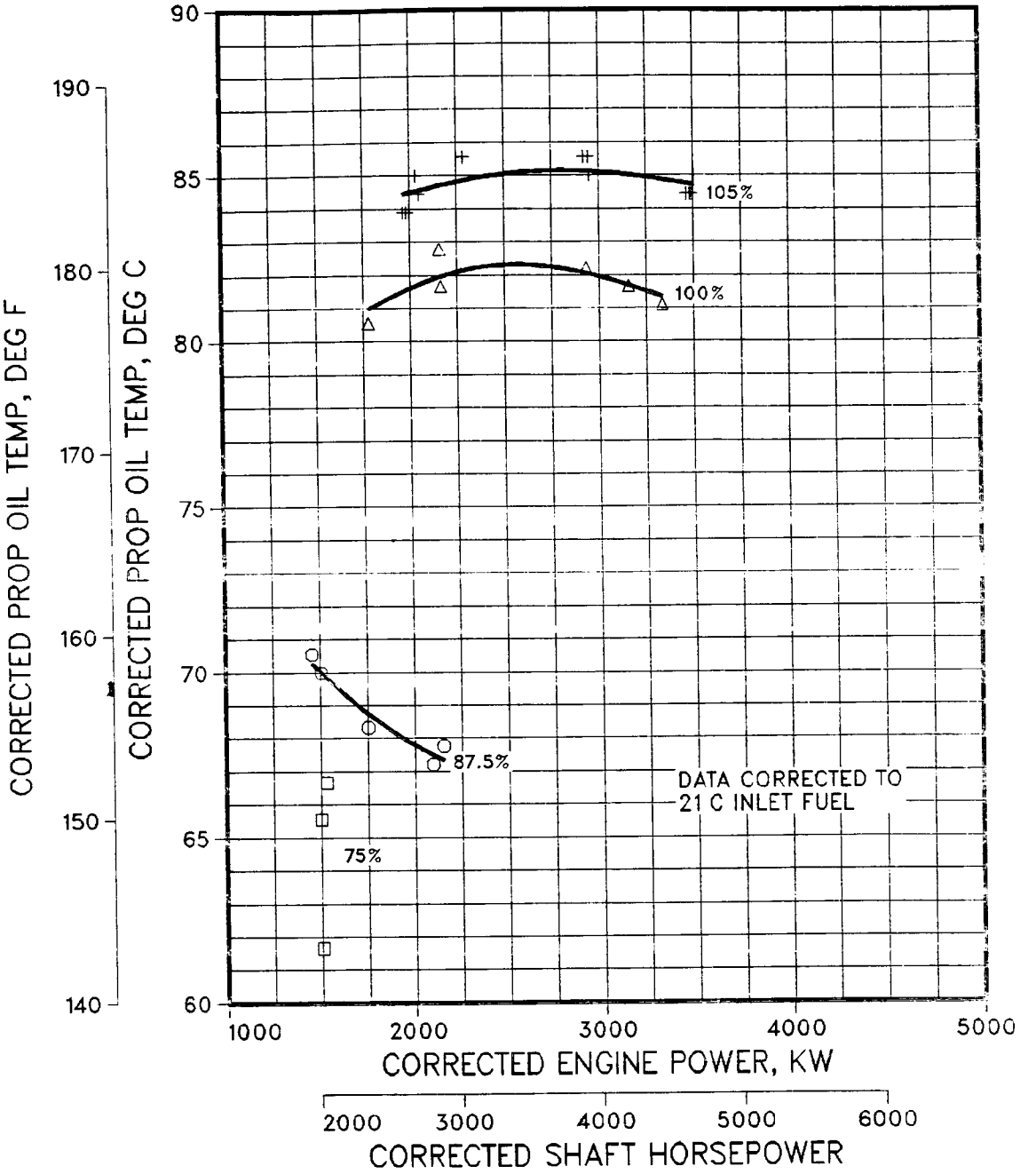

Figure 9.15. PTA Static Propfan Fluid Temperature

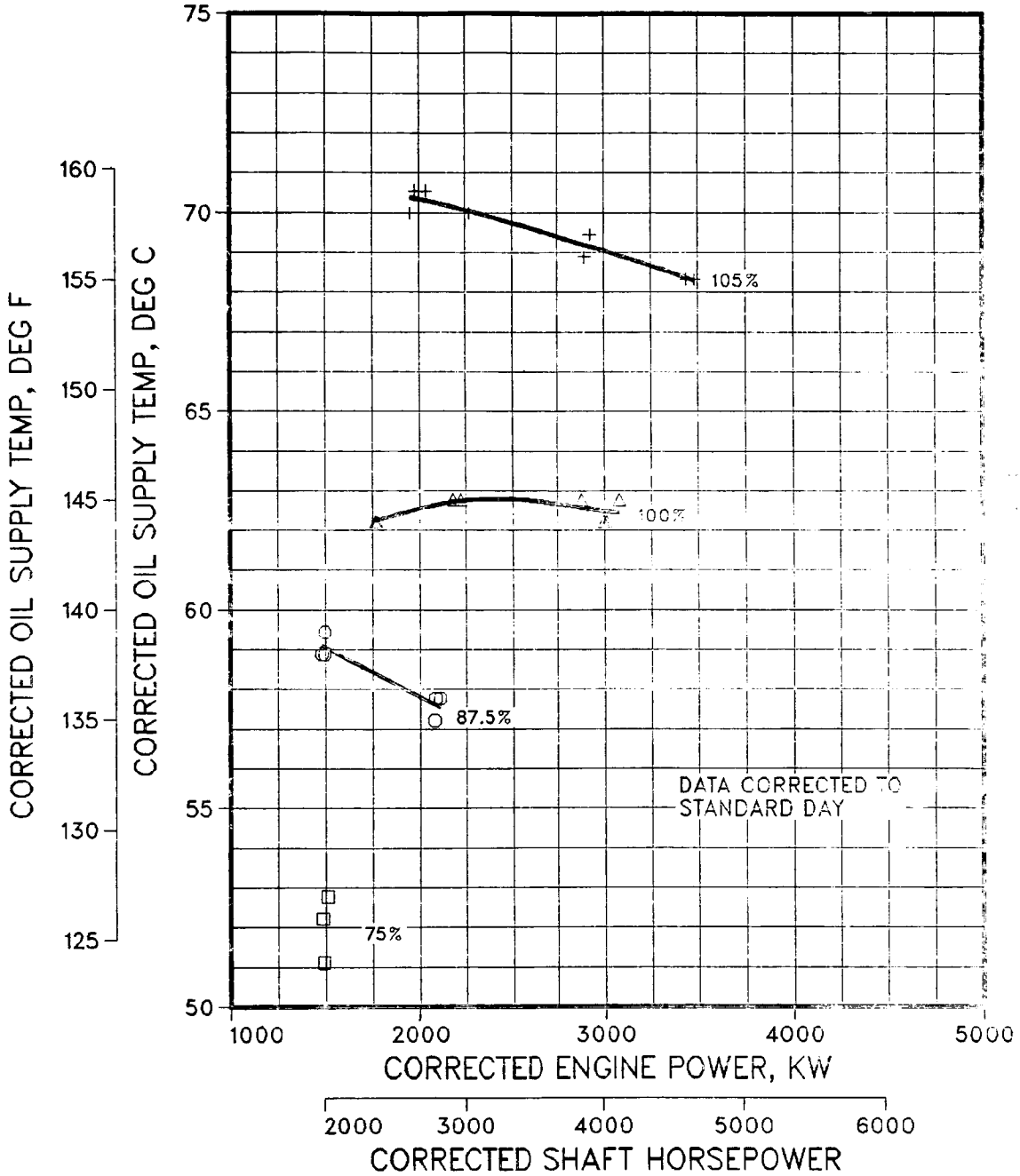

Figure 9.16. PTA Static Drive System Oil Temperature

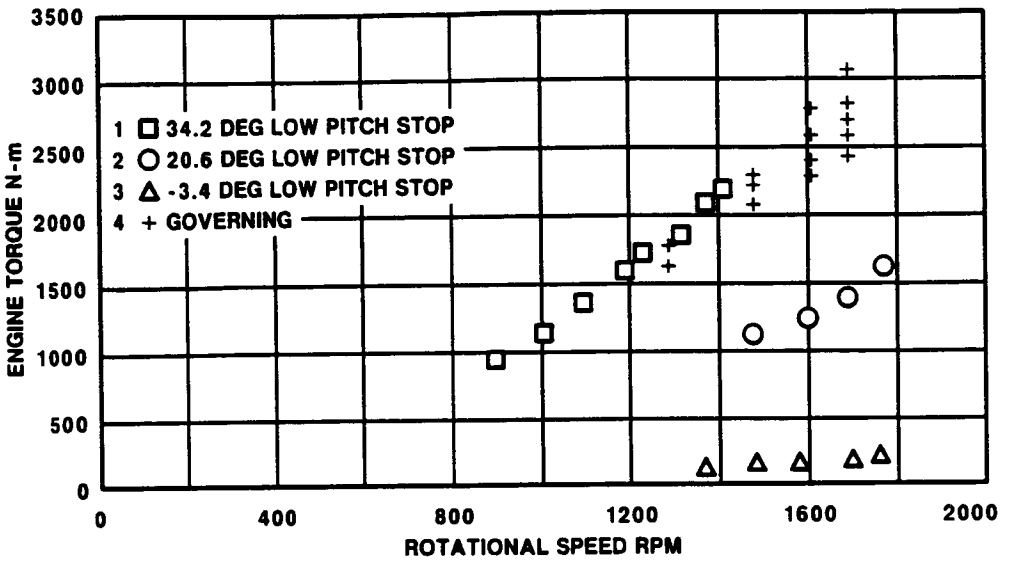

Figure 9.17. Stress Survey Conditions Selected for Data Analysis

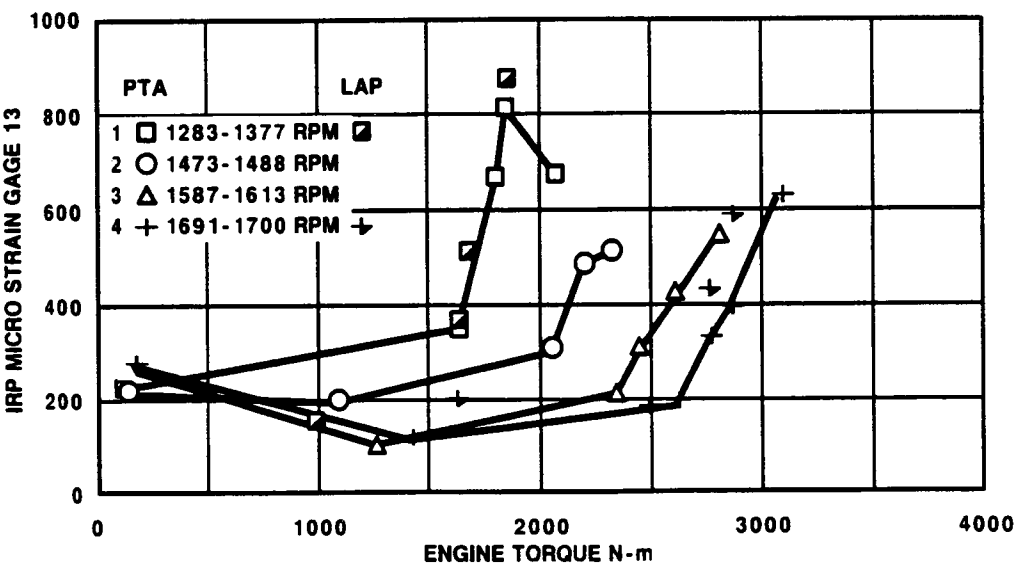

Figure 9.18. Tip Bending Gage Strain Variation With Torque

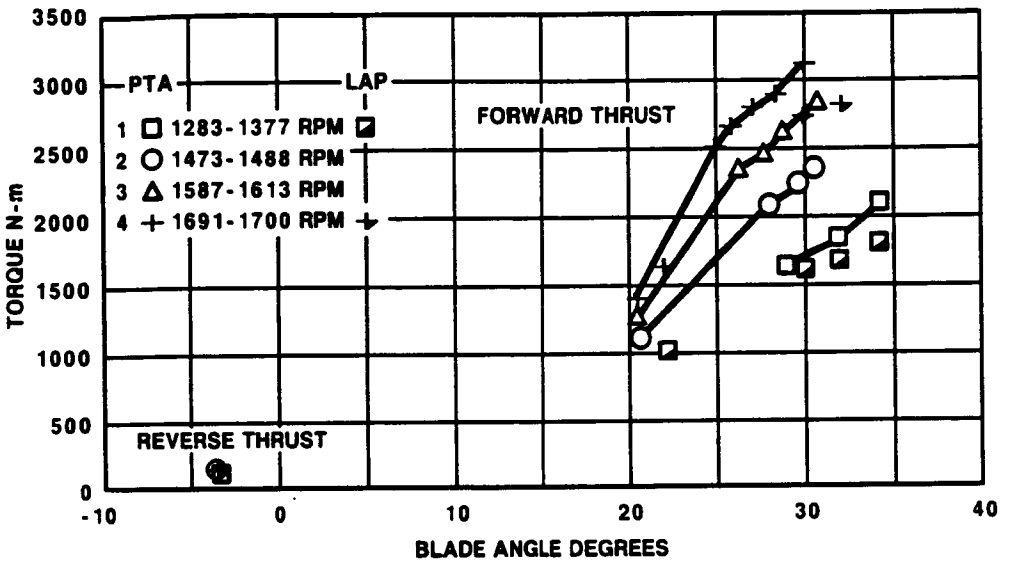

Figure 9.19. SR-7L Torque Change With Blade Angle

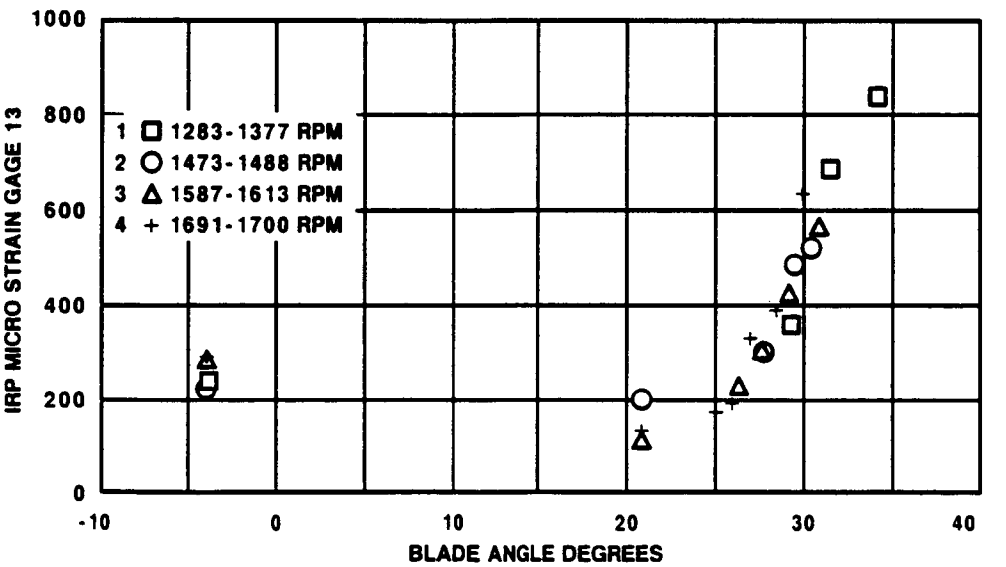

Figure 9.20. Tip Bending Gage Strain Variation With Blade Angle

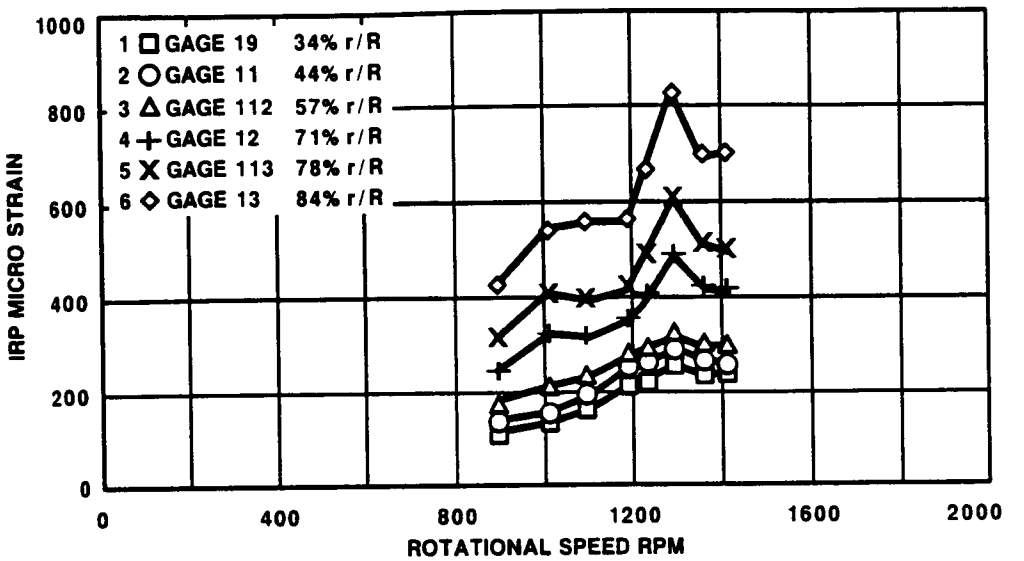

Figure 9.21. Blade 1 Vibratory Strain Distribution at 34.2 Degrees Blade Angle

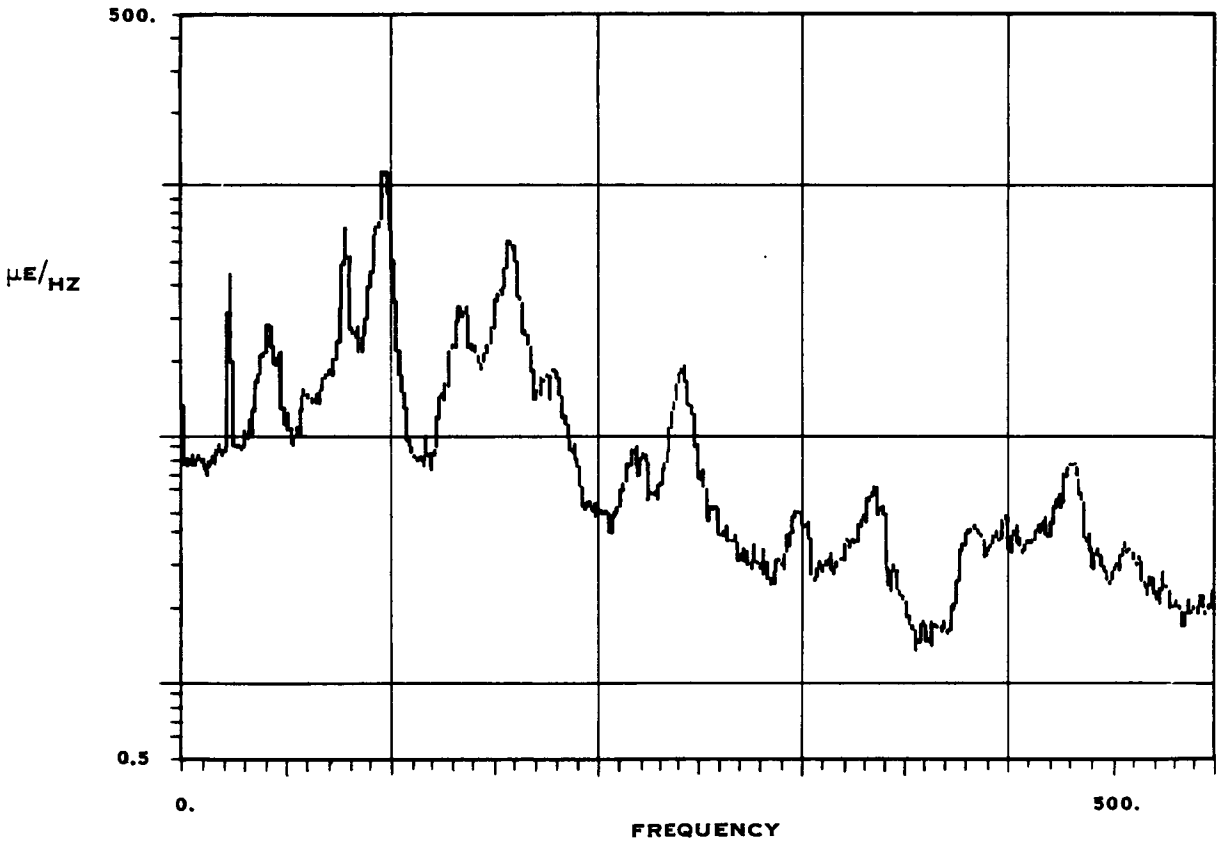

Figure 9.22. Frequency Content of the Tip Bending Gage 13 - Run 14 at 1400 RPM, 34.2° Blade Angle

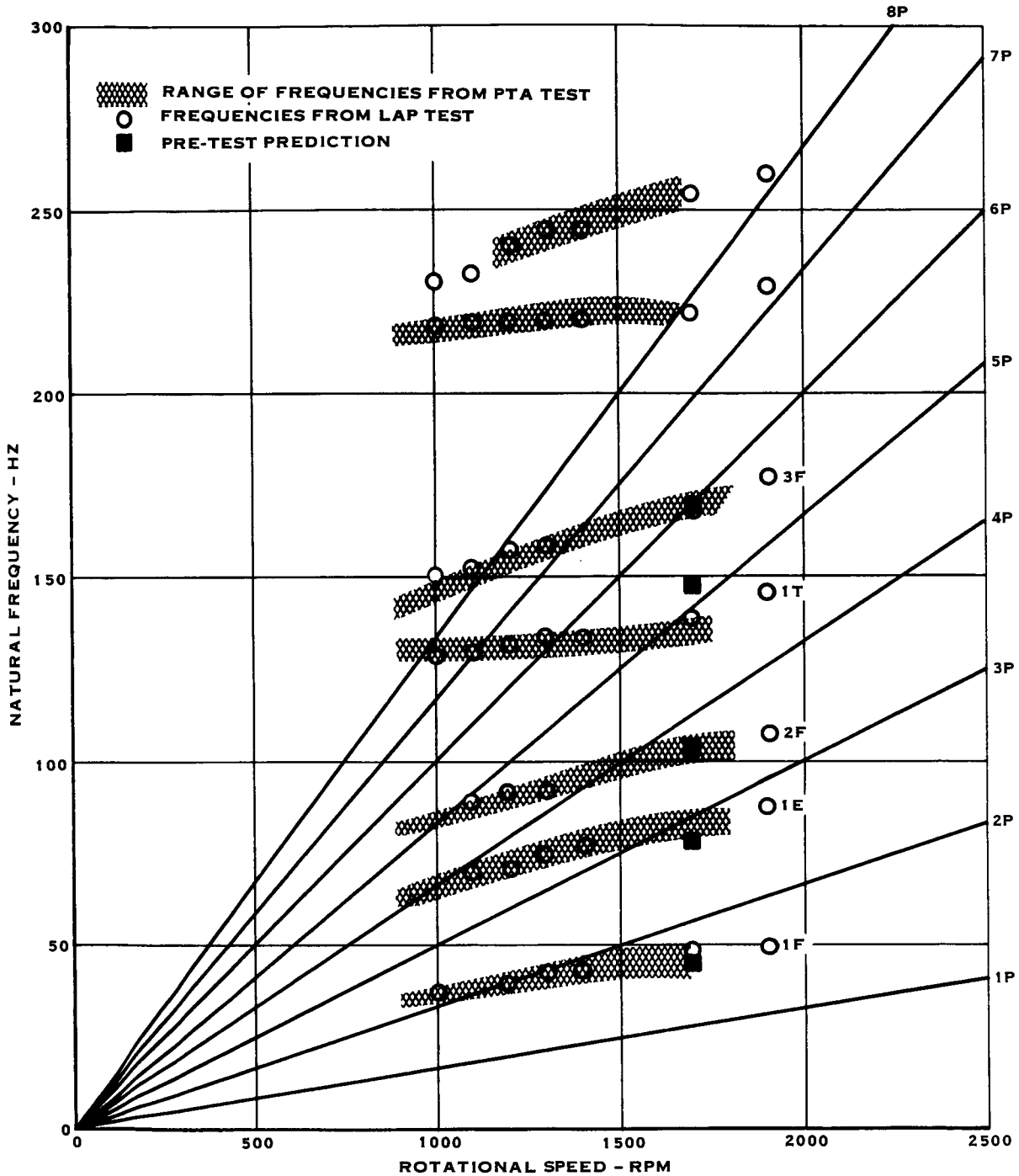

Figure 9.23. Comparison of SR-7L Blade Natural Frequency - Test Results to Prediction

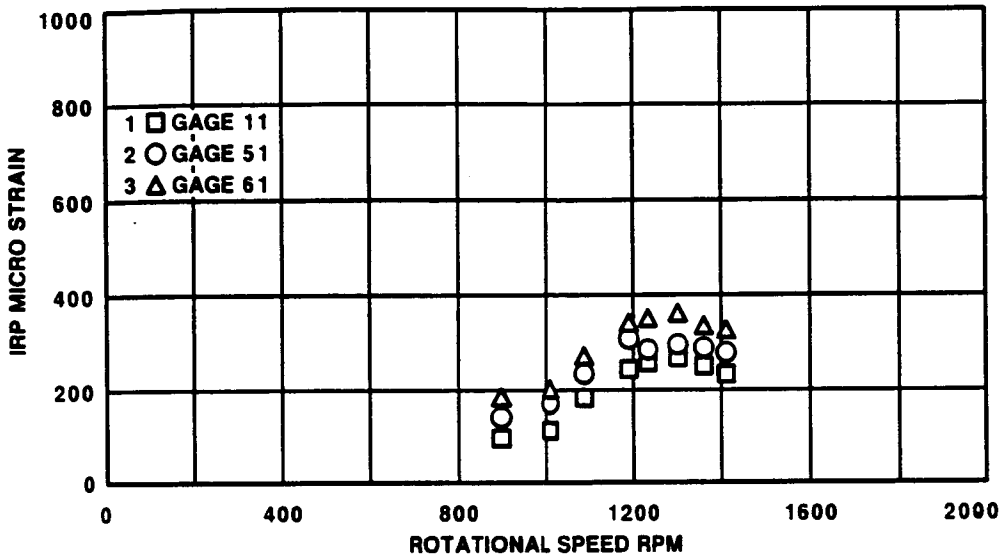

Figure 9.24. Inboard Bending Gage Vibratory Strain at 34.2° Blade Angle

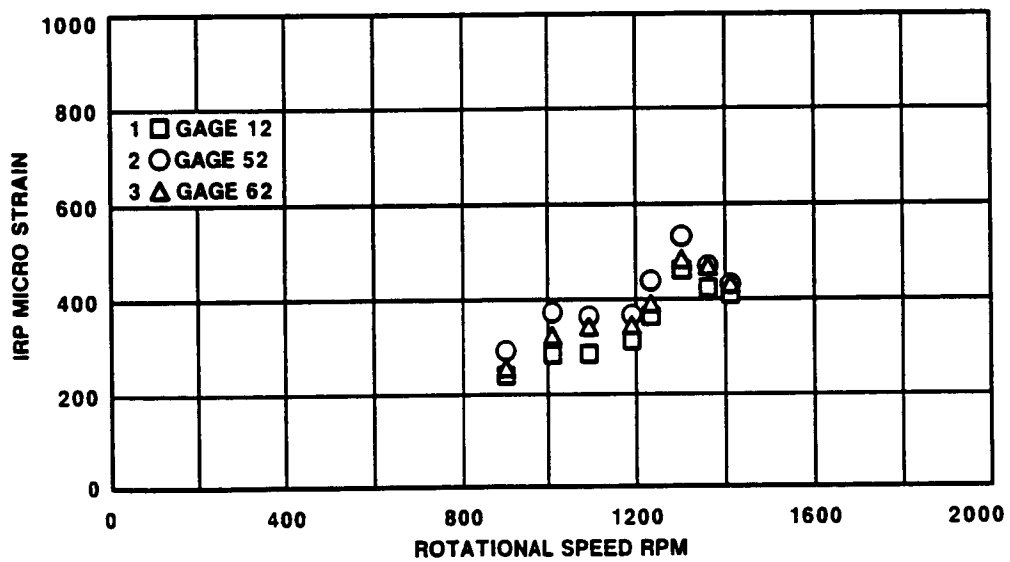

Figure 9.25. Mid-Blade Bending Gage Vibratory Strain at 34.2° Blade Angle

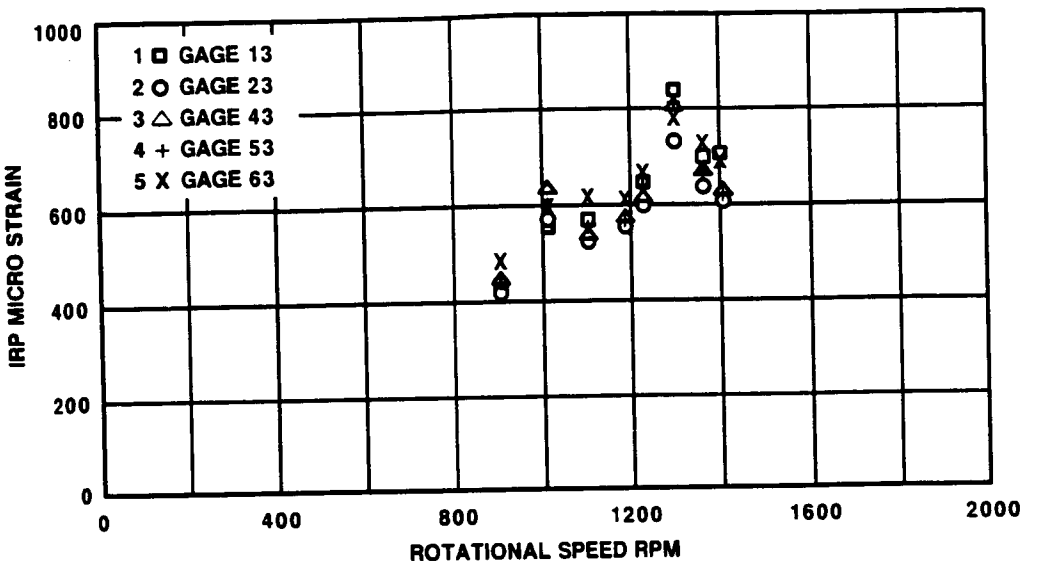

Figure 9.26. Tip Bending Gage Vibratory Strain at 34.2° Blade Angle

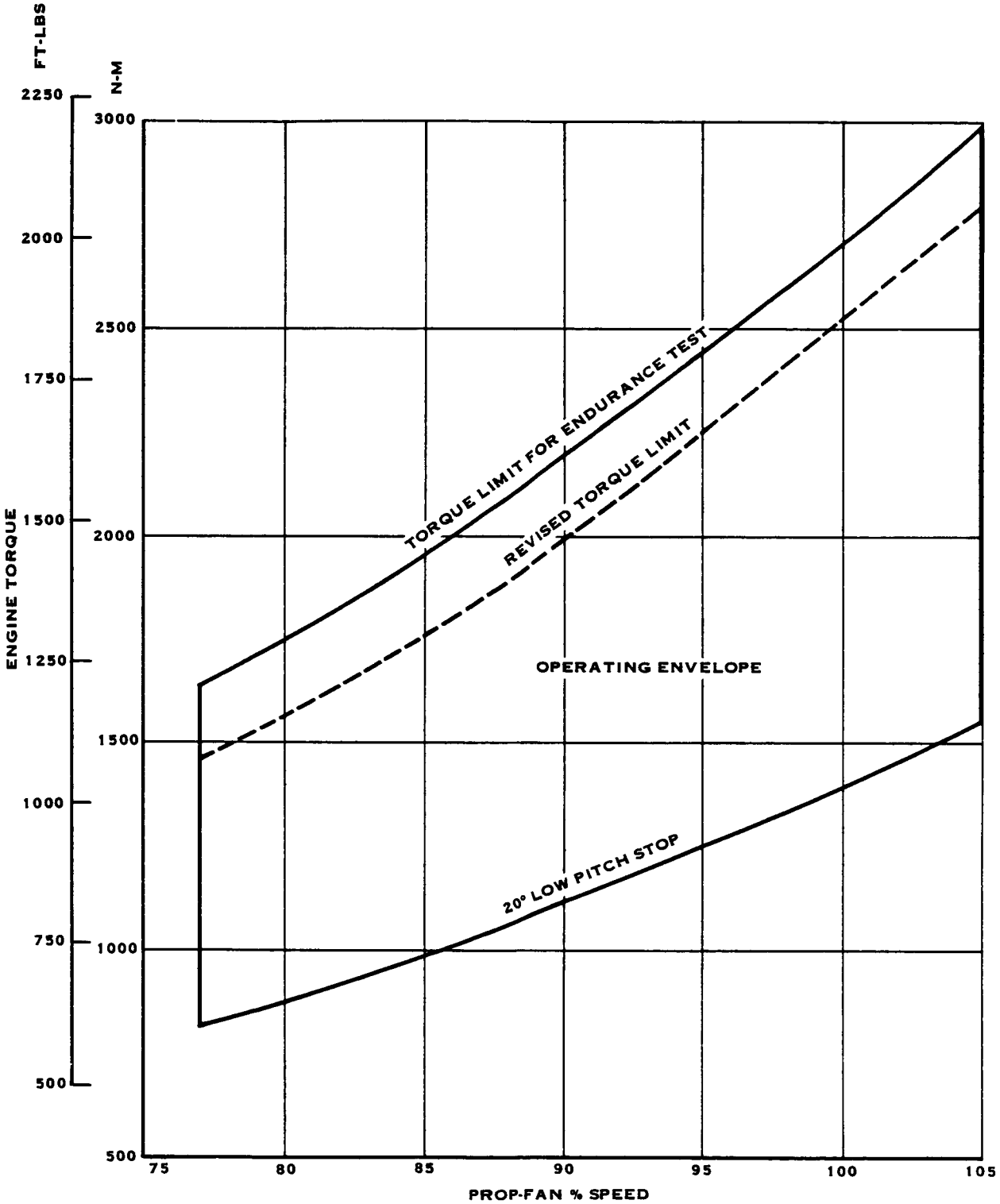

Figure 9.27. Static Operating Envelope With Revised Torque Limit

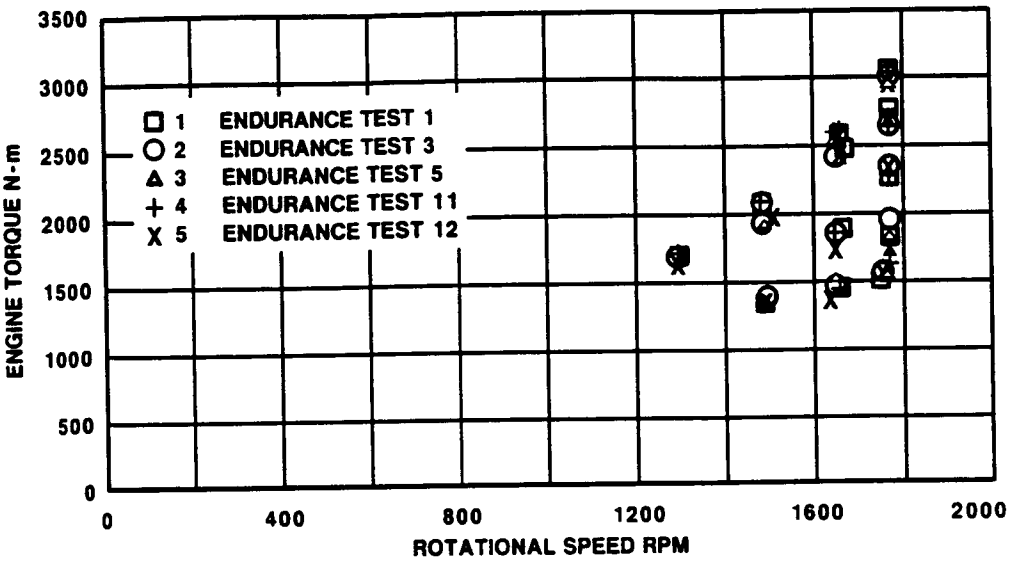

Figure 9.28. Endurance Test Conditions Selected for Data Analysis

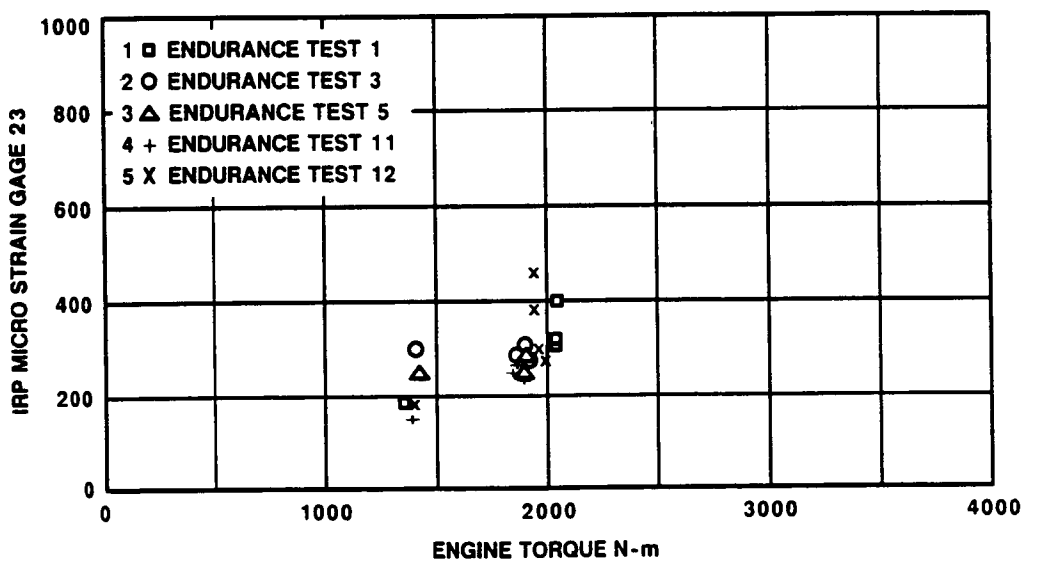

Figure 9.29. Tip Bending Gage Vibratory Strain at 77% Speed

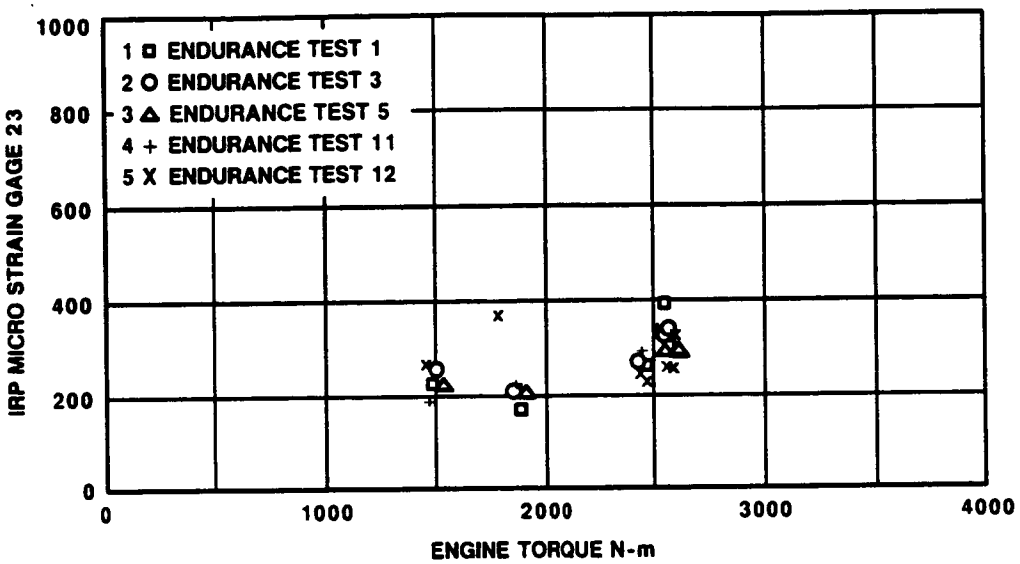

Figure 9.30. Tip Bending Gage Vibratory Strain at 87.5% Speed

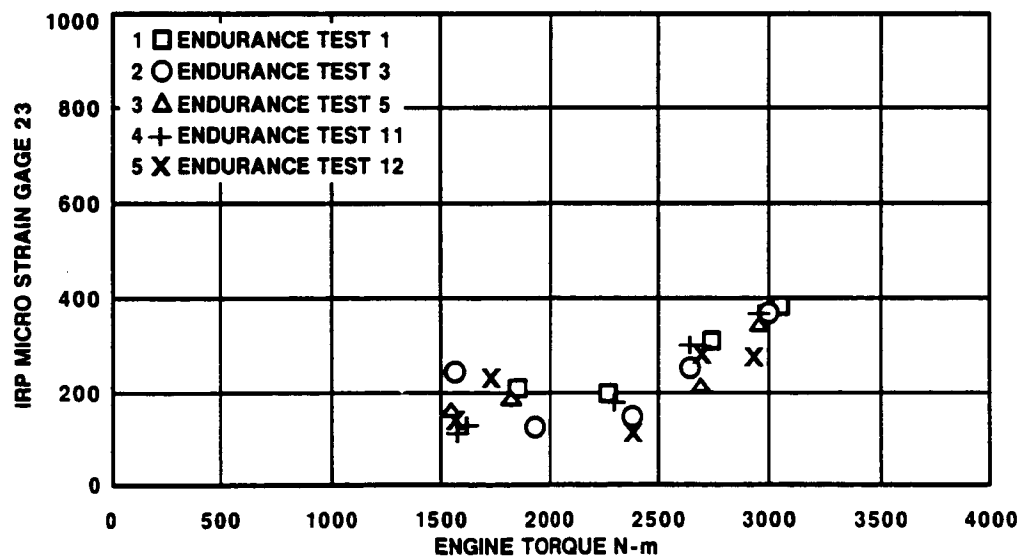

Figure 9.31. Tip Bending Gage Vibratory Strain at 105% Speed

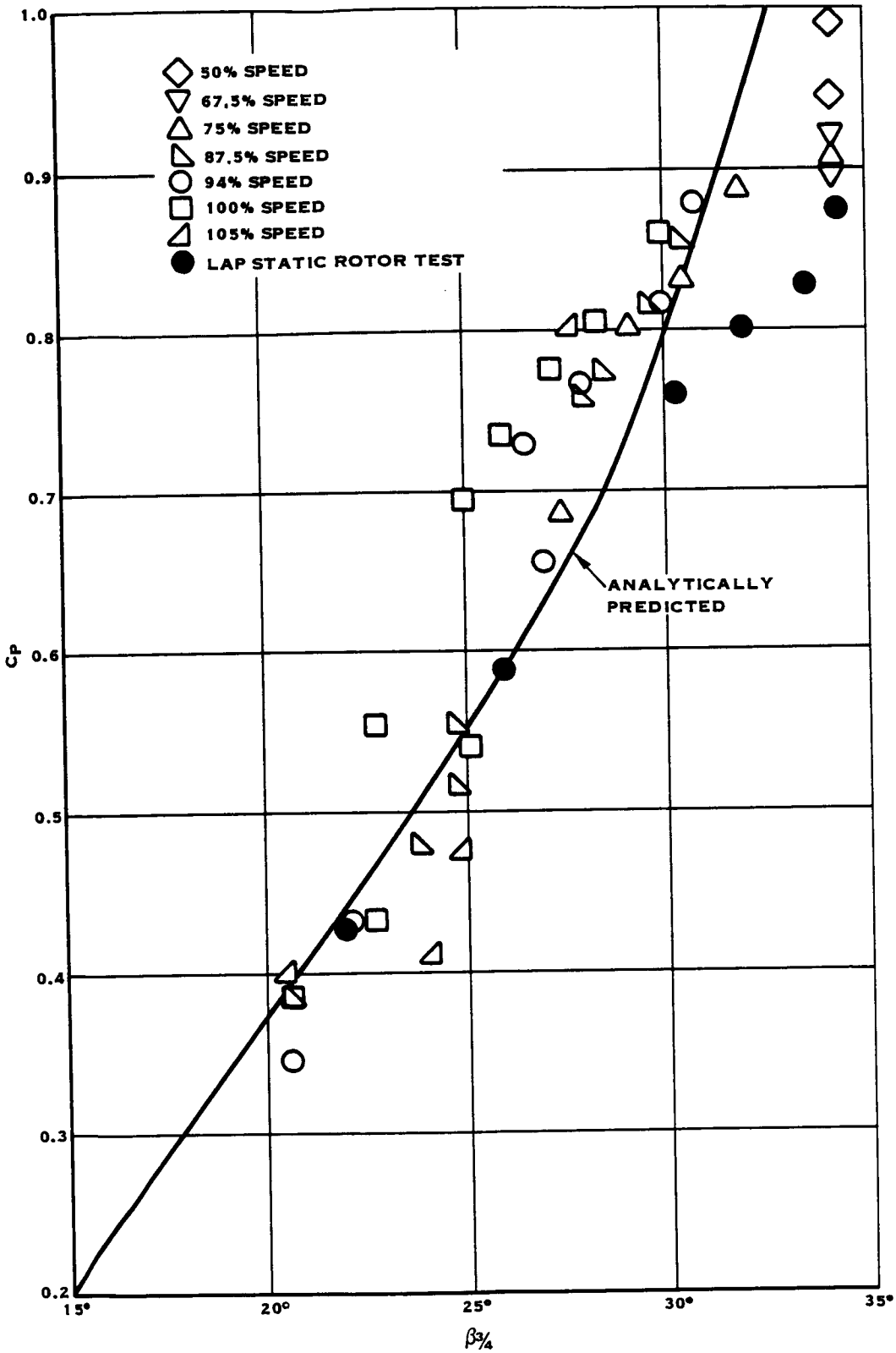

Figure 9.32. SR-7L Static Performance - Power Coefficient vs Blade Angle

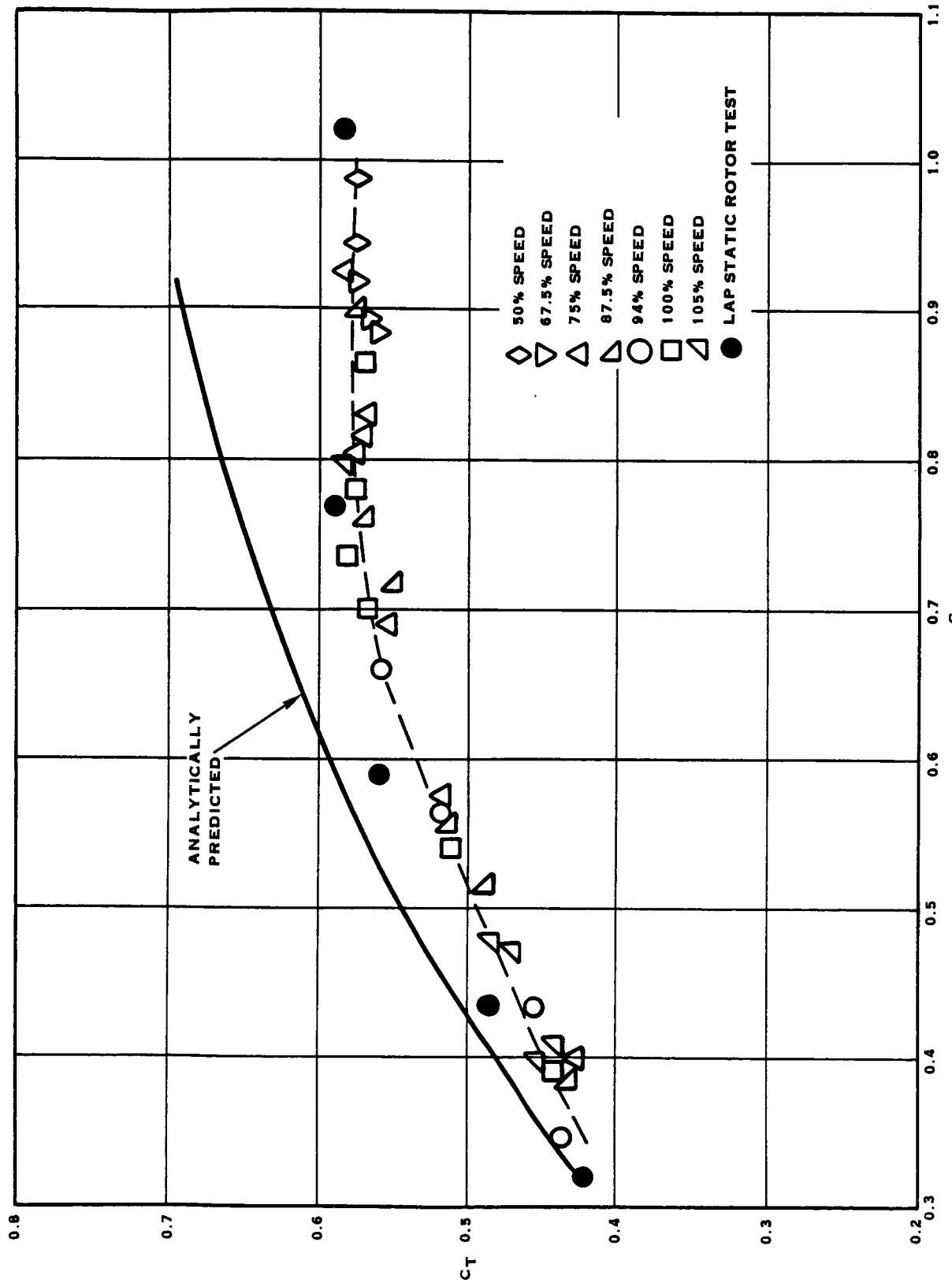

Figure 9.33. SR-7L Static Performance - Thrust Coefficient vs Power Coefficient

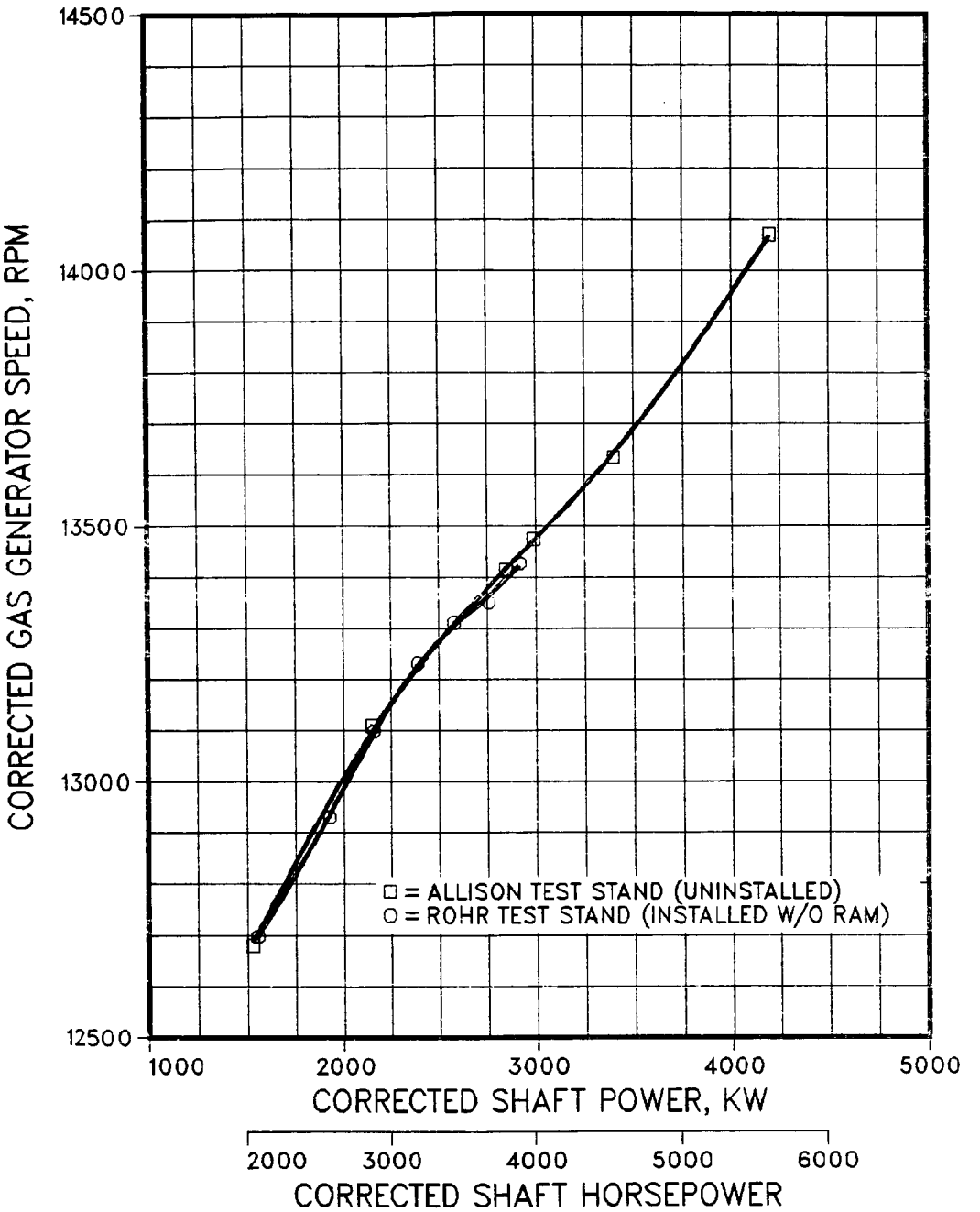

Figure 9.34. Unity Ram Gas Generator Speed - Installed Versus Uninstalled - 100% N_p Speed

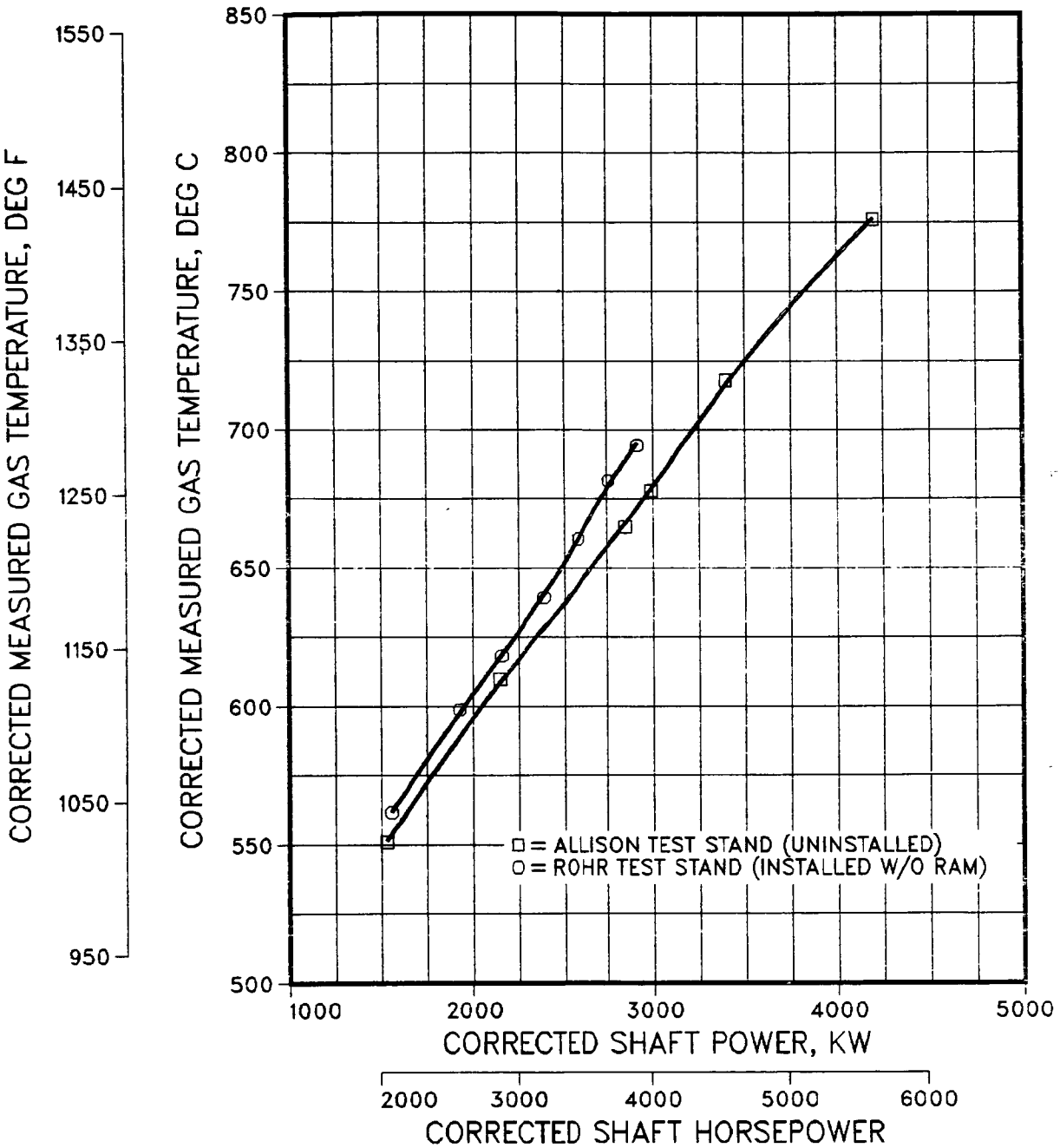

Figure 9.35. Unity Ram MGT - Installed Versus Uninstalled - 100% N_p Speed

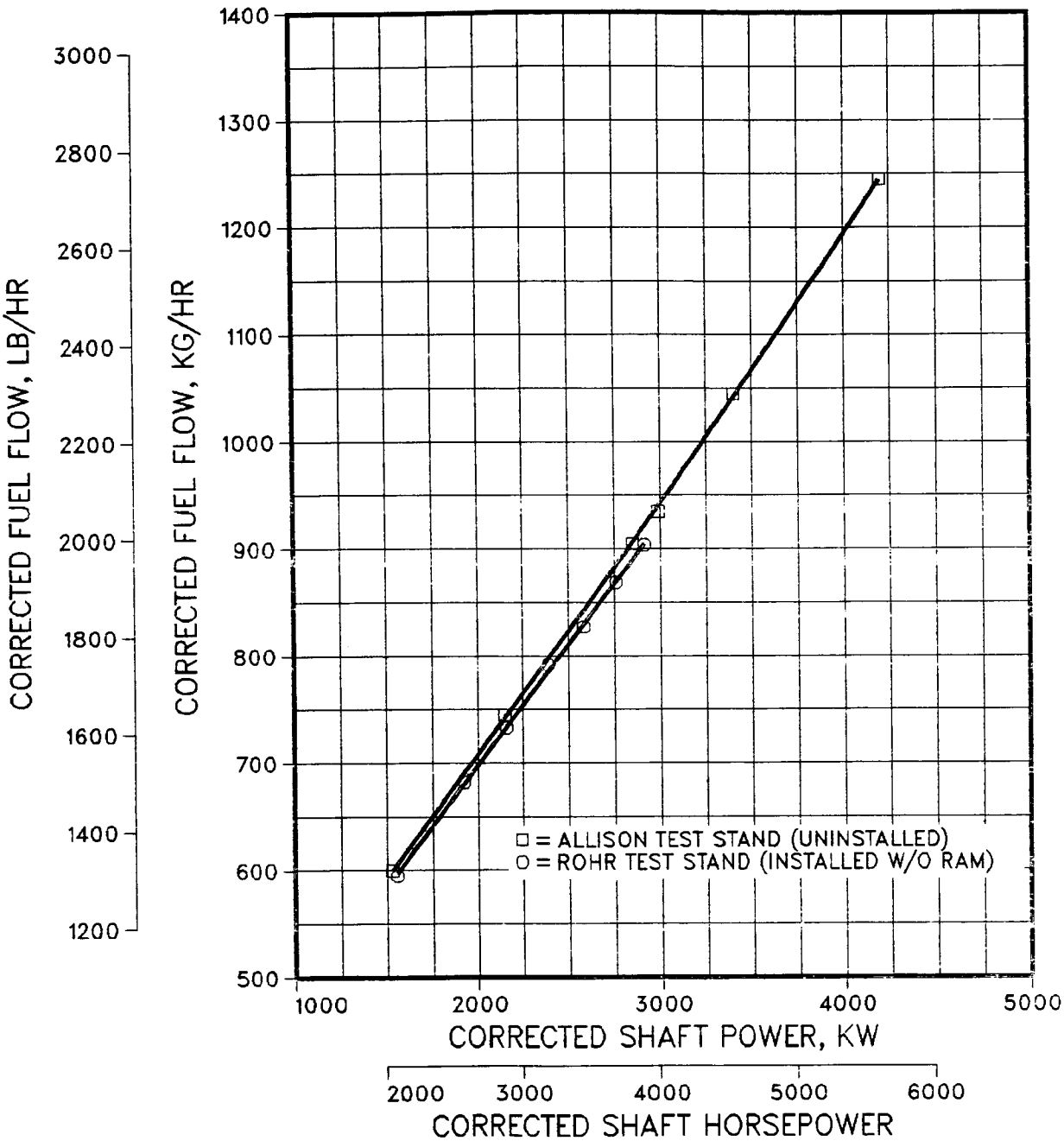

Figure 9.36. Unity Ram Fuel Flow - Installed Versus Uninstalled - 100% N_p Speed

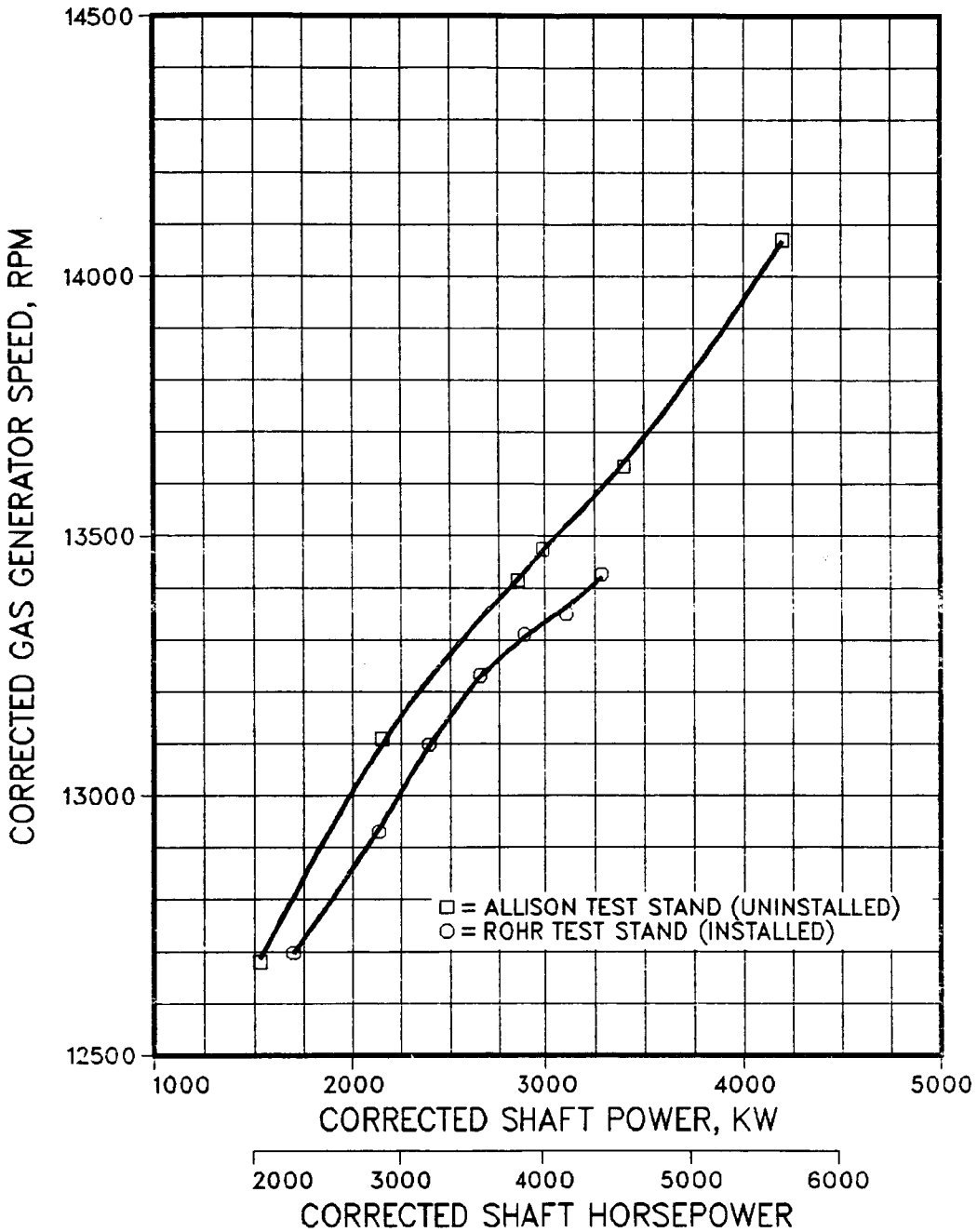

Figure 9.37. Corrected Gas Generator Speed - Installed Versus Uninstalled - 100% N_p Speed

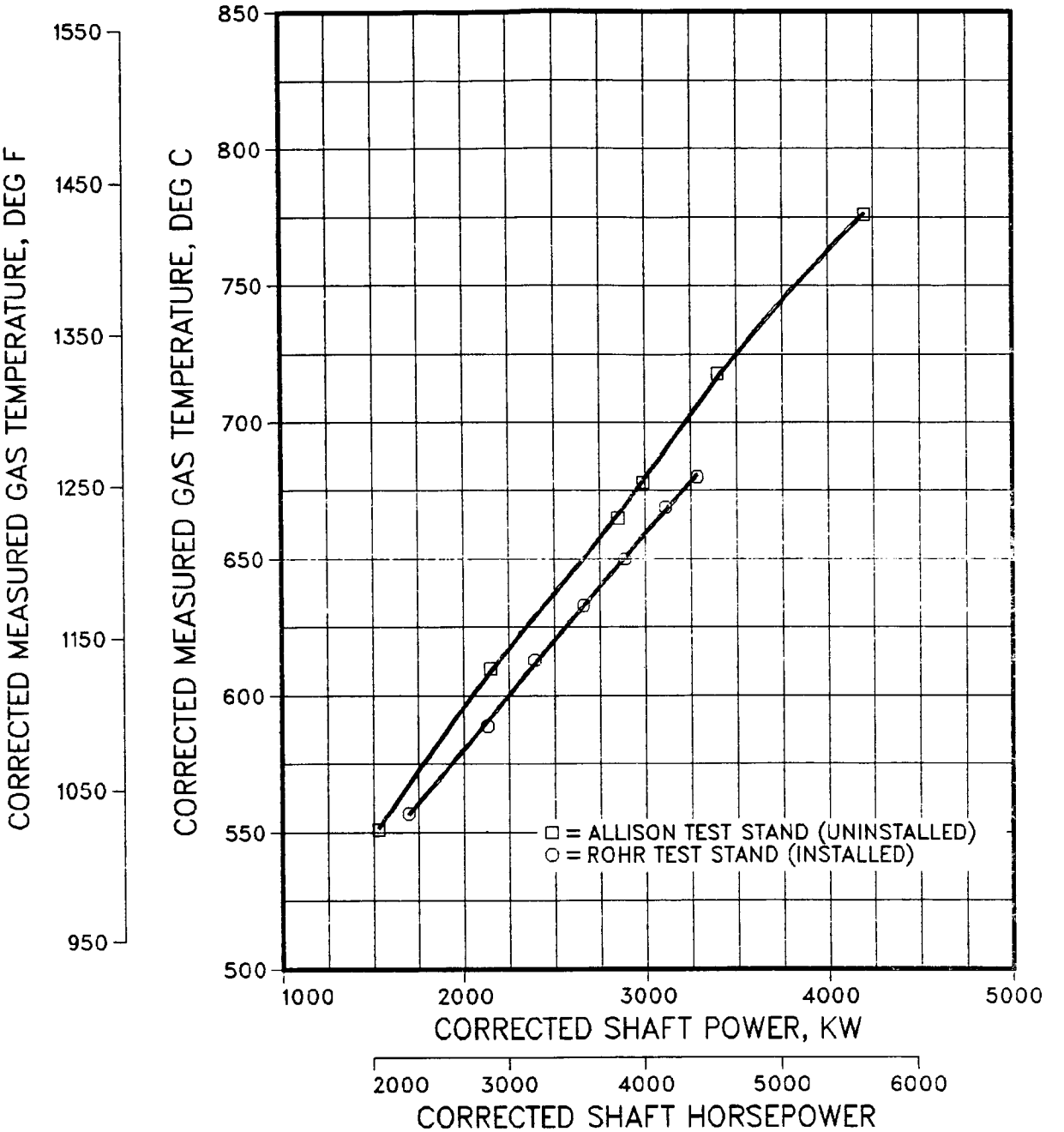

Figure 9.38. Corrected MGT - Installed Versus Uninstalled - 100% N_p Speed

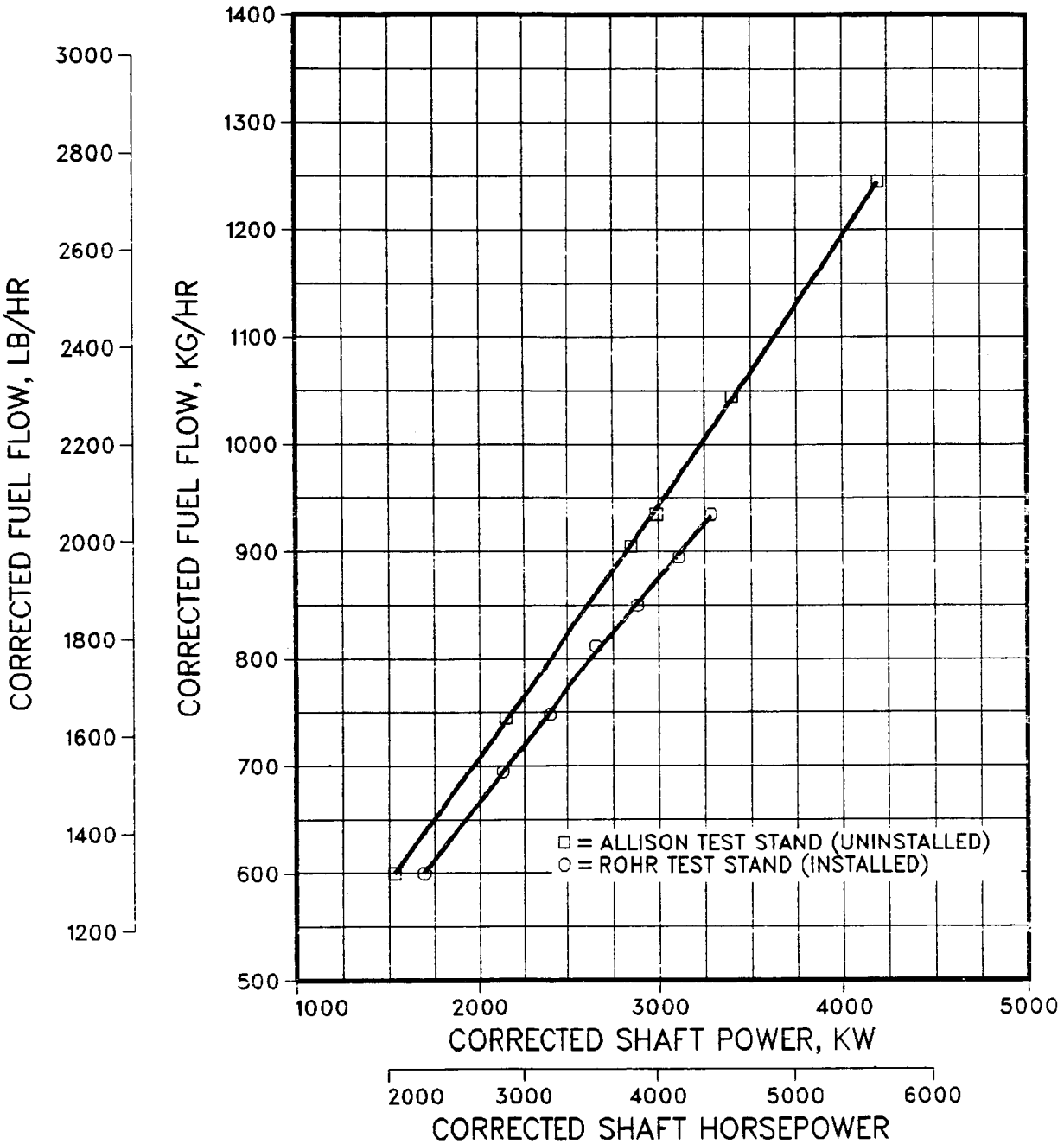

Figure 9.39. Corrected Fuel Flow - Installed Versus Uninstalled - 100% N_p Speed

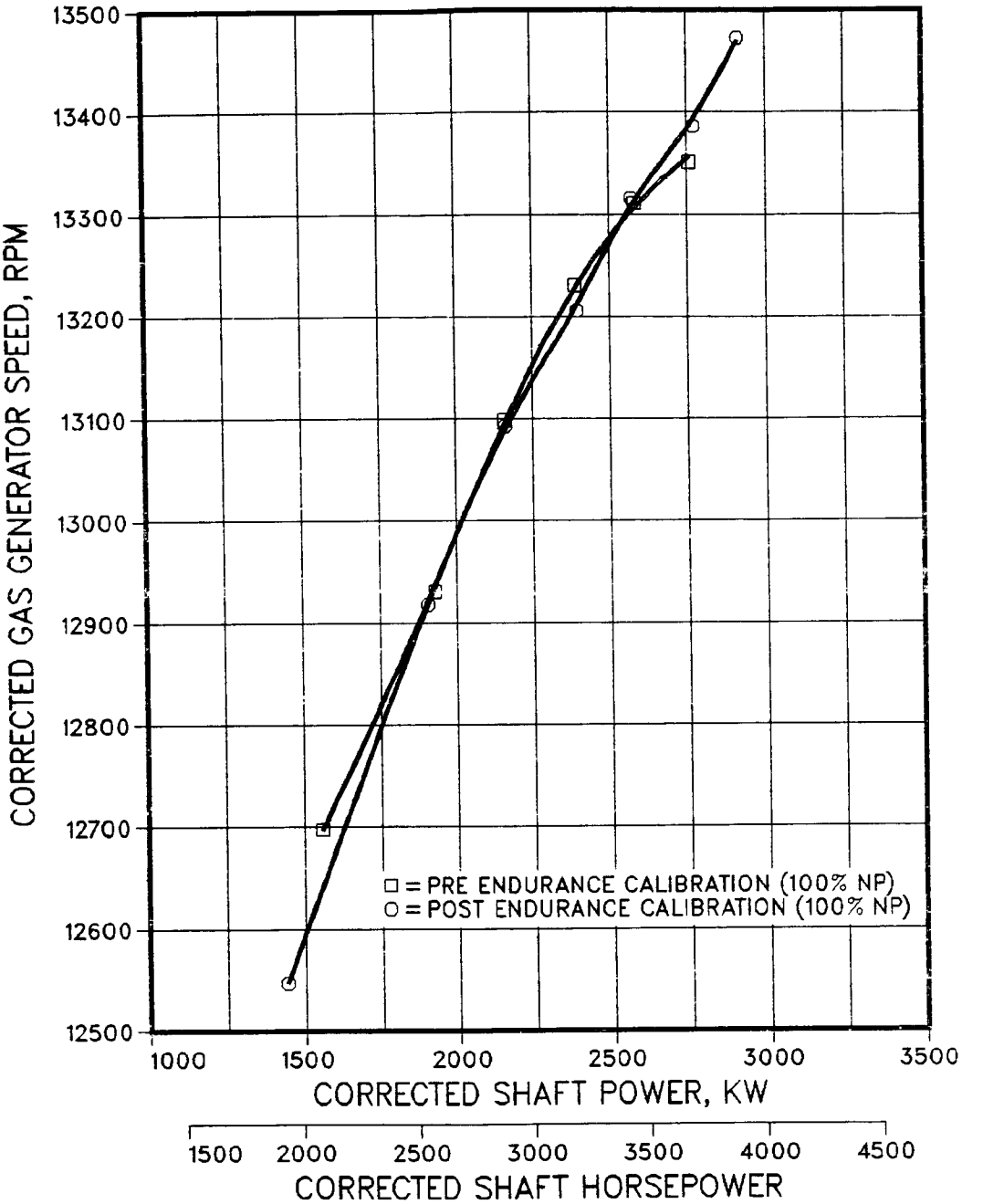

Figure 9.40. Corrected Gas Generator Speed - Pre- Versus Post-Endurance - 100% N_p Speed

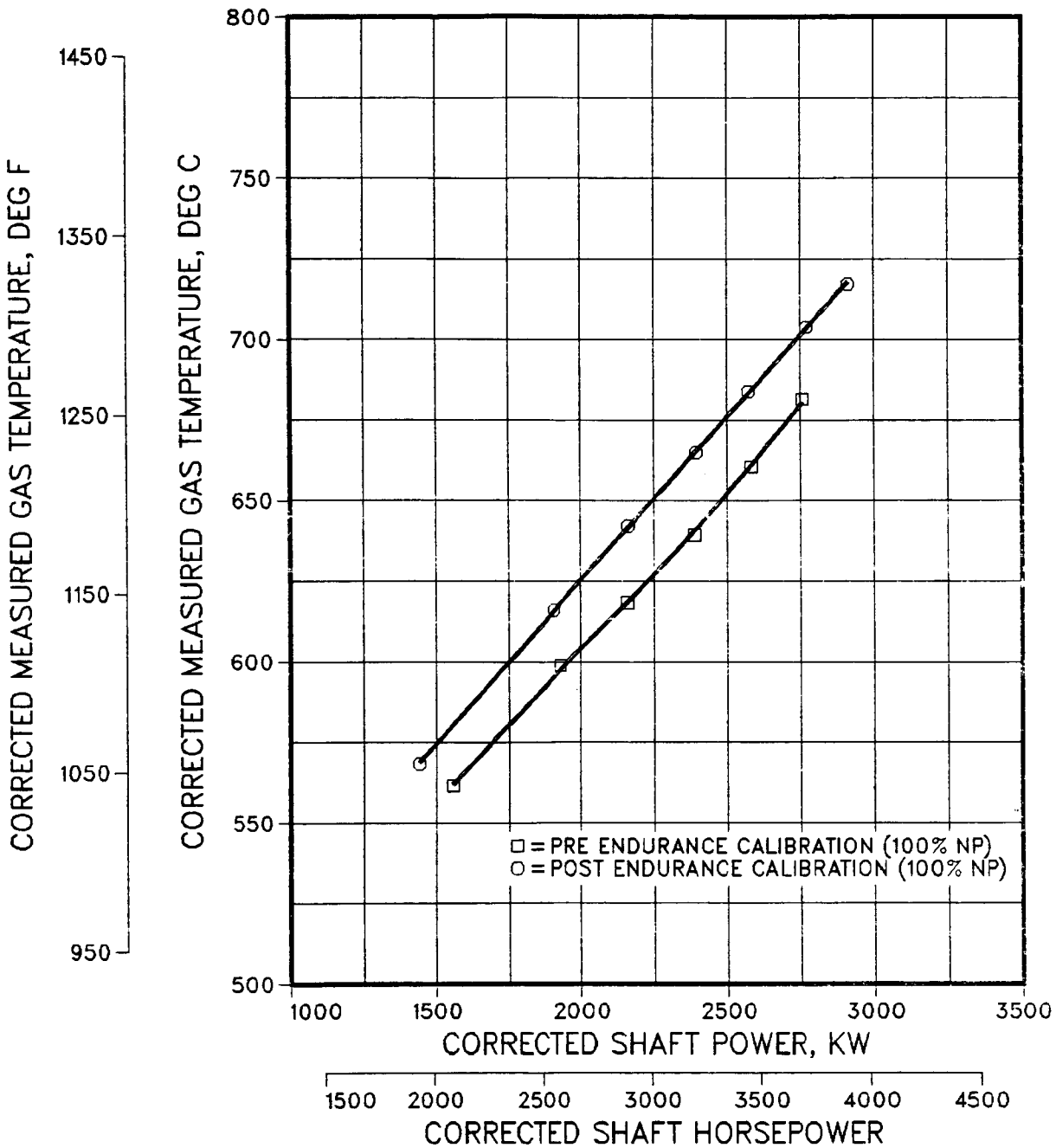

Figure 9.41. Corrected MGT - Pre- Versus Post-Endurance - 100% N_p Speed

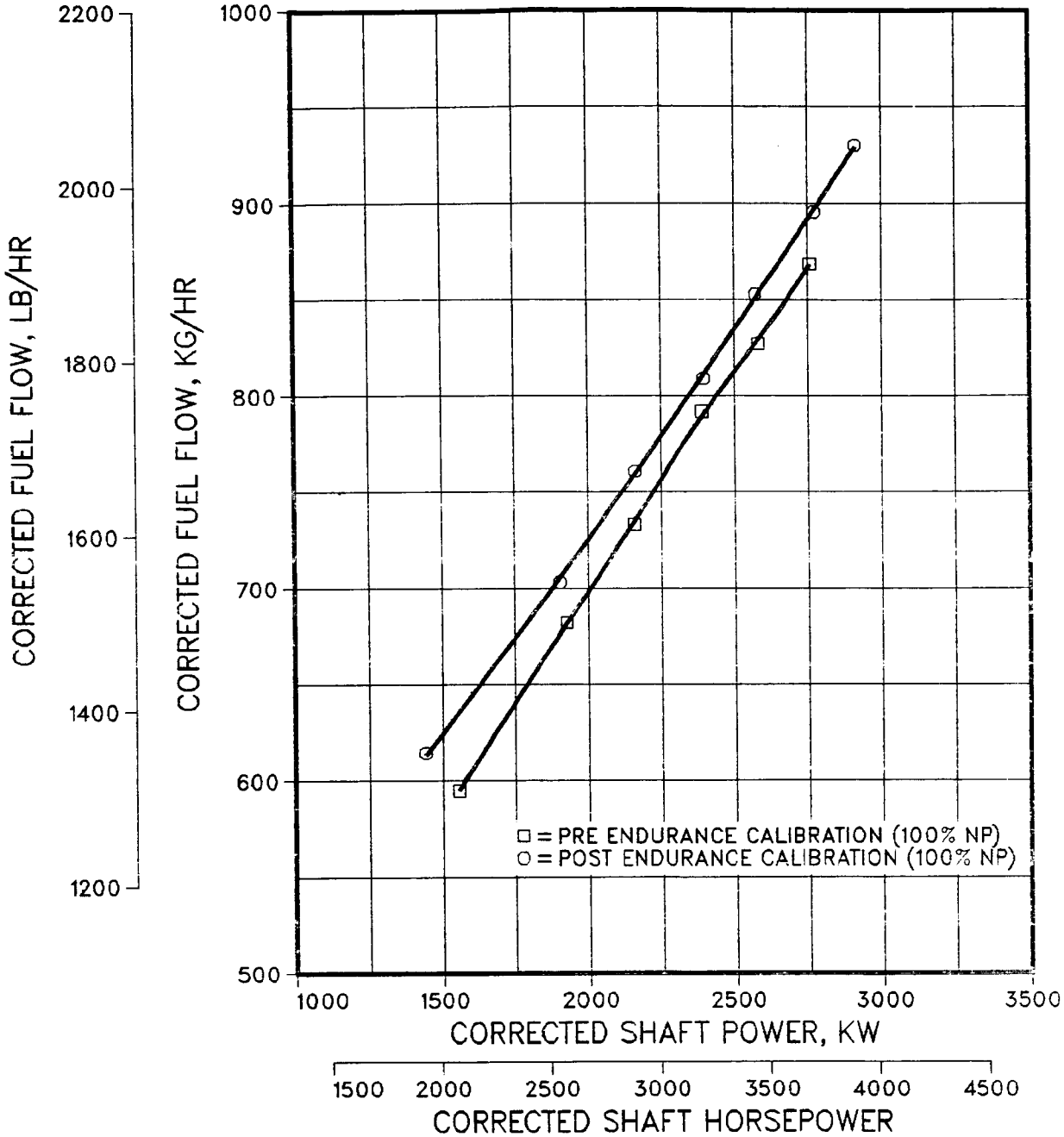

Figure 9.42. Corrected Fuel Flow - Pre- Versus Post-Endurance - 100% N_p Speed

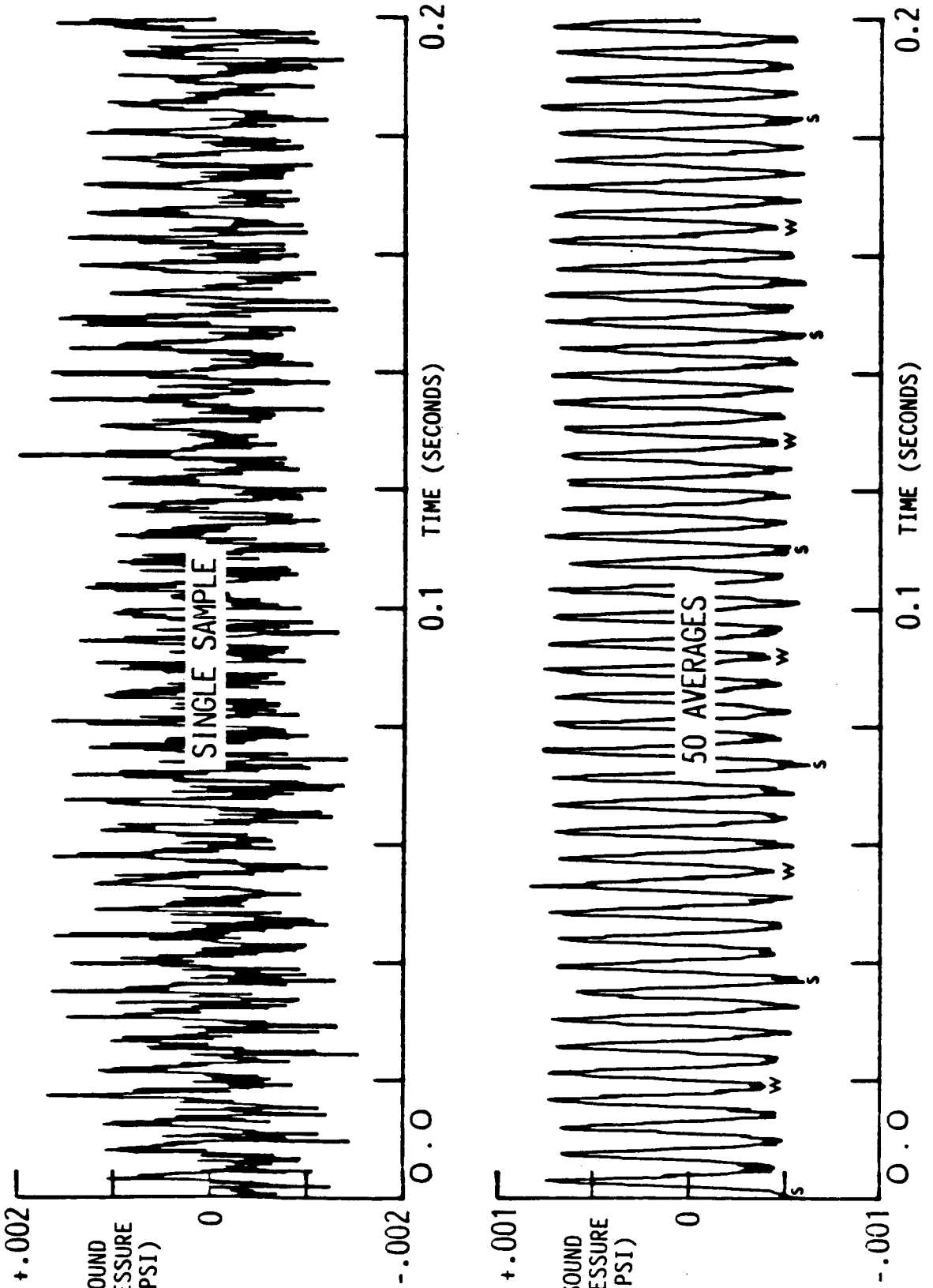

Figure 9.43. Ground Level Sound Pressures - 45.7 m, 90° Azimuth, 1732 KW, 100% N_p Speed (200 ms Time Histories)

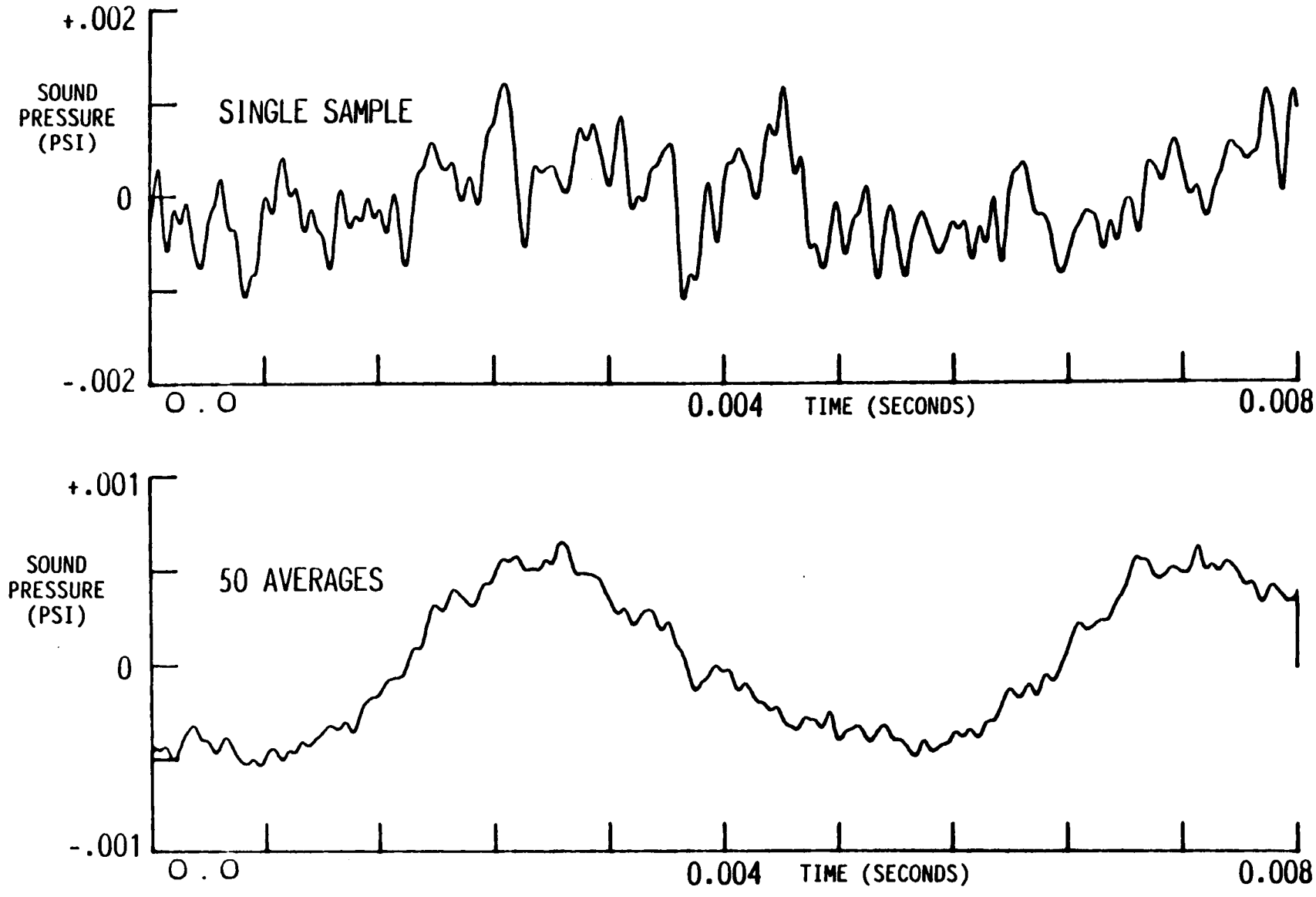

Figure 9.44. Ground Level Sound Pressures - 45.7 m, 90° Azimuth, 1732 KW, 100% N_p Speed (8 ms Time Histories)

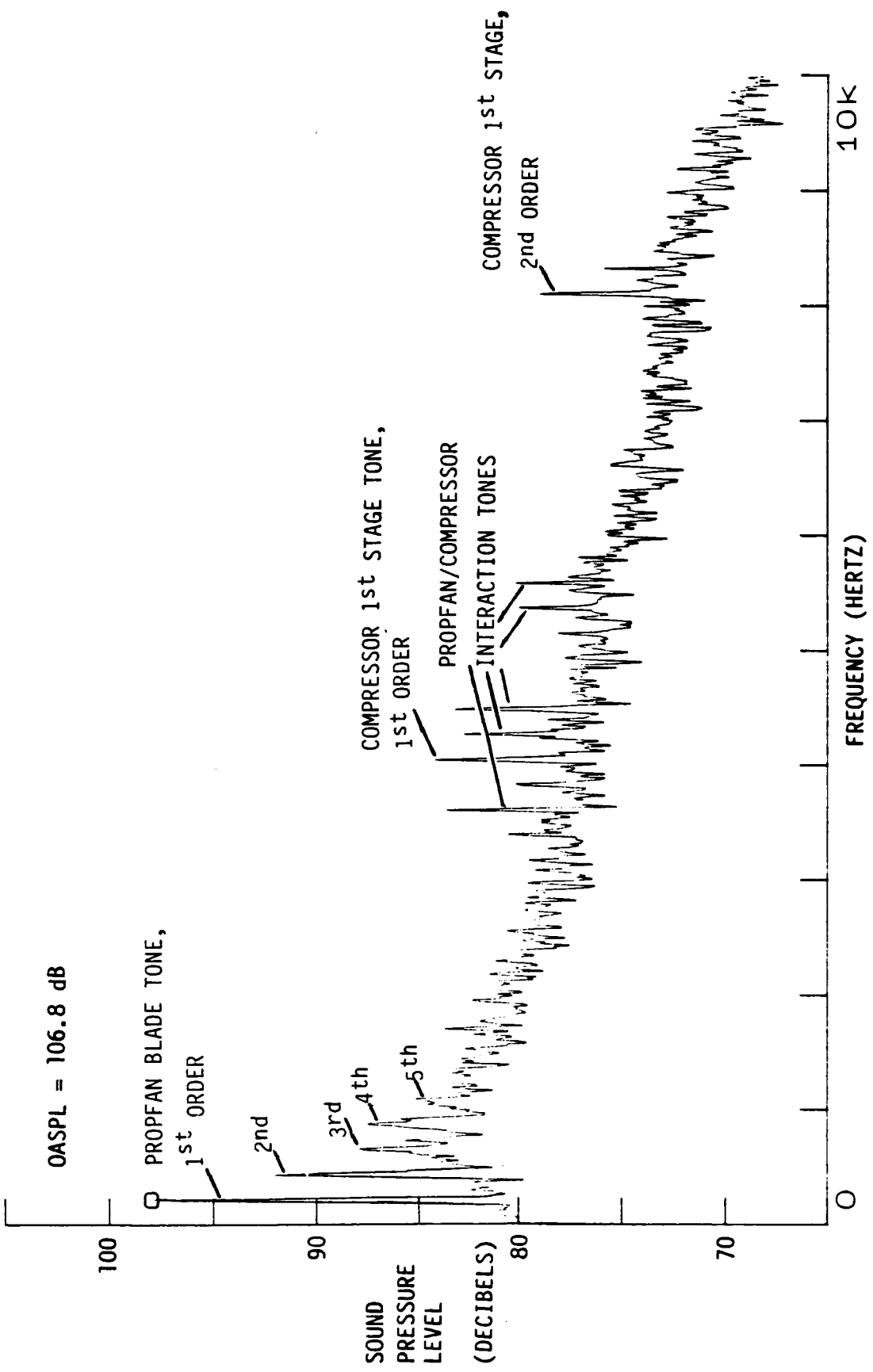

Figure 9.45. Ground Level Noise Spectrum - 45.7 m, 30° Azimuth, 1732 KW, 100% N_p Speed

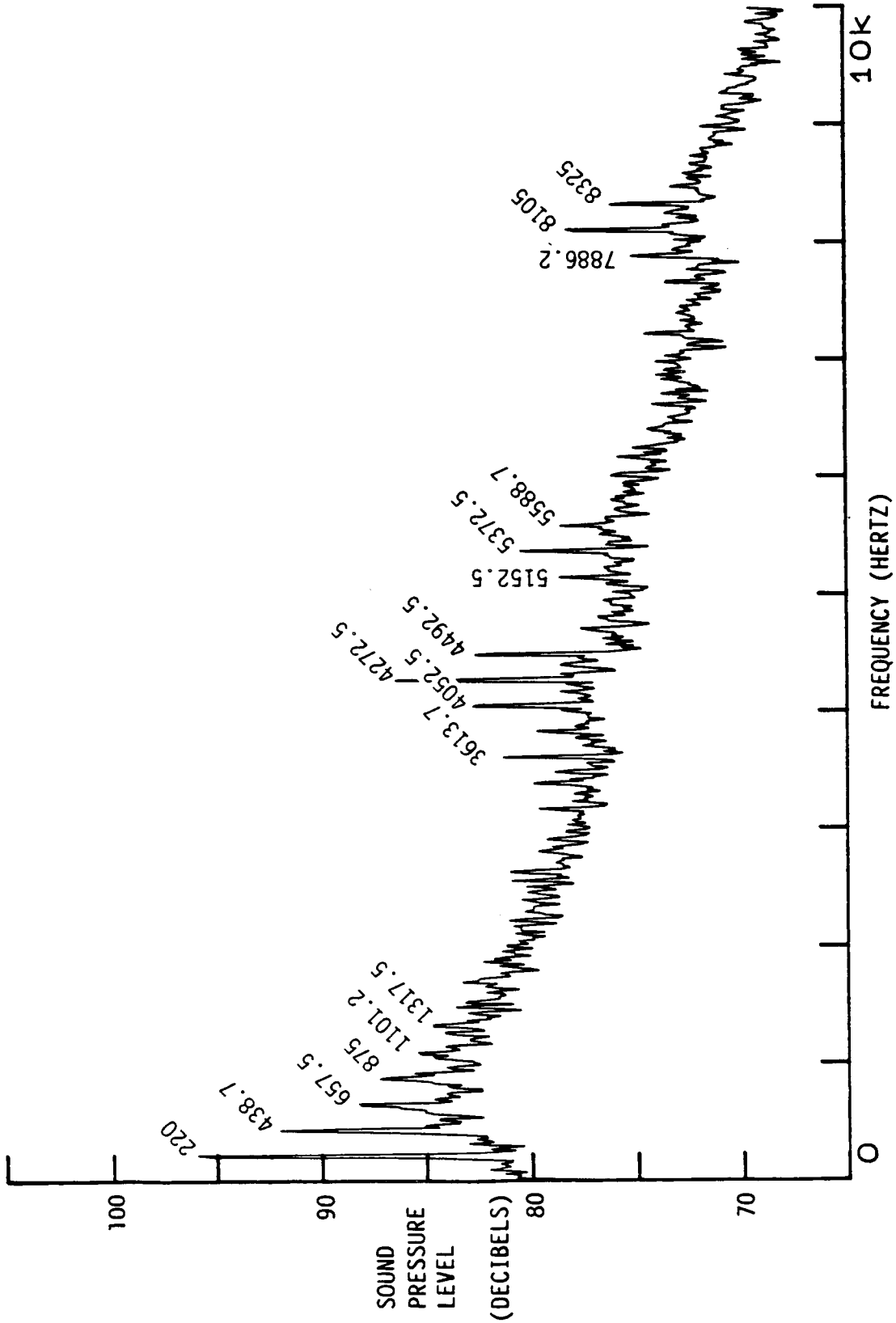

Figure 9.46. Ground Level Noise Spectrum - 45.7 m, 30° Azimuth, 1732 KW, 100% N_p Speed (High Resolution (10x) Frequency Analysis)

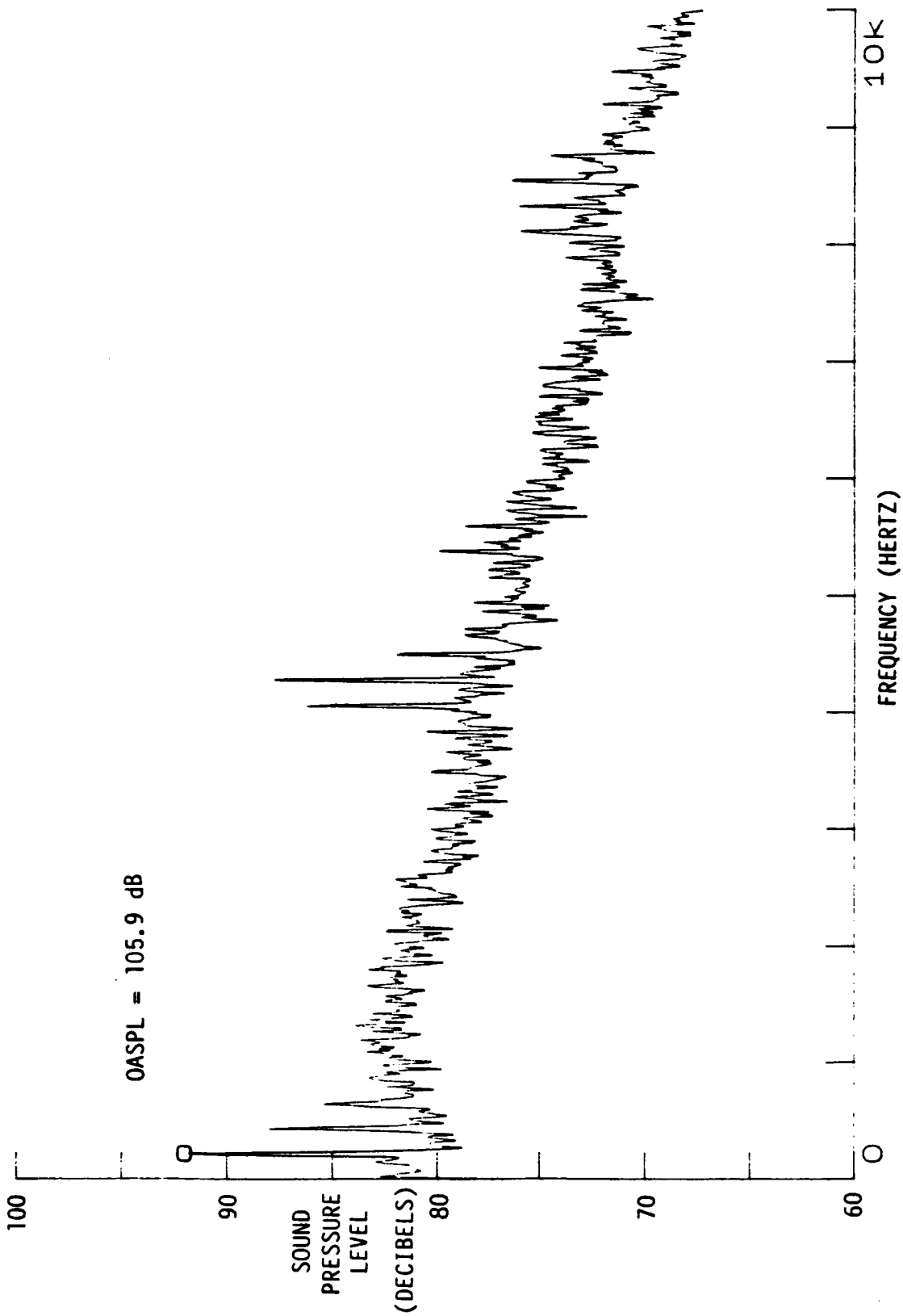

Figure 9.47. Ground Level Noise Spectrum - 45.7 m, 60° Azimuth, 1732 KW, 100% N_p Speed

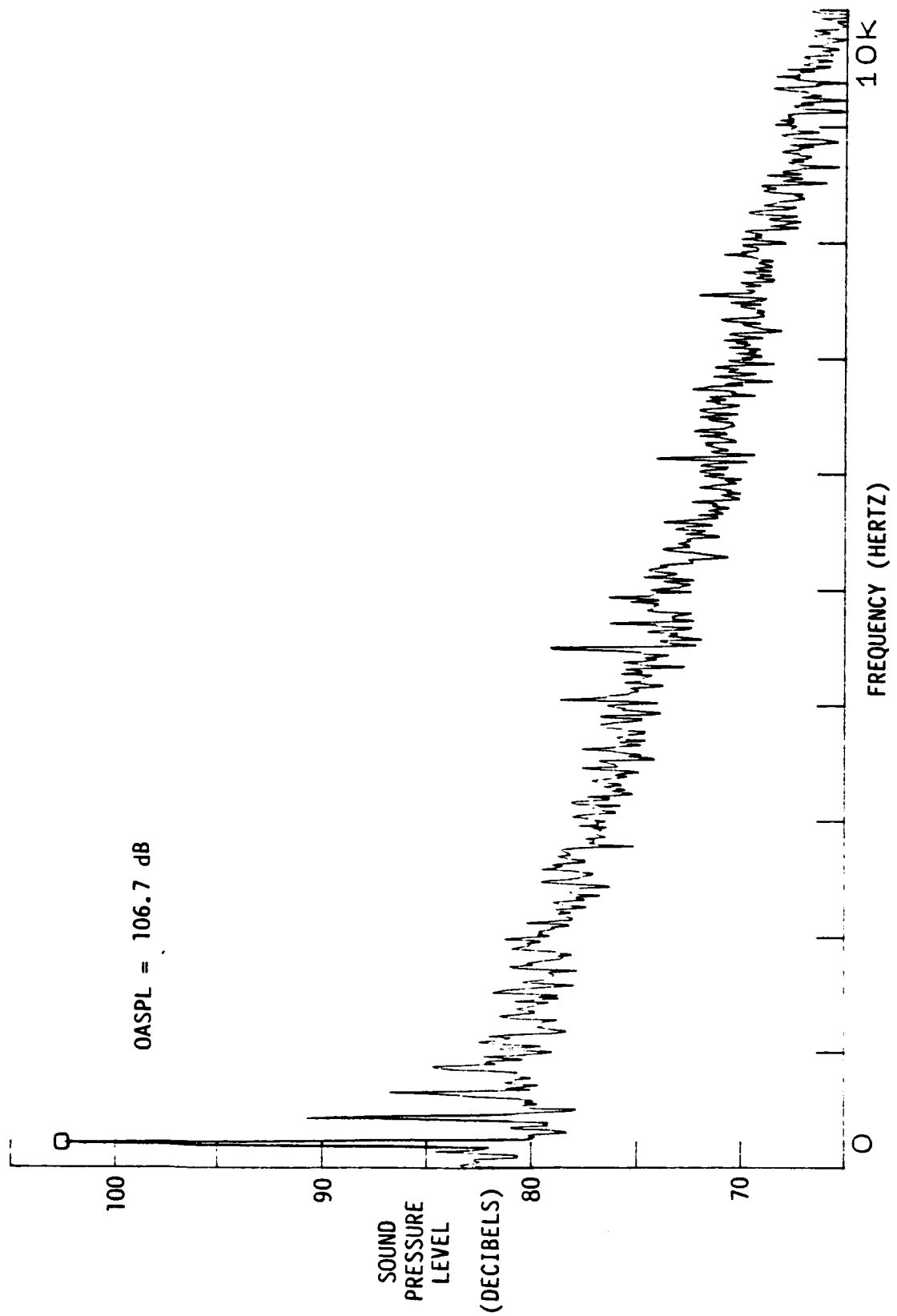

Figure 9.48. Ground Level Noise Spectrum - 45.7 m, 90° Azimuth, 1732 KW, 100% N_p Speed

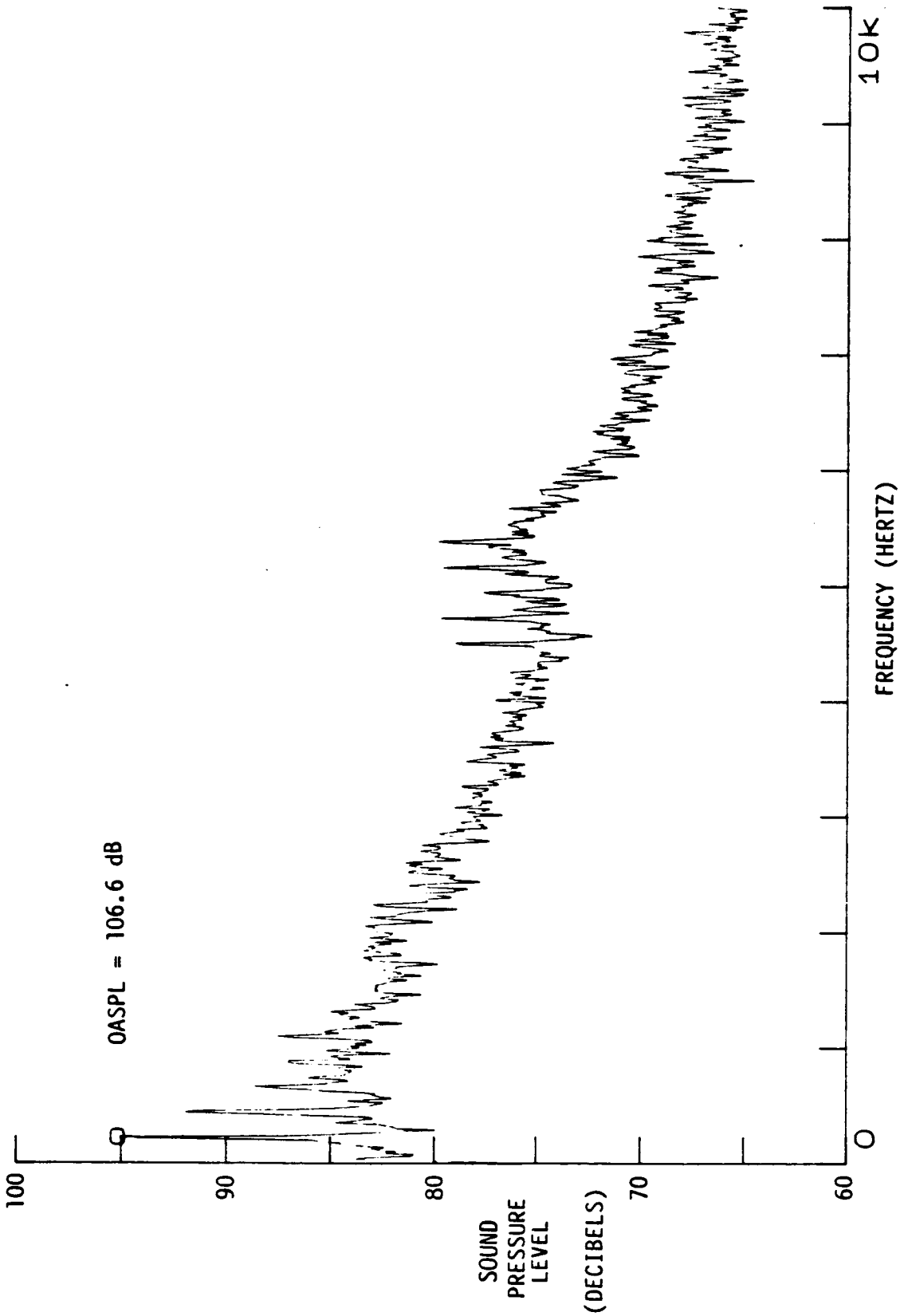

Figure 9.49. Ground Level Noise Spectrum - 45.7 m, 120° Azimuth, 1732 Kw, 100% N_p Speed

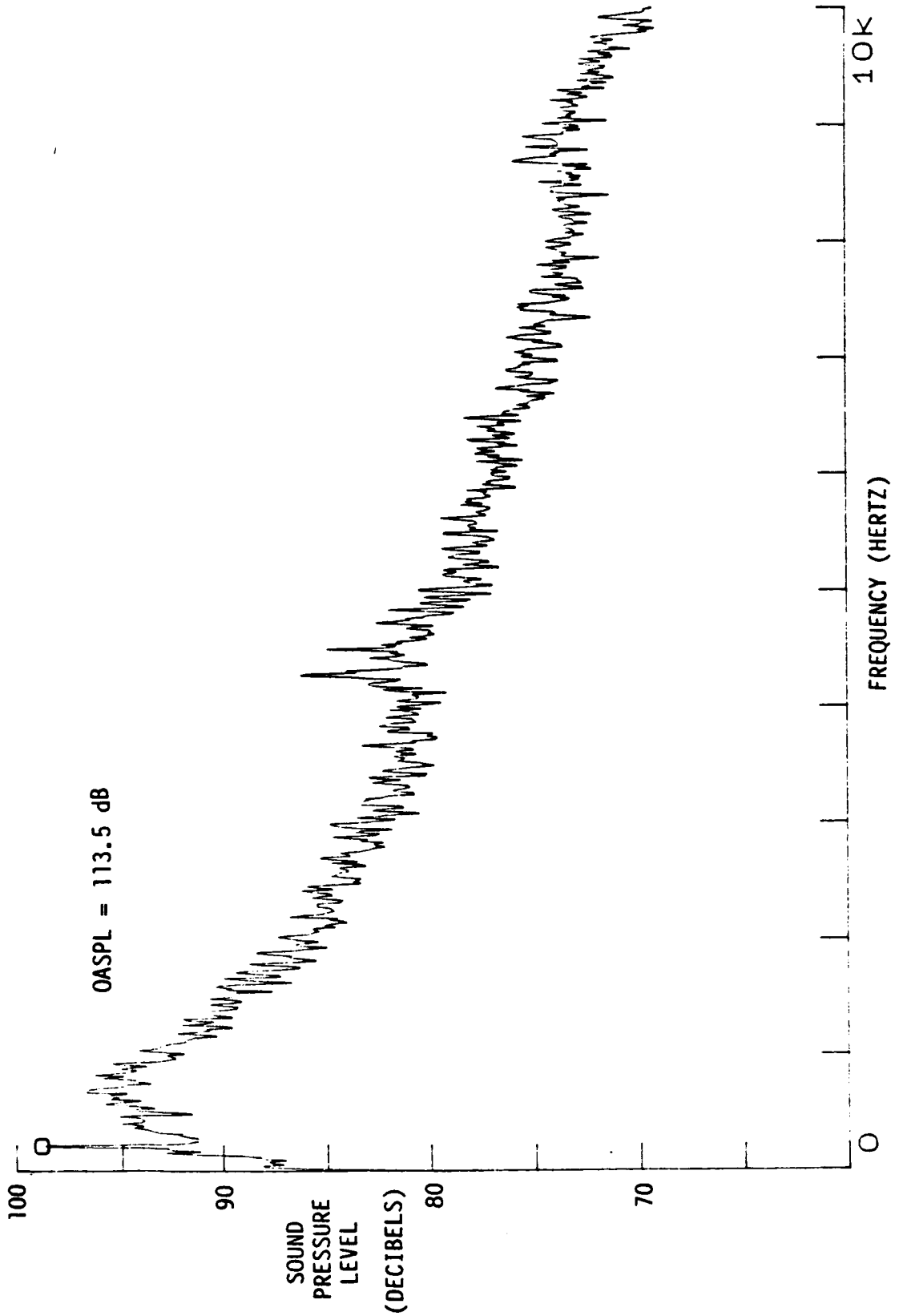

Figure 9.50. Ground Level Noise Spectrum - 45.7 m, 60° Azimuth, 3007 KW, 100% N_p Speed

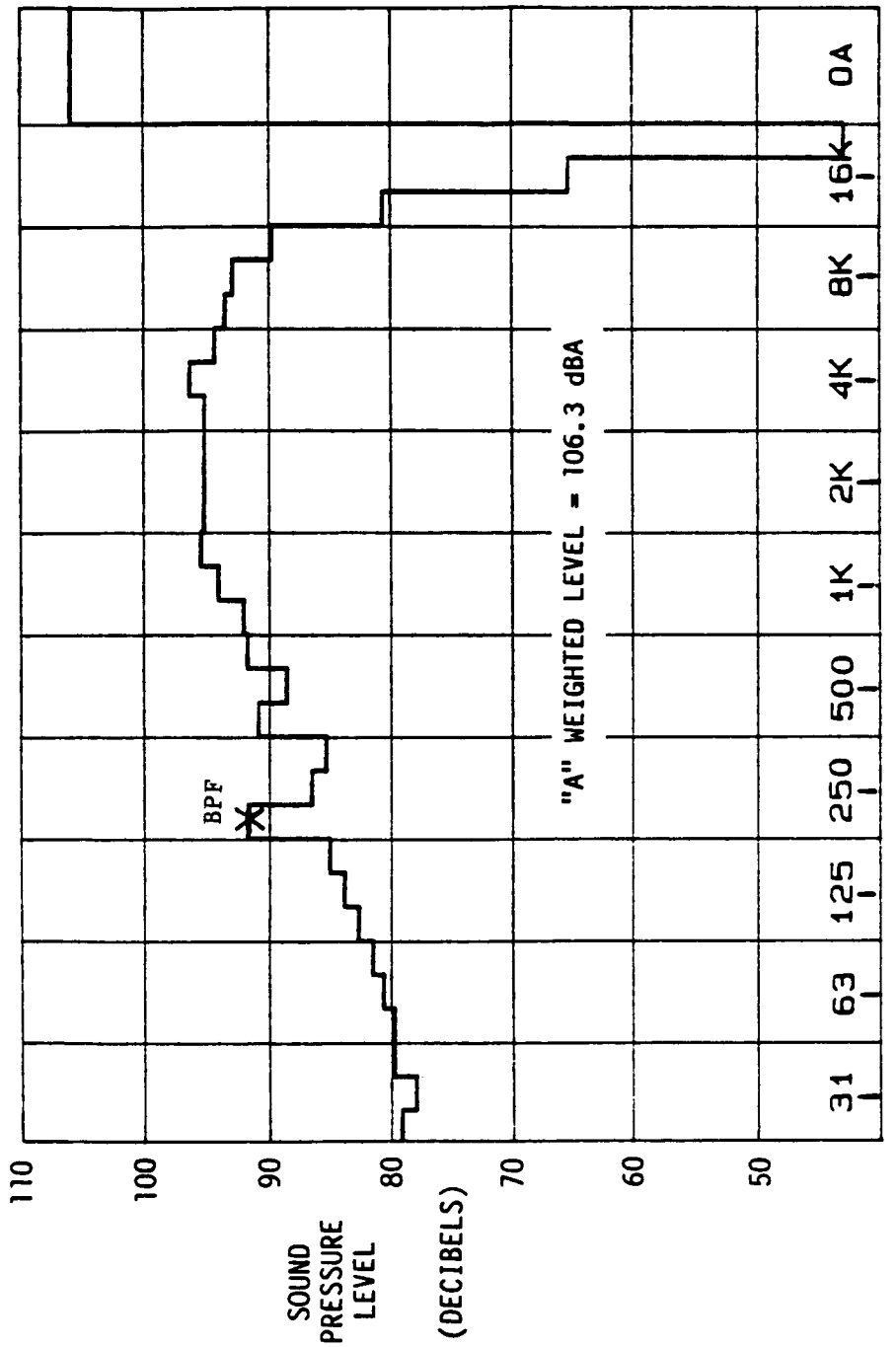

Figure 9.51. Ground Level One-Third Octave Noise Spectrum - 45.7 m, 60° Azimuth, 1732 KW, 100% N_p Speed

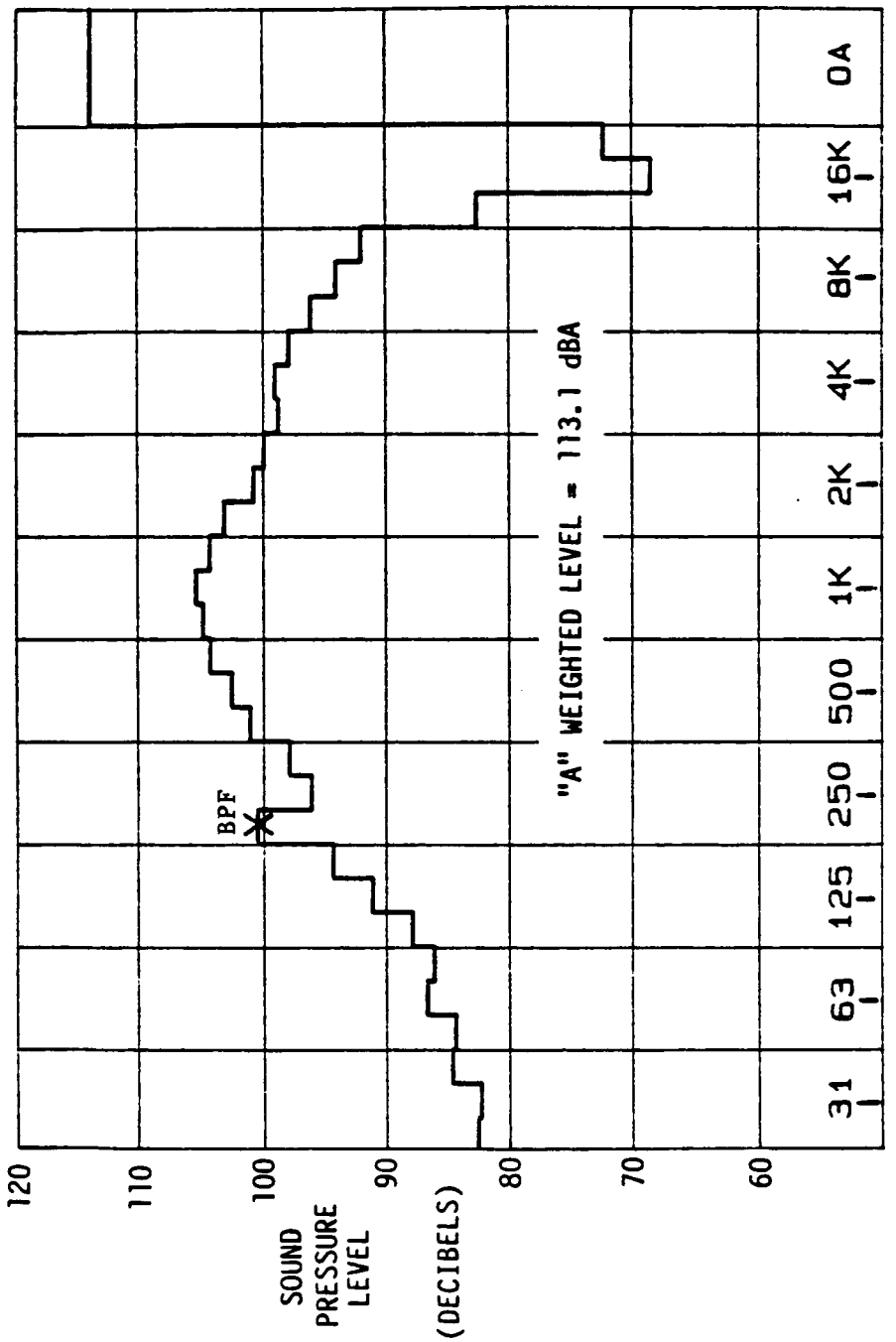

Figure 9.52. Ground Level One-Third Octave Noise Spectrum - 45.7 m, 60° Azimuth, 3007 KW, 100% N_p Speed

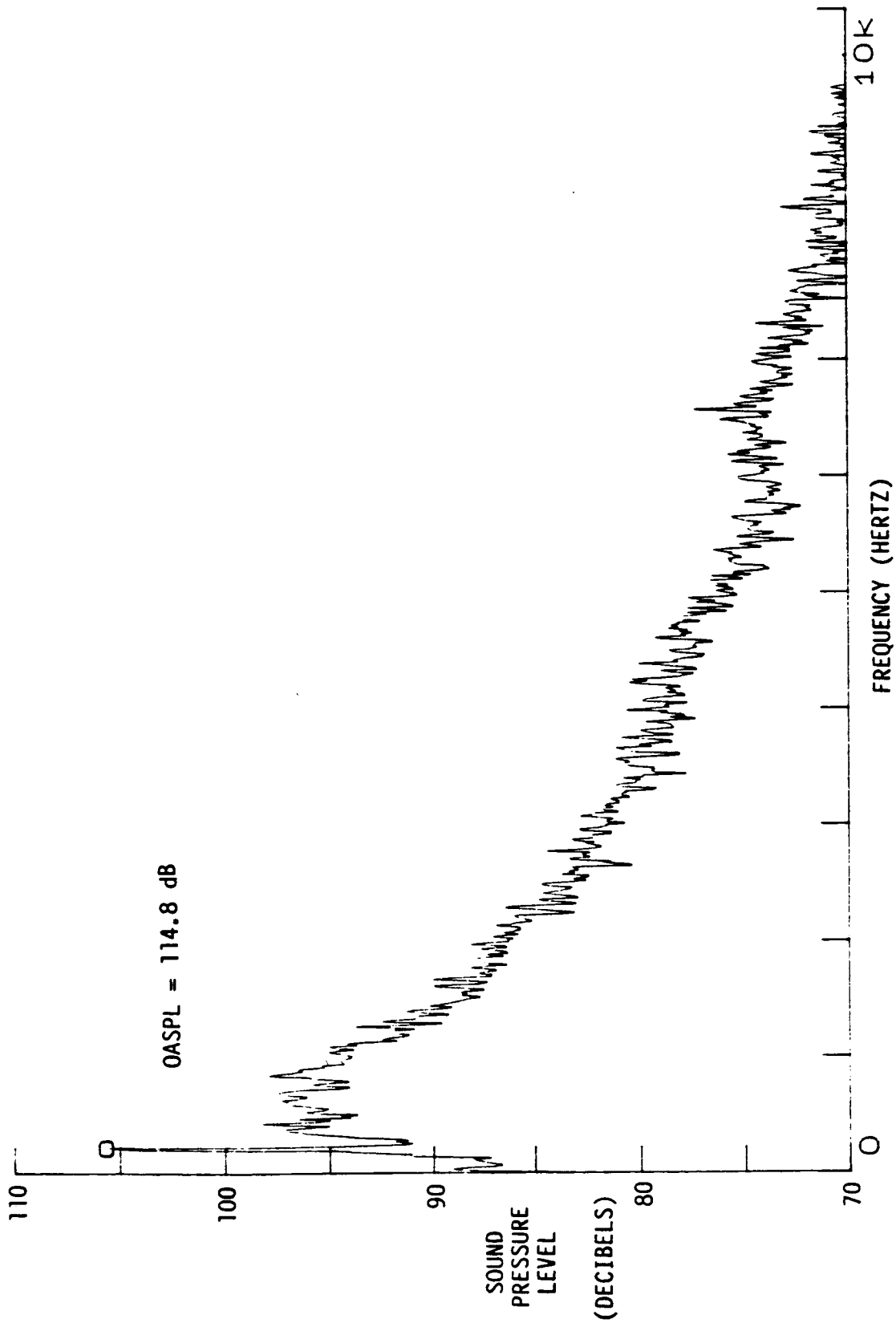

Figure 9.53. Ground Level Noise Spectrum - 45.7 m, 90° Azimuth, 3007 KW, 100% N_p Speed

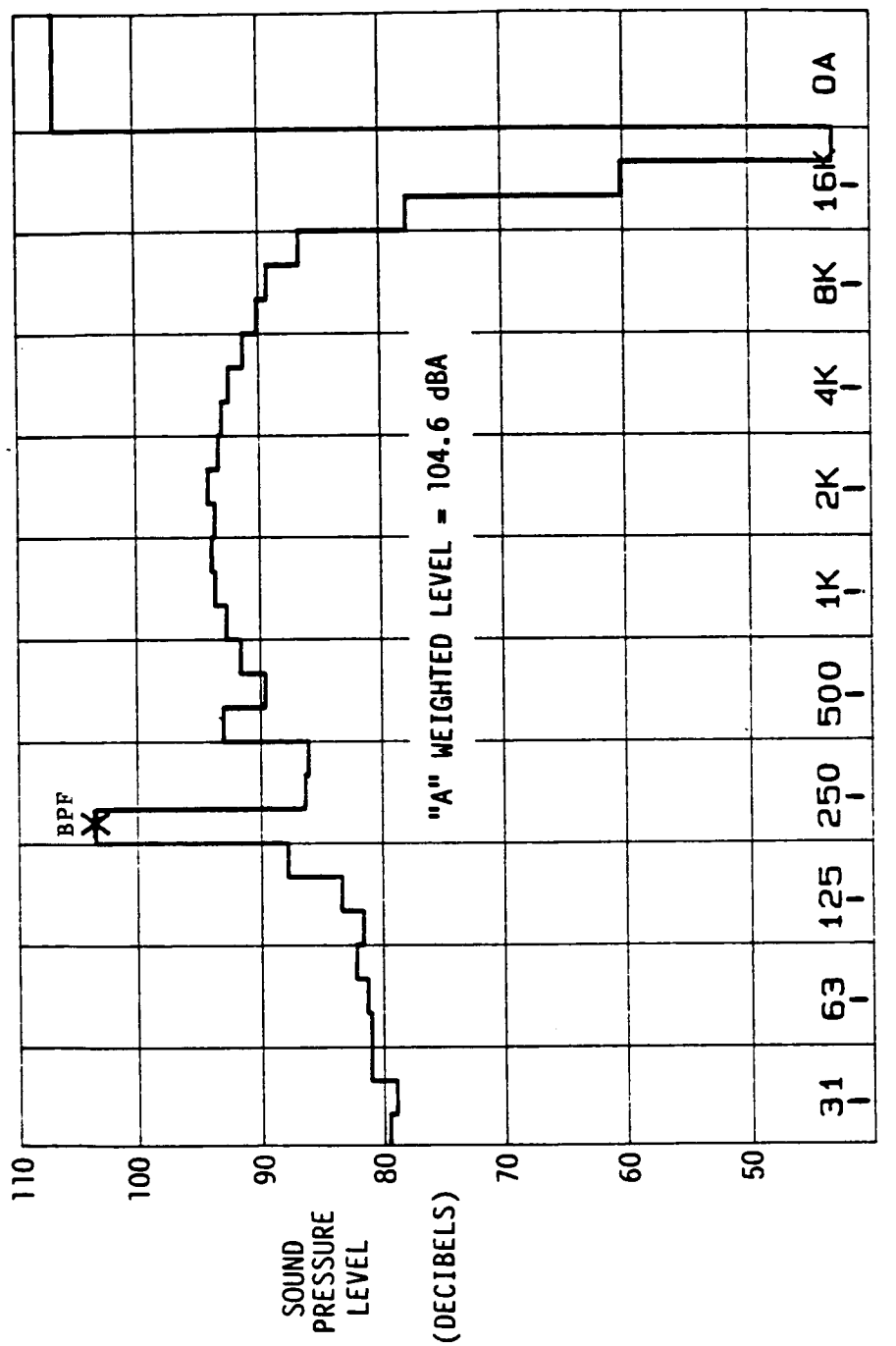

Figure 9.54. Ground Level One-Third Octave Noise Spectrum - 45.7 m, 90° Azimuth, 1732 KW, 100% N_p Speed

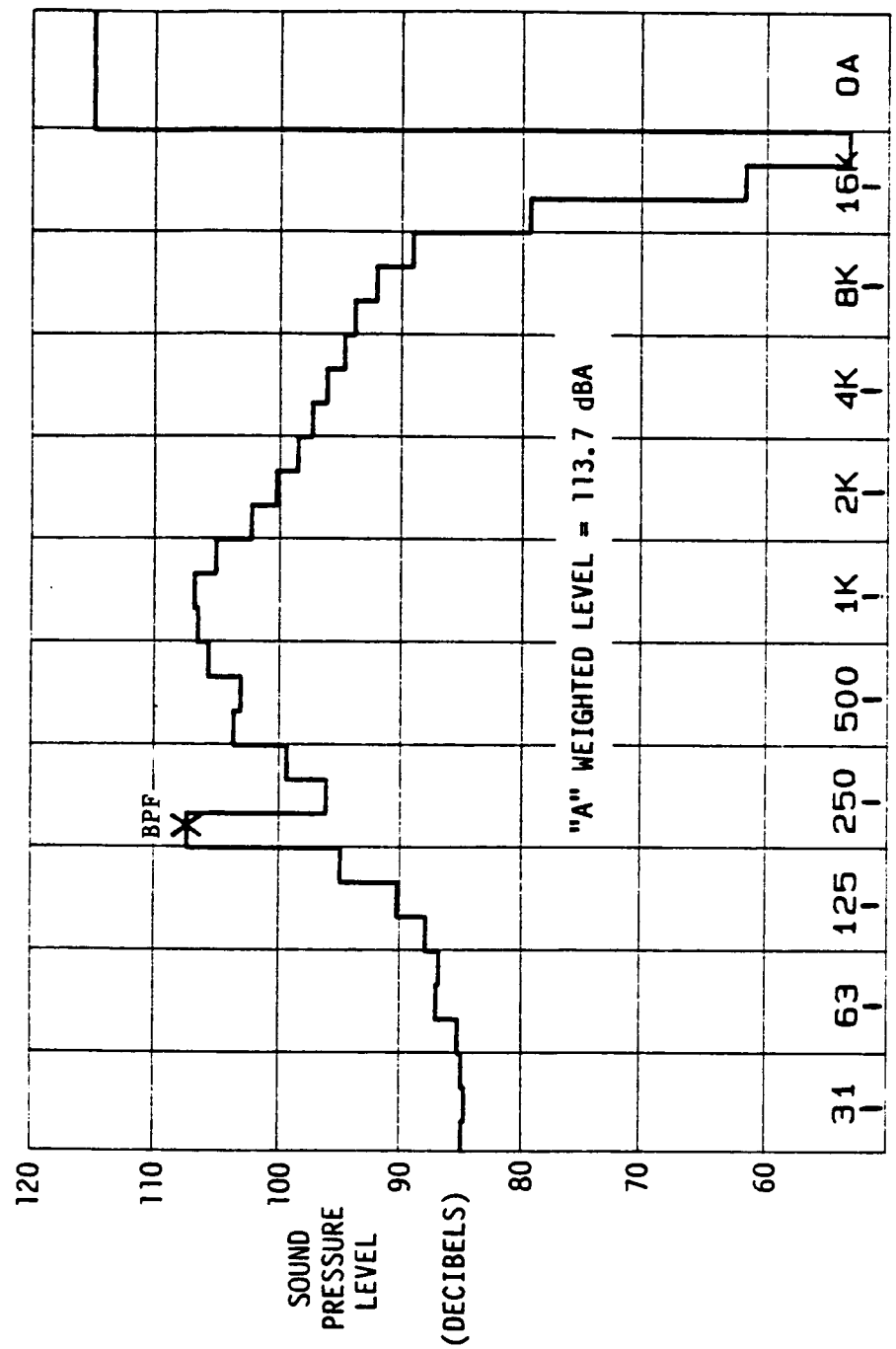

Figure 9.55. Ground Level One-Third Octave Noise Spectrum - 45.7 m, 90° Azimuth, 3007 KW, 100% N_p Speed

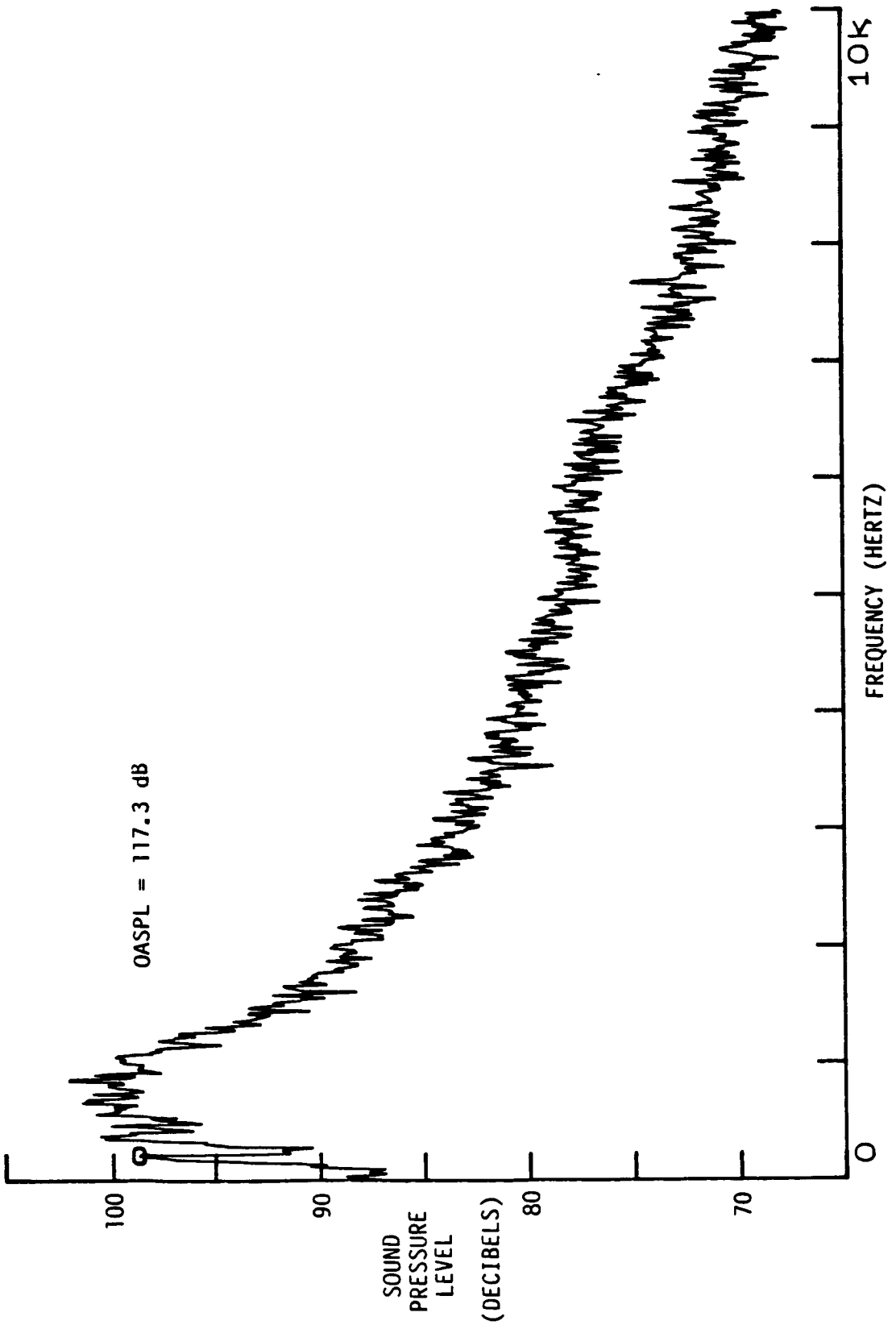

Figure 9.56. Ground Level Noise Spectrum - 45.7 m, 120° Azimuth, 3007 KW, 100% N_p Speed

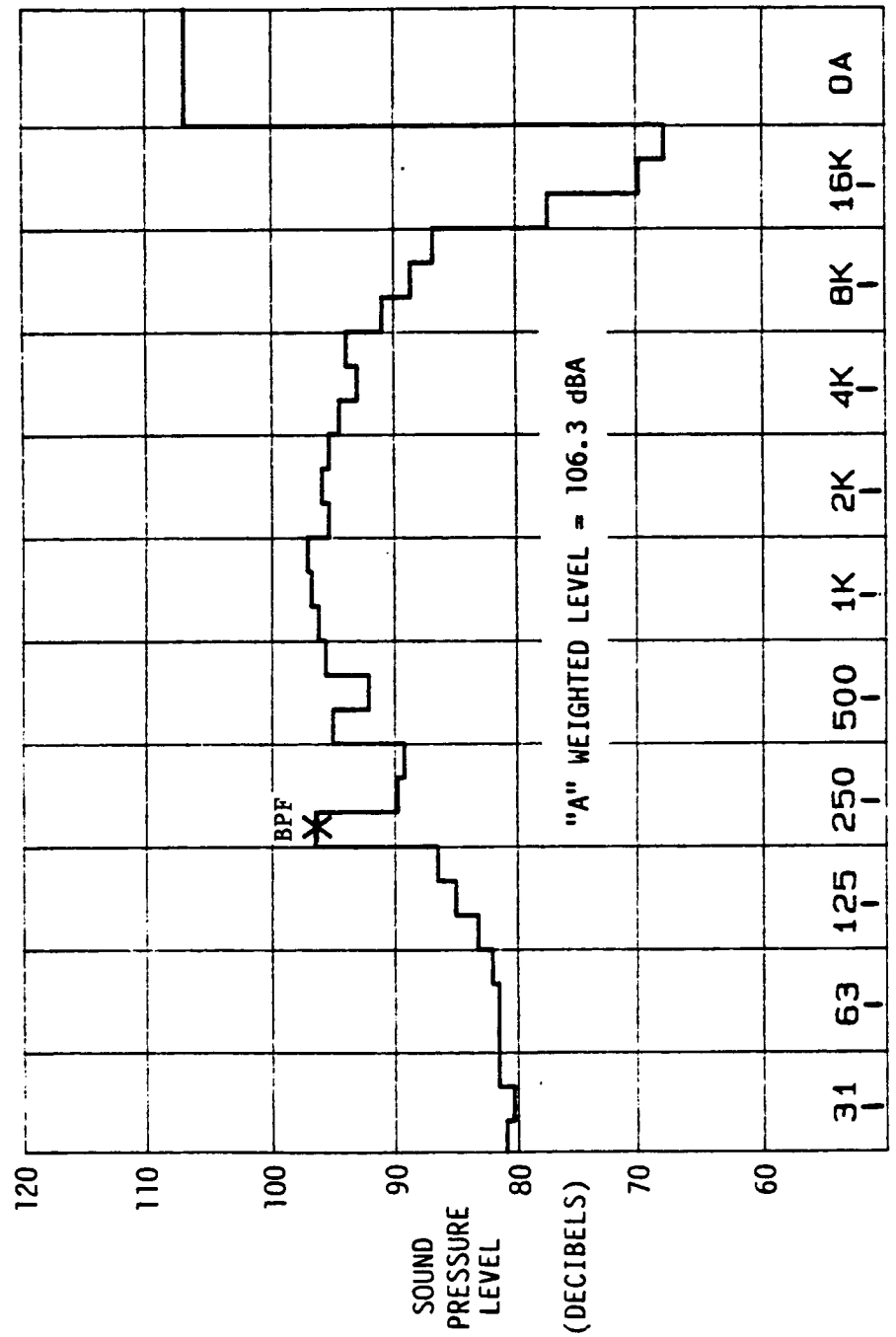

Figure 9.57. Ground Level One-Third Octave Noise Specturm - 45.7 m, 120° Azimuth, 1732 Kw, 100% N_p Speed

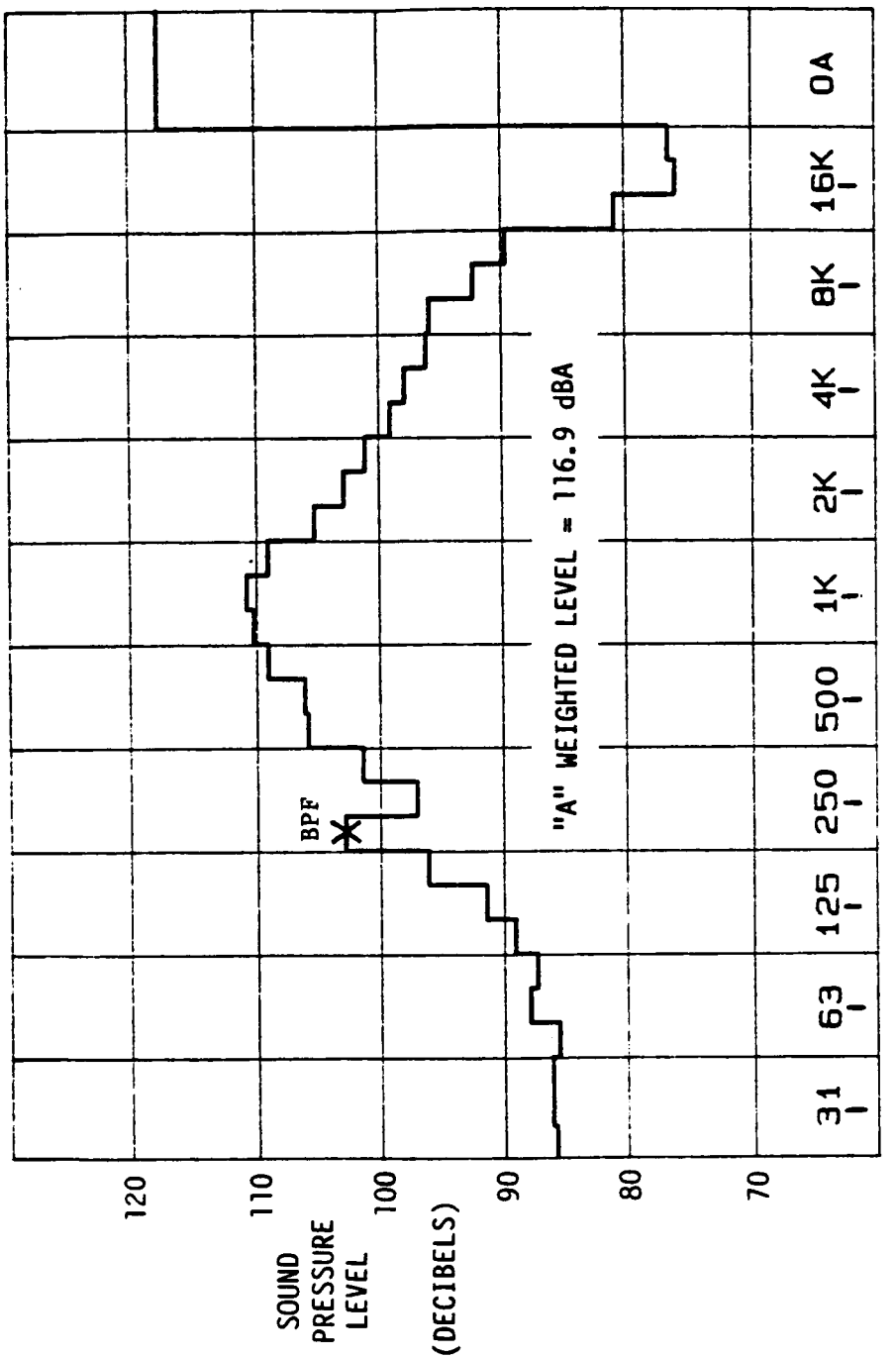

Figure 9.58. Ground Level One-Third Octave Noise Spectrum - 45.7 m, 120° Azimuth, 3007 KW, 100% N_p Speed

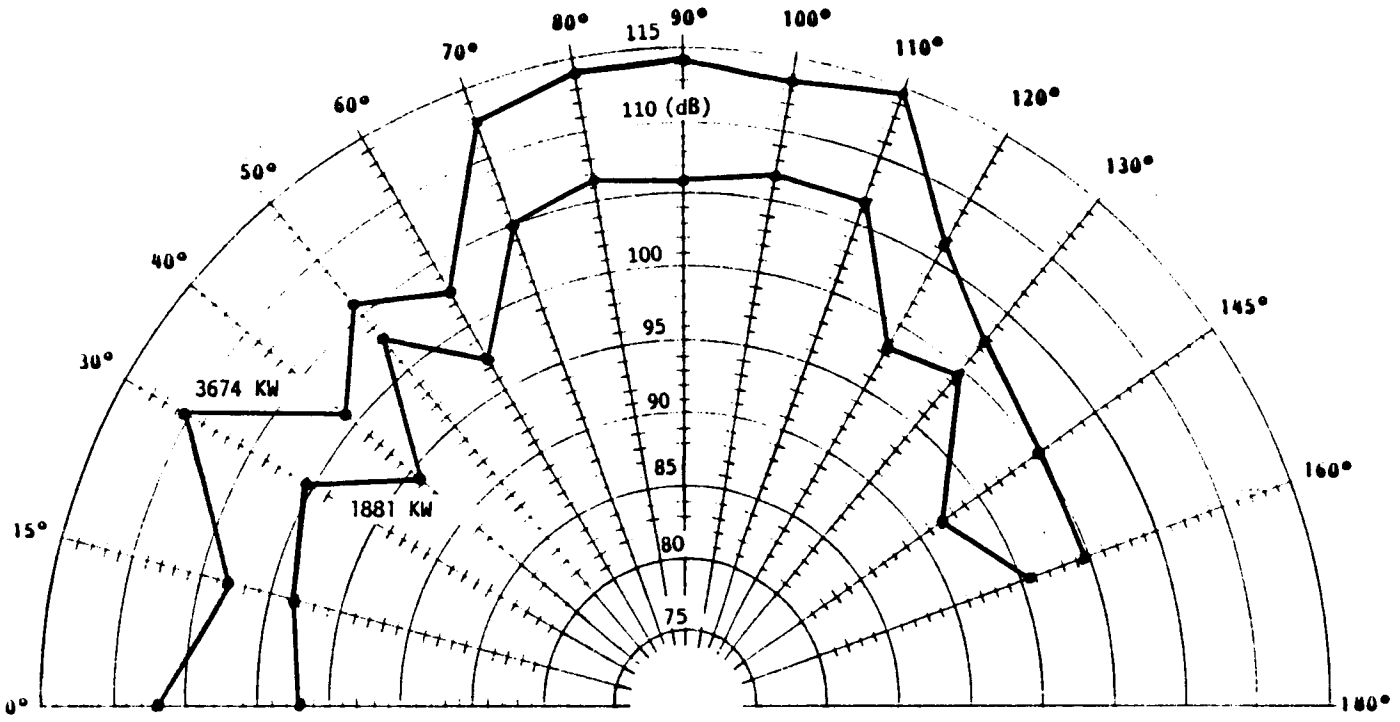

Figure 9.59. Ground Level First Order Blade Passage SPL - 45.7 m, 105% N_p Speed

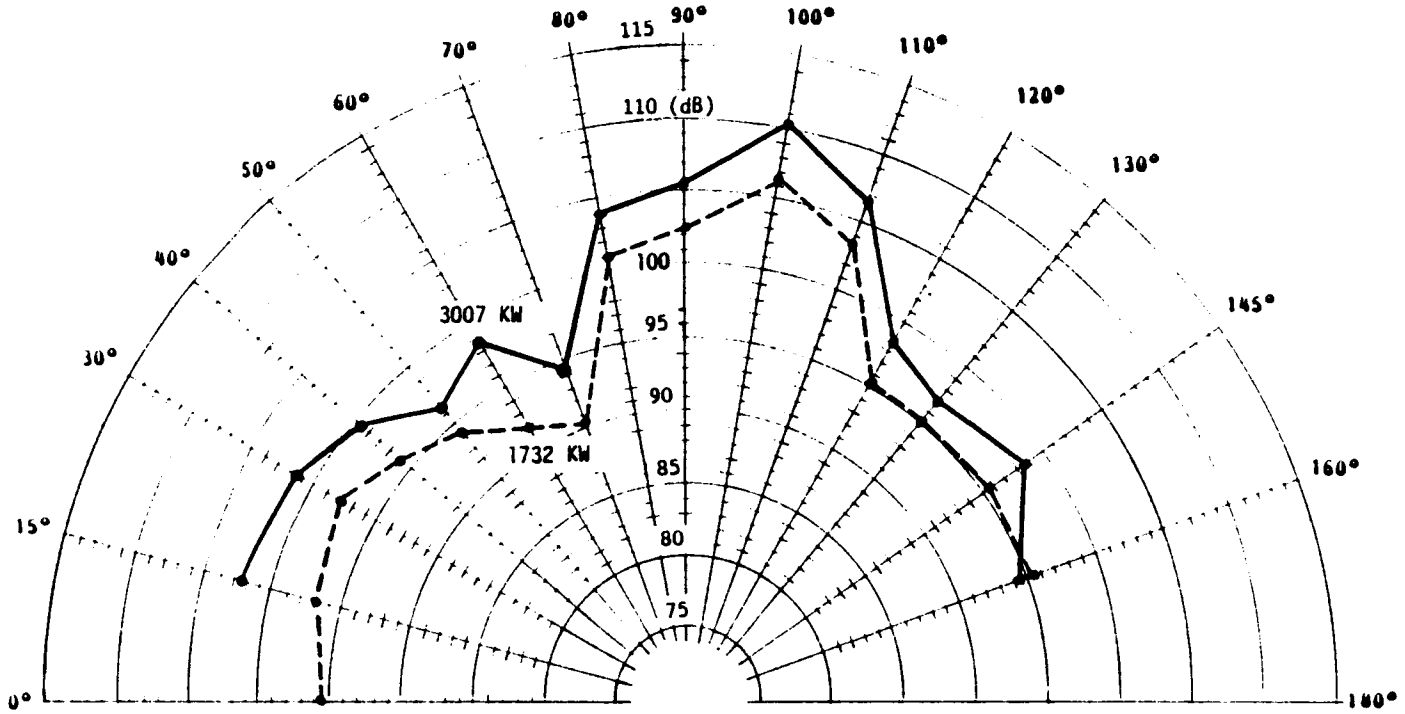

Figure 9.60. Ground Level First Order Blade Passage SPL - 45.7 m, 100% N_p Speed

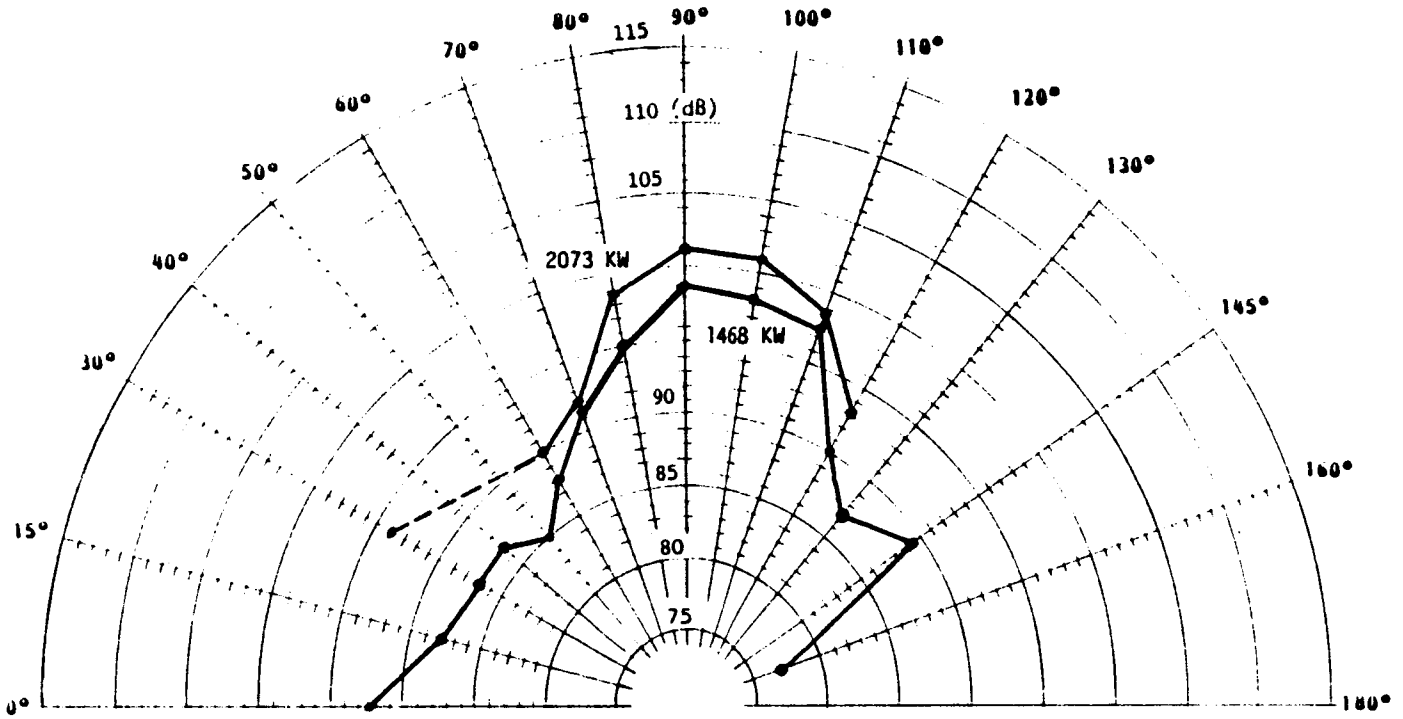

Figure 9.61. Ground Level First Order Blade Passage SPL - 45.7 m, 87.5% N_p Speed

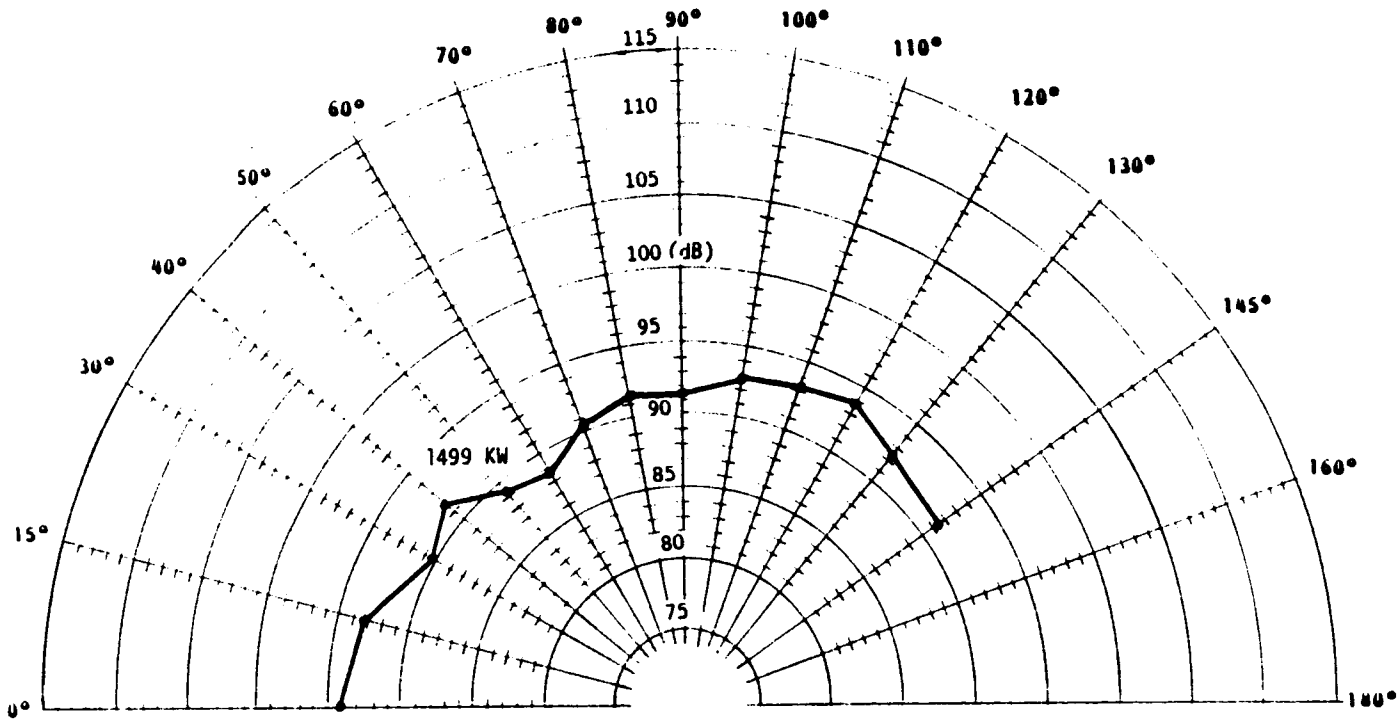

Figure 9.62. Ground Level First Order Blade Passage SPL - 45.7 m, 75% N_p Speed

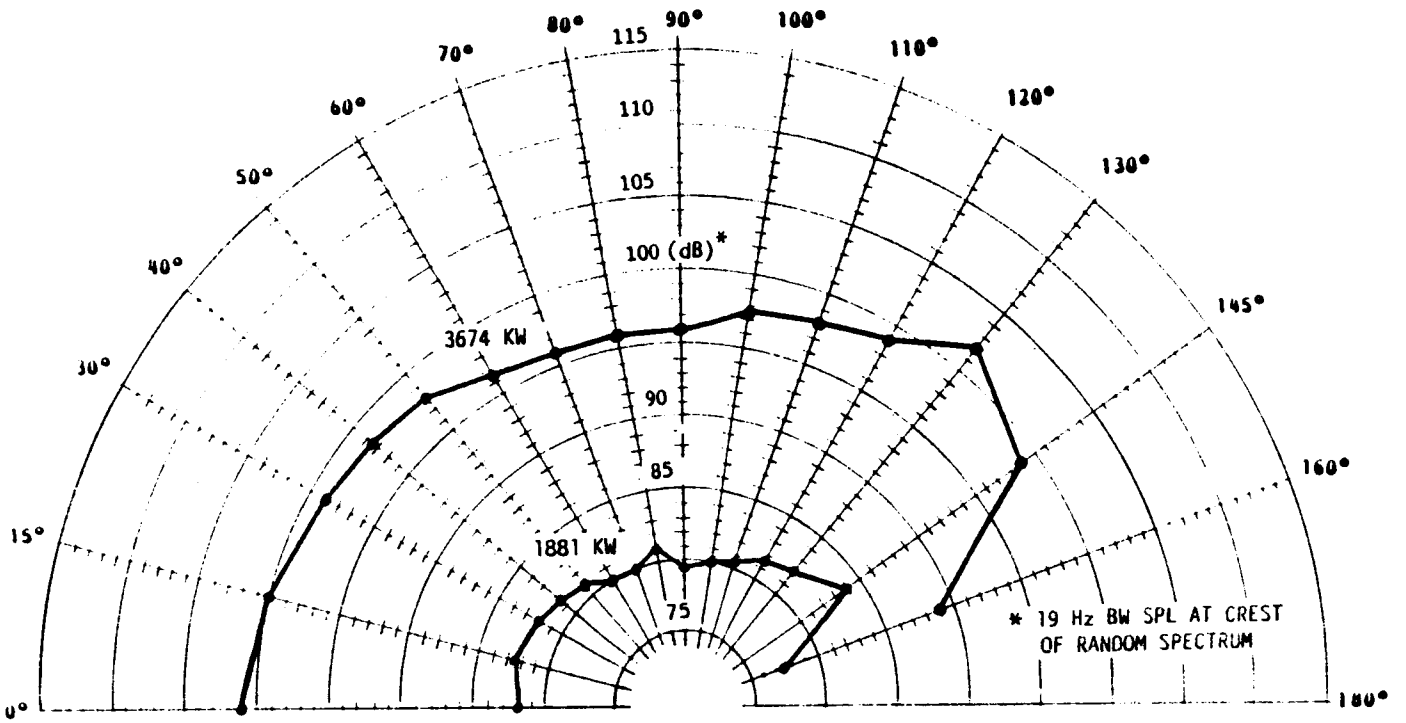

Figure 9.63. Ground Level Random Noise - 45.7 m, 105% N_p Speed

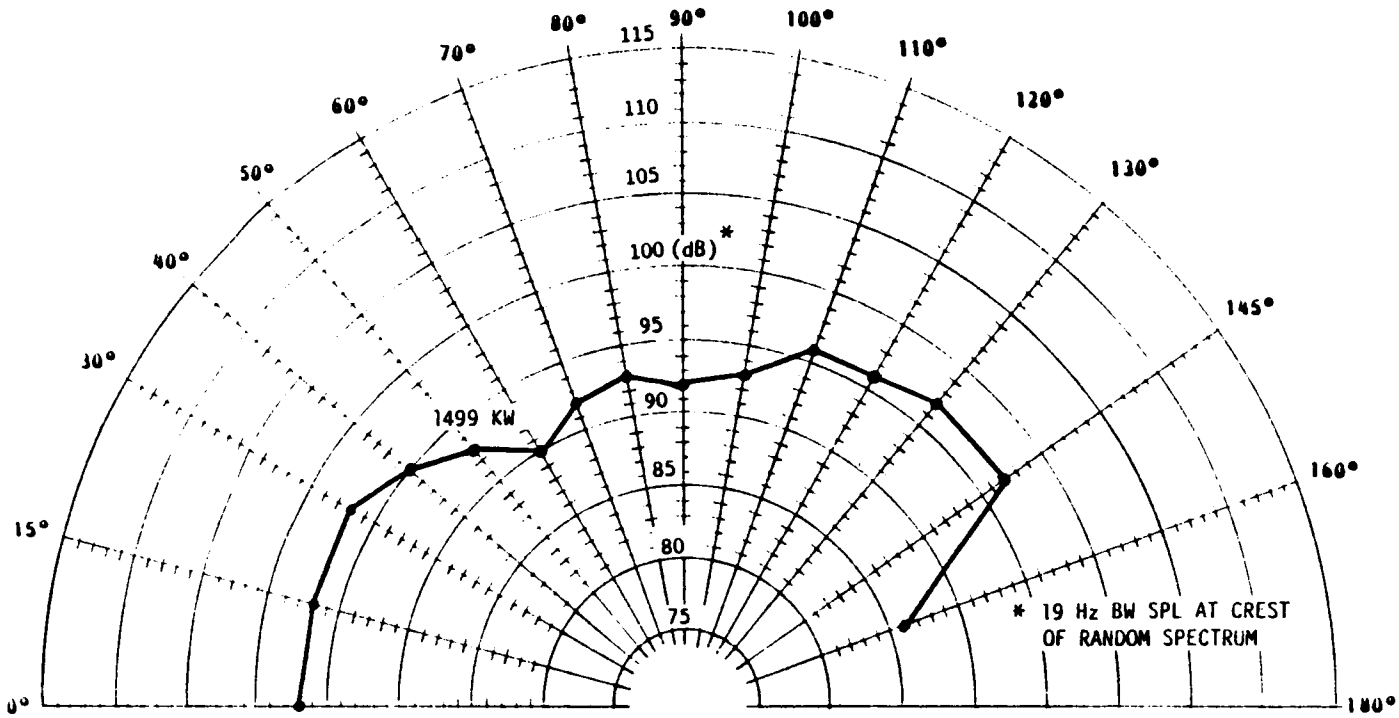

Figure 9.64. Ground Level Random Noise - 45.7 m, 75% N_p Speed

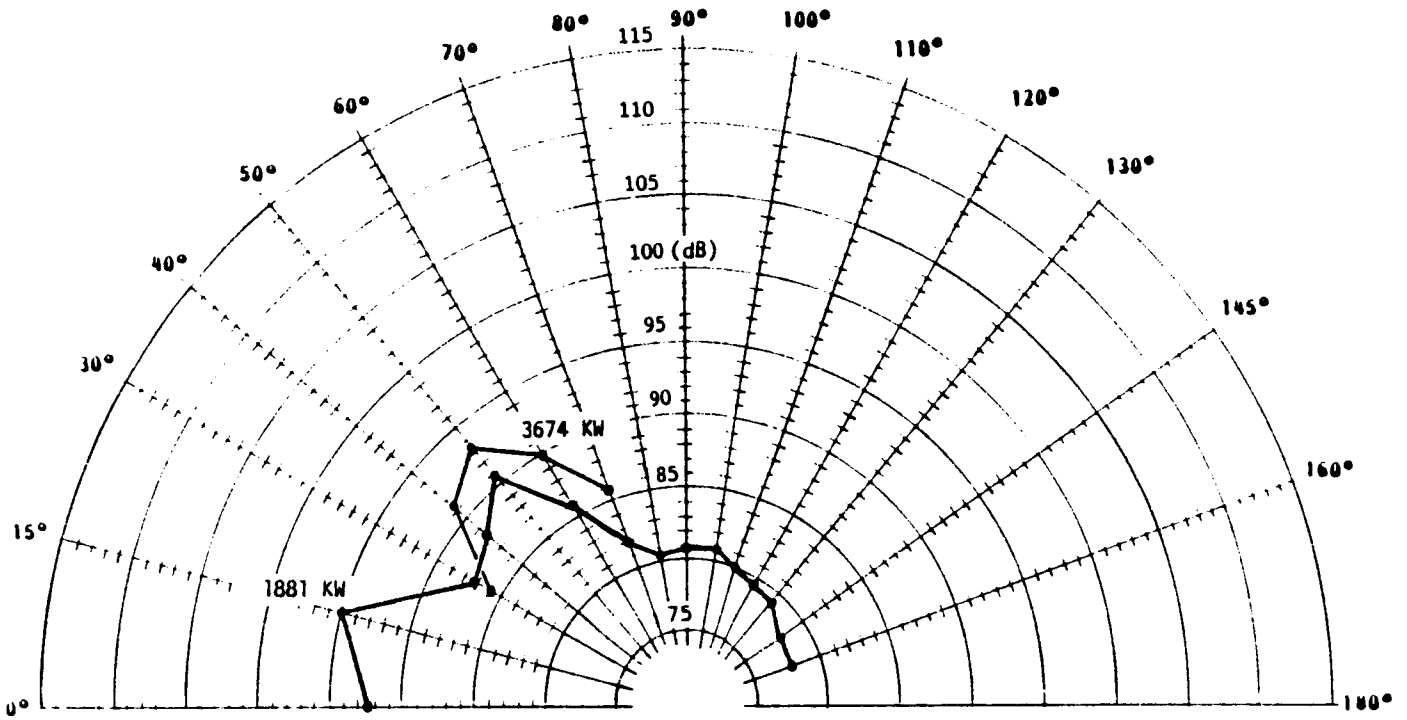

Figure 9.65. Ground Level Strongest Compressor Tone SPL's - 45.7 m, 105% N_p Speed

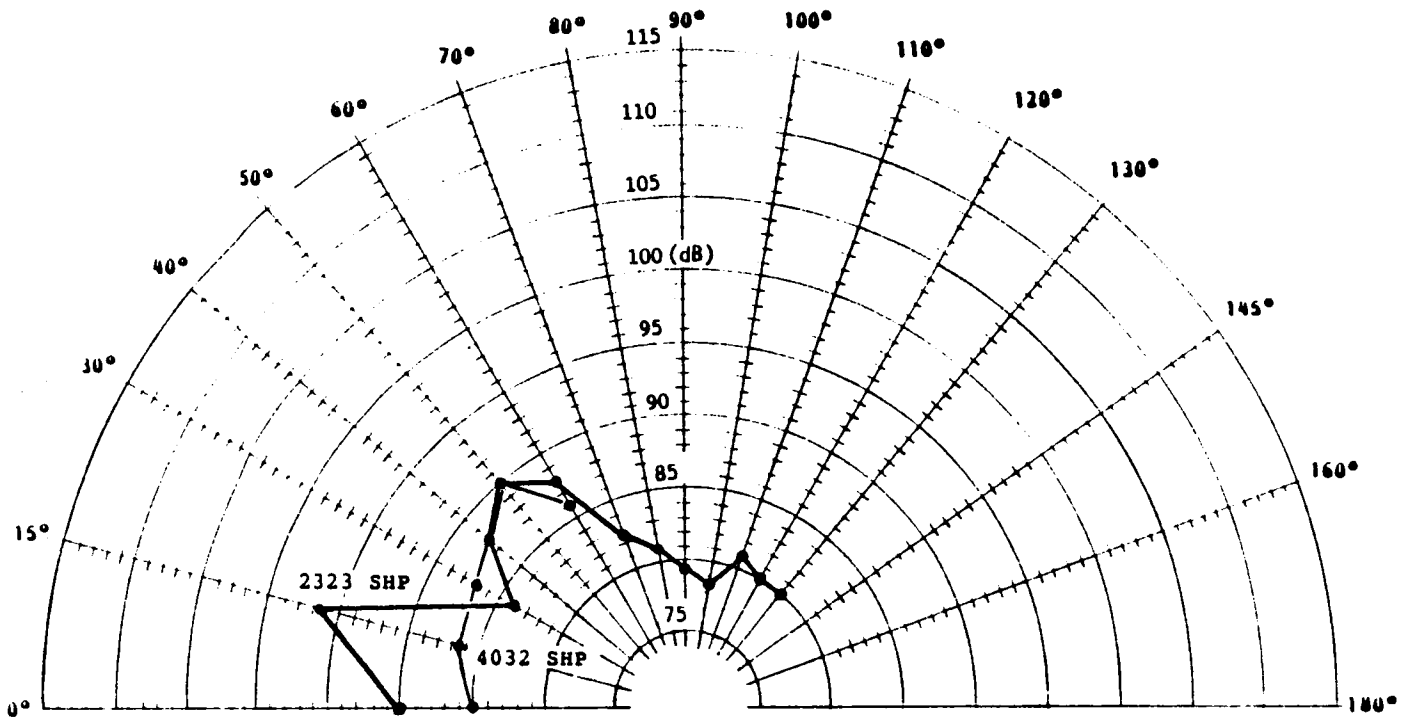

Figure 9.66. Ground Level Strongest Compressor Tone SPL's - 45.7 m, 100% N_p Speed

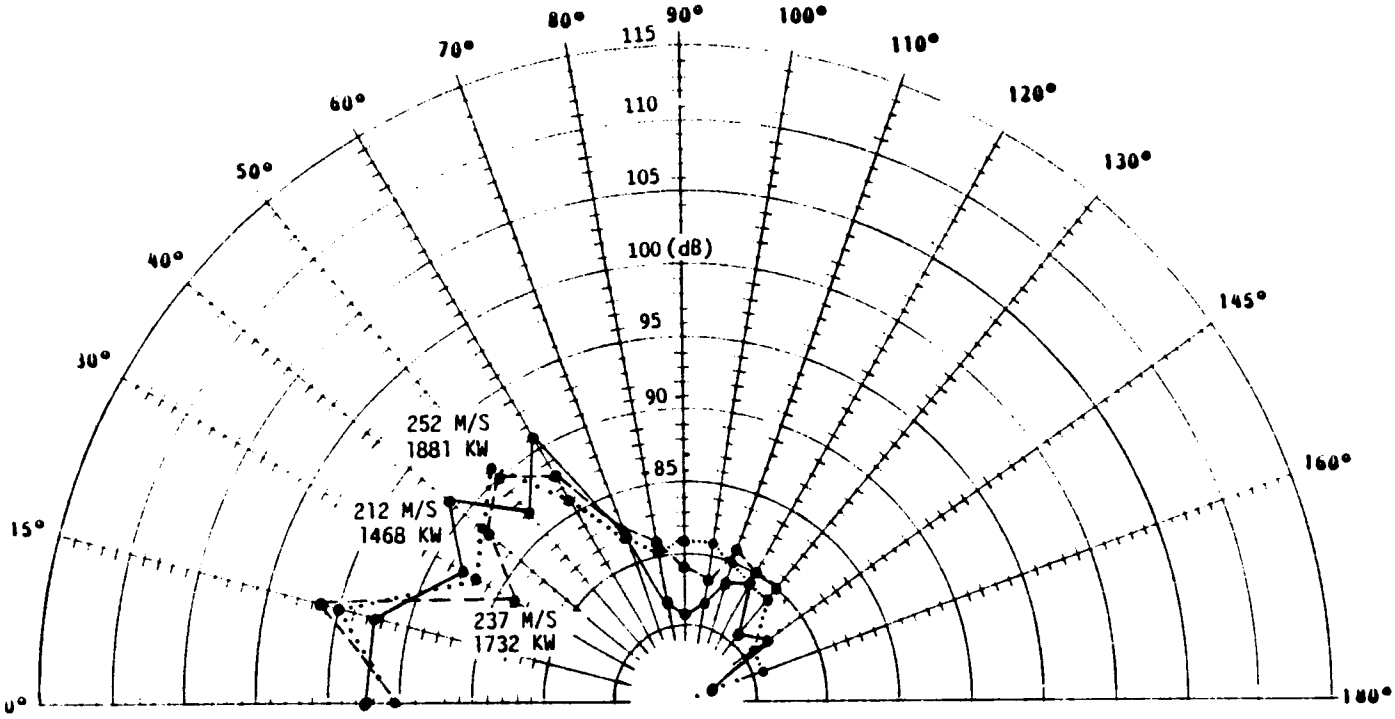

Figure 9.67. Ground Level Strongest Compressor Tone SPL's - 45.7 m, Minimum Test Powers

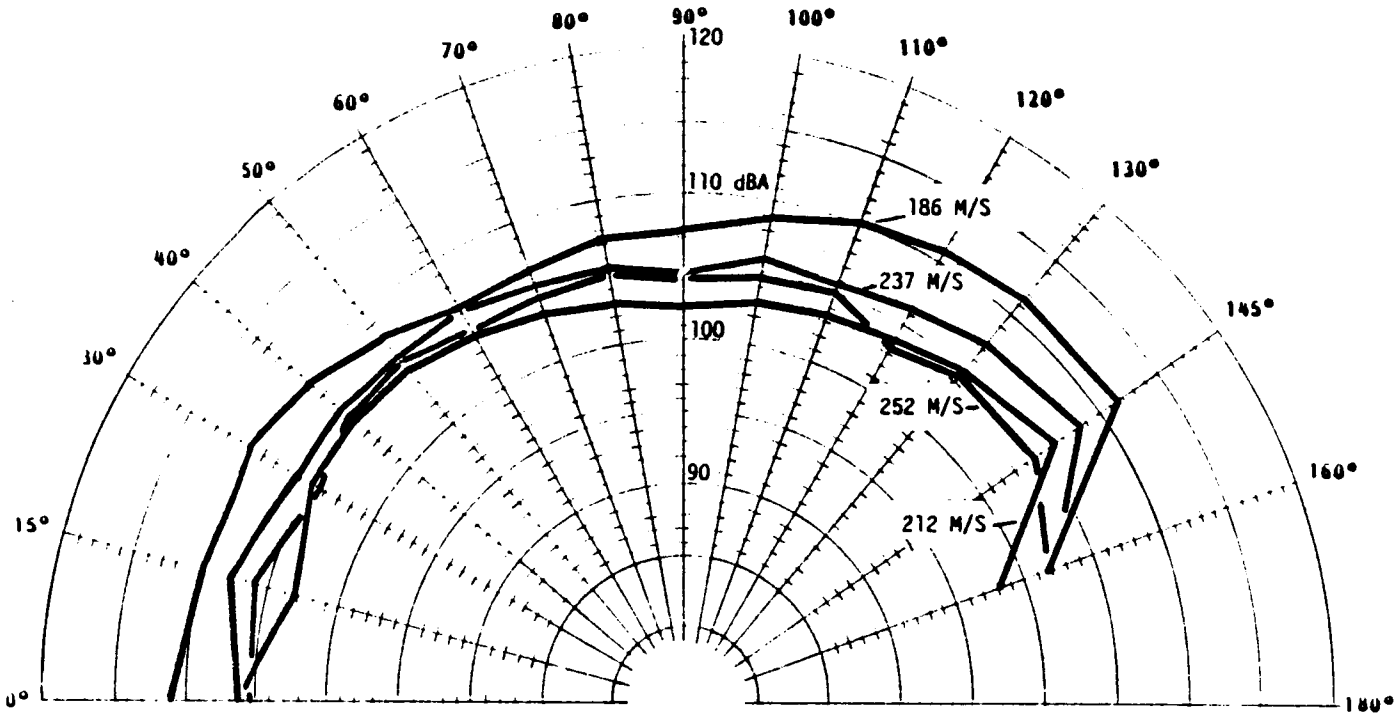

Figure 9.68. Ground Level Subjective Noise Level - 45.7 m, Minimum Test Powers

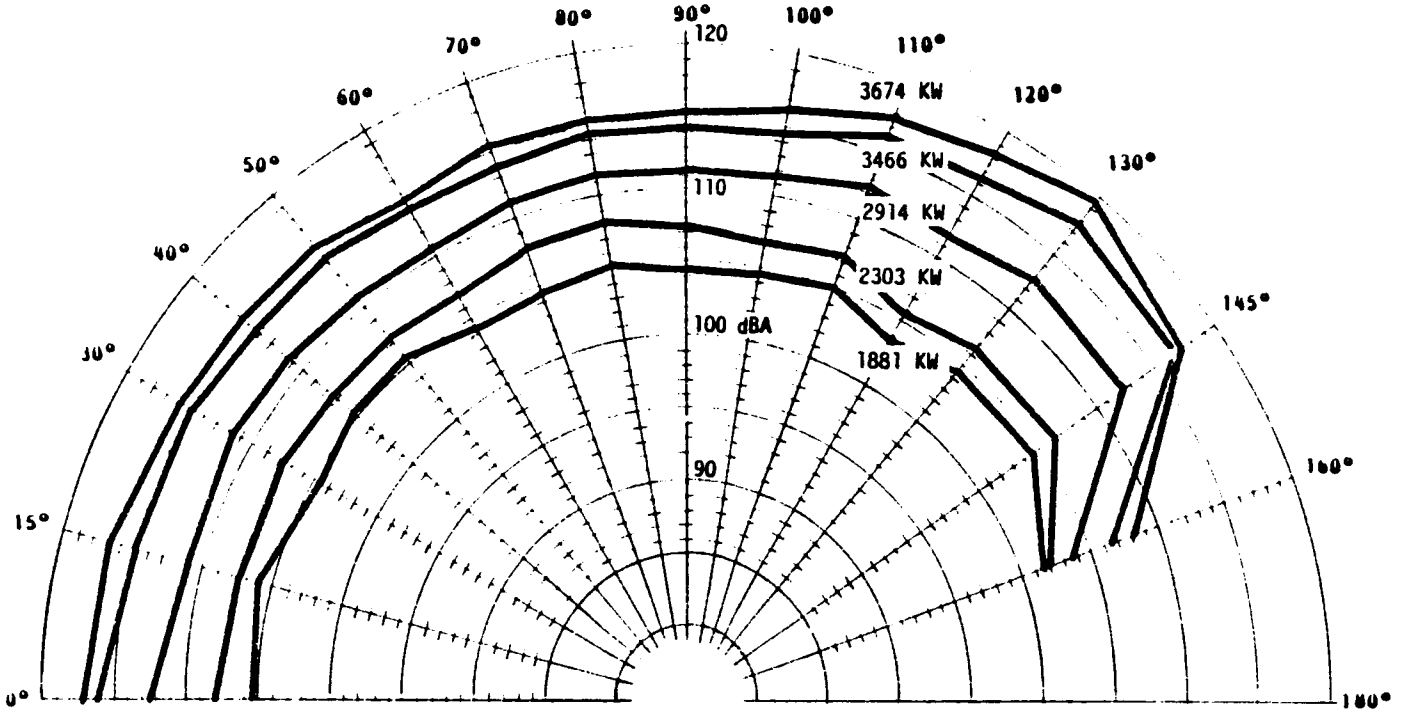

Figure 9.69. Ground Level Subjective Noise Level - 45.7 m, 105% N_p Speed

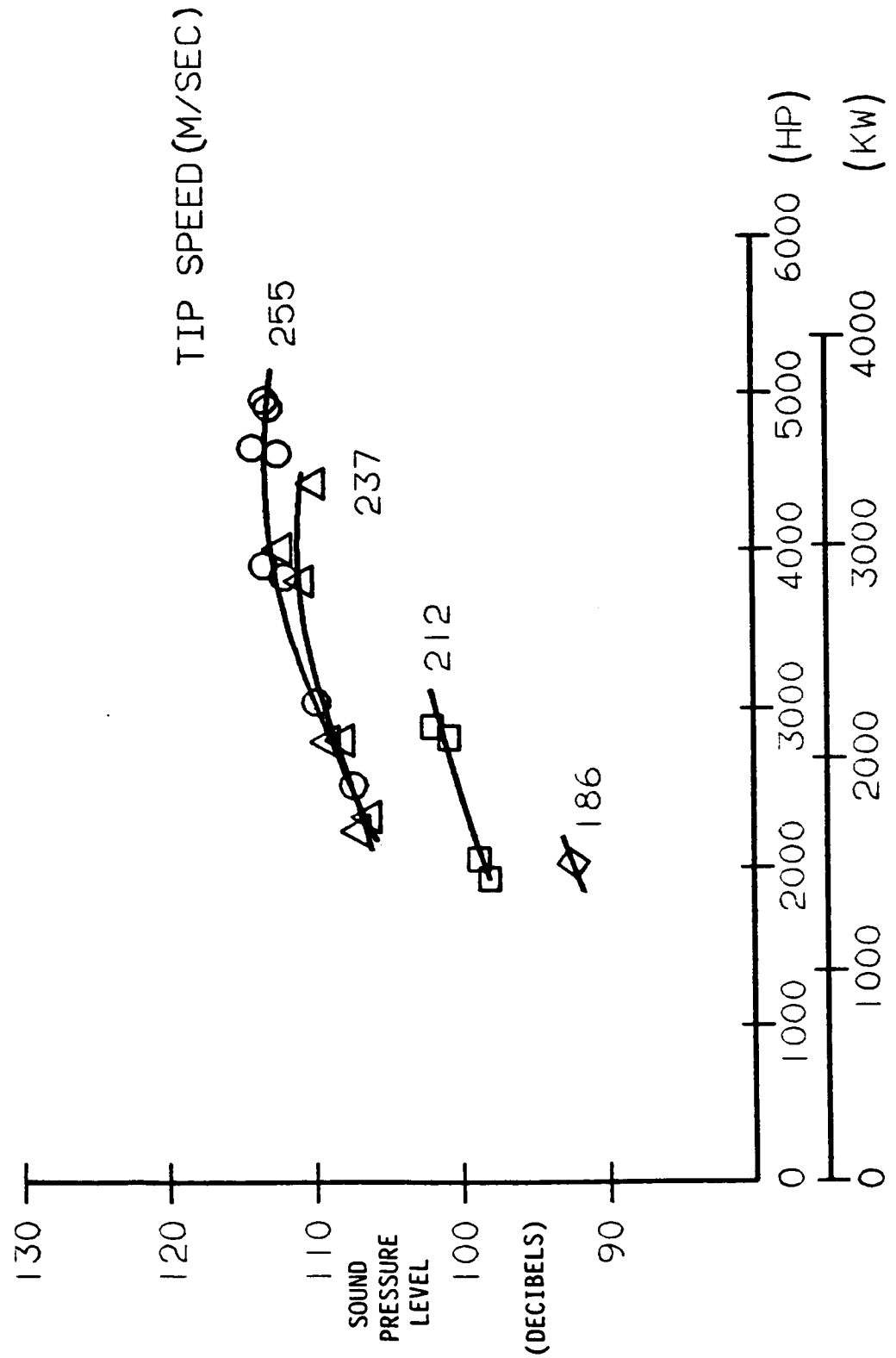

Figure 9.70. Ground Level First Order Blade Noise Dependence on Power - 45.7 m, 100° Azimuth

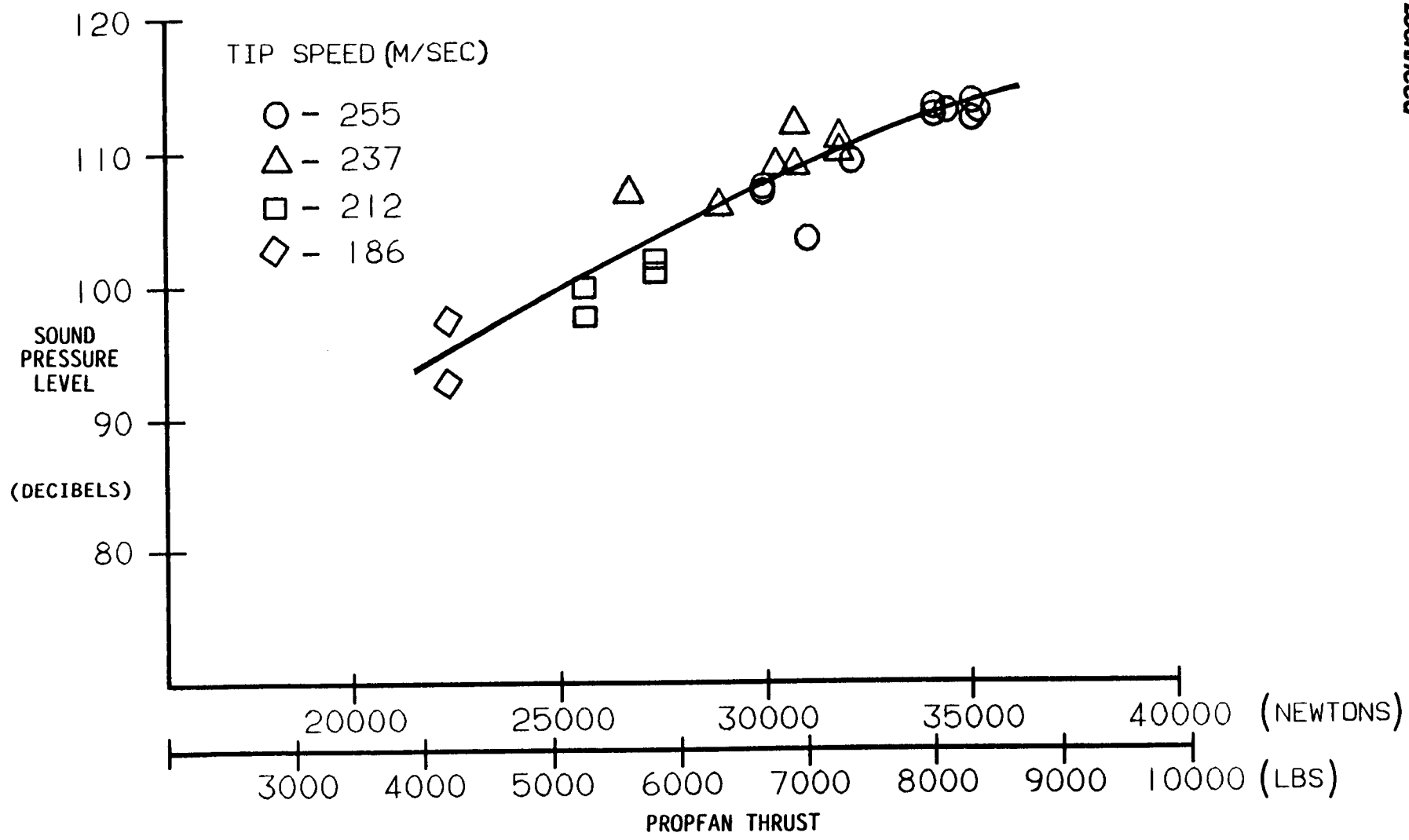

Figure 9.71. Ground Level First Order Blade Noise Dependence on Thrust - 45.7 m, 100° Azimuth

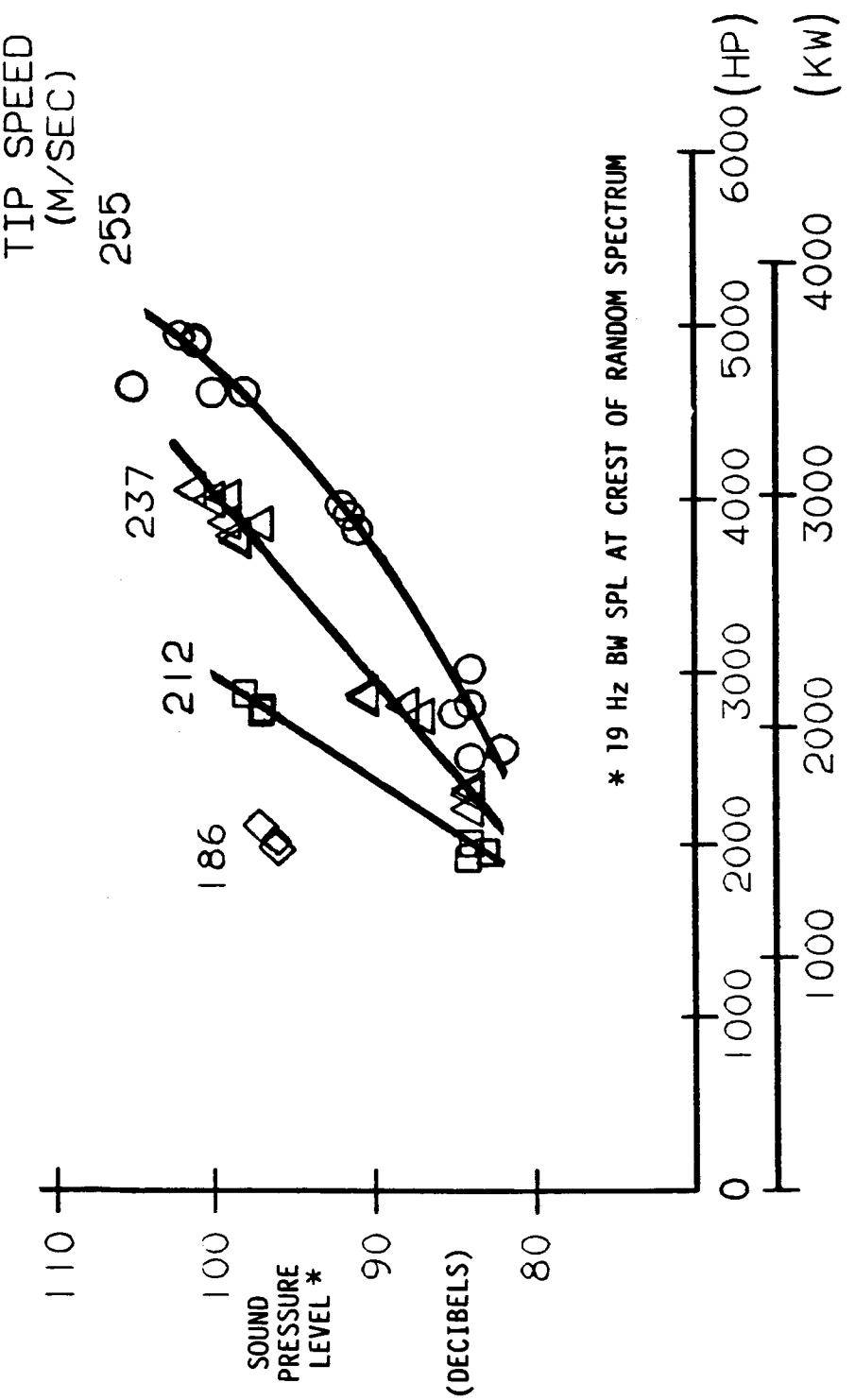

Figure 9.72. Ground Level Random Noise Dependence on Power - 45.7 m, 130° Azimuth

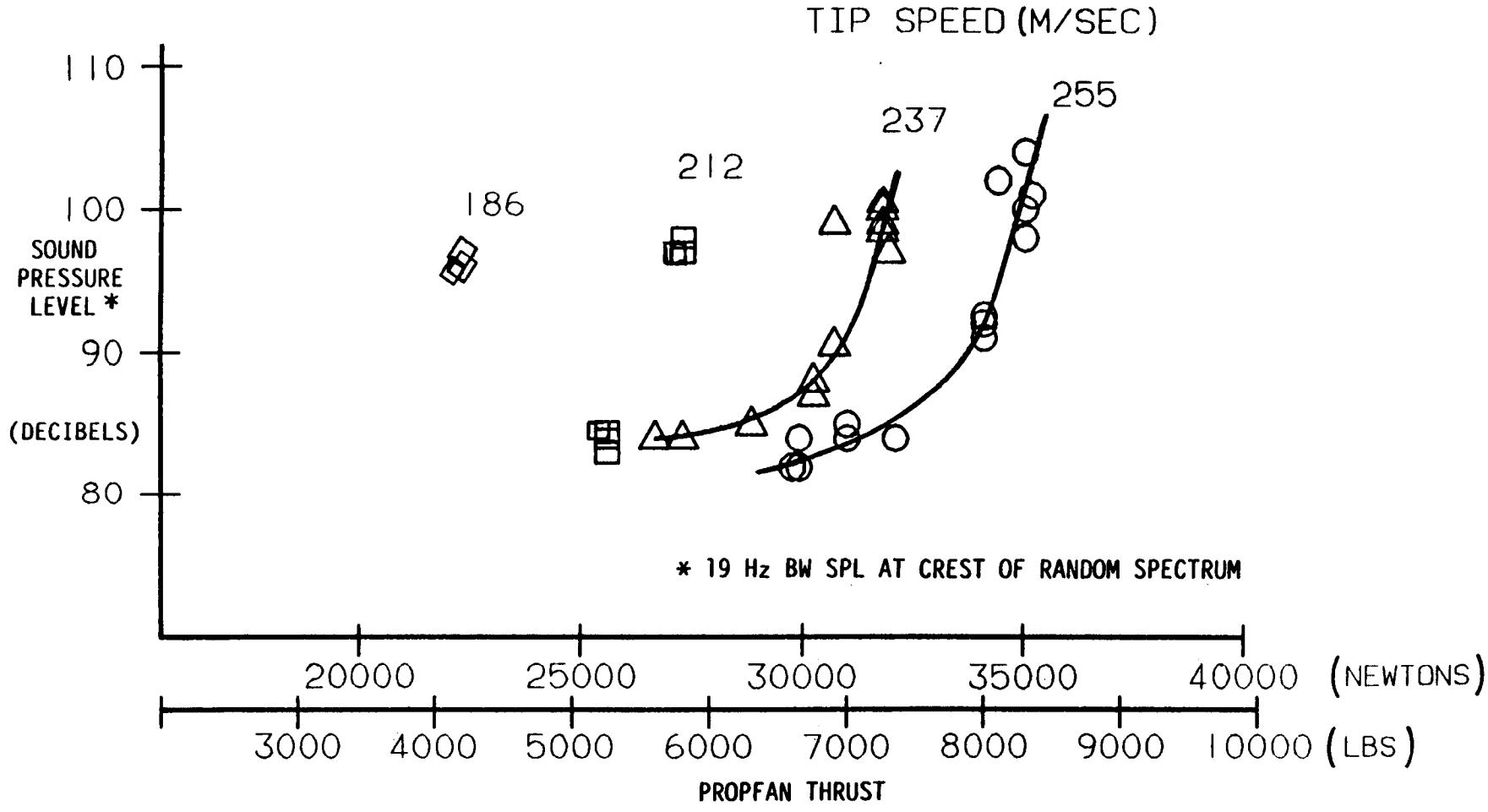

Figure 9.73. Ground Level Random Noise Dependence on Thrust - 45.7 m, 130° Azimuth

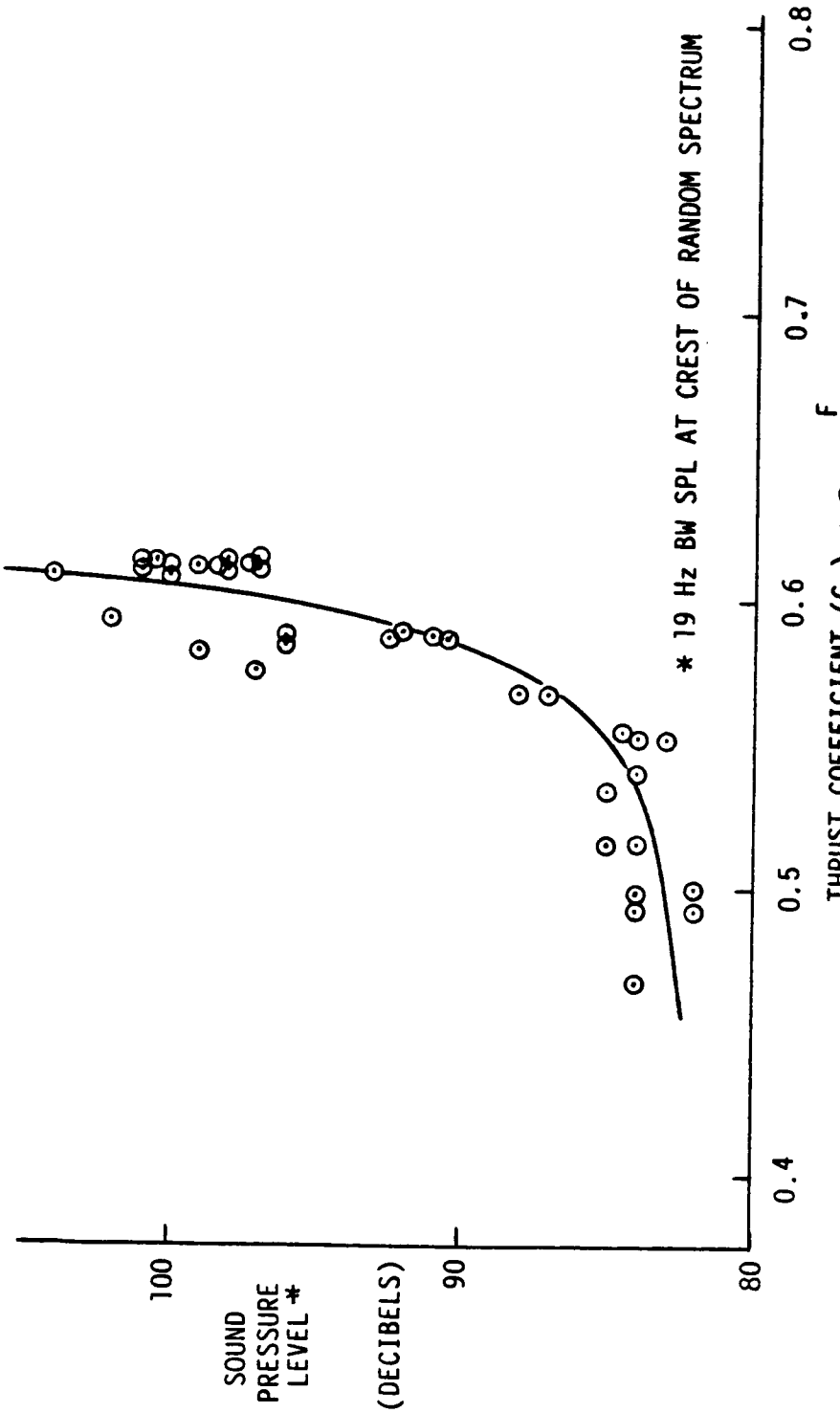

Figure 9.74. Ground Level Random Noise Relationship to Thrust Coefficient - 45.7 m, 130° Azimuth

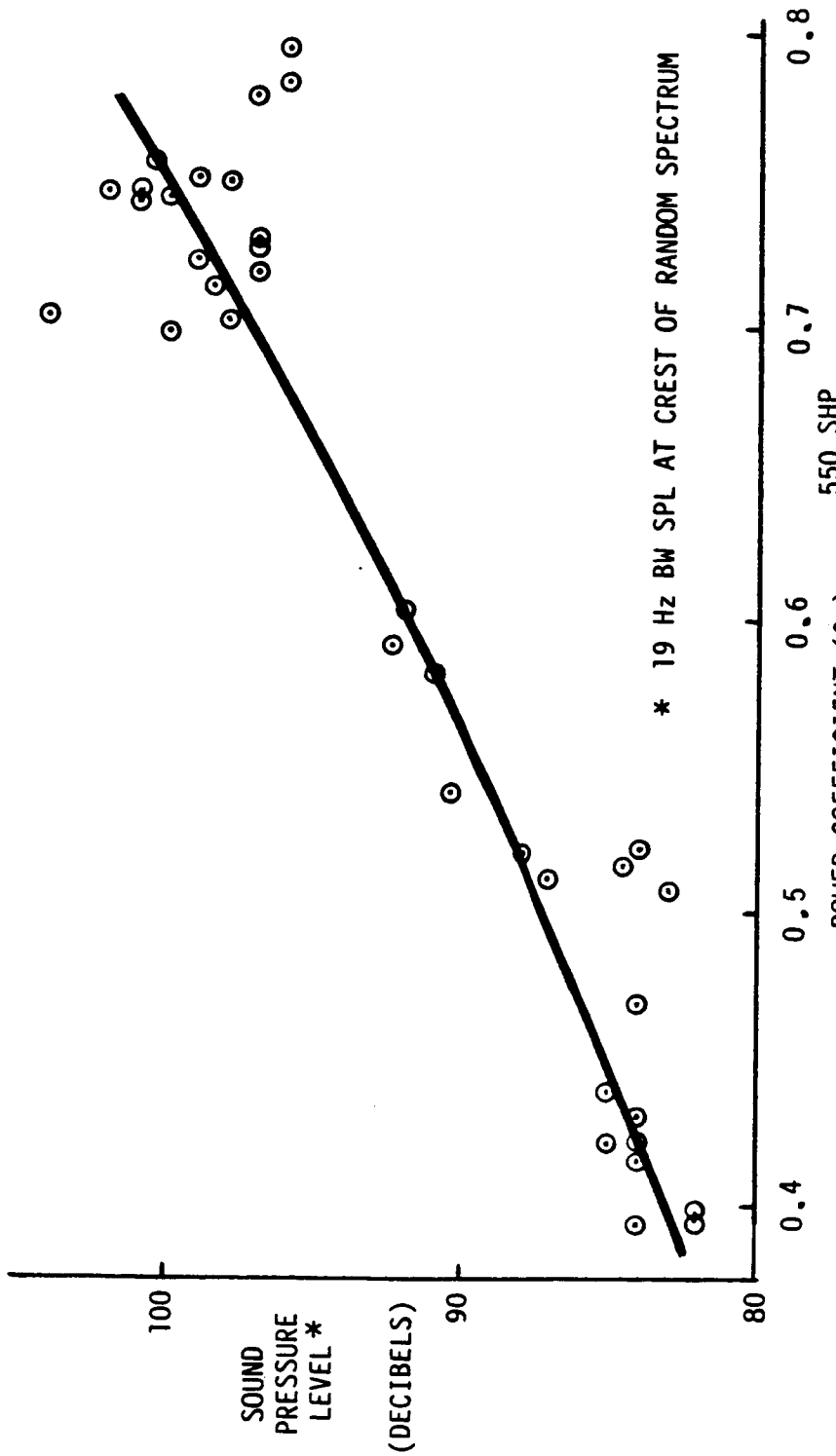

Figure 9.75. Ground Level Random Noise Relationship to Power Coefficient - 45.7 m, 130° Azimuth

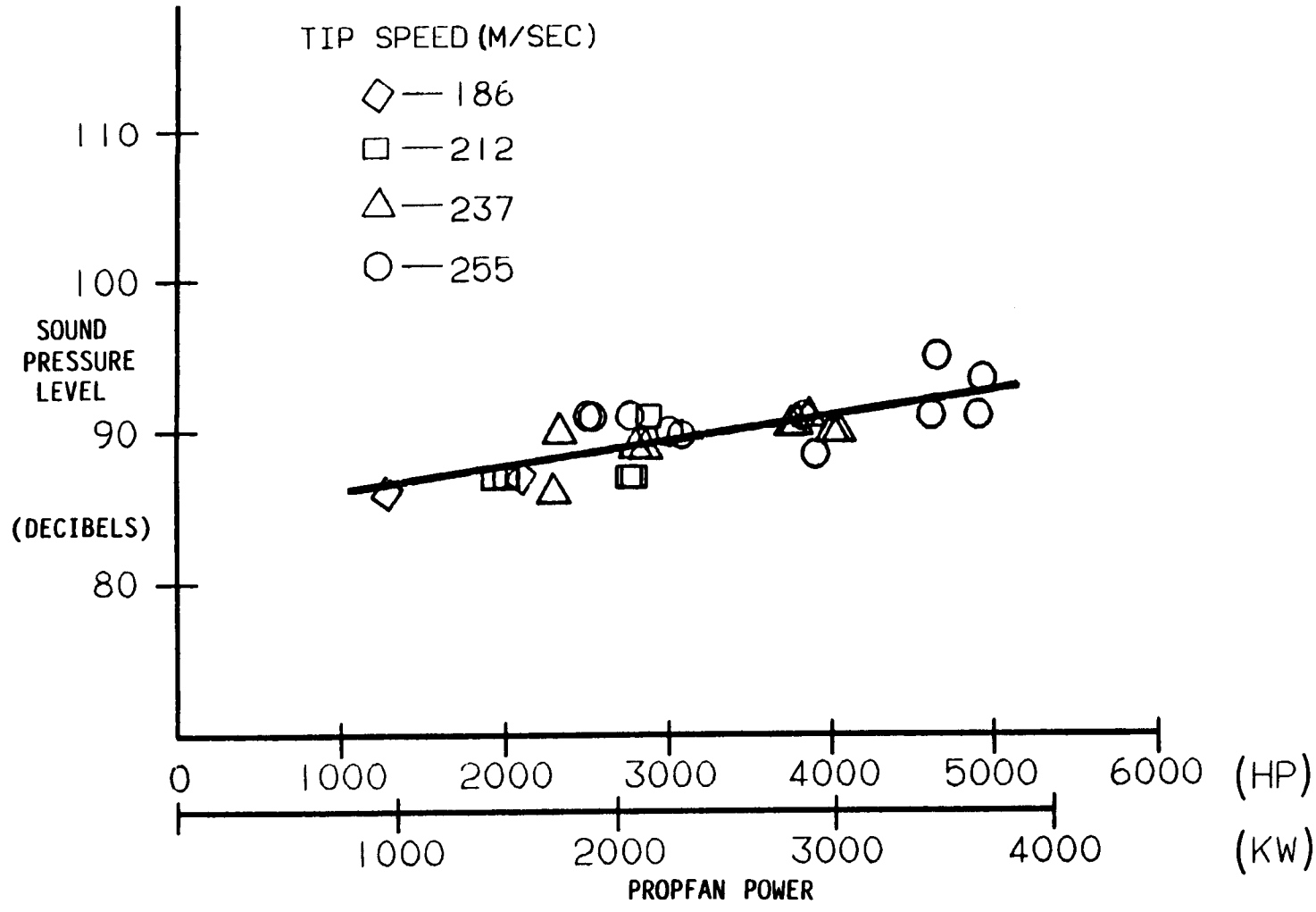

Figure 9.76. Ground Level Compressor/Propfan Interaction Tone Noise Dependence on Power - 45.7 m, 50° Azimuth

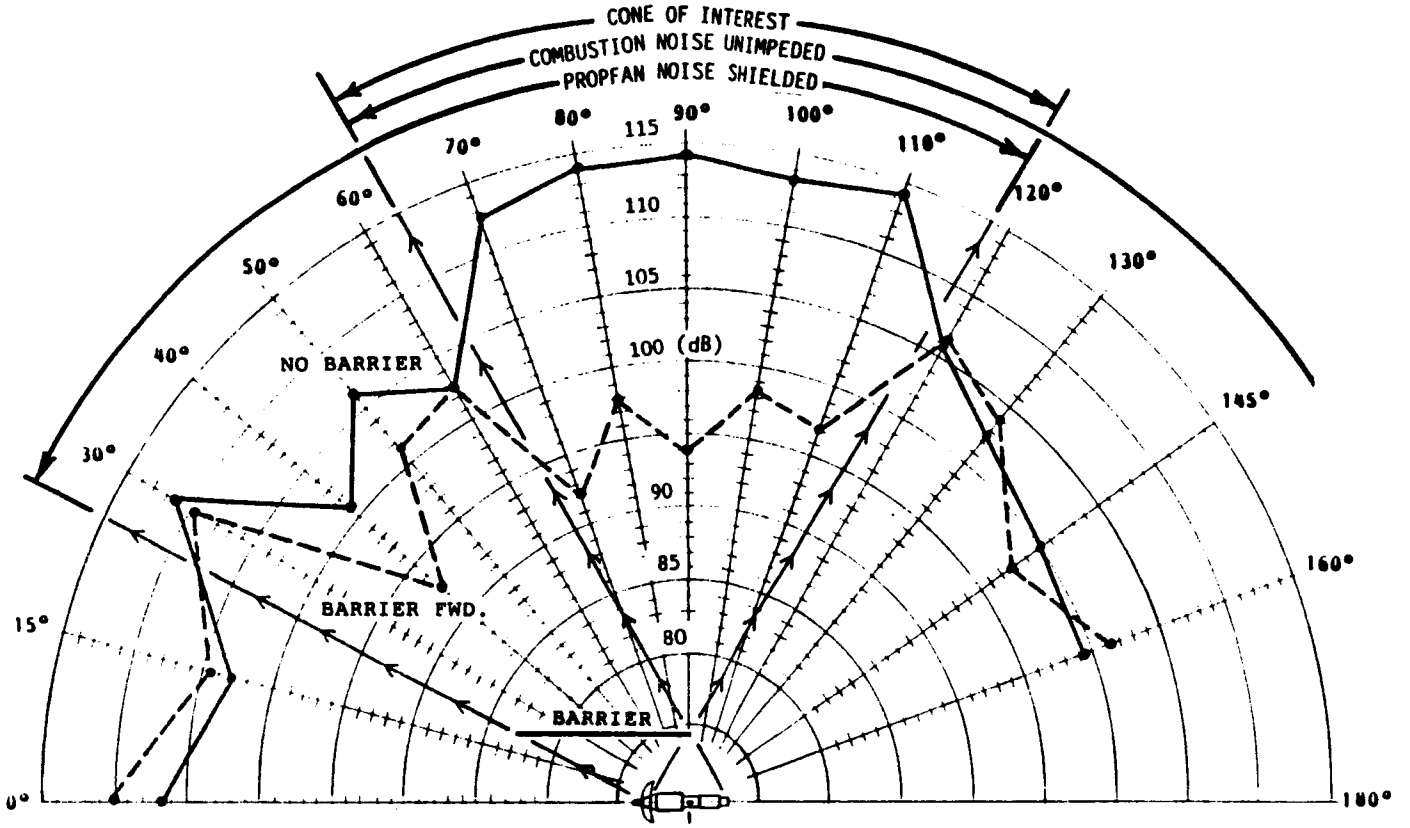

Figure 9.77. Barrier Effect on Ground Level First Order Blade Passage SPL - 45.7 m, 3675 KW, 105% N_p Speed

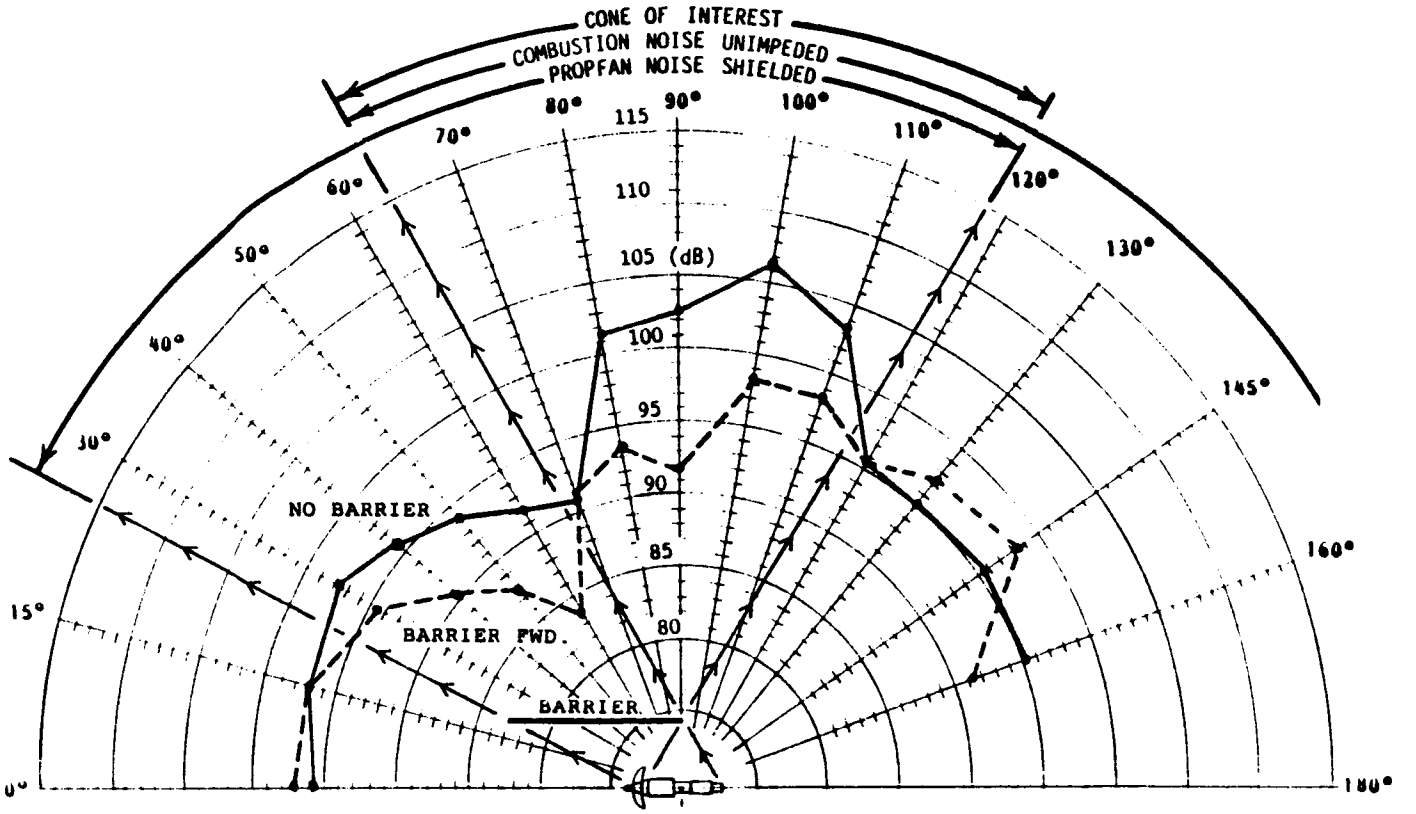

Figure 9.78. Barrier Effect on Ground Level First Order Blade Passage SPL - 45.7 m, 1643 to 1732 KW, 100% N_p Speed

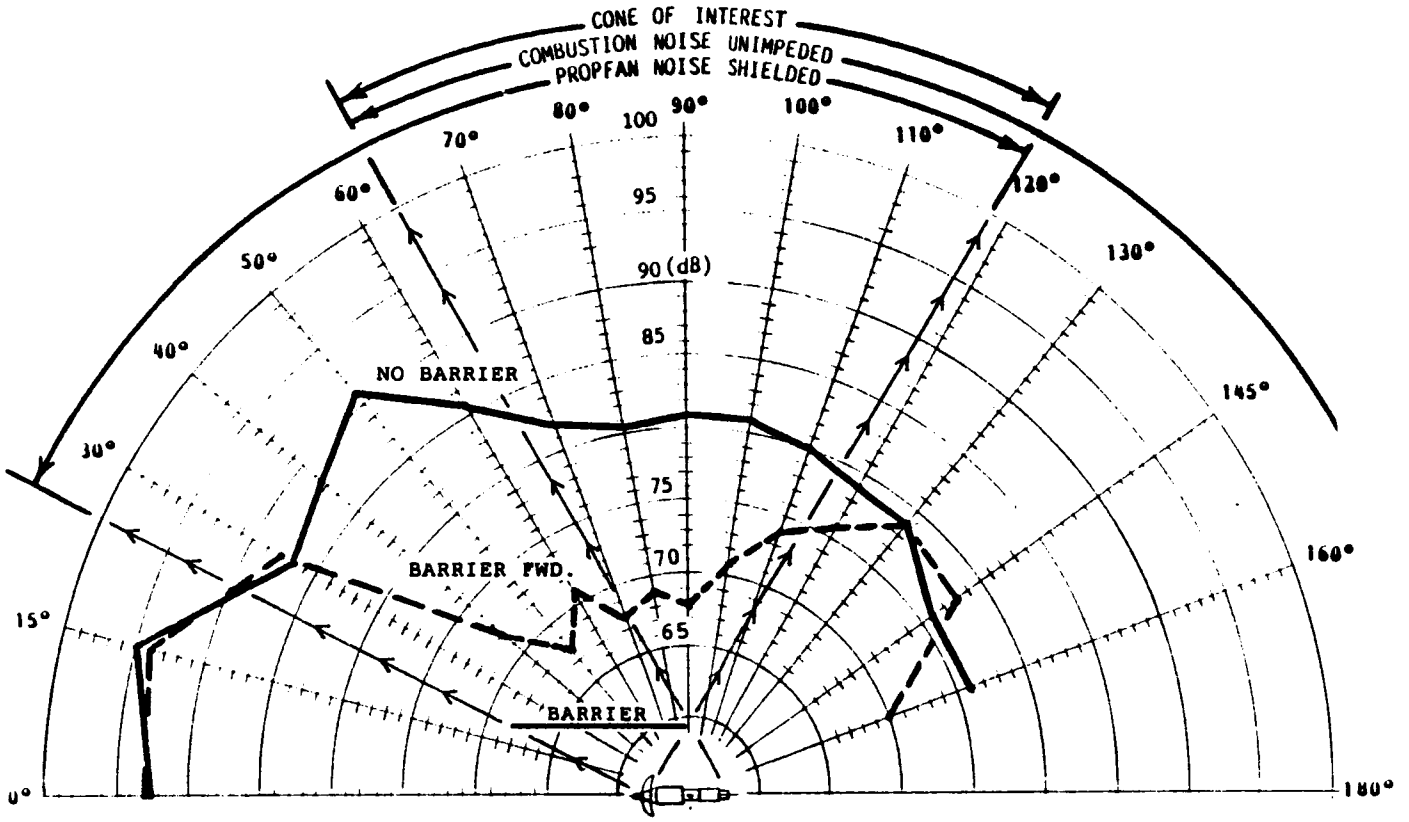

Figure 9.79. Barrier Effect on Ground Level Strongest Compressor Tone SPL's - 45.7 m, 1881 to 1903 KW, 105% N_p Speed

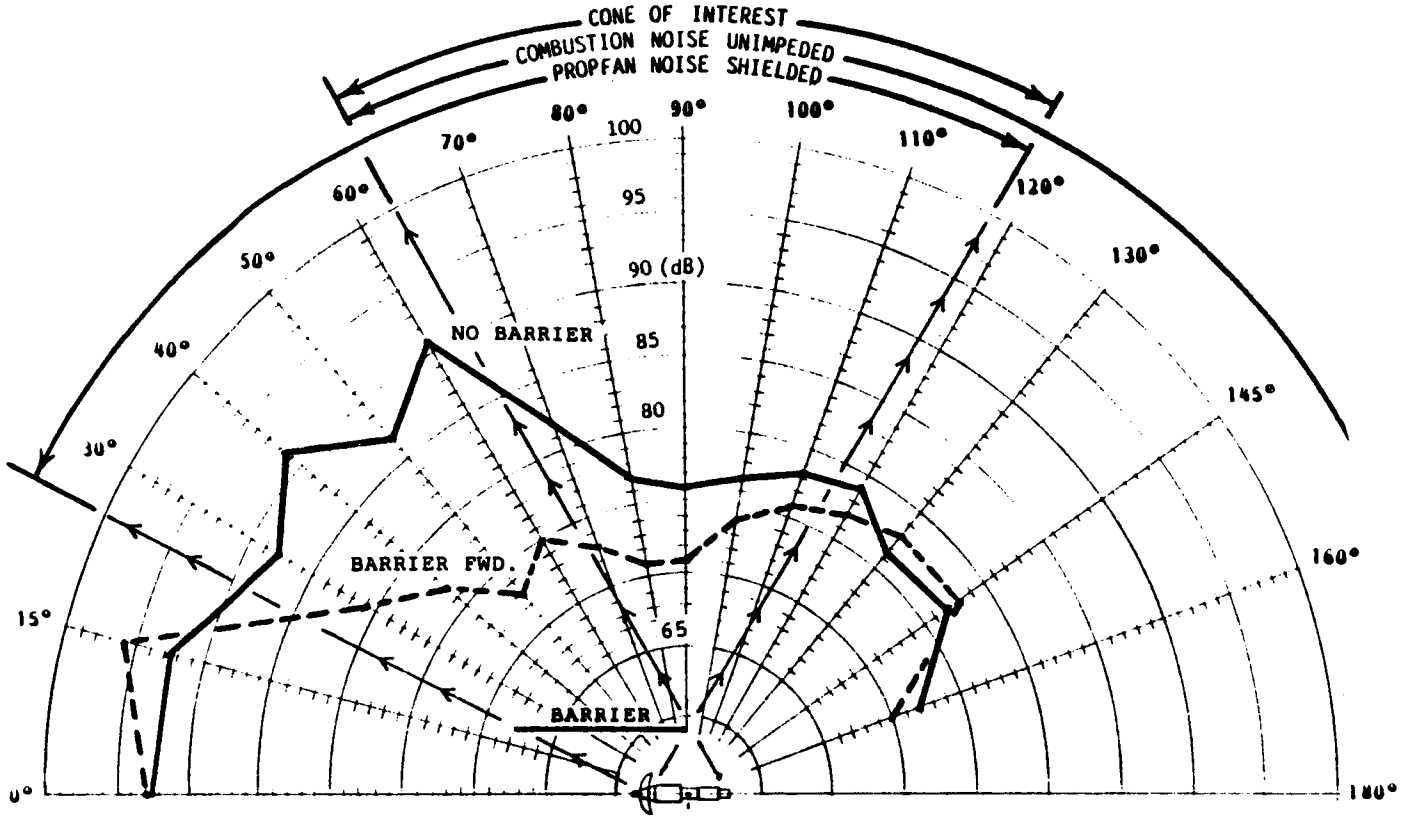

Figure 9.80. Barrier Effect on Ground Level Strongest Compressor Tone SPL's - 45.7 m, 1460 KW, 87.5% N_p Speed

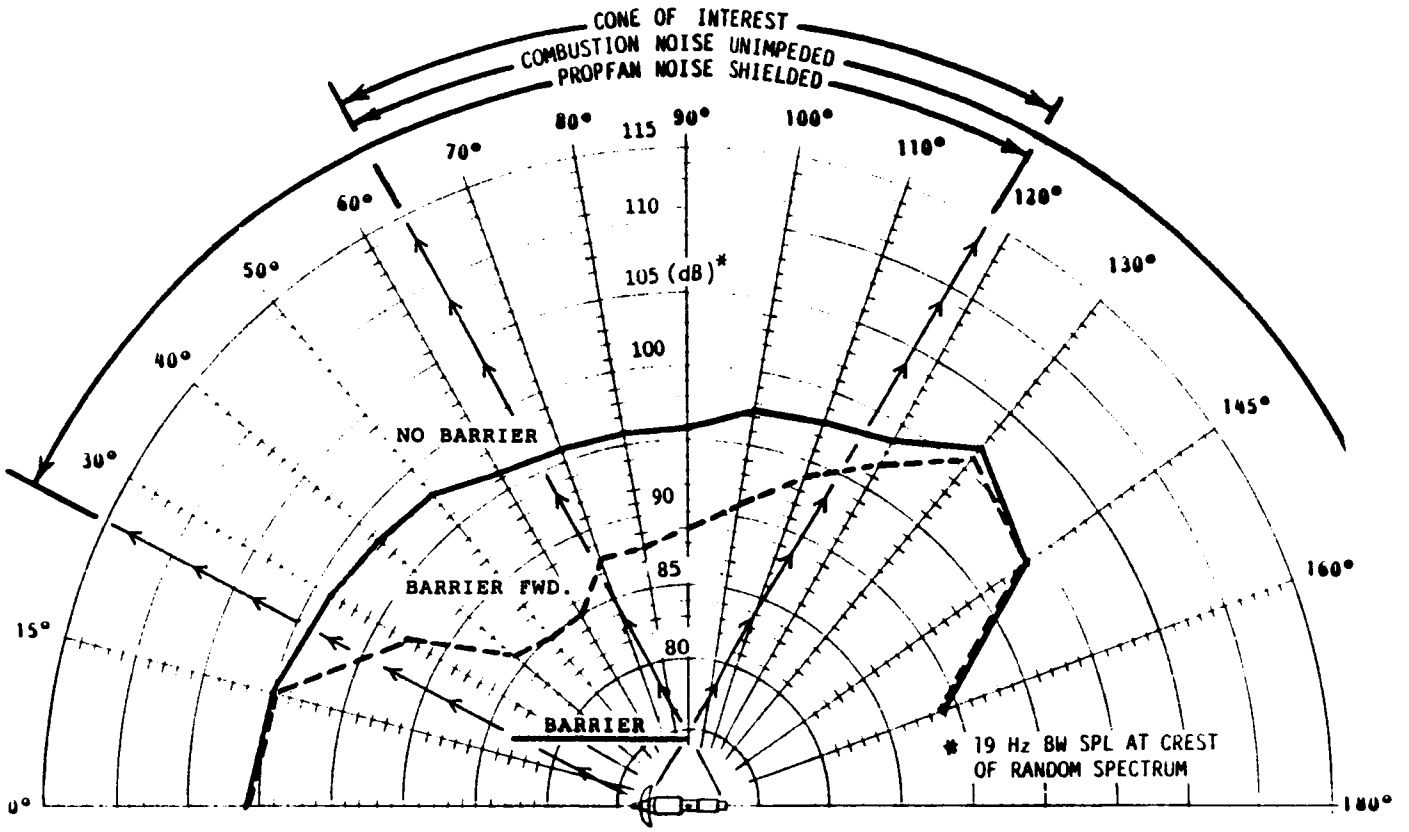

Figure 9.81. Barrier Effect on Ground Level Random Noise - 45.7 m, 3675 KW, 105% N_p Speed

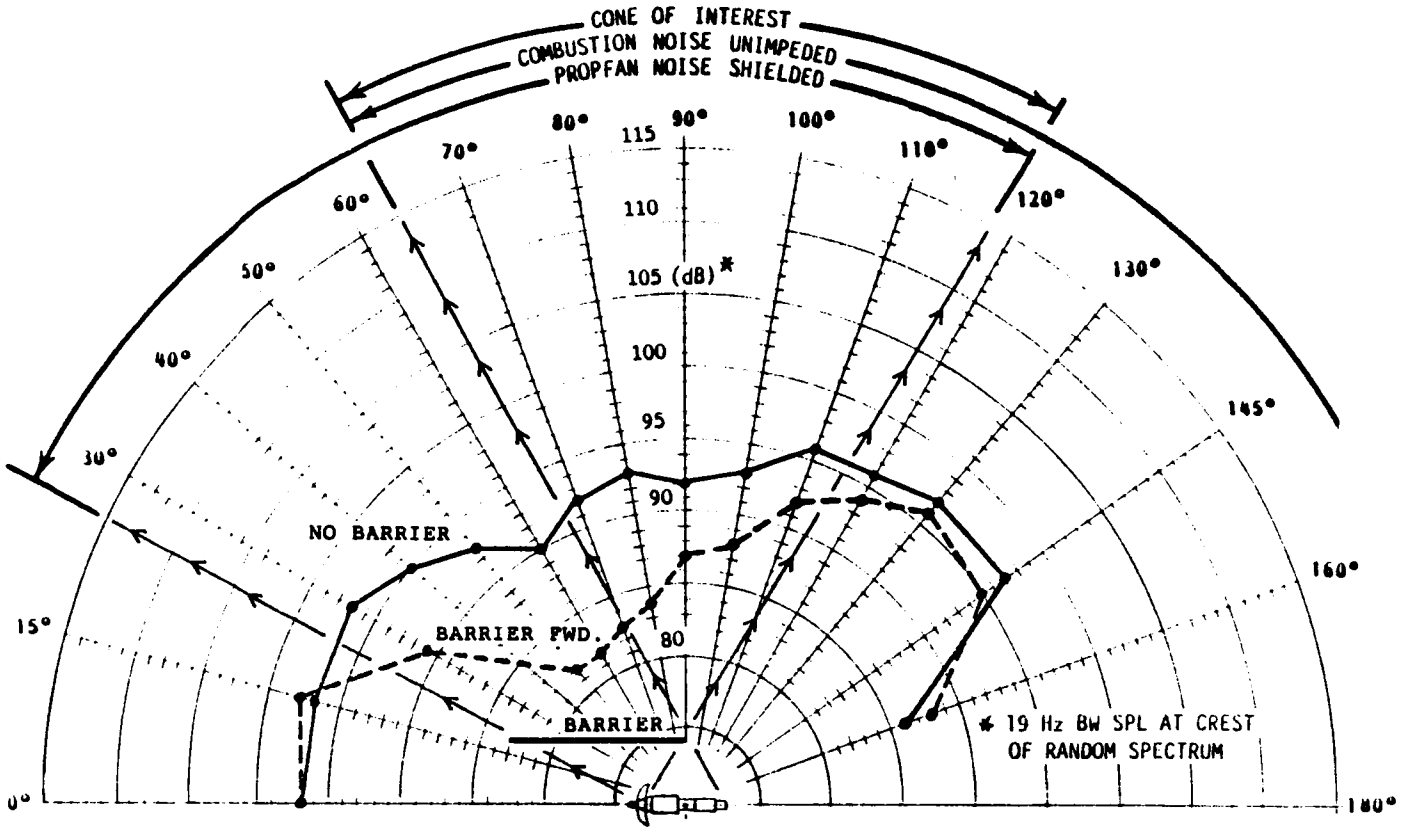

Figure 9.82. Barrier Effect on Ground Level Random Noise - 45.7 m, 1490 KW, 75% N_p Speed

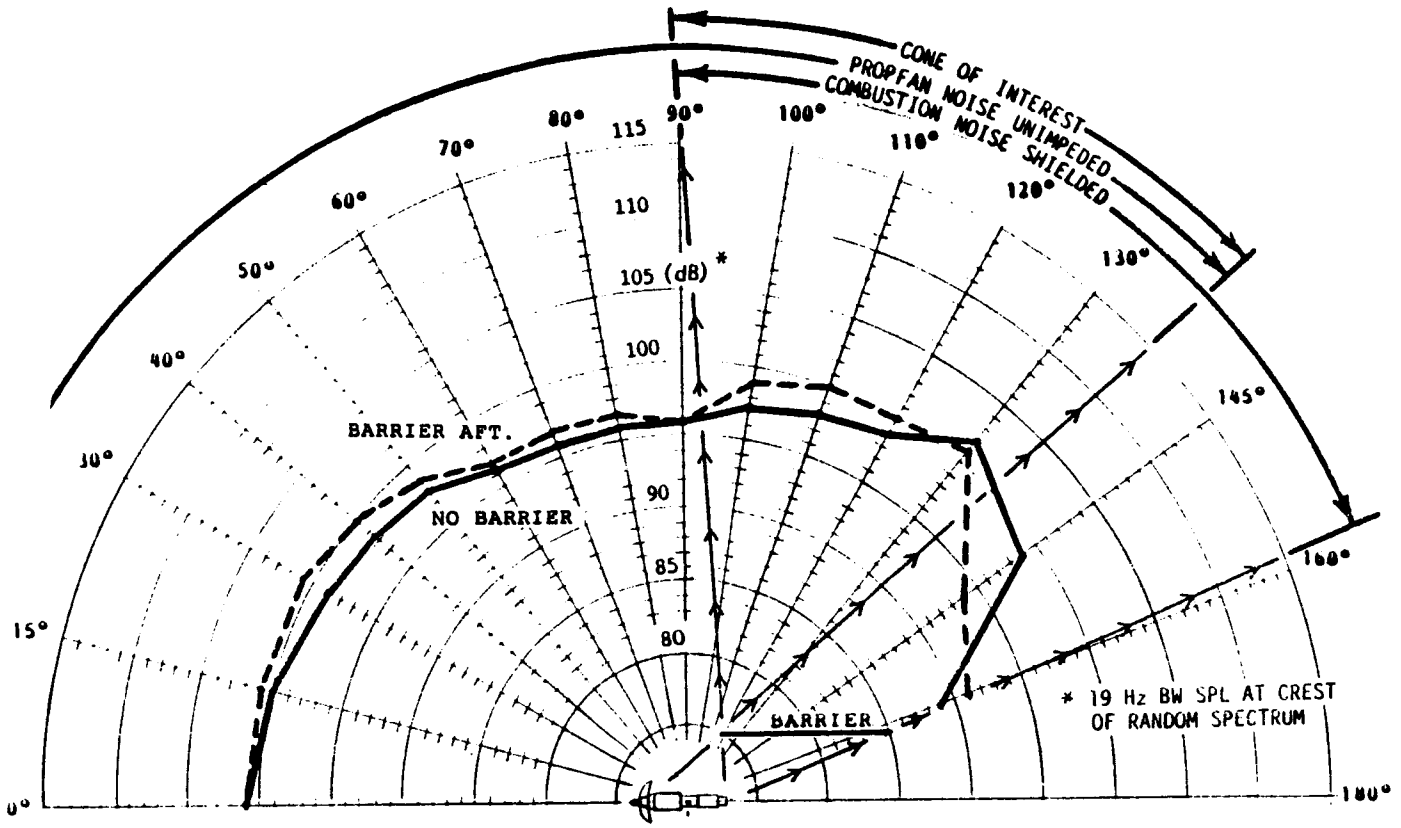

Figure 9.83. Barrier Effect on Ground Level Random Noise - 45.7 m, 3665 KW, 105% N_p Speed

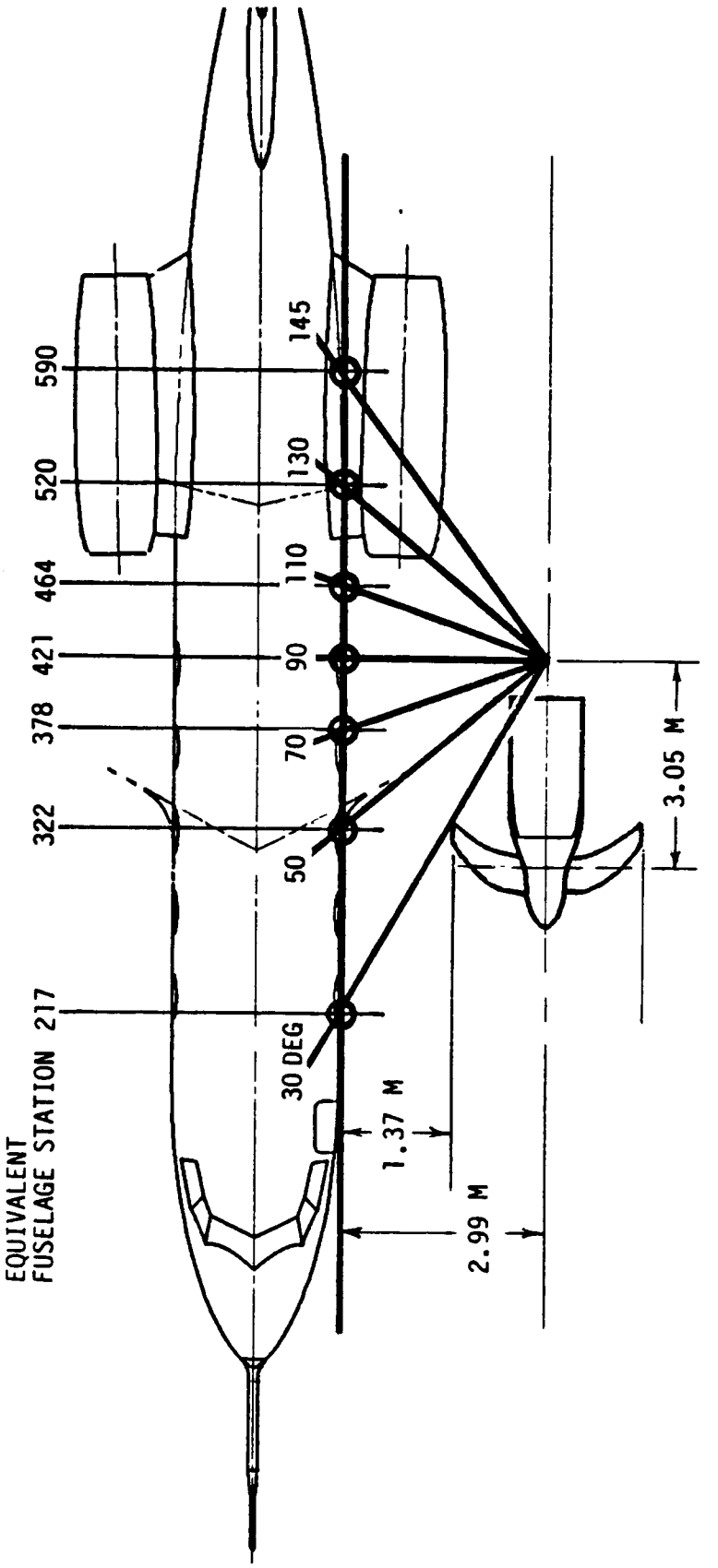

Figure 9.84. Near-Field Microphone Locations Relative to Testbed Aircraft Fuselage

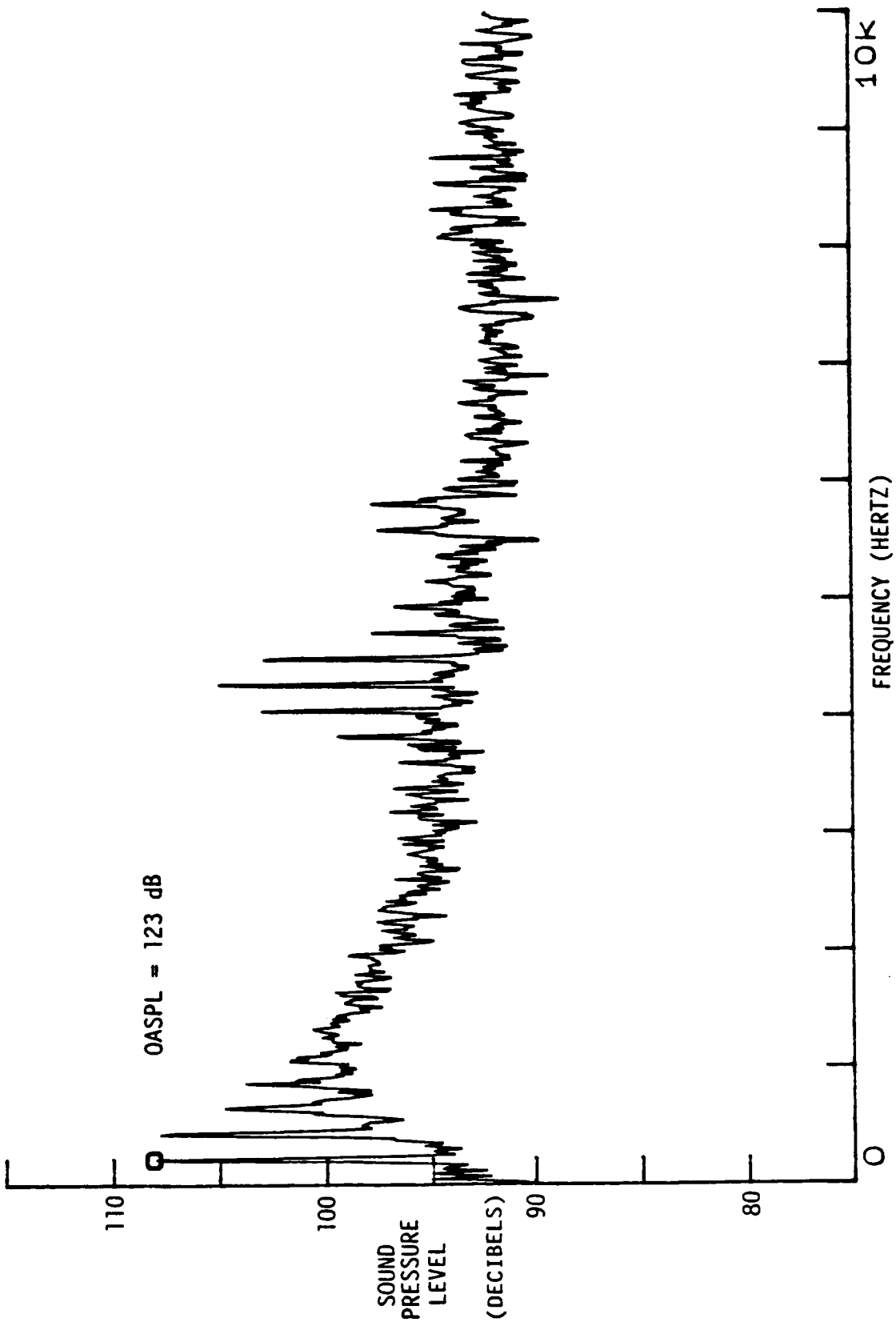

Figure 9.85. Centerline Heigth Noise Spectrum - 2.99 m, 30° Azimuth (FS 217), 1732 KW, 100% N_p Speed

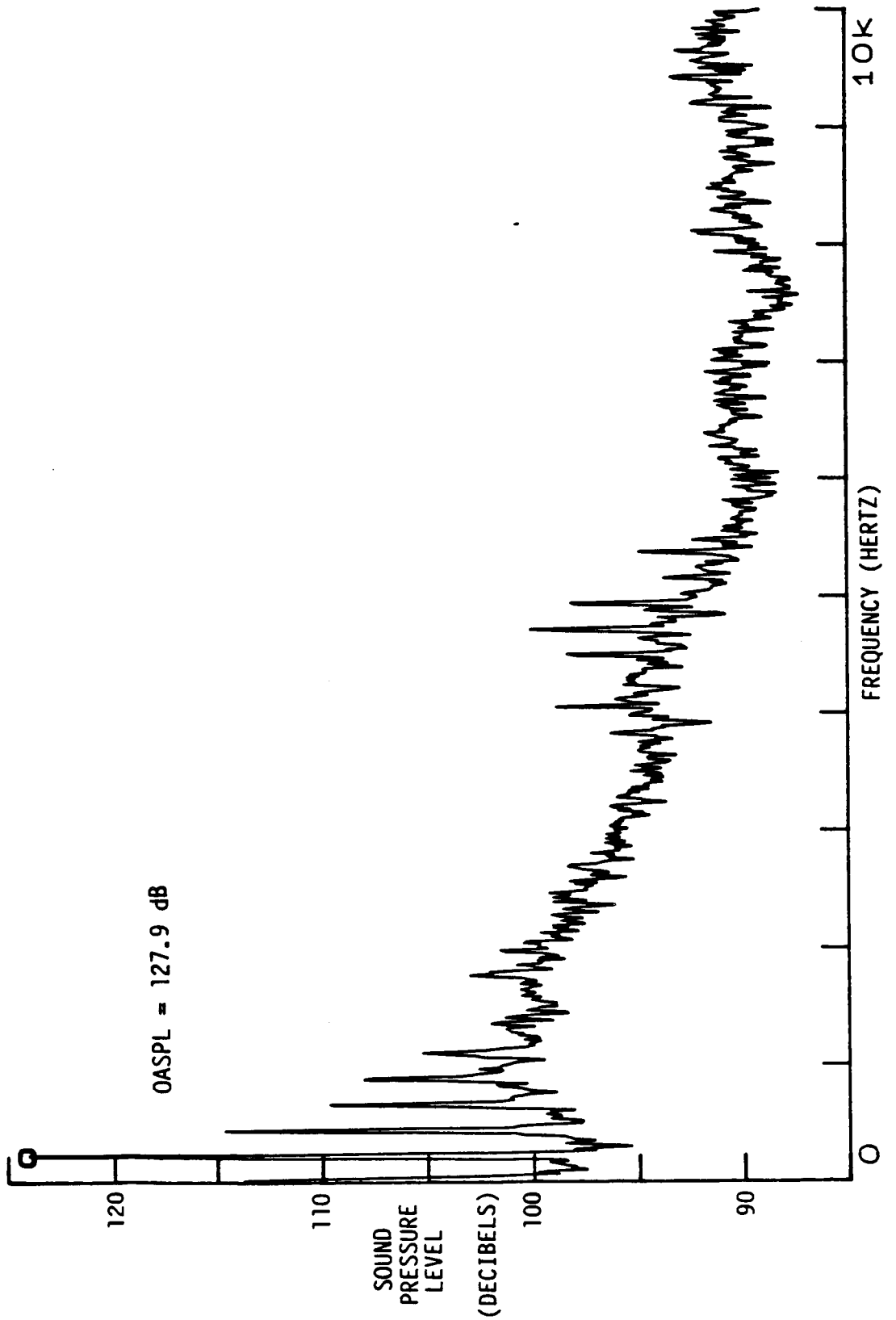

Figure 9.86. Centerline Height Noise Spectrum - 2.99 m, 50° Azimuth (FS 322), 1732 KW, 100% N_p Speed

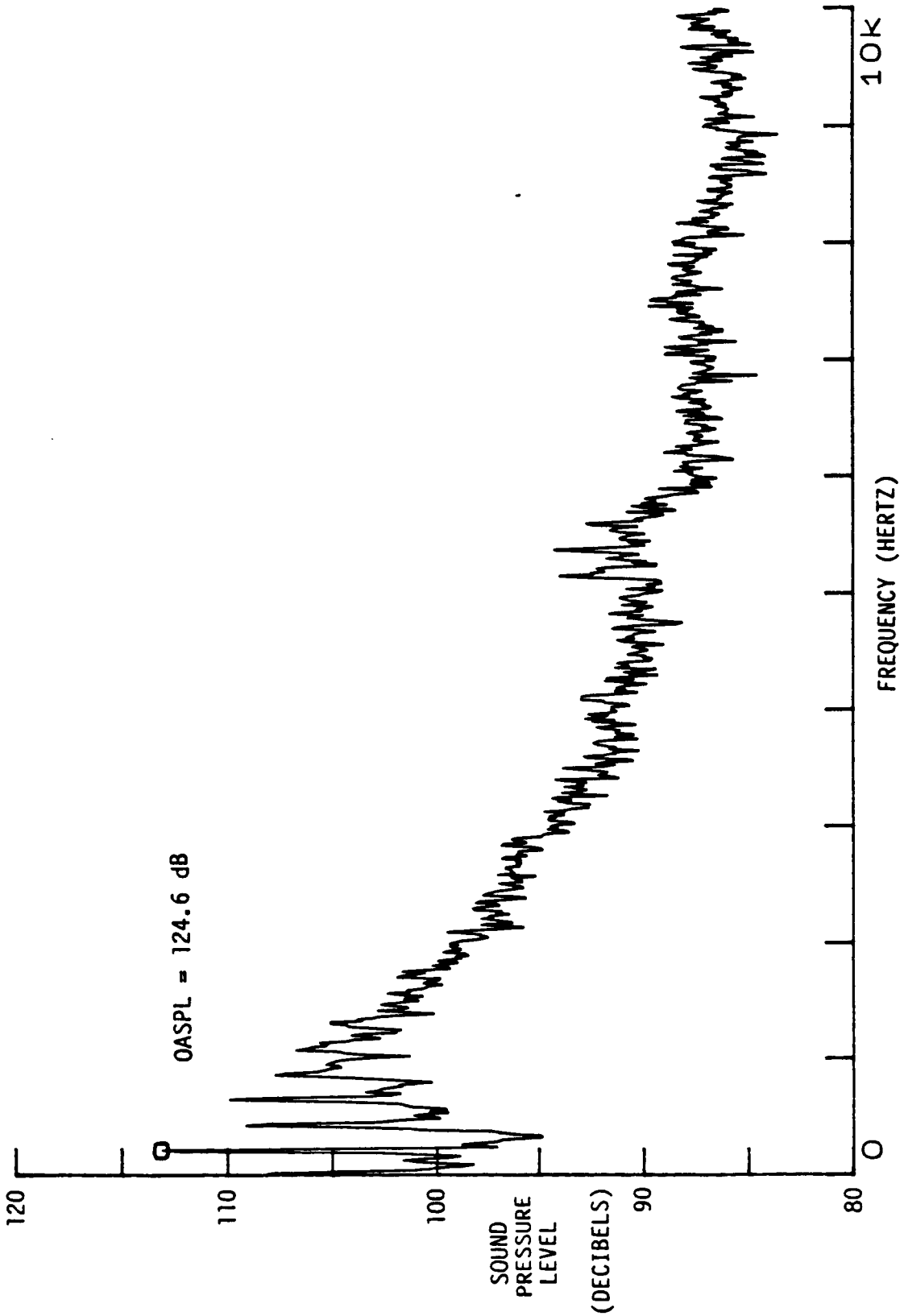

Figure 9.87. Centerline Height Noise Spectrum - 2.99 m, 90° Azimuth (FS 421), 1732 KW, 100% N_p Speed

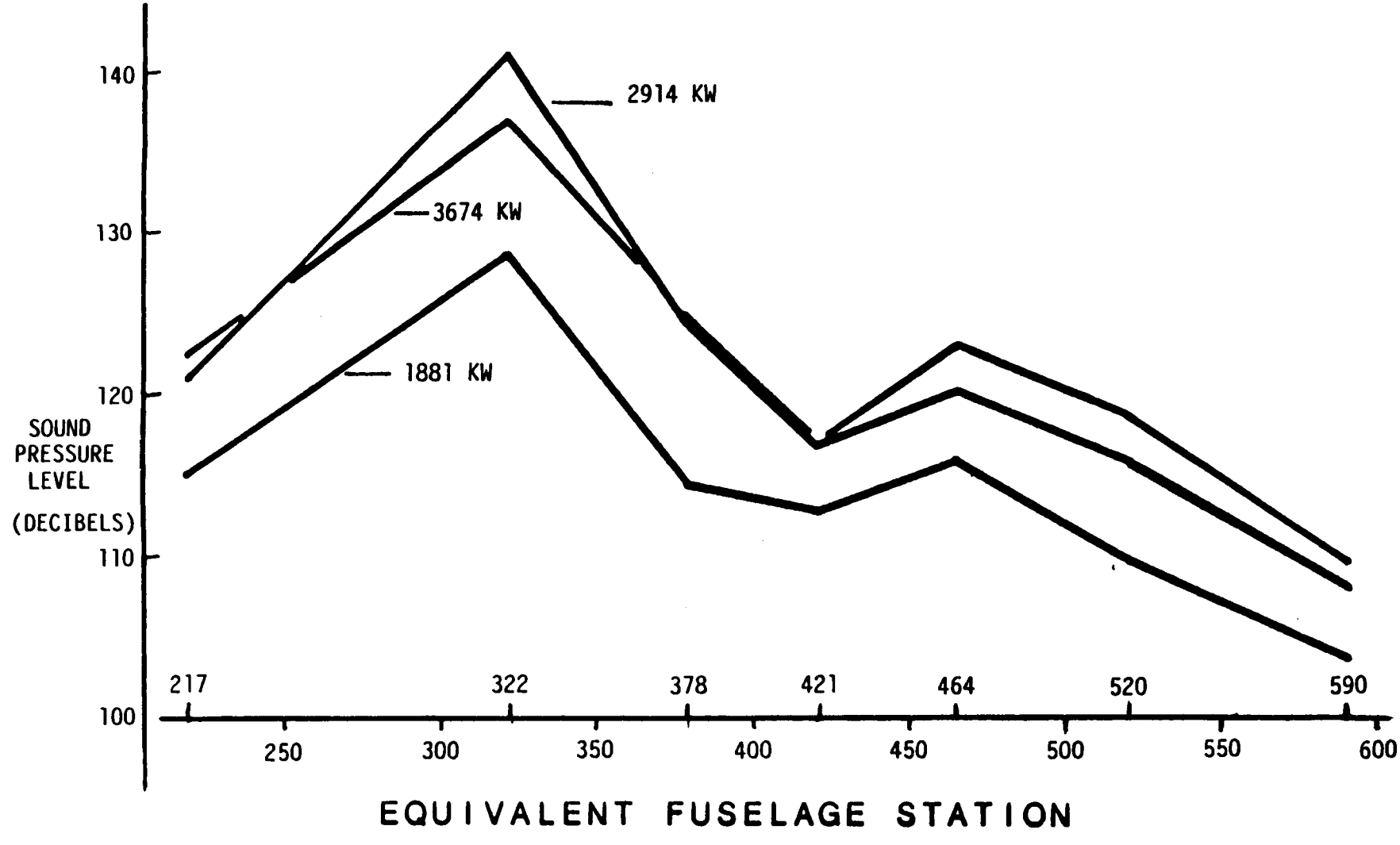

Figure 9.88. Centerline Height First Order Blade Passage SPL - 2.99 m, 105% N_p Speed

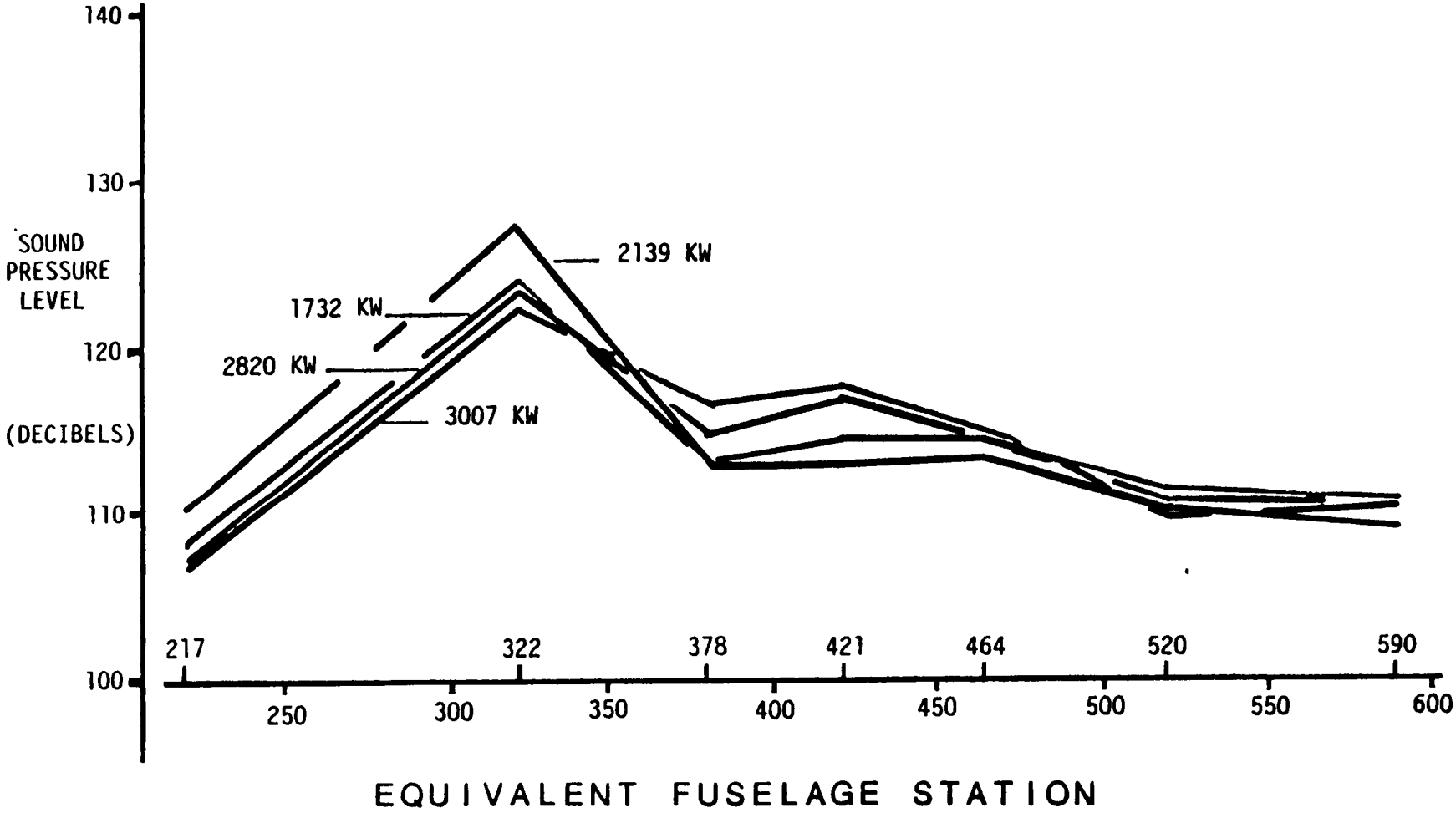

Figure 9.89. Centerline Height First Order Blade Passage SPL - 2.99 m, 100% N_p Speed

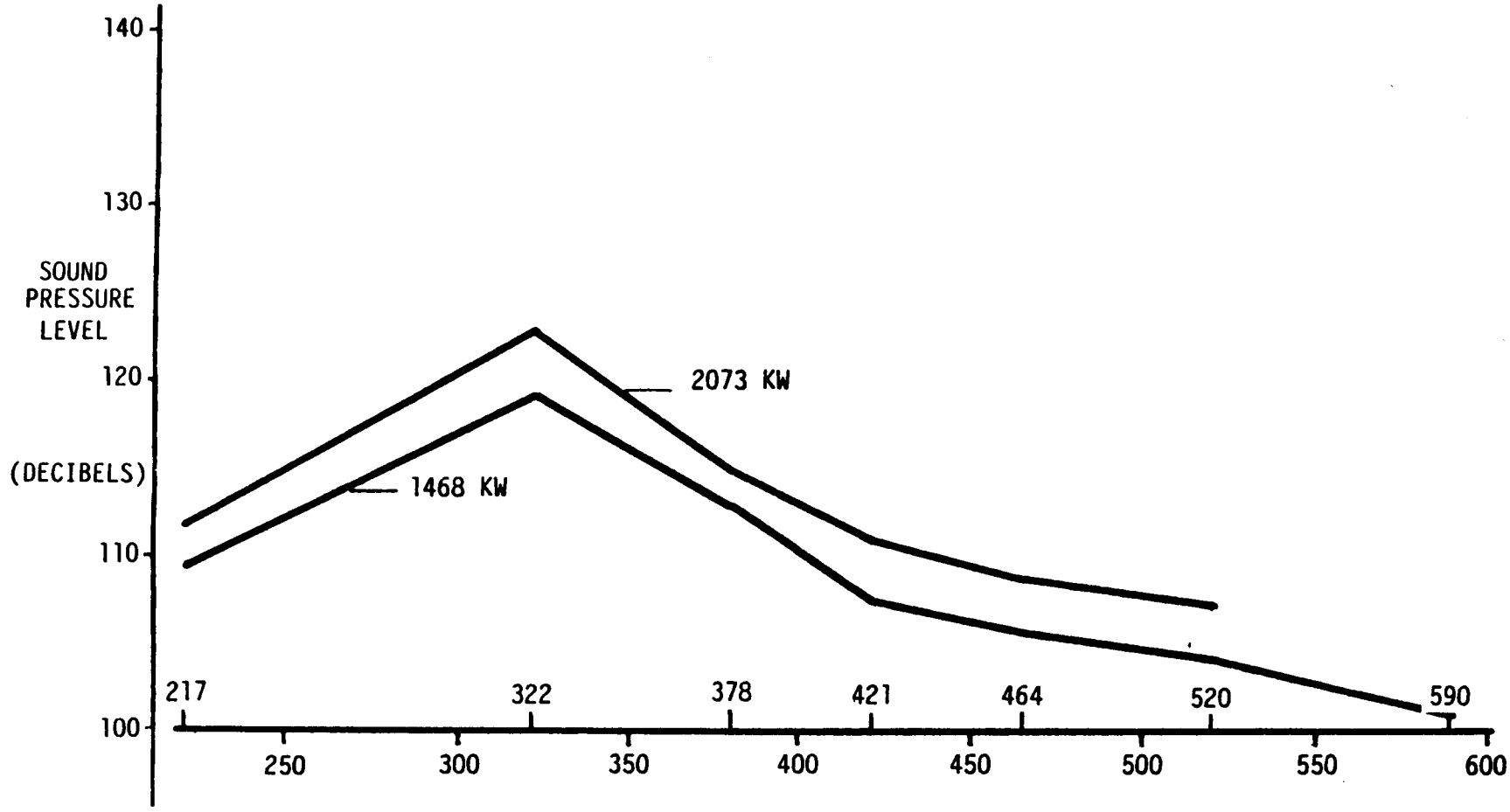

Figure 9.90. Centerline Height First Order Blade Passage SPL - 2.99 m, 87.5% N_p Speed

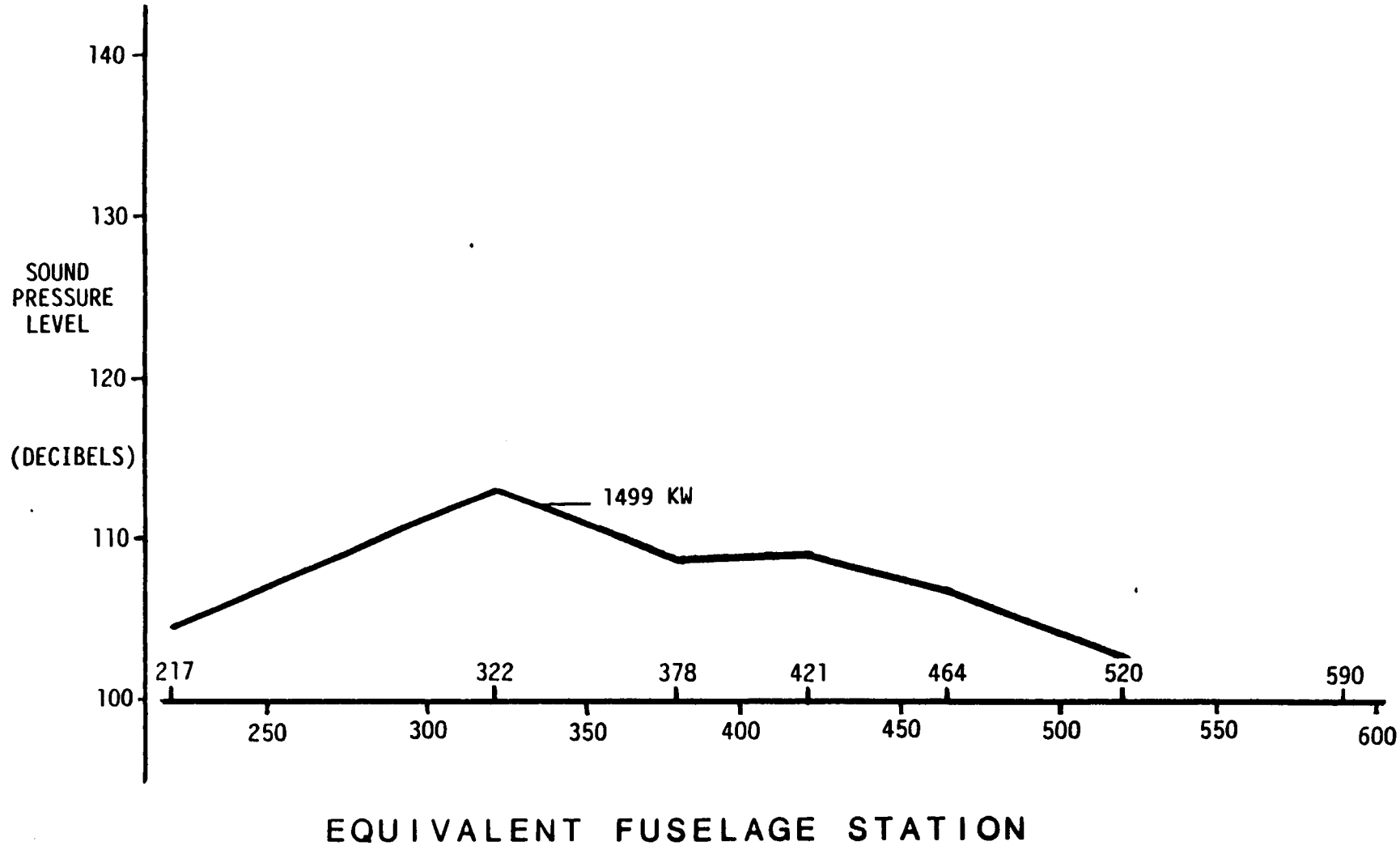

Figure 9.91. Centerline Height First Order Blade Passage SPL - 2.99 m, 75% N_p Speed

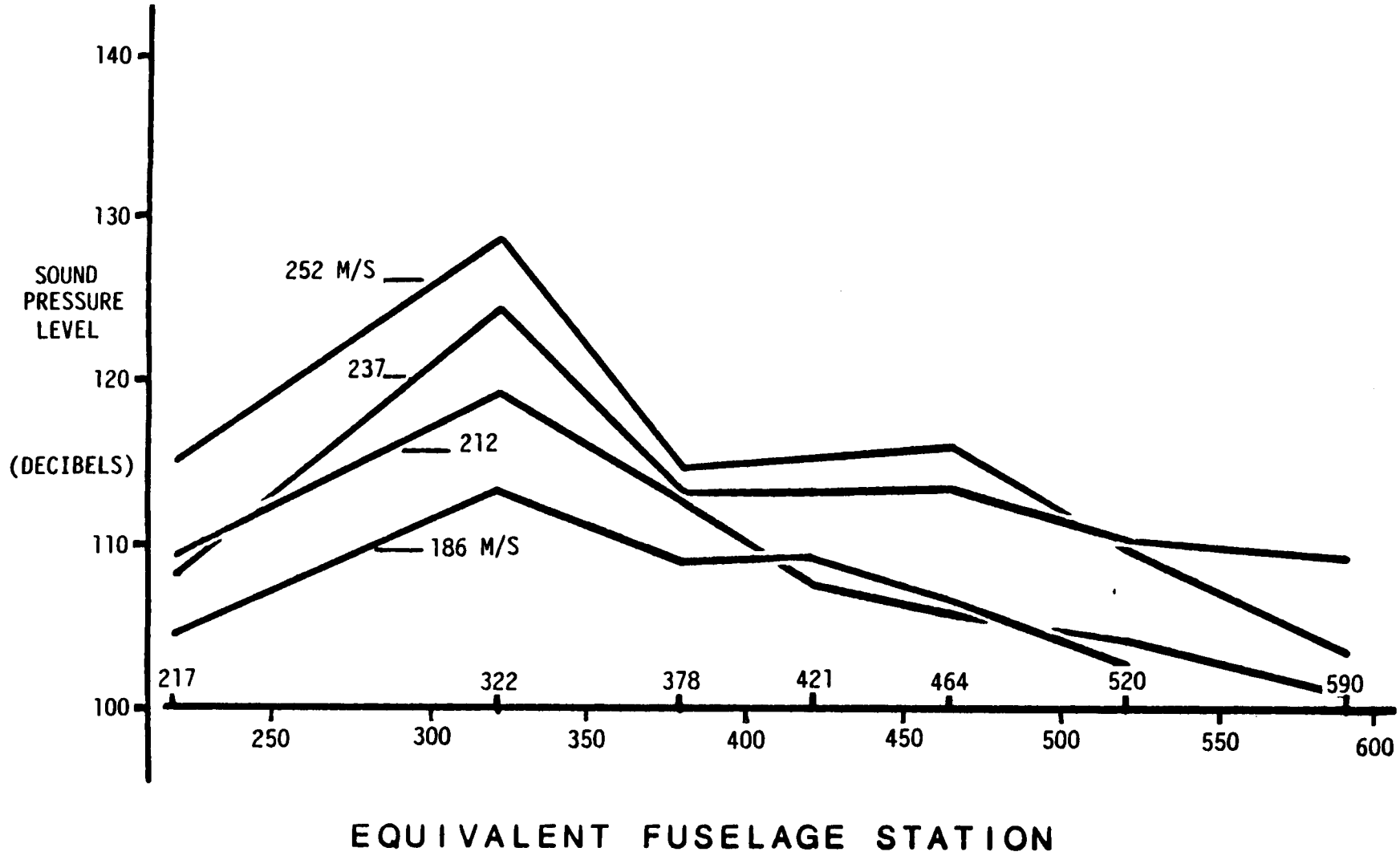

Figure 9.92. Centerline Height First Order Blade Passage SPL - 2.99 m, 1468 to 1881 KW

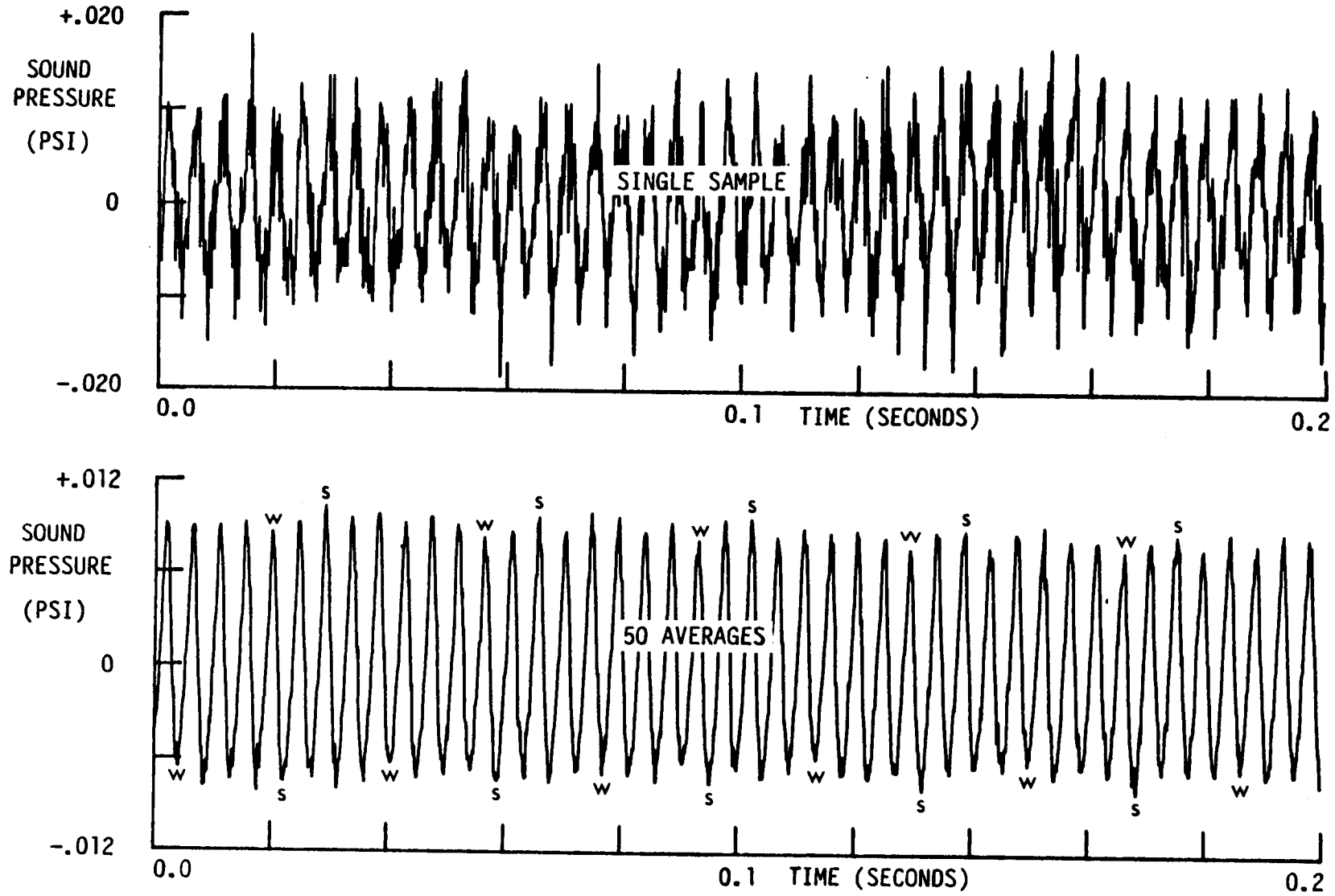

Figure 9.93. Centerline Height Sound Pressures - 2.99 m, 50° Azimuth (FS 322), 1732 KW, 100% N_p Speed (200 ms Time Histories)

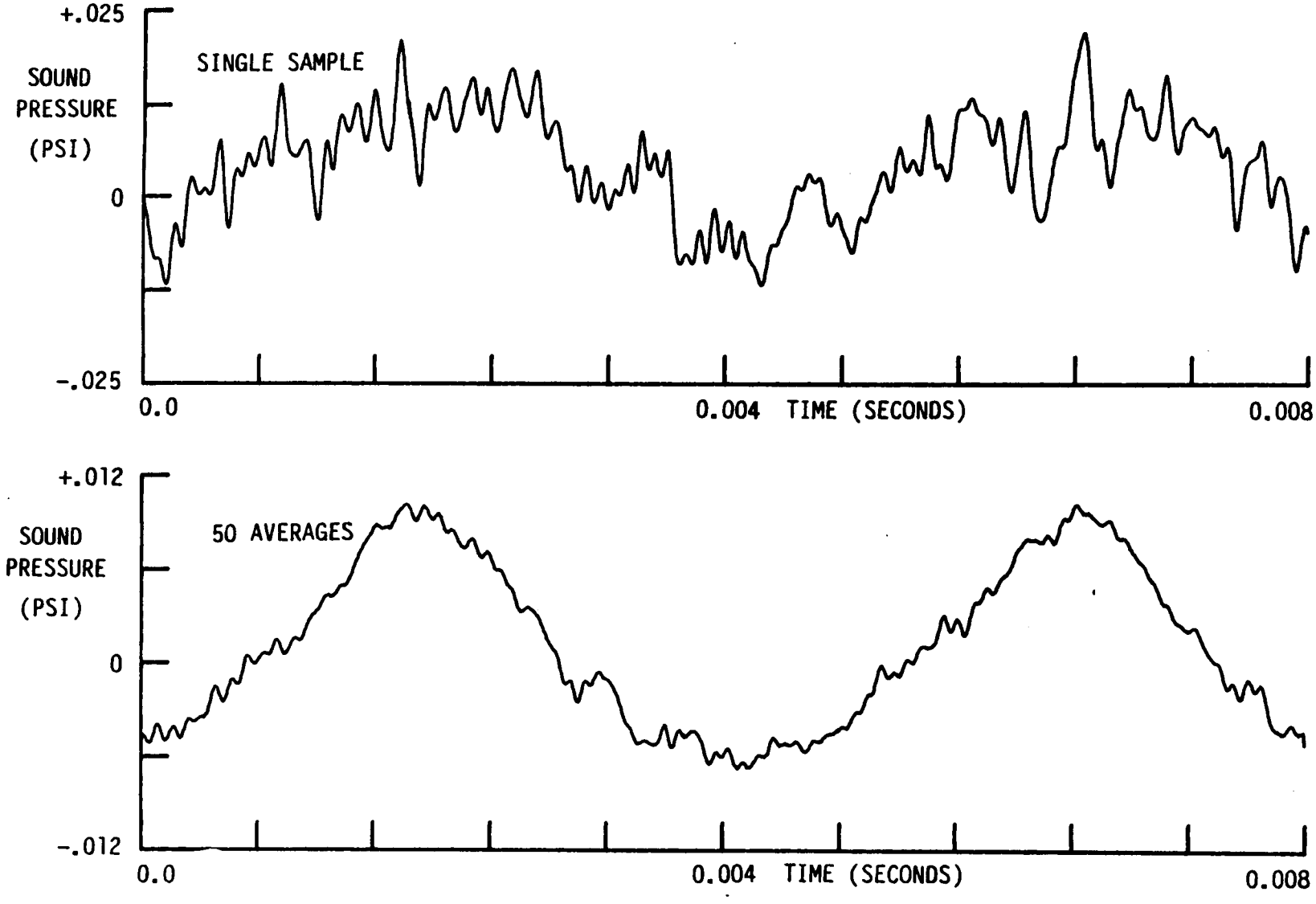

Figure 9.94. Centerline Height Sound Pressures - 2.99 m, 50° Azimuth (FS 322), 1732 KW, 100% N_p Speed (8 ms Time Histories)

REFERENCES

1. "Propfan Test Assessment Propulsion System Static Test and Instrumentation Plan", Lockheed-Georgia Company, LG86ER0008, February 1986, Revised May 1986.

2. "Propfan Test Assessment Propfan Propulsion System Static Test Informal Report", Lockheed-Georgia Company, PTA-86/5-0177, NASA-24339 DRD 221-02, August 1986.

3. "SR-7L Prop-Fan PTA Static Engine Test Report", Chuck de George and Jay Turnberg, Hamilton Standard Division, United Technologies Corporation, October 1986.

4. PTA Program Coordination Memo, "Acoustic Tailpipe Static Test Results Review", T. F. Dowell and J. Gamble, Rohr Industries, August 1986.

5. "Work Plan for the Propfan Test Assessment (PTA) Program", Lockheed-Georgia Company, LG84ER0136, November 1984, Revised April 1985.

1. Report No.	2. Government Accession No.	3. Recipient's Catalog No.
CR - 179613		

4. Title and Subtitle

Propfan Test Assessment
Propfan Propulsion System
Static Test Report

5. Report Date

May 1987

6. Performing Organization Code

7. Author(s)

D. M. O'Rourke

8. Performing Organization Report No.

LG86ER0173

10. Work Unit No.

9. Performing Organization Name and Address

Lockheed-Georgia Company
86 South Cobb Drive
Marietta, GA 30063

11. Contract or Grant No.

NAS3-24339

13. Type of Report and Period Covered

Contractor Report
Feb-June 1986

12. Sponsoring Agency Name and Address

NASA Lewis Research Center
21000 Brookpark Road
Cleveland, OH 44135

14. Sponsoring Agency Code

15. Supplementary Notes

NASA Technical Monitor - D. C. Reemsnyder
NASA Project Manager - E. J. Graber

16. Abstract

The Propfan Test Assessment (PTA) propulsion system successfully completed over 50 hours of extensive static ground tests, including a 36 hour endurance test. All major systems performed as expected, verifying that the large-scale 2.74m (9 foot) diameter propfan, engine, gearbox, controls, subsystems and flight instrumentation will be satisfactory with minor modifications for the upcoming PTA flight tests on the GII aircraft in early 1987.

A test envelope was established for static ground operation to maintain propfan blade stresses within limits for propfan rotational speeds up to 105% (1783 rpm) and power levels up to 3880 kW (5200 SHP). Transient tests verified stable, predictable response of the engine power and propfan speed controls. Installed engine TSFC was better than expected, probably due to the excellent inlet performance coupled with the supercharging effect of the propfan.

Near-and far-field noise spectra contained three dominant components, which were dependent on power, tip speed, and direction. The components were propfan blade tones, propfan random noise, and compressor/propfan interaction noise. No significant turbine noise or combustion noise was evident.

17. Key Words (Suggested by Author(s))	18. Distribution Statement
Propfan Propfan Test Assessment (PTA) Advanced Propeller Static Test	General Release

19. Security Classif. (of this report)	20. Security Classif. (of this page)	21. No. of pages	22. Price*
Unclassified	Unclassified		

*For sale by the National Technical Information Service, Springfield, Virginia 22161